Identification and characterization of selected secondary metabolite biosynthetic pathways from *Xenorhabdus nematophila*

Dissertation
zur Erlangung des Doktorgrades
der Naturwissenschaften

vorgelegt beim Fachbereich Biowissenschaften (15)
der Johann Wolfgang Goethe-Universität
in Frankfurt am Main

von

Daniela Reimer

aus Offenbach am Main

Frankfurt 2013
(D 30)

vom Fachbereich Biowissenschaften (15) der Johann Wolfgang Goethe-Universität als Dissertation angenommen.

Dekan: Prof. Dr. Starzinski-Powitz
Gutachter: Prof. Dr. Helge B. Bode, Prof. Dr. Eckhard Boles
Datum der Disputation: 22.08.2013

Meinen Eltern

"Two roads diverged in a yellow wood,
And sorry I could not travel both
And be one traveler, long I stood
And looked down one as far as I could
To where it bent in the undergrowth;

Then took the other, as just as fair,
And having perhaps the better claim,
Because it was grassy and wanted wear;
Though as for that the passing there
Had worn them really about the same,

And both that morning equally lay
In leaves no step had trodden black.
Oh, I kept the first for another day!
Yet knowing how way leads on to way,
I doubted if I should ever come back.

I shall be telling this with a sigh
Somewhere ages and ages hence:
Two roads diverged in a wood, and I -
I took the one less traveled by,
And that has made all the difference."*

---

* Robert Frost, poem "The road not taken", published in the collection Mountain Interval, Henry Holt and Company, New York, 1916.

Table of contents

Abstract

Bacteria of the genera *Xenorhabdus* and *Photorhabdus* are entomopathogenic bacteria symbiotically associated with entomopathogenic nematodes belonging to the genera *Steinernema* and *Heterorhabditis*, respectively. Detailed studies for the understanding of the regulation system in the tripartial mutualism-pathogenesis relationship between the bacteria, the nematode and the infected host have shown that secondary metabolites produced by the bacteria are either involved in the pathogenesis against numerous insect larvae or play an important role in the symbiosis towards the nematode. Several classes of structurally diverse secondary metabolites with a broad spectrum of bioactivities (e.g. antibacterial, insecticidal, antifungal) are known from different *Xenorhabdus* and *Photorhabdus* strains and are produced by nonribosomal peptide synthetases (NRPS) and the fatty acid synthase (FAS)-related polyketide synthases (PKS) or even hybrids thereof.

During this work, xenocoumacin 1 (XCN 1) and 2 (XCN 2), the major antimicrobial compounds produced by *Xenorhabdus nematophila* and their corresponding biosynthetic gene cluster were identified and studied in detail. Although both compounds show antibiotic activity against Gram-positive bacteria, XCN 1 is much more active and additionally shows good activity against different fungi. Xenocoumacins are synthesized via a non colinear hybrid PKS/NRPS multienzyme (*xcnA-N*), consisting of six transcriptional units identified by real time PCR. The biosynthesis can be divided into enzymes responsible for the biosynthesis of the core structure (XcnAFHIJKL), including the hydroxymalonyl-ACP (XcnBCDE), in proteins involved in an interesting drug activation mechanism (XcnAG) and for a resistance conferring inactivation pathway (XcnMN).

Five different prexenocoumacins are formed by the xenocoumacin biosynthetic machinery as inactive prodrugs inside the cytoplasm. XcnG, a bifunctional protein with a periplasmic peptidase domain and three additional transmembrane helices cleaves the acylated D-asparagine residue from all prexenocoumacin derivatives to form the bioactive XCN 1 as sole compound. Furthermore, XCN 1 is secreted by an ABC transporter TolC-like protein complex and is thought to be involved in killing microbes living inside the insect gut or other bacterial food competitors during the infection cycle and the nematode development. As XCN 1 is also toxic to the producing strain, this compound is taken up by *X. nematophila* and a detoxification by XcnMN via a conversion of XCN 1 into the less active XCN 2 occurs due to a new type of pyrrolidine ring formation. A desaturase (XcnN) and a saccharopine dehydrogenase-like enzyme (XcnM) are essential for this unusual transformation via two new identified intermediates and the catalytic reaction is regulated by the response regulator OmpR. OmpR was identified as a negative regulator of *xcnA-L* required for the biosynthesis of XCN 1 and as a positive regulator responsible for the self-resistance mechanism. The differential expression may therefore be part of a response to balance the necessary level between XCN 1 and XCN 2 to avoid self-toxicity and as a result to optimize the fitness of the strain.

Astonishingly, homologues of the membrane-bound and D-asparagine-specific peptidase (XcnG) and the encoding NRPS for the starting module (XcnA) for the acylated D-asparagine residue

were identified in many different bacterial genera. Thus indicating a widespread and important mechanism for the activation of secondary metabolites as it was earlier only known from ribosomal biosynthesis and should be considered especially during the *in silico* analysis of secondary metabolite biosynthetic gene clusters and their predicted products during large-scale genome mining approaches.

Moreover, six novel linear peptides named rhabdopeptides (RDPs) have been identified after the identification of the corresponding *rdp* gene cluster using a promoter trap strategy (IVET) for the detection of insect inducible genes. Detailed analysis revealed that these compounds participate in virulence towards insects and are produced upon bacterial infection of a suitable insect host. As rhabdopeptide production is initially upregulated upon infections but *rdp* mutant strains display no severe virulence defect, rhabdopeptides are suggested to function during the insect bioconversion and nematode reproduction phases of the *Xenorhabdus* life cycle due to an abundant production after the insect death. The structures of the highly *N*-methylated nonribosomally derived rhabdopeptides were deduced exclusively from stable isotope labeling experiments combined with detailed mass spectrometric analysis and represent a new class of *N*-methylated peptides carrying a decarboxylated amino acid.

Besides rhabdopeptides, a new xenortide derivative from *X. nematophila* and the cyclic GameXPeptides from *P. luminescens* were identified and their structures were elucidated. The combination of labeling experiments and mass spectrometry enables a rapid identification of building blocks. In particular it allows to distinguish between isobar amino acids such as leucine and isoleucine in nonribosomally produced peptides. The established methods are especially important techniques, when isolation of compounds might be a challenging task as the microorganism produces the interesting compound in minute amounts or with many different derivatives in complex mixtures. Furthermore, stable isotope labeling can be used as a method to determine the absolute amino acid configuration of compounds directly in the producer strain without derivatization reagents. Labeling of amino acids used in transaminase deficient mutant strains enables to determine the absolute configuration as in a conversion to a D-amino acid one label is exchanged. Hence, in this work the absolute configuration of the GameXPeptides was successfully determined.

Zusammenfassung

6 Zusammenfassung

Bakterien des Genus *Xenorhabdus* und *Photorhabdus* sind entomopathogen, leben in Symbiose mit entomopathogenen Nematoden der Gattungen *Steinernema* bzw. *Heterorhabditis* und sind pathogen gegenüber verschiedenen Insekten einschließlich der Ordnung Lepidoptera. Verschiedene Untersuchungen des dreigeteilten Mutualismus-Pathogenese Verhältnisses zwischen Bakterium, Nematode und infizierter Insektenlarve haben gezeigt, dass von den Bakterien produzierte Sekundärmetabolite in der Pathogenese gegen eine Vielzahl an Insektenlarven oder in der Symbiose mit den Nematoden eine wichtige Rolle spielen. Verschiedene strukturell unterschiedliche Klassen an Sekundärmetaboliten mit einem breiten Spektrum an Bioaktivitäten sind aus unterschiedlichen *Xenorhabdus* und *Photorhabdus* Stämmen bekannt. Ungefähr 7,5 % des Genoms in *Xenorhabdus nematophila* codiert für den Sekundärmetabolismus, was im Vergleich zu *Streptomyces coelicolor* mit nur 4,5 % einen großen Anteil darstellt. Vergleicht man *Xenorhabdus* und *Photorhabdus* miteinander, so sind aus *Xenorhabdus* Arten mehr unterschiedliche Sekundärmetabolite bekannt. Beispielsweise weist Nematophin eine antifungische und antibakterielle Aktivität, auch gegenüber dem klinisch relevanten Bakterium *Staphylococcus aureus* auf. Für zyklische Depsipeptide wie Szentiamid aus *Xenorhabdus szentirmaii* konnte eine Aktivität gegenüber dem Parasiten *Plasmodium falciparum*, dem Erreger von Malaria, gezeigt werden. Die meisten Sekundärmetabolite werden von nichtribosomalen Peptidsynthetasen (NRPS) und den der Fettsäuresynthase (FAS)-ähnlichen Polyketidsynthasen (PKS) oder Hybriden beider Enzymsysteme hergestellt.

Während dieser Arbeit wurden Xenocoumacin 1 (XCN 1) und 2 (XCN 2), die wichtigsten antimikrobiellen Substanzen von *Xenorhabdus nematophila*, und das dazu gehörige Biosynthese Gencluster identifiziert und im Detail untersucht. Obwohl beide Substanzen antibakterielle Aktivität gegenüber Gram-positiven Bakterien aufweisen, zeigt XCN 1 eine höhere Aktivität und weist zudem eine gute Aktivität gegenüber verschiedenen Pilzen auf. Xenocoumacine werden von einem nicht co-linearen PKS/NRPS Hybrid Multienzymkomplex (*xcnA-N*), bestehend aus sechs transkriptionalen Einheiten synthetisiert. Die Biosynthese kann in verschiedene Teile untergliedert werden: Enzyme, die für die Biosynthese der Kernstruktur (XcnAFHIJKL), inklusive der Hydroxymalonyl-ACP Biosynthese (XcnBCDE) verantwortlich sind und Proteine, die an einem interessanten Mechanismus für die Prodrug Aktivierung (XcnAG) und an einem resistenzvermittelndem Biosyntheseweg der Inaktivierung (XcnMN) beteiligt sind.

Strukturelle Bausteine wie das seltene Hydroxymalonyl, welches aus 1,3-Bisphophoglycerat mit Hilfe von vier Enzymen umgewandelt wird, sind ausführlich in der Biosynthese von Zwittermicin in *Bacillus cereus* beschrieben. Eine Inaktivierung von *xcnC* und genaue Analyse von XcnBCDE belegen eine Beteiligung an der Biosynthese der Hydroxymalonyl Einheit. Xenocoumacin stellt somit einen weiteren Naturstoff mit dieser seltenen Verlängerungseinheit dar.

Auf Grund der aus der Literatur bekannten Xenocoumacin Derivate 1 und 2 schlug die erste Vorhersage und Aufklärung des Biosyntheseweges fehl. Da das Biosynthese Gencluster ein NRPS Modul mehr vorweist als für die Synthese der Strukturen benötigt und konservierte katalytisch wichtige Sequenzmotive keine hohe Ähnlichkeit aufwiesen, wurde dieses fälschlicherweise als inaktiv postuliert. Inaktivierungen der Gene des Biosynthese Genclusters, denen bisher keine Rollen zugewiesen werden konnten, lieferten jedoch den entscheidenden Hinweis. Deletionsstudien von XcnG zeigten anstatt der Xenocoumacin Produktion die Bildung fünf inaktiver Xenocoumacin-Vorstufen, die *N*-terminal ein D-Asparagin verknüpft mit unterschiedlichen Acylresten tragen. Somit konnte als Biosynthesemodel das folgende Schema postuliert werden:

Fünf verschiedene Prexenocoumacine werden von der Xenocoumacin Biosynthese Maschinerie innerhalb des Zytoplasmas als inaktive Vorstufen, sogenannte Prodrugs, produziert. XcnG, ein bifunktionales Protein mit einer periplasmatischen Peptidase Domäne und drei zusätzlichen Transmembranhelices spaltet den acylierten D-Asparaginrest von allen Prexenocoumacinen ab und wandelt die Vorstufen somit in das bioaktive XCN 1 um. Daraufhin wird XCN 1 von einem ABC Transporter-TolC-ähnlichem Komplex aus der Zelle ausgeschleust.

Erstaunlicherweise wurden homologe Proteine der membrangebundenen D-Asparagin-spezifischen Peptidase (XcnG) und dem NRPS Startmodul (XcnA) für den acylierten D-Asparaginrest in vielen verschiedenen bakteriellen Gattungen identifiziert. Diese Entdeckung zeigt auf, dass dieser wichtige Aktivierungsmechanismus für Sekundärmetabolite weit verbreitet ist und bei *in silico* Vorhersagen von Sekundärmetabolit Genclustern und den dazugehörigen Substanzen berücksichtig werden sollte. Solch eine Aktivierung war bis zu dieser Arbeit nur aus der ribosomalen Biosynthese von Proteinen bekannt.

Homologe von XcnG konnten in den Biosynthesegenclustern von Amicoumacin und Zwittermicin aus *Bacillus* spp., von Colibactin aus *Escherichia coli* und anderen Gattungen wie zum Beispiel *Clostridium*, bei denen die produzierte Substanz noch unbekannt ist, identifiziert werden. Detaillierte Analyse des strukturellen Aufbaus erlaubte eine Klassifizierung in Typ I und Typ II Peptidasen. Typ I Peptidasen, wie XcnG, weisen eine Signalsequenz für den Transport des Proteins in das Periplasma, die katalytisch aktive Peptidase Domäne sowie drei Transmembranhelices, die der Verankerung in der Membran dienen, auf. Typ II Peptidasen wie zum Beispiel ZmaM aus der Zwittermicin Biosynthese hingegen haben zusätzlich einen aus sechs Transmembranhelices bestehenden ABC-Transporter und damit insgesamt neun Transmembranhelices. Im Genom von *X. nematophila* konnten drei Kandidaten gefunden werden, die vermutlich die Funktion des ABC-Transporters übernehmen könnten. Heterologe Expression der Peptidase in *E. coli* konnte zeigen, dass

der Transmembranteil von XcnG nicht nur für die Verankerung in der Membran zuständig ist, sondern auch für die Aktivität benötigt wird.

XcnG und das homologe ClbP, die Peptidase aus dem Colibactin Biosynthesegencluster, weisen eine hohe strukturelle Ähnlichkeit mit Klasse C β-Lactamasen (AmpC) auf. Mit Hilfe eines Homologiemodells konnte dieser Typ Peptidasen der MEROPS S12 Enzym Familie zugeordnet werden, die Serin-Typ D-Ala-D-Ala-Carboxypeptidasen umfasst. Als katalytische Triade konnten Serin, Lysin und Tyrosin nachgewiesen werden. Obwohl der *N*-terminale Rest in allen Beispielen als acyliertes D-Asparagin gezeigt oder vorhergesagt werden konnte, scheint sich diese Klasse der Peptidasen weiter in verschiedenen Spezifitäten zu unterscheiden. Heterologe Expression der Zwittermicin und Amicoumacin Peptidasen zeigte keine Spaltung der isolierten Prexenocoumacine. Wobei hingegen die Expression einer Peptidase aus *Xenorhabdus bovienii* eine Spaltung ermöglichte. Auch, wenn die Struktur des dazugehörigen Genclusters aus *X. bovenii* noch unbekannt ist, konnte anhand der Strukturvorhersage gezeigt werden, dass die auf den acylierten D-Asparaginrest folgende Aminosäure eine hohe Ähnlichkeit zu Arginin aus Xenocoumacin aufweist. Zwittermicin und Amicoumacin hingegen tragen an dieser Position ein Serin bzw. Aspartat.

Während dem Bakterien-Nematoden-Lebenszyklus, spielt Xenocoumacin 1 eine wichtige Rolle in der Abwehr von um Nahrung konkurrierende Mikroben, die im Insektenmagen und Boden leben. Da XCN 1 selbst toxisch für das produzierende Bakterium ist, wird die Substanz als Selbstschutzmechanismus wieder von *X. nematophila* aufgenommen und strukturell verändert. XcnMN wandeln XCN 1 über eine bislang unbekannte Pyrrolidinringbildung in das weniger aktive XCN 2 um. Eine Desaturase (XcnN) und ein der Saccharopine Dehydrogenase ähnliches Enzym (XcnM) sind essentiell für diese ungewöhnliche Umwandlung. XCN 1 wird von XcnN zu einem wahrscheinlich instabilen Intermediat XCN-464 oxidiert und trägt eine Doppelbindung an der Stickstoffposition der Aminogruppe im Argininrückgrat. Die XCN 2 Bildung kann auf zwei unterschiedlichen Stoffwechselwegen erfolgen, die vermutlich beide von XcnM katalysiert sein könnten. Die Umwandlung in XCN 3, ein in dieser Arbeit neu identifiziertes Derivat, erfolgt durch einen intramolekularen Angriff der freien Aminogruppe, wobei Guanidin abgespalten wird und ein Pyrrolidinring entsteht. Alternativ kann XCN 4 durch Hydrolyse oder als Intermediat bei der Umwandlung in XCN 3 entstehen. In einem weiteren Schritt wird XCN 3 in XCN 2 reduziert. Die Umwandlung wird von dem OmpR Regulator, ein Teil des Zweikomponentensystems OmpR/EnvZ gesteuert. Das Zweikomponentensystem ist an der Regulation der Flagella und Exoenzym Biosynthese beteiligt. OmpR wurde als negativer Regulator von den für die Biosynthese von XCN 1 benötigten Genen (*xcnA-L*) und als positiver Regulator für den Resistenzmechanismus (*xcnMN*) beschrieben. Die unterschiedliche Expression kann als Teil einer Regulationskaskade für den notwendigen

Konzentrationslevel zwischen XCN 1 und XCN 2 angesehen werden. Dies erlaubt dem Produzenten, sich selbst vor der Toxizität zu bewahren und seine Fitness zu stärken.

Weiterhin konnten sechs bisher unbekannte Peptide, Rhabdopeptide genannt, und das dazu gehörige Gencluster (*rdp*) anhand einer *in vivo* Expressionstechnologie (IVET) in *Xenorhabdus nematophila* identifiziert werden. Anhand IVET können Gene, die im Insektenmodell induziert und somit positiv reguliert werden, identifiziert werden. Eine detaillierte Analyse enthüllte, dass Rhabdopeptide an der Virulenz gegenüber dem Insekt beteiligt sind und während der bakteriellen Infektion im Insektenwirt produziert werden. Obwohl die Rhabdopeptidproduktion zunächst hoch reguliert ist, zeigen *rdp* Mutanten keinen gravierenden Defekt in der Virulenz auf und weisen auch keine anderen phänotypischen Unterschiede wie zum Beispiel bei der Nematoden Kolonialisierung auf. Da die Produktion der Rhabdopeptide nach dem Tod des Insektes stark ansteigt und das Maximum erst nach 10 Tagen nach der Infektion und somit nach ungefähr acht Tagen nach dem Insektentod erreicht wird, wird angenommen, dass die Substanzen den Insektenkadaver vor Nahrungskonkurrenten schützen oder eine Rolle während der Nematoden Reproduktion im *Xenorhabdus* Lebenszyklus spielen.

Die Strukturen der stark *N*-methylierten nichtribosomal synthetisierten Rhabdopeptide wurden ausnahmslos durch Markierungsexperimente mit Aminosäuren in Kombination mit massenspektrometrischen Analysen (Tandem MS) aufgeklärt und repräsentieren eine neue Klasse von *N*-methylierten Peptiden, die eine decarboxylierte Aminosäure tragen. Die sechs Derivate unterscheiden sich in ihrer Länge und weisen einen Einbau von vier bis sechs Aminosäuren (Valin, Leucin) und als *C*-terminales Amin Phenylethylamin auf. Der Einbau von Phenylethylamin ist strukturell aus den Xenortiden bekannt und die Verwendung einer terminalen Kondensationsdomäne, die den Einbau katalysiert, wurde ausführlich in der Biosynthese von Pseudomonine beschrieben. Im Genom von *X. nematophila* konnte eine Decarboxylase identifiziert werden, die an der Bereitstellung von Phenylethylamin beteiligt ist. Im Gegensatz zu der Länge der Peptide, besteht das zugehörige Biosynthese Gencluster neben der terminalen Kondensationsdomäne hingegen nur aus drei Modulen, die die Adenylierung, *N*-Methylierung, Kondensation und Thiolierung katalysieren. Aus diesem Grund kann von einer teilweisen iterativen Nutzung ausgegangen werden.

In Bioaktivitätstest gegen verschiedene Protozoen Parasiten weisen Rhabdopeptide geringe Aktivitäten gegen *T. brucei rhodesiense*, *T. cruzi* und *P. falciparum* auf.

Strukturell verwandt zu den Rhabdopeptiden sind die Xenortide. Xenortide bestehen wie die Rhabdopeptide aus *N*-methylierten Bausteinen, unterscheiden sich aber durch den Einbau von

Phenylalanin. Das Biosynthese Gencluster zeigt eine große Sequenzhomologie mit den Rhabdopeptiden und es wird ein sogenannter Crosstalk zwischen den beiden Genclustern vermutet.

Außer den linearen Peptiden aus *Xenorhabdus* konnten vier zyklische GameXPeptide aus *P. luminescens* identifiziert und aufgeklärt werden. Eine Kombination von Markierungsexperimenten und Massenspektrometrie erlaubte eine schnelle Aufklärung von Strukturbausteinen in den nichtribosomalen GameXPeptiden. Solch eine Methode, ermöglicht selbst die Unterscheidung von isobaren Aminosäuren wie zum Beispiel Leucin und Isoleucin und stellt vor allem eine wichtige Technik dar, wenn eine Isolierung von interessanten Substanzen auf Grund von geringen produzierten Mengen oder vielen in der HPLC MS überlappenden Derivaten erschwert bzw. unmöglich ist. Eine Kultivierung des Produzenten in ^{13}C oder ^{15}N markiertem Medium ermöglicht die Bestimmung der Kohlenstoff- und Stickstoffatome. Durch inverse Fütterungsexperimente, bei denen natürlich vorkommende Aminosäuren in einen markierten Hintergrund gefüttert werden, können die Bausteine in der Substanz identifiziert werden. Erfolgt ein Einbau, ist eine Massenverschiebung zu einer geringeren Masse um die Anzahl der eingebauten Kohlenstoffe sichtbar. Am Beispiel von GameXPeptid A konnte z.B. eine Verschiebung von *m/z* 618 um -5 zu *m/z* 613 detektiert werden, was einem Einbau von Valin entspricht.

Weiterhin können Markierungsversuche mit stabilen Isotopen als Methode zur Bestimmung der absoluten Konfiguration von Aminosäuren direkt im Produzenten verwendet werden. Dies hat den Vorteil, dass keine anderweitige Derivatisierung mit unterschiedlichen Reagenzien notwendig ist. In nichtribosomalen Peptidsynthetasen wird die Epimerisierung zu einer D-Aminosäure von speziellen Epimerisierungsdomänen oder dualen Kondensations-Epimerisierungsdomänen übernommen. Um zu unterscheiden, ob eine Umwandlung durch die jeweilige Domäne katalysiert wird, erlaubt die Markierung von Aminosäuren in Transaminase-negativen Mutanten diese Bestimmung. Bei einer Umwandlung einer L-Aminosäure in eine D-Aminosäure wird eine [^{2}H]-Markierung am α-Kohlenstoff durch ein Wasserstoff aus dem Medium ausgetauscht. Im Gegensatz bleibt diese Markierung erhalten, wenn eine L-Aminosäure eingebaut wird. Durch die Anwendung dieser Methode konnte in dieser Arbeit die absolute Konfiguration der GameXPeptide erfolgreich bestimmt werden.

Introduction

Mutualistic and entomopathogenic bacteria as a source for natural products

Since ancient times knowledge of plants and their pharmaceutical metabolites have been used for human health care. A high proportion of phytomedicine, herbal pharmaceuticals, used all over the world is based on the isolation of substances discovered in plants mentioned in the traditional medicine.[31] The sources for compounds derived from nature were further extended with the advent of the so-called “Golden Age of Antibiotics” in the 1940s. Nature was recognized as a rich source for novel bioactive compounds and not only plants, but also microorganisms and fungi moved into the focus of researchers.[31] At the same time, pharmaceutical companies started on natural product discovery and also developed screening assays to test chemically synthesized compounds.[5] Another approach taken by pharmaceutical companies was the implementation of combinatorial chemistry in order to create large libraries of compounds to be tested for their bioactivity. Although, combinatorial chemistry was and is a successful technique, only one de novel compound, the antitumor compound sorafenib from Bayer, was approved as a drug in the last 30 years being derived from this approach.[111]

The role of natural products as a dominant player in drug discovery field can be highlighted by the fact that only 36 % of the small-molecule approved drugs in the period of 1981 to 2010 are based on synthetic origin. Compared to 6 % being natural products, 28 % being derived from natural products and the remaining 30 % being synthetic molecules with a natural product pharmacore or at least mimicing natural product structures.[111] In the meantime, the search for new drugs is required more than ever, as one major problem nowadays is the fact that antimicrobial drugs become ineffective due to the formation of pathogen resistance.[37] Apart from the role as antibiotics (e.g. gentamycin, vancomycin), natural products have an essential function as cytostatics (e.g. paclitaxel, doxorubicin), immunosuppressive agents (e.g. rapamycin, ciclosporin), antivirals (e.g. interferon α, darunavir), for the treatment against inflammatory diseases (e.g. azithromycin, etoricoxib) and many more.[5;111] Furthermore, drug research in the last decades was driven by the need of industrialized countries under economical aspects. As more than one billion people worldwide lack access to a functioning health care system and around 4.8 million people are killed each year by neglected diseases like malaria, typhoid fever, leishmaniasis, tuberculosis, hepatitis C and HIV/AIDS, the gap between available drug discovery programs and the global need is enormous.[29] The challenging task for the future will be to develop new drug discovery programs dealing with economical, ethical and need driven questions in a balanced way as for example the use of a "cheap" natural plant derived products to resolve health issues.[109]

As approximately 1 % of the microbial world has been taxonomically described, the diverse microbial habitats call for discovery.[31] One neglected ecological niche of microbes is the symbiotic system. Symbiosis is designated as a close physical association between two organisms belonging to different species. A beneficial symbiosis is called mutualism. Mutualistic partnerships are widespread in nature among prokaryotic and eukaryotic species and reveal many possibilities to study the

interaction of partners at the chemical and molecular level.[67;131] Genome mining projects,[85;190] heterologous expression[71] or induction of silent biosynthetic gene clusters[179] enabled to discover natural products in symbiotic systems.[32] Moreover, the research on symbiotic systems was facilitated due the discovery of natural products from previously "uncultivable" bacteria,[82] a possible co-cultivation of different organisms[194] as well as the discovery of hidden, not expected and unknown symbionts.[128;150] Not only the pharmaceutical industry with for instance the biosynthesis of natural products to generate new sources of rare drug candidates profits from symbiotic research, furthermore, symbiotic research allowed to understand natural systems in their specific ecological niche. Here, it is assumed that secondary metabolites fulfill diverse functions in symbiotic systems with respect to signaling and regulation.[32;33;36;130]

To give a short overview about the occurrence of symbiosis in various habitats with a focus on the bacterially produced secondary metabolites, some examples are highlighted (reviewed in[131]). Plants are often associated with endophytic fungi but nevertheless a well-studied symbiosis is the partnership between leguminous plants and the α-proteobacterial order Rhizobiales.[10] The bacteria are able to induce the formation of root nodules, which are then colonized by them as they offer a protective environment for fixing nitrogen. Secondary metabolites like rhizobitoxine contribute to a functional symbiosis. Rhizobitoxine was initially regarded as a plant toxin causing induction of chlorosis in soybeans but was recently identified as a beneficial player in the plant-rhizobial symbiosis by inhibiting ethylene-mediated plant defense reactions.[196] An interesting partnership and rich in secondary metabolites are lichens, associations between fungi and algae or fungi and cyanobacteria.[76] The cyanobacterium *Nostoc* sp. associated with *Peltigera canina* produces for example the chlorine-containing nostoclides with unknown function.[193] Within the marine invertebrate *Bugula neritina*, a bryozoan, the cyctotoxic macrolide bryostatin is produced, which is assumed to be synthesized by an unknown bacterial symbiont. Bryostatin belongs to the most promising drug candidates from marine vertebrates and showed an activity against different human cancer cell lines modulating protein kinase C.[110;152] Many secondary metabolites have been described from symbiotic bacteria living in the gut of insects or other arthropods. *Streptomyces anulates*, isolated from an arthropod, produces the antmicrobial endophenazines[55] and some *Bacillus* spp. associated with water beetles of the family Dytiscidae release defensive steroids.[147]

Model organisms to study symbiotic systems are insect pathogens, e.g. the entomopathogenic bacteria *Xenorhabdus* and *Photorhabdus*, living in a mutualistic association with nematodes of the genera *Steinernema* and *Heterorhabditis*, which will be discussed in more detail in the next sections. Other interesting entomopathogenic bacteria like *Pseudomonas entomophila* or the *Bacillus* spp. are not associated with a symbiotic partner. In *Pseudomonas entomophila*, a soil bacterium, only the secondary metabolites entolysin[12;183], pyoverdine and pseudomonine are known.[103] Genome analysis revealed a potential for novel compounds, which might be of broad interest as potential pharmaceuticals.[11;185] Several *Bacillus thuringiensis* strains, but also *Xenorhabdus* and *Photorhabdus*

in combination with nematodes have been successfully applied as biological control agents for plant protection against insect pests.[41] Besides insecticidal compounds, these species are a rich source for antibacterial, antifungal and nematicidal compounds, and therefore they also might be a promising resource for the pharmaceutical industry.[11]

The genera *Xenorhabdus* and *Photorhabdus* and their associated symbiotic partners

Taxonomy of entomopathogenic nematodes and bacteria

The genera *Xenorhabdus* and *Photorhabdus* are entomopathogenic bacteria symbiotically associated with entomopathogenic nematodes (EPNs) belonging to the genera *Steinernema* and *Heterorhabditis*, respectively, and are pathogenic against different insect hosts including the order of Lepidoptera.[61]

In 1929 without the knowledge of symbiotic bacteria, the first insect pathogenic nematode was isolated from the Japanese beetle grub *Popillia japonica* and described as *Neoaplectana glaseri*.[58;169]

Thirty-six years later, the first symbiotic bacteria isolates from the intestinal lumen of the nematode *Neoaplectana carpocapsae* DD-136 Weiser (now known as *Steinernema carpocapsae*) were assigned into the genus *Achromobacter* and designated by Poinar and Thomas as *Achromobacter nematophilus*.[181] Due the fact that the genus *Achromobacter* combined a number of different species, the generic name was rejected and some species belonging to this genus were transferred to the genus *Alcaligenes*[66] or to other genera.

In the following years, different symbiotic bacteria from the nematode genus *Neoaplectana* as well as the luminous bacteria NC-19 (ATCC 29304) and Hb (ATCC 29999) from a different entomopathogenic nematode genus, assigned *Heterorhabditis*,[135] were isolated. As *Achromobacter nematophilus* and the new bacteria could not be classified in one of these genera, it was necessary to create the new genus *Xenorhabdus* in 1979. The origin of the new name is based on characteristics of the phenotype and the life habitat of these bacteria combining the Greek nouns xenos (“enemy stranger”) and rhabdos (“rod”).[180] Due to the fact that both strains, the bioluminous Hb strain and *A. nematophilus* share common traits, like mutualistic relationship to nematodes and pathogenicity against insects, they were grouped into the genus *Xenorhabdus* and designated as *Xenorhabdus nematophila* and *Xenorhabdus luminescens*.[180]

In the early 1980s, the nematodes were reassigned and the name *Neoaplectana* was discontinued and replaced by *Steinernema*.[51] As *Xenorhabdus luminescens* showed many differences compared to other strains of the *Xenorhabdus* spp. isolated from different nematode species, and on the basis of the DNA-DNA hybridization by Boemare *et al.* in 1993 the new separate genus *Photorhabdus* was introduced for bacteria associated with nematodes of the genus *Heterorhabditis*.[15]

Today, *Xenorhabdus* and *Photorhabdus* are classified into the family of Enterobacteriaceae in the γ-subclass of Proteobacteria.

The life cycle of the entomopathogenic nematodes *Steinernema* and *Heterorhabditis*

The life cycle of the entomopathogenic nematodes *Steinernema* and *Heterorhabditis* is subdivided into the so-called larvae stages. The infective juvenile (IJ) represents the only stage of the nematode outside of their insect host, while carrying the bacteria in the gut. At this stage the nematode is a non-feeding and soil-dwelling larvae, encased in a double cuticle with closed mouth and anus, and able to survive for long-terms in the soil.[60] IJs of the family Heterorhabditiae use the so-called cruiser strategy to search actively in the soil for suitable insect larvae. Nematodes of the family Steinernematidae, adopted the ambusher strategy, waiting passively near the soil surface for prey to cross their way.[83] After an insect is sensed, the nematode sheds its outer cuticle to uncover mouth and anus, enters the insect through natural openings like anus, mouth and spiracles and migrates to the insect blood cavity.[157] In comparison to *Steinernema*, *Heterorhabditis* is able to penetrate directly through the thin intersegmental areas of the insect integument by using a dorsal tooth.[83] The bacteria of *Xenorhabdus* spp. are located in a part of the intestine, the so-called receptacle but not in a vesicle as it was described until 2007.[86] The bacteria are then released through defecation triggered by ingestion of the hemolymph.[157;161] Colonization of the nematode occurs at the distal portion of the receptacle (Rd), but newer studies evidence that the receptacle is open at the proximal end (Rp) by a stretched tube-like connection leading to the esophago-intestinal junction (EIJ) (Figure 1).

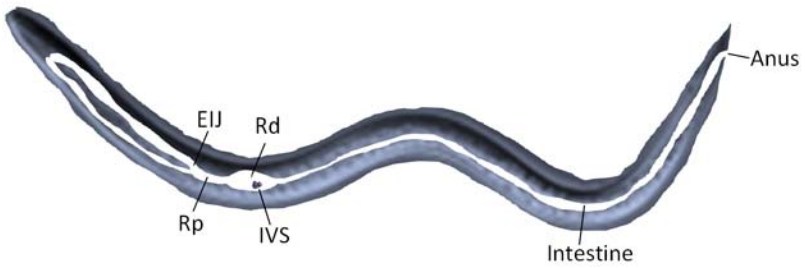

Figure 1. *Steinernema* nematode and their bacterial receptacle. *Xenorhabdus* bacteria colonize in a portion of the intestine, termed receptacle. Bacteria adhere to a cluster of spheres (intravesicular structure, IVS) in the distal receptacle end (Rd). During defecation, the bacteria are pumped through an opening and a narrow passage into the intestinal lumen towards the anus. Esophago-intestinal junction (EIJ), proximal receptacle (Rp) (the nematode is adapted from Herbert & Goodrich-Blair[70] and was modified for this figure).

After 2 h of hemolymph exposure, a 2 - 3 h enduring pulsatile movement forces the receptacle distal end to open up and the bacteria abandon the distal portion through a narrow passage into the intestinal lumen and subsequently through the anus out of the nematode. The area of the esophago-intestinal junction might be used to balance the pulsatile movement as some bacteria can be observed in this region during movement.[161]

Nematode and bacteria overcome the insect immune system and the host insect is killed within 48 h post-infection as it is described in more detail for *X. nematophila* and *S. carpocapsae* in the following paragraph. The insect cadaver is then digested by the bacteria and the nematodes undergo a complex life cycle (Figure 2).

The first stage after entering the insect is the so-called recovery phase (J3, see Figure 2). Triggered by a unknown food signal, the nematodes exit the infective stage in a developmental step that is known as recovery and transform into the fourth stage (J4) causing a toxicogenesis by releasing an immunosupressive factor that inhibits antimicrobial peptides produced by the insect.[13] J4 stages nematodes develop into egg lying female or male adults in the insect cadaver and hereby run through four juvenile stages (J1 - J4) and the adult stage up to three generations. After reproduction and depletion of all nutrients, a high nematode population density triggers the nematode development into IJs again.[136] In the case of *Steinernema*, IJs become colonized by bacteria via one or two founder bacterial cells. Finally, dependent on the size of the insect prey up to several hundred thousand individuals emerge from the empty carcass.[60]

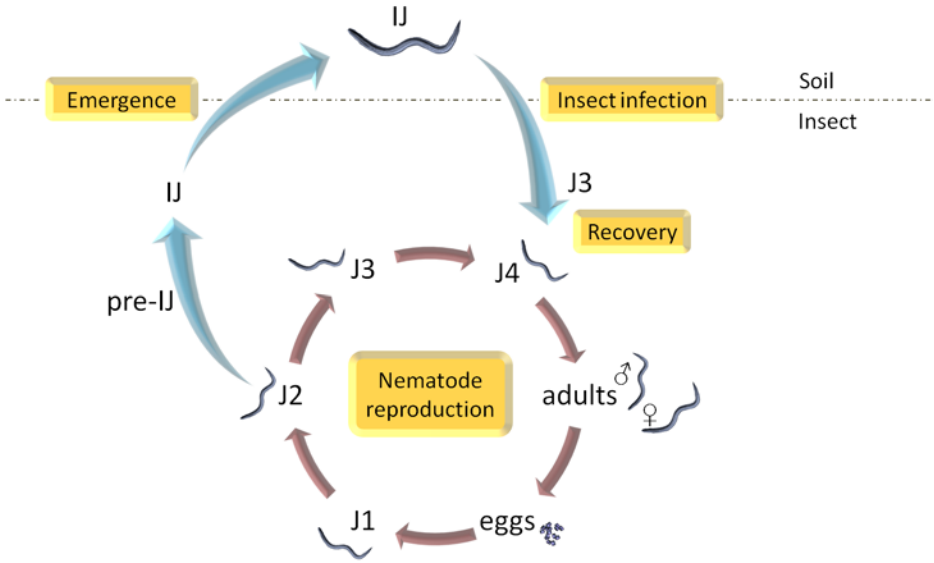

Figure 2. The *Steinernema* life cycle. The infective juvenile (IJ) nematodes infect a suitable insect host and develop into the fourth stage juvenile (J4), a developmental step that is known as recovery. During reproduction nematodes undergo four juvenile stages. Depletion of all nutrients leads to the development into IJs again and the nematodes leaf the empty carcass (the nematodes are adapted from Herbert & Goodrich-Blair[70] and were modified for this figure).

Nematodes of the genus *Heterorhabditis* undergo an alternative way of reproduction: in the first generation, IJs turn into self-fertile egg laying hermaphrodites and only in the next generations male, female and additional hermaphrodites are born. IJs are developed exclusively via intrauterine hatching and matricide.[28]

Colonization of *Steinernema* infective juveniles occurs as mentioned before by one or two founder bacterial cells in the anterior intestinal lumen, called receptacle. *S. carpocapsae* receptacle includes the two anterior intestinal cells, where the founder cells multiply to fill the space until a maximum bacterial cell density is achieved and adhere to a nematode derived cluster of spheres (intravesicular structure, IVS) surrounded by a glycan-containing mucous material (Figure 1).[101;102] In contrary to *S. carpocapsae*, where the bacteria are loosely packed within the receptacle, in *S. jollieti*, associated with *X. bovienii*, the bacterial cells are packed tightly together with IVS within a vesicle in the receptacle, a small bag with a cellophane-like envelope, to protect the cells.[170] Receptacle morphology can be grouped into five clades based on absence or presence of a vesicle within the receptacle, the quantity of clusters of spheres and of the characteristics like the size of the receptacle.[86]

Genus *Xenorhabdus*

Up to date, twenty-four highly diverse *Xenorhabdus* species are described: *X. nematophila,*[181] *X. beddingii, X. bovienii, X. poinarii,*[1] *X. japonica,*[113] *X. budapestensis, X. ehlersii, X. innexi, X. szentirmaii,*[94] *X¨indica,*[162] *X. cabanillasii, X. doucetiae, X. griffiniae, X. hominickii, X. koppenhoeferi, X. kozodoii, X. mauleonii, X. miraniensis, X. romanii, X. stockiae,*[175] *X. vietnamensis,*[173] *X. magdalenensis,*[174] *X. ishibashii*[90] and *X. khoisanae*.[44]

Xenorhabdus cells are mesophilic, Gram-negative, asporogenous, rod shaped and peritrichous flagellated with a size of 0.3 - 2 µm. In the last third of the exponential growth, spheroplasts with an average diameter of 2.6 µm can appear. Proteinaceous crystalline inclusion bodies can occur in the stationary phase and swarming of cells on soft agar can be observed. *Xenorhabdus* strains are DNAse and protease positive.[13] Additionally, they are catalase negative and are unable to reduce nitrate delineating them from other genera in the family of Enterobacteriacea.[42] Conformation of the affiliation to the family of Enterobacteriacea is predicated on phylogenetic analysis based on 16S rDNA[22] and the presence of the enterobacterial common antigen,[139] although there is only a 4 % DNA/DNA relatedness with *Escherichia coli* determined.[42]

Xenorhabdus features the capability to respond to environmental changes by changing its physical and physiological form, called phase variation.[51] Bacteria of phase I, also called primary form, occurs in the L3 stage (IJ) of the nematode life cycle.[14] In primary form, cells comprise the ability to produce secondary metabolites, to absorb dyes like bromothymol blue and to produce

proteases, lipases and phospholipases. Furthermore, primary form variants are motile and exhibit the capability to constitute protoplasmic paracrystalline inclusions. A switch to phase II variants appears spontaneously in stationary phase under *in vitro* cultivation conditions or during nematode cultivation on an artificial diet (reviewed in[50]). Adaption like the phase switching might be one mechanism for bacterial pathogens to circumvent host defense mechanisms[145] or facilitate survival outside the symbiotic niche.[51;160]

Detailed studies for the understanding of the regulation system in the tripartial mutualism-pathogenesis relationship between the bacteria, the nematode and the infected host have shown that microbial mutualism and pathogenesis in *Xenorhabdus*[30] share common molecular features for microbial adaptation to hosts and regulation between mutualism and pathogenesis like it is known from other bacteria.[67] The next section will focus on some issues of these relationships using the example of *Xenorhabdus nematophila* and *Steinernema carpocapsae*.

The mutualistic association of *X. nematophila* and *S. carpocapsae* is not mandatory, survival without each other could be observed for both genera under lab conditions.[70]

The initiation for pathogenicity of nematode-bacteria mutualism is controlled by compounds of the hemolymph of the infected insect. Exposure of the nematode to the insect gut triggers the loss of the outer cuticle and migration into the insect blood system.[157] A nutrient upshift between the nematode vesicle lumen and the hemolymph causing the release of the bacteria, suggesting a compound of the hemolymph as the release-triggering signal.[70] Mutants of *Xenorhabdus*, defective in oligopeptide transport resulted in a decreased cell growth and confirmed the hypothesis for oligopeptides as nutrient signals.[119] Furthermore, studies of the global regulator Lrp (leucine responsive regulatory protein) indicated an essential regulation for adaptation from nutrient limited to nutrient rich conditions.[30]

Survival of the bacteria within the host and in order to overcome the immune system is dependent on the properties of the cell surface.[157] Interactions with the hemocytes of the host blood system are mediated by surface proteins and structures with a binding capacity and adhesions like OpaB. OpaB describes an Ail (attachment and invasion locus)-family outer membrane protein.[125] Virulence factors like the Lrp-dependent type I fimbriae MrxA interact with their pilin subunit with the insect and are responsible for pore forming in the target cell membranes.[6] Lipopolysaccharides (LPS) are toxic to the insect hemocytes.[65] The bleb off from bacterial outer membrane vesicle and therefore the production of toxic virulence effectors might be also triggered by oligopeptides of the hemolymph.[70] Furthermore, some secondary metabolites are produced to manipulate the insect immunity. The highly active benzylideneacetone, acetylated phenylalanine-glycine-valine and cyclo-proline-tyrosine peptides as well as indoles inhibit the activation of aggregation and hemocyte nodulation in the insect hemolymph (described more in detail in the secondary metabolites section).[87;154;163]

Xenorhabdus causes insect death after 48 h by secreting multiple compounds playing a role in virulence like the Tc (toxin complex, $XptA_2B_1C_1$), the Txp40 toxin[124] and the C1 cytotoxin (XaxAB) with necrotic and apoptotic activities towards the target cells, other proteins like lipases that are secreted through the flagellar export apparatus (XlpA),[144] proteases (PrtA) and the C1 hemolysin (XaxAB) help to degrade the insect biomass. Tc toxins and the C1 cytotoxin (in *X. nematophila*: α-xenorhabdolysin) are widely spread among bacteria and could be also found in *Yersinia* spp. and *Pseudomonas* spp. and display an apoptotic and hemolytic activity.[155;184] The Tc toxin complex is composed of three class A, B and C toxin proteins, which occur in a 4:1:1 stoichiometry to each other. The class A protein plays a role in solubilizing the insect by roughening the outer membranes and inducing pore formation.[156] Class A toxin is classified into three classes: I, II and III, each showing different oral toxicities towards diverse Lepidoptera species.[26] Class B and C toxins modulate and enhance the toxicity and additionally class C, an ADP-ribosyltransferases, targets the actin cytoskeleton of the host cells.[92;156] Interestingly, the genome of *X. nematophila* encodes seven class A, three class B and three class C subunit genes referring to a broad spectra of targeting different insects.[26] A single Tc locus, that is conserved among sequenced *Photorhabdus* and *Xenorhabdus* strains, encodes two class A subunits and is flanked by genes encoding a chitinase, which can synergize insecticidal toxins by allowing the toxins access to the epithelial target cells due to digesting chitin, the major compound of insect peritropic matrixes and barrier between gut lumen and hemocoel.[26;121;191]

The genes *xlpA*, *prtA* and *xaxAB* encoding a lipase, a protease and the C1 hemolysin, respectively, responsible for converting the insect biomass into small molecules, are regulated by the FlhDC regulon, which is repressed by the OmpR/EnvZ system. Furthermore, the OmpR/EnvZ two-component system takes part in the pathogenesis as it also represses the production of some secondary metabolites.[123] Alongside, *Xenorhabdus* have to compete against several food competitors such as other insect gut microbes living in the gut of the insect or invading from the soil. Elimination of these competitors is warranted by the production of bacteriocins like xenorhabdicin, a phage tail-like bacteriocin[178] or the endoribonuclease xenocin belonging to the E3-type colicins,[159] toxin complexes[46] and secondary metabolites.[51]

As nematode and bacteria share common nutrients from the death insect, the bacteria are reducing their population size in periodical intervals to release nutrients from the death bacterial cells.[70;101] Furthermore, the intracellular inclusion PixA might be responsible for the benefit of the nematode host as PixA deficient mutants showed no attenuation in virulence and did not exhibit an effect in nematode colonization, but might serve as a protein depot.[59;70]

Studies of the global regulator Lrp shed some light on the connection between mutualism and pathogenesis and their complex regulation system. As described before, Lrp plays an important role in regulation of nematode colonization, as well as in the pathogenesis by regulating the expression of the transcriptional regulator *lrhA* (LysR homologue A). LrhA deficient mutants showed a drastic decrease

in the capability to kill insects, indicating LrhA as one of the key controlling virulence factors.[70;144] Furthermore, the signal transduction system CpxRA, a sensor histidine kinase-phosphatase complex, is involved in mutualistic and pathogenic functions. CpxRA negatively regulates the production of hemolysins, proteases and the expression of MrxA. Additionally, it positively influences the capability of motility and thereby the colonization of the nematodes in the initiation and outgrowth stages.[68;69]

Genus *Photorhabdus*

Currently, the genus *Photorhabdus* includes only three species, which might have emerged simultaneously from one ancestor. All species including further subclades noted as $C_{P\text{-}I}$, $C_{P\text{-}II}$ and $C_{P\text{-}III}$:[173] *P. luminescens* subsp. *luminescens*, *P. luminescens* subsp. *akhurstii*, *P. luminescens* subsp. *laumondii*,[49] *P. luminescens* subsp. *kayaii*,[64] *P. luminescens* subsp. *caribbeanensis*, *P. luminescens* subsp. *hainanensis*,[173] *P. luminescens* subsp. *noenieputensis*[45] ($C_{P\text{-}I}$); *P. temperata* subsp. *temperata*,[49] *P. temperata* subsp. *cinerea*,[182] *P. temperata* subsp. *khanii*, *P. temperata* subsp. *tasmaniensis*, *P. temperata* subsp. *thracensis*[64;173] ($C_{P\text{-}II}$), and as $C_{P\text{-}III}$ *P. asymbiotica* subsp. *asymbiotica*,[49] *P. asymbiotica* subsp. *australis*.[2]

All *Photorhabdus* species were isolated from infected insects or their nematode hosts, except *P. asymbiotica*, which was isolated from human wounds and identified as a human pathogen strain and not associated with nematodes.[43;129] Indeed, the bacteria disseminates bacteremic infections caused by an invasion of soft tissues, in 2006 the associated nematode symbiont was identified in Kingscliff, New South Wales, Australia.[56] Interestingly, *P. asymbiotica* infection could be actively reproduced in a human host without an insect vector, unlike of the facultative human pathogen *Wolbachia* and its associated nematode of the genus *Onchocerca volvulus*.[56;177] Furthermore, phenotypic analysis of the human pathogenic strains and the isolates from the identified Kingscliff nematode revealed differences in the production of proteases and lipases required for symbiosis and the production of stilbenes and siderophores necessary for nematode growth and development.[79;80;134] However, the role of the nematode during infection and the change of the phenotypic behavior between human pathogen and insect pathogen is still elusive.[191]

Unlike *Xenorhabdus*, *Photorhabdus* cells are catalase positive[13] and phase switch from primary to secondary form is irreversible.[57;187] A striking feature of all *Photorhabdus* species is their ability for bioluminescence.[180] Additionally, *Photorhabdus* represents the only known non-marine luminous bacterium. Sequence similarity and arrangement of the bioluminescence responsible *lux* genes alluded to a horizontal gene transfer between the marine bacteria of the genus *Vibrio* and *Photobacterium* and *Photorhabdus*.[172]

Secondary metabolites of *Xenorhabdus* and *Photorhabdus*

Until now, several classes of structurally diverse secondary metabolites with a broad spectrum including insecticidal, antifungal, antibacterial, nematicidal and cytotoxic activities are isolated and/or known from different *Xenorhabdus* and *Photorhabdus* strains. The sequencing of the genomes of several *Xenorhabdus* and *Photorhabdus* strains facilitated the search for new compound classes. Detailed genome studies revealed a large number of biosynthesis gene clusters responsible for the production of secondary metabolites. For example, in *Xenorhabdus nematophila* ATCC 19061 7.5 % and in *Photorhabdus luminescens* TT01 5.9 % of the genome encode for proteins involved in secondary metabolism.[26;40] In contrast to Streptomycetes, which encode less than 5 % for secondary metabolites (e.g. *S. coelicolor* 4.5 %).[8]

The majority of the already identified compounds comprise secondary metabolites produced by different *Xenorhabdus* strains and are shown in Figure 3 and 4.

Indole derivatives (Figure 4), isolated from *X. nematophila* and *X. bovienii,* confer antibacterial activity against several Gram-positive and Gram-negative bacteria causing a serious inhibition of RNA synthesis by inducing the accumulation of guanosine-3',5'-bis-pyrophosphate and show additional activity on fungi of medical and agricultural importance.[95;171] Recently, Seo *et al.* were successful in identifying two small indole derivatives, indole and oxindole from *X. nematophila*, also known from some *Penicillium* spp., which exhibit weak phospholipase A_2 (PLA_2) inhibitory effects (Figure 4).[154] Furthermore, the proline-tyrosine (PY) dipeptide and *p*-hydroxyphenyl propionic acid (PHPP) show the same weak inhibitory effects (Figure 3).[154;163]

Nematophin, besides activities against bacteria and fungi, displays a high activity against clinically relevant drug-resistant strains of *Staphylococcus aureus* (Figure 4).[97;98]

Phenethylamides isolated from *X. nematophila* and *X. doucetiae* show significant cytotoxicity against human cancer cell lines, such as gastric adenocarcinoma or hepatoblastoma by inducing apoptosis of carcinoma cells through a caspase activation (Figure 4).[77;120] In 2011 Proschak *et al.* identified and elucidated from *X. doucetiae* the structures of 21 phenethylamide derivatives and five additional tryptamide derivatives differing in their acyl chain length. The differences of the derivatives are based on the acyl chain that either consist straight-chain fatty acids, iso-fatty acids or desaturated fatty acids. The newly identified derivatives exhibit a stronger cytotoxic activity as observed for the previously isolated *N*-phenethyl-2-phenylacetamide. Moreover, some derivatives showed an activity against insect hemocytes.[137]

Another structural compound class is represented by the xenorhabdins and xenorxides, members of the pyrrothine class antibiotics (Figure 4). Xenorhabdins, isolated from *X. nematophila* and *X. bovienii,* but also xenorxides produced by *X. bovienii* displayed antibacterial, antifungal and insecticidal activity.[96;104]

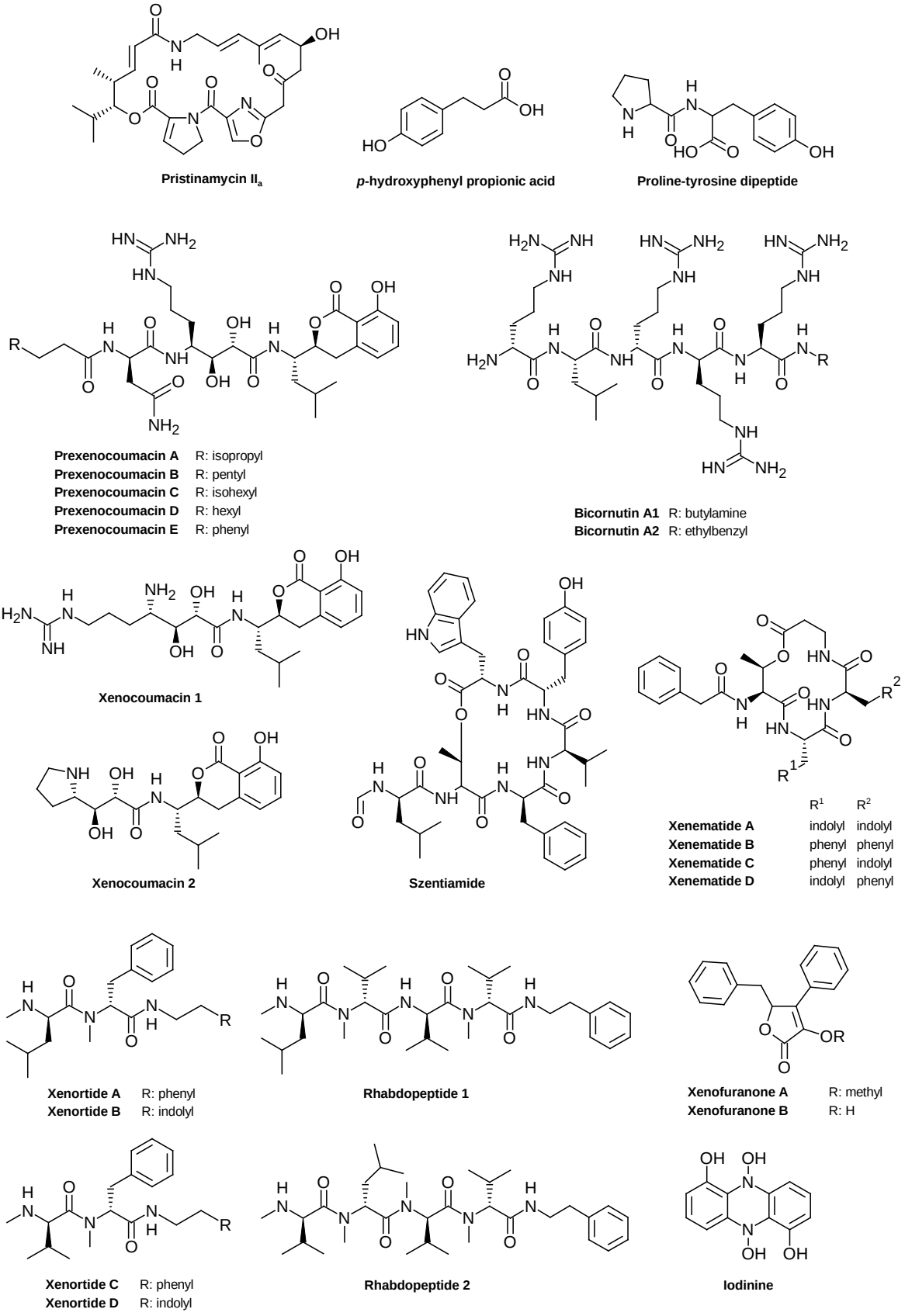

Figure 3. Secondary metabolites of different *Xenorhabdus* strains.

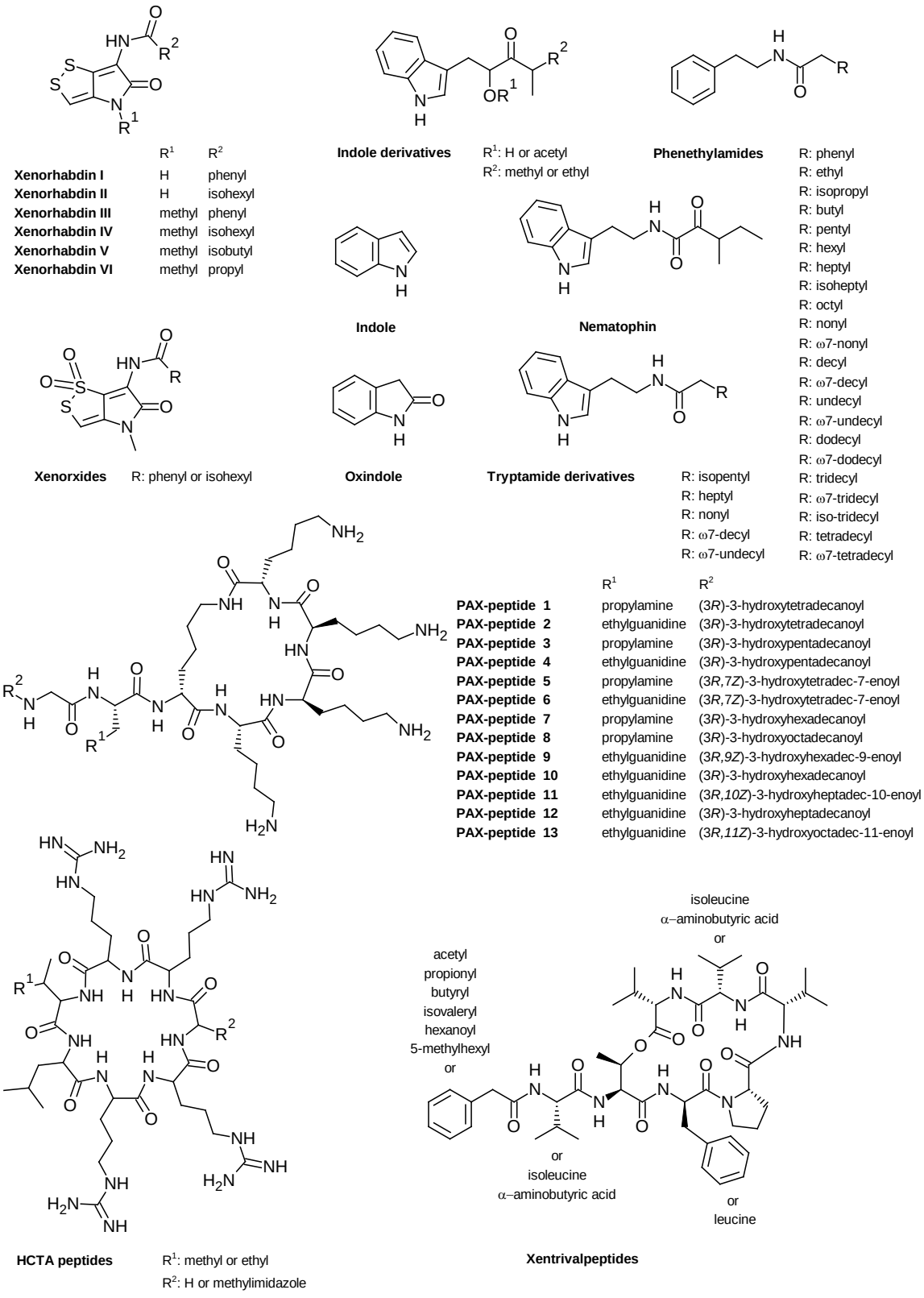

Figure 4. Further secondary metabolites of different *Xenorhabdus* strains.

A phenotypic peculiar characteristic of *Xenorhabdus szentirmaii* is its purple metallic color originated from the known phenazine pigment iodinin (Figure 3).[11] However, the major compound

class produced by *X. szentirmaii* are xenofuranones showing similarities to fungal furanones of *Aspergillus terreus*[107] (Figure 3). Xenofuranones confer a weak cytotoxic activity.[11;17] Furthermore, szentiamide (Figure 3), an *N*-formylated cyclic depsipeptide was isolated, showing activity against the malaria-causing parasite *Plasmodium falciparum*.[114;115]

To all appearances, the compound class of nonribosomally produced secondary metabolites might be the major class produced in *Xenorhabdus* spp. Depsipeptides like xenematides of *X. nematophila* are antibacterial against Gram-positive and -negative bacteria, moreover they display a moderate insecticidal activity, too (Figure 3). Xenematide biosynthesis is strongly upregulated under cultivation conditions with excess of L-proline.[33;35;93] Furthermore, linear peptides like PATA-peptides (Zhou, Q., Grundmann, F., unpublished) or gargantuanine (Kegler, C., unpublished), as well as the cyclic tetrapeptide (Bode, H.B., unpublished), the lipodepsipeptides taxlllaids (Kronenwerth, M., unpublished) and xentrivalpeptides[198] could be isolated from different *Xenorhabdus* strains and their structure elucidated. The lysine-rich cyclo PAX-peptides of *X. nematophila* confer antifungal and antibacterial activity (Figure 4).[53;62] Two linear hexapeptides (bicornutin, Figure 3) were identified from *X. budapestensis* with activity against the plant pathogens *Erwinia amylovora* and *Phytophthora nicotianae*[16;54] and four arginine-rich cyclic peptides named HCTA-peptides from *X. miraniensis* and *Xenorhabdus* sp. XPB 63.3 with an unknown function (Figure 4).[54] Xenortides[35;93] (Figure 3) as well as rhabdopeptides[141] (Figure 3) represent a class of *N*-methylated peptides containing a *C*-terminal amide and will be discussed in more detail in chapter 5 and the concluding remarks.

The major class of compounds in *X. nematophila* xenocoumacins exhibit a broad antibacterial activity against Gram-positive bacteria and overall possess an antiulcer activity (Figure 3). Furthermore, xenocoumacin 1 has an antifungal activity.[105] The biosynthesis of xenocoumacin via a hybrid polyketide synthase (PKS)/nonribosomal peptide synthetase (NRPS) multienzyme complex and its regulation were investigated in detail and will be discussed in chapter 1 – 3, revealing an interesting drug activation mechanism, which is widespread among different bacteria taxa.[122;142;143]

Another compound produced in *X. nematophila* by a hybrid PKS/NRPS is pristinamycin II_a, until recently only known from *Streptomcyes* strains (Figure 3).[20] Pristinamycin also known as virginiamycin M, is used with its associated branched cyclic hexadepsipeptide virginiamycin S as a synergistic two-compound streptagramin antibiotic, is a clinically applied drug for the treatment of infections caused by multidrug-resistant pathogens.[108;138]

Benzylidenacetone (BZA) from *X. nematophila* and *Photorhabdus temperata* exhibits an antibacterial activity against plant-pathogenic Gram-negative bacteria such as *Agrobacterium vitis* and *Pectobacterium carotovorum*[78] (Figure 5). Of great importance was the identification of BZA as a key player in the pathogenesis of the bacteria-nematode complex. BZA affects the insect immunosupression by acting as an inhibitor of the phospholipase A_2 (PLA_2). Inhibition of the phospholipase A_2, a key enzyme in the eicosanoid pathway, prevents the biosynthesis of prostaglandins and leukotrienes, which mediate the nonself recognition of insect signals against

pathogens and therefore suppresses the immune response.[87;126;154] Additional PAL_2 inhibitors were identified in both species, like the cis-cyclo-proline-tyrosine (cis-cyclo-PY) dipeptide and the acetylated phenylalanine-glycine-valine (Ac-FGV) tripeptide (Figure 5).[154;163]

Rhabduscin, an isocyanide- and aminoglycosyl-functionalized tyrosine derivative is produced by *X. nematophila* and *Photorhabdus luminescens* and its aglycone is known from the human pathogen *Vibrio cholera* (Figure 5).[21;36] Rhabduscin is localized at or near the periphery of the bacterial cell wall and serves as an inhibitor of the phenoloxidase, which takes an important part in the melanization pathway of the insect's immune system.[33;36]

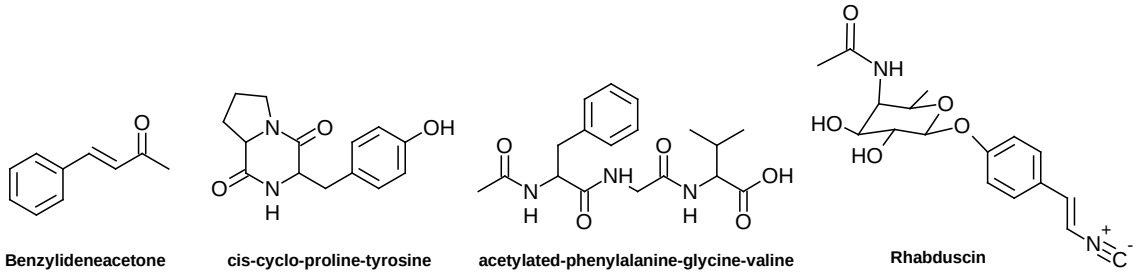

Figure 5. Secondary metabolites of different *Xenorhabdus* and *Photorhabdus* strains.

Up to now, in *P. luminsecens* a gene cluster for a carbapenem-backbone could be identified and analyzed (Figure 6).[39] The β-lactam antibiotics of the carbapenem group are known from other organisms like *Streptomyces* and the Gram-negative *Erwinia* and *Serratia* species.[127;192] In *Photorhabdus*, the genes are expressed during exponential phase growth, but not controlled by quorum sensing (QS) as it is described for *Erwinia* and *Serratia* due the lack of the QS protein CarR.[39]

Photobactin, a catechol siderophore produced in *P. luminescens* is related to the siderophores vibriobactin and agrobactin and may contribute in the antibiosis by sequestering iron in the insect cadaver (Figure 6).[27]

Photorhabdus asymbiotica harbors a biosynthesis gene cluster with high similarity to the gene cluster of yersiniabactin, and ulbactin E, a short yersiniabactin derivative known from a marine *Altermonas* strain could be identified in the strain (Figure 6).[188]

Anthraquinones are widespread in nature and normally produced by plants. In *P. luminescens*, as only Gram-negative bacterial producer, this compound class is deduced from a type II polyketide synthase (Figure 6). Their mode of action is still unknown but the anthraquinones might act as an ant-deterrent factor.[18;81]

Recently, *P. luminescens* was described as a producer of the blue pigment indigoidine, which is also known from *Erwinia chrysanthemi* (Figure 6). In wild type strains the biosynthesis gene cluster is silent and production could only be observed in promoter exchange experiments or heterologous expression in *E. coli*.[19]

Stilbenes are well known common plant metabolites but were also identified in all *Photorhabdus* strains (Figure 6). Isopropylstilbene and ethylstilbene possess antimicrobial activity and are crucial in virulence and mutualism as food signals in the nematode recovery process.[79;81] Epoxystilbene exhibits antibacterial activity, in particular against drug-resistant *Staphylococcus aureus*, and moreover indicates cytotoxicity against three human cancer cell lines.[74] Further stilbene derivatives were identified recently, like dihydroisopropylstilbene, which mediates protection against oxidative stress in the insect hemolymph.[34;88]

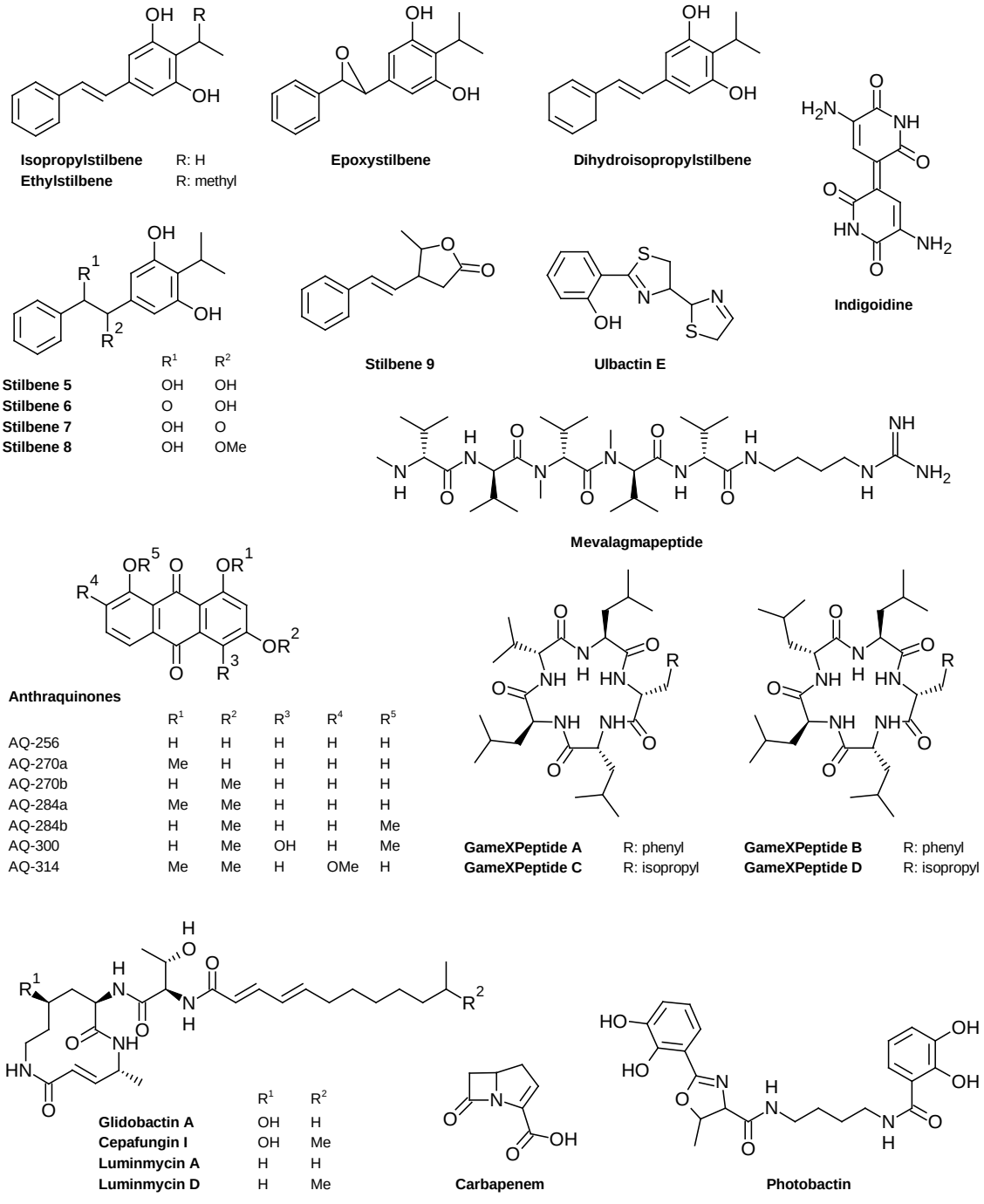

Figure 6. Secondary metabolites of different *Photorhabdus* strains.

Some nonribosomally produced peptides such as the cyclic GameXPeptides and the linear mevalagmapeptide from *P. luminescens* could be identified (Figure 6). Although, these compounds are only produced in traces, the group of Bode *et al.* succeeded in the elucidation of these compounds by exploiting genomic analysis and isotopic feeding experiments.[12] Aspects of the biosynthesis and structure elucidation will be the topic of chapter 4.

The NRPS derived glidobactins confer a broad antifungal activity and revealed cytotoxicity against tumor cell lines (Figure 6).[116-118] Glidobactins were first isolated from *Polyangium brachysporum*.[116] In 2007, Schellenberg *et al.* identified a possible biosynthesis gene cluster for the glidobactins in *P. luminescens*[149] and some of the potent proteasome inhibitor derivatives, named luminmycin and glidobactin could be isolated from *P. luminescens* and *P. asymbiotica* or heterologously expressed in *E. coli*, recently.[9;52;168;179]

Nonribosomal peptide synthetases and polyketide synthases

Many secondary metabolites with biologically interesting activities are produced by multienzyme thiotemplate mechanisms like nonribosomal peptide synthetases (NRPS) and the fatty acid synthase (FAS)-related polyketide synthases (PKS) or by a hybrid biosynthesis thereof. They use peptide bond formation and Claisen-type condensation reactions, respectively, to build larger molecules from small building blocks.

NRPSs employ large multienzyme complexes for peptide bond formation, which are organized in defined sections on protein level, termed module and domain. A module is a well-defined unit responsible for the incorporation of one specific amino acid or building block into the growing polypeptide chain.[100] Each module consists of distinct domains. Domains are highly conserved catalytically units, which catalyze the steps required for the recognition and activation of the substrates, covalent binding of the building blocks, peptide bond formation and elongation of the peptide intermediate but also for the modification and release of the final product. Domains can be analyzed and identified by their highly conserved “core-motifs” representing structural important residues for their catalytic activity.[89;158]

Modules can be subdivided into their role in the biosynthesis process such as initiation or elongation. A minimal elongation module consists of an adenylation domain, a peptidyl carrier protein and a condensation domain. These domains are required for the elongation of a single building block. Essential domains can be accompanied by tailoring enzymes responsible for modifications like methylation or epimerization. In contrast, a minimal initiation module functions without a condensation domain. However, special starter condensation domains responsible for the incorporation of fatty acids can be present.[140] NRPS assembly lines can be classified into three types: type A,

a directional synthesis called colinearity, type B, an iterative usage of some modules and type C, a non-linear usage, which includes the incorporation of small building blocks not covalently bound to the NRPS template using stand-alone domains.[106]

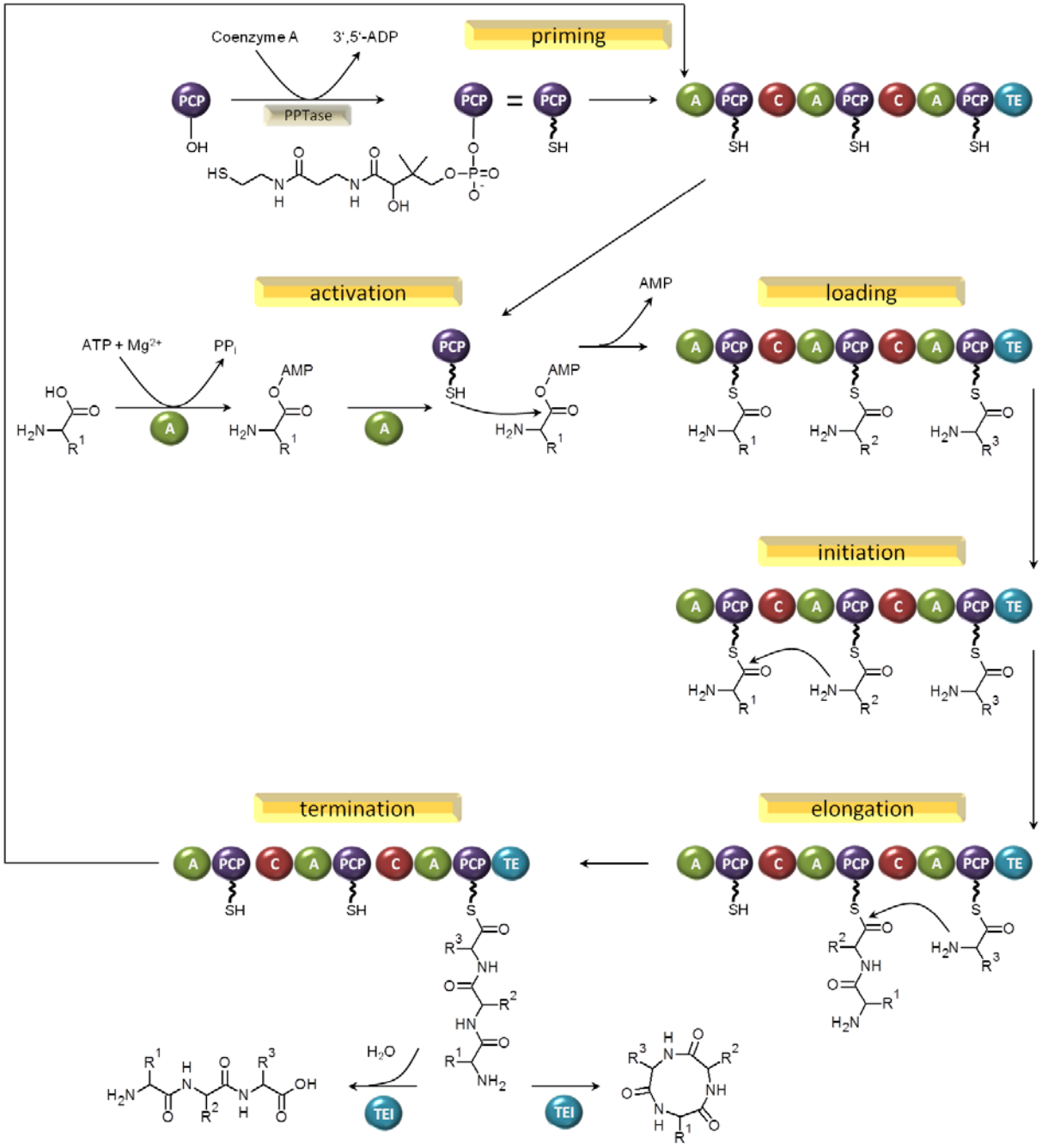

Figure 7. The nonribosomal peptide synthetic pathway. The amino acids are recognized and activated by the A domain and transferred onto the free thiolgroup of the 4'-phosphopantetheinyl residue covalently bound to the PCP. The C domain catalyzes the condensation of the peptide intermediates mediating a nucleophilic attack of the amino group of the downstream bound amino acid onto the acyl group of the upstream bound amino thioester. The release of the final product is realized by a TE domain. A: adenylation domain, PCP: peptidyl carrier protein, C: condensation domain, TE: thioesterase domain, PPTase: phosphopantetheinyl transferase.

Indispensable steps of the nonribosomal peptide biosynthetic mechanism are highlighted in Figure 7. The adenylation (A) domain is responsible for the recognition and activation of a specific amino acid. Due to sequence analysis, the A domain is classified into the superfamily of the adenylate forming enzymes and exhibit a large *N*-terminal and a small *C*-terminal subdomain. The activation of the substrate takes place in a two-step chemical reaction. In the first step, the selected amino acid is activated at the carboxy group by forming an aminoacyl adenylate intermediate by hydrolysis of adenosine-5'-triphosphate (ATP) and the release of pyrophosphate (PP_i). In the second step, the amino acid-*O*-AMP oxoester is transferred by a nucleophilic attack onto the free thiolgroup of the peptidyl carrier protein (PCP) 4'-phosphopantetheinyl cofactor to form a thioester.[158;164]

The four-helix bundle fold PCP domain, also referred to as thiolation (T) domain, is located downstream of the A domain and acts as a transporter to pass the activated and covalently bound aminoacyl adenylate intermediate between the different catalytic centers.[158;189] The activation or priming of the inactive apo-PCP domain is catalyzed by a 4'-phosphopantheinyl transferase (PPTase), which posttranslationally and covalently transfers a phosphopantetheinly group of coenzyme A to a highly conserved serine residue of the carrier protein resulting in the active *holo*-PCP.[91] Although, thiolation domains do not possess a high sequence similarity to each other, the core motif with the invariant serine residue and the second helix in the bundle resemble indispensable elements for the functionality of the PCP. The elongation and formation of peptide bonds between the amino acyl substrates is catalyzed by the condensation (C) domain, which mediates a nucleophilic attack of the free α-amino group of the downstream carrier protein bound amino acid onto the acyl group of the upstream bound amino thioester.[7] Condensation domains exhibit a V-shape like conformation with an acceptor site for the nucleophile at one subdomain and a donor site for the electrophile at the other subdomain allowing PCPs to dock their substrates.[84;146] Furthermore, C domains possess a selectivity for the acceptor substrate.[84] Subsequently, the growing peptide is passed from one to the next downstream located module until the last PCP domain is reached. A type I thioesterase (TEI) domain catalyzes the release of the final product by a peptide internal nucleophilic attack or the hydrolysis of water resulting in a macrocylic or linear product.[23;158] Type II thioesterases (TEII) are stand-alone proteins acting in *trans* and are responsible for removing short acyl chains from the 4'-phosphopantetheinyl groups or the release of misprimed substrates.[153;195]

The diversity of nonribosomally produced peptides can be increased by further modifications catalyzed by editing domains. Most commonly distributed are epimerization (E) domains or dual condensation-epimerization (C/E) domains, which are responsible for the conversion of L- into D-amino acids.[84;165] Furthermore, oxazoline or thiazoline rings are formed by cyclization (Cy) domains, which catalyze the addition of the thiol and hydroxyl side chain of cysteine or serine and threonine to the upstream amide carbonyl followed by dehydration, respectively.[84] Oxidation (Ox) and reduction (R) domains affect the oxidation state of the building blocks.[151] Methylation of amino acids is catalyzed by *N*- and *C*-methyltransferases (*N*-MT, *C*-MT) using *S*-adenosylmethionine (SAM) as

methyl donor, which is translocated to the amino or carbonyl group of the thioesterified amino acid.[3;148]

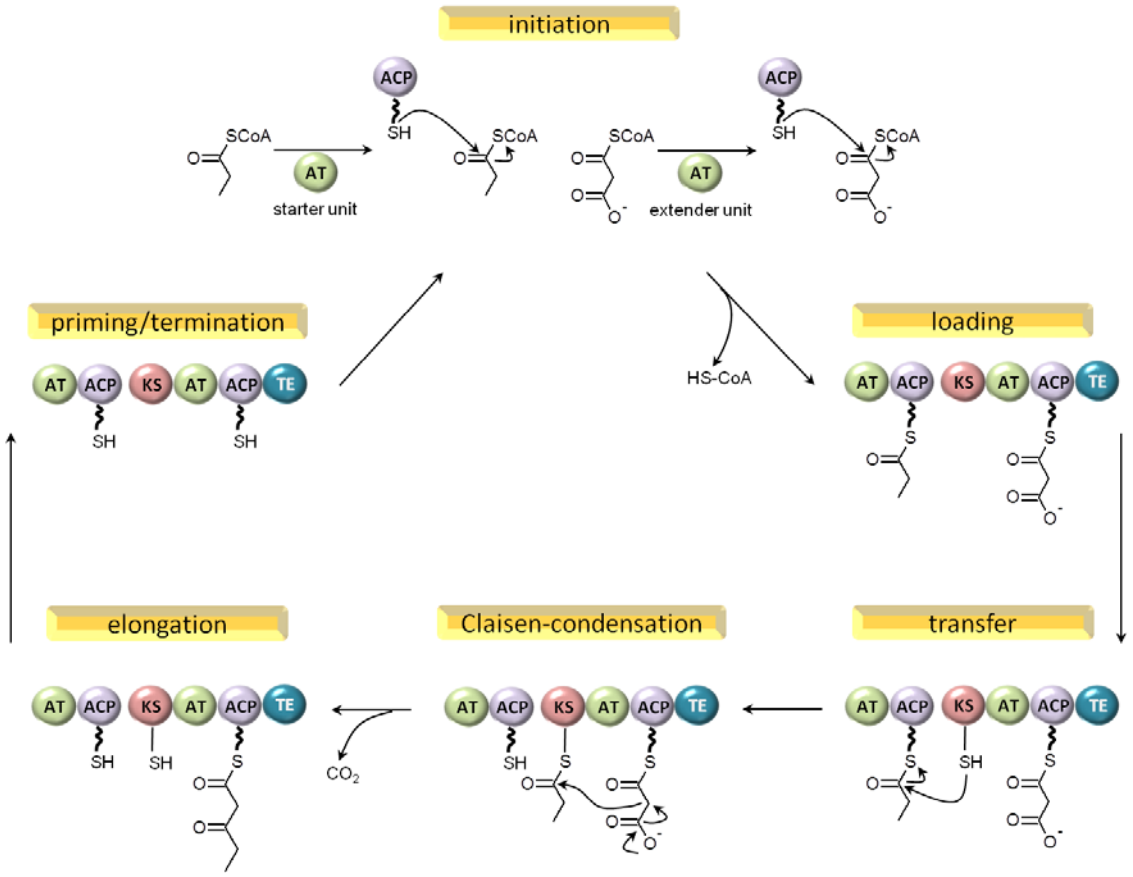

Figure 8. The type I polyketide synthetic pathway representing a minimal module of AT, ACP and KS domains. The AT domains catalyzes the selection of the starter- and extender units and the translocation of them onto the thiol group of the 4'-phosphopantetheinyl of the ACP domain. The ACP bound intermediate of the upstream located module is transferred to the KS domain catalyzing the Claisen-condensation resulting in an extended ACP-bound bound β-ketoacyl intermediate. ACP priming and product release by the TE domain takes place at it is described for NRPS. AT: acyltransferase domain, ACP: acyl carrier protein, KS: ketosynthase domain, TE: thioesterase domain.

Polyketide natural products are synthesized by PKSs similar to the closely related biosynthesis of fatty acids by FASs. A striking feature of PKS is their ability for optional reductive modifications of the β-ketoacyl derivative to theoretically enable an enormous structural diversity.[99;167]

On the basis of their assembly line organization, bacterial PKSs have been classified into three categories. Type I PKS consists of multifunctional enzymes and is organized in modules and domains incorporating single extender units as already explained for NRPS. Polyketides are synthesized following the colinearity rule.[166] The mechanism of type I PKS will be discussed in more detail in the next section. Type II PKS are dissociable monofunctional and discrete enzymes, which are used

iteratively. The minimal PKS consists of two ketosynthase units (KS_α and KS_β) and an acyl carrier protein (ACP). The nascent poly-β-keto intermediate is defined by additional ketoreductases (KR), cyclases (CYC) and aromatases (ARO).[72] Type III PKS comprises multifunctional enzymes of the chalcone and stilbene synthase family. Using CoA-linked substrates instead of ACP bound derivatives, the complete biosynthesis is guided by a single active site catalyzing condensation, extension, cyclization and aromatization reactions resulting in typical mono- and bicyclic aromatic compounds.[4;167]

The type I PKS minimal module harbors an acyltransferase (AT) domain, an ACP domain and a ketosynthase (KS) domain. In addition, a variable set of domains involved in the constitution of the redox state of the β-keto position can be present: ketoreductase (KR), dehydratase (DH) and enoyl reductase (ER).[73]

Selection of starter units (e.g. propionyl- or acetyl-CoA) and malonyl- or methylmalonyl-CoA as extender units is catalyzed by an AT domain transferring the C_2, C_3 or C_4 acyl group to the thiol group of the 4'-phosphopantetheinyl of the ACP domain.[38;63;167] The ACP domain is activated in the same way as the PCP. Apart from the predominantly used malonyl- and methylmalonyl building blocks, a variety of other extender units such as hydroxymalonate, aminomalonate, 2-ethylmalonate and methoxymalonate can be incorporated.[24;25] The polyketide intermediate of the upstream located module is transferred to a highly conserved cysteine residue in the active site of the KS domain, which catalyzes the condensation by decarboxylating and mediating a nucleophilic attack of the upstream KS-bound acyl thioester resulting in a two carbon extended ACP-bound β-ketoacyl intermediate (Figure 8).[48] Further modifications are catalyzed by the KR domain reducing the β-ketoacyl group to a β-hydroxyacyl group in a stereospecific and NADPH dependent step. The DH domain dehydrates the β-hydroxyacyl into an α,β-enoyl intermediate, which can be further reduced by the ER domain into a fully saturated α,β-acyl group using NADPH (Figure 9). The complete "reductive loop" is not mandatory and contributes to the PKS diversity as already mentioned before.[167;176] The reduced or unreduced ACP-bound intermediate is passed to the following KS for another chain elongation step. Finally, the release of the full length acyl chain is catalyzed by a TE as described for NRPS.[167]

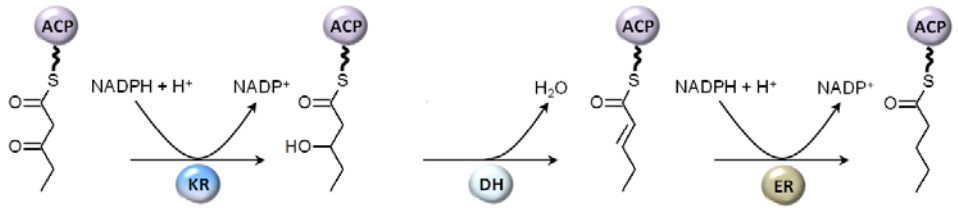

Figure 9. The optional β-carbon "reductive loop" catalyzed by the KR, DH and ER domains. The KR domain reduces the β-ketoacyl group to a β-hydroxyacyl group, which is subsequently dehydrated by the DH domain into an α,β-enoyl intermediate and further reduced by the ER domain into an α,β-acyl group. KR: ketoreductase domain, DH: dehydratase domain, ER: enoyl reductase domain.

Interestingly, besides the mentioned canonical *cis*-AT, integrated in a module, many bacteria reveal another PKS system with a freestanding *trans*-AT. Phylogenetic analysis of *cis*- and *trans*-AT revealed a different and independent evolution of both systems from FAS-like systems. The *cis*-AT might be evolved by gene duplication of individual modules, whereas *trans*-AT might be developed by horizontal gene transfer.[133] Based on this analysis, KS of *trans*-AT clusters could be classified according to their substrate specificity into 16 different clades, e.g. α-methylated olefinic thioesters, nonbranched saturated intermediates or D-configurated hydroxyl substrates.[112;132]

The structural diversity already enabling an unlimited number of natural products is further expanded by PKS/NRPS hybrids and the fact that NRPS are not limited on proteinogenic amino acids like in ribosomal biosynthesis.[47] Moreover, a coupling between the primary and the secondary metabolism is possible like in the case of the tRNA-dependent aminoacyltransferase catalyzing a transfer of aminoacyl on the NRPS assembly line.[197] Additionally, postsynthetical modifications such as glycosylation[75] and halogenations could take place.[186]

Reference list

1. **Akhurst, R. J. and N. E. Boemare**. 1988. A numerical taxonomic study of the genus *Xenorhabdus* (Enterobacteriaceae) and proposed elevation of the subspecies of *X. nematophilus* to species. J. Gen. Microbiol. 134:1835-1845.

2. **Akhurst, R. J., N. E. Boemare, P. H. Janssen, M. M. Peel, D. A. Alfredson, and C. E. Beard**. 2004. Taxonomy of Australian clinical isolates of the genus *Photorhabdus* and proposal of *Photorhabdus asymbiotica* subsp. *asymbiotica* subsp. nov. and *P. asymbiotica* subsp. *australis* subsp. nov. Int. J. Syst. Evol. Microbiol. 54:1301-1310.

3. **Ansari, M. Z., J. Sharma, R. S. Gokhale, and D. Mohanty**. 2008. In silico analysis of methyltransferase domains involved in biosynthesis of secondary metabolites. BMC Bioinf. 9:454.

4. **Austin, M. B. and J. P. Noel**. 2003. The chalcone synthase superfamily of type III polyketide synthases. Nat. Prod. Rep. 20:79-110.

5. **Baker, D. D., M. Chu, U. Oza, and V. Rajgarhia**. 2007. The value of natural products to future pharmaceutical discovery. Nat. Prod. Rep. 24:1225-1244.

6. **Banerjee, J., J. Singh, M. C. Joshi, S. Ghosh, and N. Banerjee**. 2006. The cytotoxic fimbrial structural subunit of *Xenorhabdus nematophila* is a pore-forming toxin. J. Bacteriol. 188:7957-7962.

7. **Belshaw, P. J., C. T. Walsh, and T. Stachelhaus**. 1999. Aminoacyl-CoAs as probes of condensation domain selectivity in nonribosomal peptide synthesis. Science 284:486-489.

8. **Bentley, S. D., K. F. Chater, A. M. Cerdeno-Tarraga, G. L. Challis, N. R. Thomson, K. D. James, D. E. Harris, M. A. Quail, H. Kieser, D. Harper, A. Bateman, S. Brown, G. Chandra, C. W. Chen, M. Collins, A. Cronin, A. Fraser, A. Goble, J. Hidalgo, T. Hornsby, S. Howarth, C. H. Huang, T. Kieser, L. Larke, L. Murphy, K. Oliver, S. O'Neil, E. Rabbinowitsch, M. A. Rajandream, K. Rutherford, S. Rutter, K. Seeger, D. Saunders, S. Sharp, R. Squares, S. Squares, K. Taylor, T. Warren, A. Wietzorrek, J. Woodward, B. G. Barrell, J. Parkhill, and D. A. Hopwood**. 2002. Complete genome sequence of the model actinomycete *Streptomyces coelicolor* A3(2). Nature 417:141-147.

9. **Bian, X., A. Plaza, Y. Zhang, and R. Müller**. 2012. Luminmycins A-C, Cryptic Natural Products from *Photorhabdus luminescens* Identified by Heterologous Expression in *Escherichia coli*. J. Nat. Prod. 75:1652-1655.

10. **Bladergroen, M. R. and H. P. Spaink**. 1998. Genes and signal molecules involved in the rhizobia-leguminoseae symbiosis. Curr. Opin. Plant Biol. 1:353-359.

11. **Bode, H. B.** 2009. Entomopathogenic bacteria as a source of secondary metabolites. Curr. Opin. Chem. Biol. 13:224-230.

12. **Bode, H. B., D. Reimer, S. W. Fuchs, F. Kirchner, C. Dauth, C. Kegler, W. Lorenzen, A. O. Brachmann, and P. Grün**. 2012. Determination of the absolute configuration of peptide natural products by using stable isotope labeling and mass spectrometry. Chem. Eur. J. 18:2342-2348.

13. **Boemare, N. and R. J. Akhurst**. 2006. Genera *Photorhabdus* and *Xenorhabdus*. Prokaryotes 6:451-494.

14. **Boemare, N. E. and R. J. Akhurst**. 1988. Biochemical and physiological characterization of colony form variants in *Xenorhabdus* spp. (Enterobacteriaceae). J. Gen. Microbiol. 134:751-761.

15. **Boemare, N. E., R. J. Akhurst, and R. G. Mourant**. 1993. DNA relatedness between *Xenorhabdus* spp. (Enterobacteriaceae), symbiotic bacteria of entomopathogenic nematodes, and a proposal to transfer *Xenorhabdus luminescen*s to a new genus, *Photorhabdus gen. nov.* Int. J. Syst. Bacteriol. 43:249-255.

16. **Boszormenyi, E., T. Ersek, A. Fodor, A. M. Fodor, L. S. Foldes, M. Hevesi, J. S. Hogan, Z. Katona, M. G. Klein, A. Kormany, S. Pekar, A. Szentirmai, F. Sztaricskai, and R. A. J. Taylor**. 2009. Isolation and activity of *Xenorhabdus* antimicrobial compounds against the plant pathogens *Erwinia amylovora* and *Phytophthora nicotianae*. J. Appl. Microbiol. 107:746-759.

17. **Brachmann, A. O., S. Forst, G. M. Furgani, A. Fodor, and H. B. Bode**. 2006. Xenofuranones A and B: phenylpyruvate dimers from *Xenorhabdus szentirmaii*. J. Nat. Prod. 69:1830-1832.

18. **Brachmann, A. O., S. A. Joyce, H. Jenke-Kodama, G. Schwär, D. J. Clarke, and H. B. Bode**. 2007. A type II polyketide synthase is responsible for anthraquinone biosynthesis in *Photorhabdus luminescens*. ChemBioChem 8:1721-1728.

19. **Brachmann, A. O., F. Kirchner, C. Kegler, S. C. Kinski, I. Schmitt, and H. B. Bode**. 2012. Triggering the production of the cryptic blue pigment indigoidine from *Photorhabdus luminescens*. J. Biotechnol. 157:96-99.

20. **Brachmann, A. O., D. Reimer, W. Lorenzen, A. E. Augusto, Y. Kopp, J. Piel, and H. B. Bode**. 2012. Reciprocal cross talk between fatty acid and antibiotic biosynthesis in a nematode symbiont. Angew. Chem. Int. Ed. 51:12086-12089.

21. **Brady, S. F., J. D. Bauer, M. F. Clarke-Pearson, and R. Daniels**. 2007. Natural products from *isnA*-containing biosynthetic gene clusters recovered from the genomes of cultured and uncultured bacteria. J. Am. Chem. Soc. 129:12102.

22. **Brunel, B., A. Givaudan, A. Lanois, R. J. Akhurst, and N. Boemare**. 1997. Fast and accurate identification of *Xenorhabdus* and *Photorhabdus* species by restriction analysis of PCR-amplified 16S rRNA genes. Appl. Environ. Microbiol. 63:574-580.

23. **Bruner, S. D., T. Weber, R. M. Kohli, D. Schwarzer, M. A. Marahiel, C. T. Walsh, and M. T. Stubbs**. 2002. Structural basis for the cyclization of the lipopeptide antibiotic surfactin by the thioesterase domain SrfTE. Structure 10:301-310.

24. **Chan, Y. A., M. T. Boyne, A. M. Podevels, A. K. Klimowicz, J. Handelsman, N. L. Kelleher, and M. G. Thomas**. 2006. Hydroxymalonyl-acyl carrier protein (ACP) and aminomalonyl-ACP are two additional type I polyketide synthase extender units. Proc. Natl. Acad. Sci. 103:14349-14354.

25. **Chan, Y. A., A. M. Podevels, B. M. Kevany, and M. G. Thomas**. 2009. Biosynthesis of polyketide synthase extender units. Nat. Prod. Rep. 26:90-114.

26. **Chaston, J. M., G. Suen, S. L. Tucker, A. W. Andersen, A. Bhasin, E. Bode, H. B. Bode, A. O. Brachmann, C. E. Cowles, K. N. Cowles, C. Darby, L. de Leon, K. Drace, Z. J. Du, A. Givaudan, E. E. H. Tran, K. A. Jewell, J. J. Knack, K. C. Krasomil-Osterfeld, R. Kukor, A. Lanois, P. Latreille, N. K. Leimgruber, C. M. Lipke, R. Y. Liu, X. J. Lu, E. C. Martens, P. R. Marri, C. Medigue, M. L. Menard, N. M. Miller, N. Morales-Soto, S. Norton, J. C. Ogier, S. S. Orchard, D. Park, Y. Park, B. A. Qurollo, D. R. Sugar, G. R.**

Richards, Z. Rouy, B. Slominski, K. Slominski, H. Snyder, B. C. Tjaden, R. van der Hoeven, R. D. Welch, C. Wheeler, B. S. Xiang, B. Barbazuk, S. Gaudriault, B. Goodner, S. C. Slater, S. Forst, B. S. Goldman, and H. Goodrich-Blair. 2011. The Entomopathogenic Bacterial Endosymbionts *Xenorhabdus* and *Photorhabdus*: Convergent Lifestyles from Divergent Genomes. PLoS ONE 6:e27909.

27. **Ciche, T. A., M. Blackburn, J. R. Carney, and J. C. Ensign**. 2003. Photobactin: a catechol siderophore produced by *Photorhabdus luminescens*, an entomopathogen mutually associated with *Heterorhabditis bacteriophora* NC1 nematodes. Appl. Environ. Microbiol. 69:4706-4713.

28. **Ciche, T. A., K. S. Kim, B. Kaufmann-Daszczuk, K. C. Q. Nguyen, and D. H. Hall**. 2008. Cell invasion and matricide during *Photorhabdus luminescens* transmission by *Heterorhabditis bacteriophora* nematodes. Appl. Environ. Microbiol. 74:2275-2287.

29. **Cordell, G. A. and M. D. Colvard**. 2012. Natural products and traditional medicine: turning on a paradigm. J. Nat. Prod. 75:514-525.

30. **Cowles, K. N., C. E. Cowles, G. R. Richards, E. C. Martens, and H. Goodrich-Blair**. 2007. The global regulator Lrp contributes to mutualism, pathogenesis and phenotypic variation in the bacterium *Xenorhabdus nematophila*. Cell. Microbiol. 9:1311-1323.

31. **Cragg, G. M. and D. J. Newman**. 2001. Medicinals for the millennia: The historical record. Ann. N. Y. Acad. Sci. 953:3-25.

32. **Crawford, J. M. and J. Clardy**. 2011. Bacterial symbionts and natural products. Chem. Commun. 47:7559-7566.

33. **Crawford, J. M., R. Kontnik, and J. Clardy**. 2010. Regulating alternative lifestyles in entomopathogenic bacteria. Curr. Biol. 20:69-74.

34. **Crawford, J. M., S. A. Mahlstedt, S. J. Malcolmson, J. Clardy, and C. T. Walsh**. 2011. Dihydrophenylalanine: a prephenate-derived *Photorhabdus luminescens* antibiotic and intermediate in dihydrostilbene biosynthesis. Chem. Biol. 18:1102-1112.

35. **Crawford, J. M., C. Portmann, R. Kontnik, C. T. Walsh, and J. Clardy**. 2011. NRPS substrate promiscuity diversifies the xenematides. Org. Lett. 13:5144-5147.

36. **Crawford, J. M., C. Portmann, X. Zhang, M. B. Roeffaers, and J. Clardy**. 2012. Small molecule perimeter defense in entomopathogenic bacteria. Proc. Natl. Acad. Sci. 109:10821-10826.

37. **Dantas, G., M. O. A. Sommer, R. D. Oluwasegun, and G. M. Church**. 2008. Bacteria subsisting on antibiotics. Science 320:100-103.

38. **Del Vecchio, F., H. Petkovic, S. G. Kendrew, L. Low, B. Wilkinson, R. Lill, J. Cortes, B. A. Rudd, J. Staunton, and P. F. Leadlay**. 2003. Active-site residue, domain and module swaps in modular polyketide synthases. J. Ind. Microbiol. Biotechnol. 30:489-494.

39. **Derzelle, S., E. Duchaud, F. Kunst, A. Danchin, and P. Bertin**. 2002. Identification, characterization, and regulation of a cluster of genes involved in carbapenem biosynthesis in *Photorhabdus luminescens*. Appl. Environ. Microbiol. 68:3780-3789.

40. **Duchaud, E., C. Rusniok, L. Frangeul, C. Buchrieser, A. Givaudan, S. Taourit, S. Bocs, C. Boursaux-Eude, M. Chandler, J. F. Charles, E. Dassa, R. Derose, S. Derzelle, G. Freyssinet, S. Gaudriault, C. Medigue, A. Lanois, K. Powell, P. Siguier, R. Vincent, V. Wingate, M. Zouine, P. Glaser, N. Boemare, A. Danchin, and F. Kunst**. 2003. The genome

sequence of the entomopathogenic bacterium *Photorhabdus luminescens*. Nat. Biotechnol. 21:1307-1313.

41. **Ehlers, R. U.** 2001. Mass production of entomopathogenic nematodes for plant protection. Appl. Microbiol. Biotechnol. 56:623-633.

42. **Farmer, J. J.** 1984. Other genera of the family Enterobacteriaceae, p. 506-516. *In* N. N. Krieg and J. G. Holt (eds.), Bergey's Manual of systematic Bacteriology, Williams & Williams. Baltimore, MD.

43. **Farmer, J. J., III, J. H. Jorgensen, P. A. Grimont, R. J. Akhurst, G. O. Poinar, Jr., E. Ageron, G. V. Pierce, J. A. Smith, G. P. Carter, and K. L. Wilson**. 1989. *Xenorhabdus luminescens* (DNA hybridization group 5) from human clinical specimens. J. Clin. Microbiol. 27:1594-1600.

44. **Ferreira, T., C. A. van Reenen, A. Endo, C. Sproer, A. P. Malan, and L. M. Dicks**. 2013. Description of *Xenorhabdus khoisanae* sp. nov., the symbiont of the entomopathogenic nematode *Steinernema khoisanae*. Int. J. Syst. Evol. Microbiol. in press, http://dx.doi.org/10.1099/ijs.0.049049-0

45. **Ferreira, T., C. A. van Reenen, S. Pages, P. Tailliez, A. P. Malan, and L. M. Dicks**. 2012. Description of *Photorhabdus luminescens* subsp. *noenieputensis* subsp. nov., a symbiotic bacterium associated with a new *Heterorhabditis* species related to *Heterorhabditis indica*. Int. J. Syst. Evol. Microbiol. in press, http://dx.doi.org/10.1099/ijs.0.044388-0

46. **ffrench-Constant, R. and N. Waterfield**. 2006. An ABC guide to the bacterial toxin complexes. Adv. Appl. Microbiol. 58:169-183.

47. **Finking, R. and M. A. Marahiel**. 2004. Biosynthesis of nonribosomal peptides. Annu. Rev. Microbiol. 58:453-488.

48. **Fischbach, M. A. and C. T. Walsh**. 2006. Assembly-line enzymology for polyketide and nonribosomal peptide antibiotics: logic, machinery, and mechanisms. Chem. Rev. 106:3468-3496.

49. **Fischer-Le Saux, M., V. Viallard, B. Brunel, P. Normand, and N. E. Boemare**. 1999. Polyphasic classification of the genus *Photorhabdus* and proposal of new taxa: *P. luminescens* subsp. *luminescens* subsp. nov., *P. luminescens* subsp. *akhurstii* subsp. nov., *P. luminescens* subsp. *laumondii* subsp. nov., *P. temperata* sp. nov., *P. temperata* subsp. *temperata* subsp. nov. and *P. asymbiotica* sp. nov. Int. J. Syst. Bacteriol. 49 Pt 4:1645-1656.

50. **Forst, S., B. Dowds, N. E. Boemare, and E. Stackebrandt**. 1997. *Xenorhabdus* and *Photorhabdus* spp.: Bugs that kill bugs. Annu. Rev. Microbiol. 51:47-72.

51. **Forst, S. and K. Nealson**. 1996. Molecular biology of the symbiotic-pathogenic bacteria *Xenorhabdus* spp. and *Photorhabdus* spp. Microbiol. Rev. 60:21-43.

52. **Fu, J., X. Bian, S. Hu, H. Wang, F. Huang, P. M. Seibert, A. Plaza, L. Xia, R. Müller, A. F. Stewart, and Y. Zhang**. 2012. Full-length RecE enhances linear-linear homologous recombination and facilitates direct cloning for bioprospecting. Nat. Biotechnol. 30:440-446.

53. **Fuchs, S. W., A. Proschak, T. W. Jaskolla, M. Karas, and H. B. Bode**. 2011. Structure elucidation and biosynthesis of lysine-rich cyclic peptides in *Xenorhabdus nematophila*. Org. Biomol. Chem. 9:3130-3132.

54. **Fuchs, S. W., C. C. Sachs, C. Kegler, F. I. Nollmann, M. Karas, and H. B. Bode**. 2012. Neutral loss fragmentation pattern based screening for arginine-rich natural products in *Xenorhabdus* and *Photorhabdus*. Anal. Chem. 84:6948-6955.

55. **Gebhardt, K., J. Schimana, P. Krastel, K. Dettner, J. Rheinheimer, A. Zeeck, and H. P. Fiedler**. 2002. Endophenazines A-D, new phenazine antibiotics from the arthropod associated endosymbiont *Streptomyces anulatus*. I. Taxonomy, fermentation, isolation and biological activities. J. Antibiot. 55:794-800.

56. **Gerrard, J. G., S. A. Joyce, D. J. Clarke, R. H. ffrench-Constant, G. R. Nimmo, D. F. Looke, E. J. Feil, L. Pearce, and N. R. Waterfield**. 2006. Nematode symbiont for *Photorhabdus asymbiotica*. Emerg. Infect. Dis. 12:1562-1564.

57. **Gerritsen, L. J., R. G. de, and P. H. Smits**. 1992. Characterization of form variants of *Xenorhabdus luminescens.* Appl. Environ. Microbiol. 58:1975-1979.

58. **Glaser, R. W. and H. Fox**. 1930. A nematode parasite of the Japanese beetle (*Popillia Japonica* Newm.). Science 71:16-17.

59. **Goetsch, M., H. Owen, B. Goldman, and S. Forst**. 2006. Analysis of the PixA inclusion body protein of *Xenorhabdus nematophila*. J. Bacteriol. 188:2706-2710.

60. **Goodrich-Blair, H.** 2007. They've got a ticket to ride: *Xenorhabdus nematophila-Steinernema carpocapsae* symbiosis. Curr. Opin. Microbiol. 10:225-230.

61. **Goodrich-Blair, H. and D. J. Clarke**. 2007. Mutualism and pathogenesis in *Xenorhabdus* and *Photorhabdus*: two roads to the same destination. Mol. Microbiol. 64:260-268.

62. **Gualtieri, M., A. Aumelas, and J. O. Thaler**. 2009. Identification of a new antimicrobial lysine-rich cyclolipopeptide family from *Xenorhabdus nematophila*. J. Antibiot. 62:295-302.

63. **Haydock, S. F., J. F. Aparicio, I. Molnar, T. Schwecke, A. König, A. F. A. Marsden, I. S. Galloway, J. Staunton, and P. F. Leadley**. 1995. Divergent structural motifs correlated with the substrate specificity of (methyl)malonyl-CoA:acylcarrier protein transacylase domains in the modular polyketide synthases. FEBS Lett. 374:246-248.

64. **Hazir, S., E. Stackebrandtz, E. Lang, P. Schumann, R. U. Ehlers, and N. Keskin**. 2004. Two new subspecies of *Photorhabdus luminescens*, Isolated from *Heterorhabditis bacteriophora* (Nematoda : Heterorhabditidae): *Photorhabdus luminescens* subsp *kayaii* subsp nov and *Photorhabdus luminescens* subsp *thracensis* subsp nov. Syst. Appl. Microbiol. 27:36-42.

65. **He, H., H. A. Snyder, and S. Forst**. 2004. Unique organization and regulation of the mrx fimbrial operon in *Xenorhabdus nematophila*. Microbiology 150:1439-1446.

66. **Hendrie, M. S., A. J. Holding, and J. M. Shewan**. 1974. Emended descriptions of genus alcaligenes and of *Alcaligenes faecalis* and proposal that generic name *Achromobacter* be rejected - status of named species of *Alcaligenes* and *Achromobacter* - request for an opinion. Int. J. Syst. Bacteriol. 24:534-550.

67. **Hentschel, U., M. Steinert, and J. Hacker**. 2000. Common molecular mechanisms of symbiosis and pathogenesis. Trends Microbiol. 8:226-231.

68. **Herbert Tran, E. E., A. W. Andersen, and H. Goodrich-Blair**. 2009. CpxRA influences *Xenorhabdus nematophila* colonization initiation and outgrowth in *Steinernema carpocapsae* nematodes through regulation of the *nil* locus. Appl. Environ. Microbiol. 75:4007-4014.

69. **Herbert, E. E., K. N. Cowles, and H. Goodrich-Blair**. 2007. CpxRA regulates mutualism and pathogenesis in *Xenorhabdus nematophila*. Appl. Environ. Microbiol. 73:7826-7836.

70. **Herbert, E. E. and H. Goodrich-Blair**. 2007. Friend and foe: the two faces of *Xenorhabdus nematophila*. Nat. Rev. Microbiol. 5:634-646.

71. **Hertweck, C.** 2009. Hidden biosynthetic treasures brought to light. Nat. Chem. Biol. 5:450-452.

72. **Hertweck, C., A. Luzhetskyy, Y. Rebets, and A. Bechthold**. 2007. Type II polyketide synthases: gaining a deeper insight into enzymatic teamwork. Nat. Prod. Rep. 24:162-190.

73. **Hopwood, D. A.** 1997. Genetic contributions to understanding polyketide synthases. Chem. Rev. 97:2465-2497.

74. **Hu, K. J., J. X. Li, B. Li, J. M. Webster, and G. H. Chen**. 2006. A novel antimicrobial epoxide isolated from larval *Galleria mellonella* infected by the nematode symbiont, *Photorhabdus luminescens* (Enterobacteriaceae). Bioorg. Med. Chem. 14:4677-4681.

75. **Hubbard, B. K. and C. T. Walsh**. 2003. Vancomycin assembly: nature's way. Angew. Chem. Int. Ed. 42:730-765.

76. **Huneck, S.** 1999. The significance of lichens and their metabolites. Naturwissenschaften 86:559-570.

77. **Hwang, S. Y., S. Paik, S. H. Park, H. S. Kim, I. S. Lee, S. P. Kim, W. K. Baek, M. H. Suh, T. K. Kwon, J. W. Park, J. B. Park, J. J. Lee, and S. I. Suh**. 2003. N-phenethyl-2-phenylacetamide isolated from *Xenorhabdus nematophilus* induces apoptosis through caspase activation and calpain-mediated Bax cleavage in U937 cells. Int. J. Oncol. 22:151-157.

78. **Ji, D., Y. Yi, G. H. Kang, Y. H. Choi, P. Kim, N. I. Baek, and Y. Kim**. 2004. Identification of an antibacterial compound, benzylideneacetone, from *Xenorhabdus nematophila* against major plant-pathogenic bacteria. FEMS Microbiol. Lett. 239:241-248.

79. **Joyce, S. A., A. O. Brachmann, I. Glazer, L. Lango, G. Schwär, D. J. Clarke, and H. B. Bode**. 2008. Bacterial biosynthesis of a multipotent stilbene. Angew. Chem. Int. Ed. 47:1942-1945.

80. **Joyce, S. A. and D. J. Clarke**. 2003. A *hexA* homologue from *Photorhabdus* regulates pathogenicity, symbiosis and phenotypic variation. Mol. Microbiol. 47:1445-1457.

81. **Joyce, S. A., L. Lango, and D. J. Clarke**. 2011. The regulation of secondary metabolism and mutualism in the insect pathogenic bacterium *Photorhabdus luminescens*. Adv. Appl. Microbiol 76:1-25.

82. **Kaeberlein, T., K. Lewis, and S. S. Epstein**. 2002. Isolating "uncultivable" microorganisms in pure culture in a simulated natural environment. Science 296:1127-1129.

83. **Kaya, H. K. and R. Gaugler**. 1993. Entomopathogenic nematodes. Annu. Rev. Entomol. 38:181-206.

84. **Keating, T. A., C. G. Marshall, C. T. Walsh, and A. E. Keating**. 2002. The structure of VibH represents nonribosomal peptide synthetase condensation, cyclization and epimerization domains. Nat. Struct. Biol. 9:522-526.

85. **Kersten, R. D., Y. L. Yang, Y. Q. Xu, P. Cimermancic, S. J. Nam, W. Fenical, M. A. Fischbach, B. S. Moore, and P. C. Dorrestein**. 2011. A mass spectrometry-guided genome mining approach for natural product peptidogenomics. Nat. Chem. Biol. 7:794-802.

86. **Kim, S. K., Y. Flores-Lara, and Stock S.P.** 2012. Morphology and ultrastructure of the bacterial receptacle in *Steinernema* nematodes (Nematoda: Steinernematidae). J. Invertebr. Pathol. 110:366-374.

87. **Kim, Y., D. Ji, S. Cho, and Y. Park**. 2005. Two groups of entomopathogenic bacteria, *Photorhabdus* and *Xenorhabdus*, share an inhibitory action against phospholipase A2 to induce host immunodepression. J. Invertebr. Pathol. 89:258-264.

88. **Kontnik, R., J. M. Crawford, and J. Clardy**. 2010. Exploiting a global regulator for small molecule discovery in *Photorhabdus luminescens*. ACS Chem. Biol. 5:659-665.

89. **Konz, D. and M. A. Marahiel**. 1999. How do peptide synthetases generate structural diversity? Chem. Biol. 6:R39-R48.

90. **Kuwata, R., L. H. Qiu, W. Wang, Y. Harada, M. Yoshida, E. Kondo, and T. Yoshiga**. 2012. *Xenorhabdus ishibashii* sp. nov., a bacterium from the entomopathogenic nematode *Steinernema aciari*. Int. J. Syst. Evol. Microbiol. in press, http://dx.doi.org/10.1099/ijs.0.041145-0

91. **Lambalot, R. H., A. M. Gehring, R. S. Flugel, P. Zuber, M. LaCelle, M. A. Marahiel, R. Reid, C. Khosla, and C. T. Walsh**. 1996. A new enzyme superfamily - the phosphopantetheinyl transferases. Chem. Biol. 3:923-936.

92. **Lang, A. E., G. Schmidt, A. Schlosser, T. D. Hey, I. M. Larrinua, J. J. Sheets, H. G. Mannherz, and K. Aktories**. 2010. *Photorhabdus luminescens* Toxins ADP-Ribosylate Actin and RhoA to Force Actin Clustering. Science 327:1139-1142.

93. **Lang, G., T. Kalvelage, A. Peters, J. Wiese, and J. F. Imhoff**. 2008. Linear and cyclic peptides from the entomopathogenic Bacterium *Xenorhabdus nematophilus*. J. Nat. Prod. 71:1074-1077.

94. **Lengyel, K., E. Lang, A. Fodor, E. Szallas, P. Schumann, and E. Stackebrandt**. 2005. Description of four novel species of *Xenorhabdus*, family Enterobacteriaceae: *Xenorhabdus budapestensis* sp. nov., *Xenorhabdus ehlersii* sp. nov., *Xenorhabdus innexi* sp. nov., and *Xenorhabdus szentirmaii* sp. nov. Syst. Appl. Microbiol. 28:115-122.

95. **Li, J., G. Chen, J. M. Webster, and E. Czyzewska**. 1995. Antimicrobial metabolites from a bacterial symbiont. J. Nat. Prod. 58:1081-1086.

96. **Li, J., K. Hu, and J. M. Webster**. 1998. Antibiotics from *Xenorhabdus* spp. and *Photorhabdus* spp. (Enterobacterialceae). Chem. Hereocycl. Compd. 34:1331-1339.

97. **Li, J. X., G. H. Chen, and J. M. Webster**. 1997. Nematophin, a novel antimicrobial substance produced by *Xenorhabdus nematophilus* (Enterobactereaceae). Can. J. Microbiol. 43:770-773.

98. **Li, J. X., G. H. Chen, and J. M. Webster**. 1997. Synthesis and antistaphylococcal activity of nematophin and its analogs. Bioorg. Med. Chem. Lett. 7:1349-1352.

99. **Malpartida, F. and D. A. Hopwood**. 1984. Molecular cloning of the whole biosynthetic pathway of a *Streptomyces* antibiotic and its expression in a heterologous host. Nature 309:462.

100. **Marahiel, M. A., T. Stachelhaus, and H. D. Mootz**. 1997. Modular peptide synthetases involved in nonribosomal peptide synthesis. Chem. Rev. 97:2651-2674.

101. **Martens, E. C., K. Heungens, and H. Goodrich-Blair**. 2003. Early colonization events in the mutualistic association between *Steinernema carpocapsae* nematodes and *Xenorhabdus nematophila* bacteria. J. Bacteriol. 185:3147-3154.

102. **Martens, E. C., F. M. Russell, and H. Goodrich-Blair**. 2005. Analysis of *Xenorhabdus nematophila* metabolic mutants yields insight into stages of *Steinernema carpocapsae* nematode intestinal colonization. Mol. Microbiol. 58:28-45.

103. **Matthijs, S., G. Laus, J. M. Meyer, K. Abbaspour-Tehrani, M. Schafer, H. Budzikiewicz, and P. Cornelis**. 2009. Siderophore-mediated iron acquisition in the entomopathogenic bacterium *Pseudomonas entomophila* L48 and its close relative *Pseudomonas putida* KT2440. Biometals 22:951-964.

104. **McInerney, B. V., R. P. Gregson, M. J. Lacey, R. J. Akhurst, G. R. Lyons, S. H. Rhodes, D. R. Smith, L. M. Engelhardt, and A. H. White**. 1991. Biologically active metabolites from *Xenorhabdus* spp., Part 1. Dithiolopyrrolone derivatives with antibiotic activity. J. Nat. Prod. 54:774-784.

105. **McInerney, B. V., W. C. Taylor, M. J. Lacey, R. J. Akhurst, and R. P. Gregson**. 1991. Biologically active metabolites from *Xenorhabdus* spp., Part 2. Benzopyran-1-one derivatives with gastroprotective activity. J. Nat. Prod. 54:785-795.

106. **Mootz, H. D., D. Schwarzer, and M. A. Marahiel**. 2002. Ways of assembling complex natural products on modular nonribosomal peptide synthetases. ChemBioChem 3:490-504.

107. **Morishima, H., Fujita, K., Nakano, M., Atsumi, S., Ookubo, M., Kitagawa, M., Matsumoto, H., Okunyama, A., Okabe, T., Suda, H., and Nishimura, S.** Jpn. Kokai Tokkyo Koho. 1994.

108. **Namwat, W., Y. Kamioka, H. Kinoshita, Y. Yamada, and T. Nihira**. 2002. Characterization of virginiamycin S biosynthetic genes from *Streptomyces virginiae*. Gene 286:283-290.

109. **Ndjonka, D., L. N. Rapado, A. M. Silber, E. Liebau, and C. Wrenger**. 2013. Natural products as a source for treating neglected parasitic diseases. Int. J. Mol. Sci. 14:3395-3439.

110. **Nelson, T. J. and D. L. Alkon**. 2009. Neuroprotective versus tumorigenic protein kinase C activators. Trends Biochem. Sci. 34:136-145.

111. **Newman, D. J. and G. M. Cragg**. 2012. Natural products as sources of new drugs over the 30 years from 1981 to 2010. J. Nat. Prod. 75:311-335.

112. **Nguyen, T., K. Ishida, H. Jenke-Kodama, E. Dittmann, C. Gurgui, T. Hochmuth, S. Taudien, M. Platzer, C. Hertweck, and J. Piel**. 2008. Exploiting the mosaic structure of trans-acyltransferase polyketide synthases for natural product discovery and pathway dissection. Nat. Biotechnol. 26:225-233.

113. **Nishimura, Y., A. Hagiwara, T. Suzuki, and S. Yamanaka**. 1994. *Xenorhabdus japonicus* sp-nov associated with the nematode *Steinernema kushidai*. World J. Microbiol. Biotechnol. 10:207-210.

114. **Nollmann, F. I., A. Dowling, M. Kaiser, K. Deckmann, S. Grosch, R. ffrench-Constant, and H. B. Bode**. 2012. Synthesis of szentiamide, a depsipeptide from entomopathogenic

Xenorhabdus szentirmaii with activity against *Plasmodium falciparum*. Beilstein. J. Org. Chem. 8:528-533.

115. **Ohlendorf, B., S. Simon, J. Wiese, and J. F. Imhoff**. 2011. Szentiamide, an *N*-formylated cyclic depsipeptide from *Xenorhabdus szentirmaii* DSM 16338T. Nat. Prod. Commun. 6:1247-1250.

116. **Oka, M., Y. Nishiyama, S. Ohta, H. Kamei, M. Konishi, T. Miyaki, T. Oki, and H. Kawaguchi**. 1988. Glidobactins A, B and C, new antitumor antibiotics. I. Production, isolation, chemical properties and biological activity. J. Antibiot. 41:1331-1337.

117. **Oka, M., H. Ohkuma, H. Kamei, M. Konishi, T. Oki, and H. Kawaguchi**. 1988. Glidobactins D, E, F, G and H; minor components of the antitumor antibiotic glidobactin. J. Antibiot. 41:1906-1909.

118. **Oka, M., K. Yaginuma, K. Numata, M. Konishi, T. Oki, and H. Kawaguchi**. 1988. Glidobactins A, B and C, new antitumor antibiotics. II. Structure elucidation. J. Antibiot. 41:1338-1350.

119. **Orchard, S. S. and H. Goodrich-Blair**. 2004. Identification and functional characterization of a *Xenorhabdus nematophila* oligopeptide permease. Appl. Environ. Microbiol. 70:5621-5627.

120. **Paik, S., Y. H. Park, S. I. Suh, H. S. Kim, I. S. Lee, M. K. Park, C. S. Lee, and S. H. Park**. 2001. Unusual cytotoxic phenethylamides from *Xenorhabdus nematophilus*. Bull. Korean Chem. Soc. 22:372-374.

121. **Pardo-Lopez, L., C. Munoz-Garay, H. Porta, C. Rodriguez-Almazan, M. Soberon, and A. Bravo**. 2009. Strategies to improve the insecticidal activity of Cry toxins from *Bacillus thuringiensis*. Peptides 30:589-595.

122. **Park, D., K. Ciezki, R. van der Hoeven, S. Singh, D. Reimer, H. B. Bode, and S. Forst**. 2009. Genetic analysis of xenocoumacin antibiotic production in the mutualistic bacterium *Xenorhabdus nematophila*. Mol. Microbiol. 73:938-949.

123. **Park, D. and S. Forst**. 2006. Co-regulation of motility, exoenzyme and antibiotic production by the EnvZ-OmpR-FlhDC-FliA pathway in *Xenorhabdus nematophila*. Mol. Microbiol. 61:1397-1412.

124. **Park, J. M., M. Kim, J. Min, S. M. Lee, K. S. Shin, S. D. Oh, S. J. Oh, and Y. H. Kim**. 2012. Proteomic identification of a novel toxin protein (Txp40) from *Xenorhabdus nematophila* and its insecticidal activity against larvae of *Plutella xylostella*. J Agric. Food Chem. 60:4053-4059.

125. **Park, Y., E. E. Herbert, C. E. Cowles, K. N. Cowles, M. L. Menard, S. S. Orchard, and H. Goodrich-Blair**. 2007. Clonal variation in *Xenorhabdus nematophila* virulence and suppression of *Manduca sexta* immunity. Cell Microbiol. 9:645-656.

126. **Park, Y., Y. Kim, and D. Stanley**. 2004. The bacterium *Xenorhabdus nematophila* inhibits phospholipases A2 from insect, prokaryote, and vertebrate sources. Naturwissenschaften 91:371-373.

127. **Parker, W. L., M. L. Rathnum, J. S. Wells, Jr., W. H. Trejo, P. A. Principe, and R. B. Sykes**. 1982. SQ 27,860, a simple carbapenem produced by species of *Serratia* and *Erwinia*. J. Antibiot. 35:653-660.

128. **Partida-Martinez, L. P. and C. Hertweck**. 2005. Pathogenic fungus harbours endosymbiotic bacteria for toxin production. Nature 437:884-888.

129. **Peel, M. M., D. A. Alfredson, J. G. Gerrard, J. M. Davis, J. M. Robson, R. J. McDougall, B. L. Scullie, and R. J. Akhurst**. 1999. Isolation, identification, and molecular characterization of strains of *Photorhabdus luminescens* from infected humans in Australia. J. Clin. Microbiol. 37:3647-3653.

130. **Piel, J.** 2004. Metabolites from symbiotic bacteria. Nat. Prod. Rep. 21:519-538.

131. **Piel, J.** 2009. Metabolites from symbiotic bacteria. Nat. Prod. Rep. 26:338-362.

132. **Piel, J.** 2010. Biosynthesis of polyketides by trans-AT polyketide synthases. Nat. Prod. Rep. 27:996-1047.

133. **Piel, J., D. Hui, N. Fusetani, and S. Matsunaga**. 2003. Targeting modular polyketide synthases with iteratively acting acyltransferases from metagenomes of uncultured bacterial consortia. Environ. Microbiol. 6:921-927.

134. **Plichta, K. L., S. A. Joyce, D. Clarke, N. Waterfield, and S. P. Stock**. 2009. *Heterorhabditis gerrardi* n. sp. (Nematoda: Heterorhabditidae): the hidden host of *Photorhabdus asymbiotica* (Enterobacteriaceae: gamma-Proteobacteria). J. Helminthol. 83:309-320.

135. **Poinar, G. O. Jr., G. M. Thomas, and R. Hess**. 1977. Characterization of the specific bacterium associated with *Heterorhabditis bacteriophora* Poinar (Heterorhabditidae; Rhabditida). Nematologica 23:97-112.

136. **Popiel, I., D. L. Grove, and M. J. Friedman**. 1989. Infective juvenile formation in the insect parasitic nematode *Steinernema feltiae*. Parasitology 99:77-81.

137. **Proschak, A., K. Schultz, J. Herrmann, A. J. Dowling, A. O. Brachmann, R. ffrench-Constant, R. Müller, and H. B. Bode**. 2011. Cytotoxic fatty acid amides from *Xenorhabdus*. ChemBioChem 12:2011-2015.

138. **Pulsawat, N., S. Kitani, and T. Nihira**. 2007. Characterization of biosynthetic gene cluster for the production of virginiamycin M, a streptogramin type A antibiotic, in *Streptomyces virginiae*. Gene 393:31-42.

139. **Ramia, S., E. Neter, and D. J. Brenner**. 1982. Production of enterobacterial common antigen as an aid to classification of newly identified species of the families Enterobacteriaceae and *Vibrionaceae*. Int. J. Syst. Bacteriol. 32:395-398.

140. **Rausch, C., I. Hoof, T. Weber, W. Wohlleben, and D. H. Huson**. 2007. Phylogenetic analysis of condensation domains in NRPS sheds light on their functional evolution. BMC Evol. Biol. 7:78-92.

141. **Reimer, D., K. N. Cowles, F. I. Nollmann, H. Goodrich-Blair, and H. B. Bode**. 2013. Rhabdopeptides from entomopathogenic bacteria as examples for insect-associated secondary metabolites. ChemBioChem, submitted.

142. **Reimer, D., E. Luxenburger, A. O. Brachmann, and H. B. Bode**. 2009. A new type of pyrrolidine biosynthesis is involved in the late steps of xenocoumacin production in *Xenorhabdus nematophila*. ChemBioChem 10:1997-2001.

143. **Reimer, D., K. M. Pos, M. Thines, P. Grün, and H. B. Bode**. 2011. A natural prodrug activation mechanism in nonribosomal peptide synthesis. Nat. Chem. Biol. 7:888-890.

144. **Richards, G. R., E. E. Herbert, Y. Park, and H. Goodrich-Blair**. 2008. *Xenorhabdus nematophila lrhA* is necessary for motility, lipase activity, toxin expression, and virulence in *Manduca sexta* insects. J. Bacteriol. 190:4870-4879.

145. **Robertson, B. D. and T. F. Meyer**. 1992. Genetic variation in pathogenic bacteria. Trends Genet. 8:422-427.

146. **Samel, S. A., G. Schoenafinger, T. A. Knappe, M. A. Marahiel, and L. O. Essen**. 2007. Structural and functional insights into a peptide bond-forming bidomain from a nonribosomal peptide synthetase. Structure. 15:781-792.

147. **Schaaf, O. and K. Dettner**. 2000. Polyunsaturated monoglycerides and a pregnadiene in defensive glands of the water beetle *Agabus affinis*. Lipids 35:543-550.

148. **Schauwecker, F., F. Pfennig, N. Grammel, and U. Keller**. 2000. Construction and in vitro analysis of a new bi-modular polypeptide synthetase for synthesis of *N*-methylated acyl peptides. Chem. Biol. 7:287-297.

149. **Schellenberg, B., L. Bigler, and R. Dudler**. 2007. Identification of genes involved in the biosynthesis of the cytotoxic compound glidobactin from a soil bacterium. Environ. Microbiol. 9:1640-1650.

150. **Schmidt, E. W.** 2008. Trading molecules and tracking targets in symbiotic interactions. Nat. Chem. Biol. 4:466-473.

151. **Schneider, T. L., B. Shen, and C. T. Walsh**. 2003. Oxidase domains in epothilone and bleomycin biosynthesis: thiazoline to thiazole oxidation during chain elongation. Biochemistry. 42:9722-9730.

152. **Schwartsmann, G., A. B. da Rocha, J. Mattei, and R. Lopes**. 2003. Marine-derived anticancer agents in clinical trials. Expert. Opin. Investig. Drugs 12:1367-1383.

153. **Schwarzer, D., H. D. Mootz, U. Linne, and M. A. Marahiel**. 2002. Regeneration of misprimed nonribosomal peptide synthetases by type II thioesterases. Proc. Natl. Acad. Sci. 99:14083-14088.

154. **Seo, S., S. Lee, Y. Hong, and Y. Kim**. 2012. Phospholipase A2 inhibitors synthesized by two entomopathogenic bacteria, *Xenorhabdus nematophila* and *Photorhabdus temperata* subsp. *temperata*. Appl. Environ. Microbiol. 78:3816-3823.

155. **Sergeant, M., L. Baxter, P. Jarrett, E. Shaw, M. Ousley, C. Winstanley, and J. A. W. Morgan**. 2006. Identification, typing, and insecticidal activity of *Xenorhabdus* isolates from entomopathogenic nematodes in United Kingdom soil and characterization of the *xpt* toxin loci. Appl. Environ. Microbiol. 72:5895-5907.

156. **Sheets, J. J., T. D. Hey, K. J. Fencil, S. L. Burton, W. Ni, A. E. Lang, R. Benz, and K. Aktories**. 2011. Insecticidal toxin complex proteins from *Xenorhabdus nematophilus*: structure and pore formation. J. Biol. Chem. 286:22742-22749.

157. **Sicard, M., K. Brugirard-Ricaud, S. Pages, A. Lanois, N. E. Boemare, M. Brehelin, and A. Givaudan**. 2004. Stages of infection during the tripartite interaction between *Xenorhabdus nematophila*, its nematode vector, and insect hosts. Appl. Environ. Microbiol. 70:6473-6480.

158. **Sieber, S. A. and M. A. Marahiel**. 2005. Molecular mechanisms underlying nonribosomal peptide synthesis: approaches to new antibiotics. Chem. Rev. 105:715-738.

159. **Singh, J. and N. Banerjee**. 2008. Transcriptional analysis and functional characterization of a gene pair encoding iron-regulated xenocin and immunity proteins of *Xenorhabdus nematophila*. J. Bacteriol. 190:3877-3885.

160. **Smigielski, A. J., R. J. Akhurst, and N. E. Boemare**. 1994. Phase variation in *Xenorhabdus nematophilus* and *Photorhabdus luminescens*: Differences in respiratory activity and membrane energization. Appl. Environ. Microbiol. 60:120-125.

161. **Snyder, H., S. P. Stock, S. K. Kim, Y. Flores-Lara, and S. Forst**. 2007. New insights into the colonization and release processes of *Xenorhabdus nematophila* and the morphology and ultrastructure of the bacterial receptacle of its nematode host, *Steinernema carpocapsae*. Appl. Environ. Microbiol. 73:5338-5346.

162. **Somvanshi, V. S., E. Lang, S. Ganguly, J. Swiderski, A. K. Saxena, and E. Stackebrandt**. 2006. A novel species of *Xenorhabdus*, family Enterobacteriaceae: *Xenorhabdus indica* sp. nov., symbiotically associated with entomopathogenic nematode *Steinernema thermophilum* Ganguly and Singh, 2000. Syst. Appl. Microbiol. 29:519-525.

163. **Song, C. J., S. Seo, S. Shrestha, and Y. Kim**. 2011. Bacterial metabolites of an entomopathogenic bacterium, *Xenorhabdus nematophila*, inhibit a catalytic activity of phenoloxidase of the diamondback moth, *Plutella xylostella*. J. Microbiol. Biotechnol. 21:317-322.

164. **Stachelhaus, T., H. D. Mootz, and M. A. Marahiel**. 1999. The specificity-conferring code of adenylation domains in nonribosomal peptide synthetases. Chem. Biol. 6:493-505.

165. **Stachelhaus, T. and C. T. Walsh**. 2000. Mutational analysis of the epimerization domain in the initiation module PheATE of gramicidin S synthetase. Biochemistry. 39:5775-5787.

166. **Staunton, J.** 1998. Combinatorial biosynthesis of erythromycin and complex polyketides. Curr. Opin. Chem. Biol. 2:339-345.

167. **Staunton, J. and K. J. Weissman**. 2001. Polyketide biosynthesis: a millennium review. Nat. Prod. Rep. 18:380-416.

168. **Stein, M. L., P. Beck, M. Kaiser, R. Dudler, C. F. Becker, and M. Groll**. 2012. One-shot NMR analysis of microbial secretions identifies highly potent proteasome inhibitor. Proc. Natl. Acad. Sci. 109:18367-18371.

169. **Steiner, G.** 1929. *Neoaplectana glaseri* n.g., n.sp. (Oxyuridae), a new nemic parasite of the Japanese beetle (*Popillia japonica* Newm.). Journal of the Washington Academy of Sciences 19:436-440.

170. **Sugar, D. R., K. E. Murfin, J. M. Chaston, A. W. Andersen, G. R. Richards, L. deLeon, J. A. Baum, W. P. Clinton, S. Forst, B. S. Goldman, K. C. Krasomil-Osterfeld, S. Slater, S. P. Stock, and H. Goodrich-Blair**. 2012. Phenotypic variation and host interactions of *Xenorhabdus bovienii* SS-2004, the entomopathogenic symbiont of *Steinernema jollieti* nematodes. Environ. Microbiol 14:924-939.

171. **Sundar, L. and F. N. Chang**. 1993. Antimicrobial activity and biosynthesis of indole antibiotics produced by *Xenorhabdus nematophilus*. J. Gen. Microbiol. 139:3139-3148.

172. **Szittner, R. and E. Meighen**. 1990. Nucleotide sequence, expression, and properties of luciferase coded by lux genes from a terrestrial bacterium. J. Biol. Chem. 265:16581-16587.

173. **Tailliez, P., C. Laroui, N. Ginibre, A. Paule, S. Pages, and N. Boemare**. 2010. Phylogeny of *Photorhabdus* and *Xenorhabdus* based on universally conserved protein-coding sequences

and implications for the taxonomy of these two genera. Proposal of new taxa: *X. vietnamensis* sp. nov., *P. luminescens* subsp. *caribbeanensis* subsp. nov., *P. luminescens* subsp. *hainanensis* subsp. nov., *P. temperata* subsp. *khanii* subsp. nov., *P. temperata* subsp. *tasmaniensis* subsp. nov., and the reclassification of *P. luminescens* subsp. *thracensis* as *P. temperata* subsp. *thracensis* comb. nov. Int. J. Syst. Evol. Microbiol. 60:1921-1937.

174. **Tailliez, P., S. Pages, S. Edgington, L. M. Tymo, and A. G. Buddie**. 2012. Description of *Xenorhabdus magdalenensis* sp. nov., the symbiotic bacterium associated with *Steinernema australe*. Int. J. Syst. Evol. Microbiol. 62:1761-1765.

175. **Tailliez, P., S. Pages, N. Ginibre, and N. Boemare**. 2006. New insight into diversity in the genus *Xenorhabdus*, including the description of ten novel species. Int. J. Syst. Evol. Microbiol. 56:2805-2818.

176. **Tang, L., Y. J. Yoon, C. Y. Choi, and C. R. Hutchinson**. 1998. Characterization of the enzymatic domains in the modular polyketide synthase involved in rifamycin B biosynthesis by *Amycolatopsis mediterranei*. Gene 216:255-265.

177. **Taylor, M. J., C. Bandi, and A. Hoerauf**. 2005. *Wolbachia* bacterial endosymbionts of filarial nematodes. Adv. Parasitol. 60:245-284.

178. **Thaler, J. O., S. Baghdiguian, and N. Boemare**. 1995. Purification and characterization of Xenorhabdicin, a phage tail-like bacteriocin, from the lysogenic strain F1 of *Xenorhabdus nematophilus*. Appl. Environ. Microbiol. 61:2049-2052.

179. **Theodore, C. M., J. B. King, J. You, and R. H. Cichewicz**. 2012. Production of Cytotoxic Glidobactins/Luminmycins by *Photorhabdus asymbiotica* in Liquid Media and Live Crickets. J. Nat. Prod. 75:2007-2011.

180. **Thomas, G. M. and G. O. Poinar**. 1979. *Xenorhabdus* gen. nov., a genus of entomopathogenic nematophilic bacteria of the family Enterobacteriaceae. Int. J. Syst. Bacteriol. 29:352-360.

181. **Thomas, G. M. and G. O. Jr. Poinar**. 1965. A new bacterium, *Achromobacter nematophilus* sp. nov. (Achromobacteriaceae: Eubacteriales) associated with a nematode. Int. Bull. Bacteriol. Nomencl. Taxon. 15:249-254.

182. **Toth, T. and T. Lakatos**. 2008. *Photorhabdus temperata* subsp. *cinerea* subsp. nov., isolated from *Heterorhabditis* nematodes. Int. J. Syst. Evol. Microbiol. 58:2579-2581.

183. **Vallet-Gely, I., A. Novikov, L. Augusto, P. Liehl, G. Bolbach, M. Pechy-Tarr, P. Cosson, C. Keel, M. Caroff, and B. Lemaitre**. 2010. Association of hemolytic activity of *Pseudomonas entomophila*, a versatile soil bacterium, with cyclic lipopeptide production. Appl. Environ. Microbiol. 76:910-921.

184. **Vigneux, F., R. Zumbihl, G. Jubelin, C. Ribeiro, J. Poncet, S. Baghdiguian, A. Givaudan, and M. Brehelin**. 2007. The *xaxAB* genes encoding a new apoptotic toxin from the insect pathogen *Xenorhabdus nematophila* are present in plant and human pathogens. J. Biol. Chem. 282:9571-9580.

185. **Vodovar, N., D. Vallenet, S. Cruveiller, Z. Rouy, V. Barbe, C. Acosta, L. Cattolico, C. Jubin, A. Lajus, B. Segurens, B. Vacherie, P. Wincker, J. Weissenbach, B. Lemaitre, C. Medigue, and F. Boccard**. 2006. Complete genome sequence of the entomopathogenic and metabolically versatile soil bacterium *Pseudomonas entomophila*. Nat. Biotechnol. 24:673-679.

186. **Walsh, C. T., H. W. Chen, T. A. Keating, B. K. Hubbard, H. C. Losey, L. S. Luo, C. G. Marshall, D. A. Miller, and H. M. Patel**. 2001. Tailoring enzymes that modify nonribosomal peptides during and after chain elongation on NRPS assembly lines. Curr. Opin. Chem. Biol. 5:525-534.

187. **Wang, Y., A. L. Bilgrami, D. Shapiro-Ilan, and R. Gaugler**. 2007. Stability of entomopathogenic bacteria, *Xenorhabdus nematophila* and *Photorhabdus luminescens*, during *in vitro* culture. J. Ind. Microbiol. Biotechnol. 34:73-81.

188. **Waterfield, N. R., M. Sanchez-Contreras, I. Eleftherianos, A. Dowling, G. Yang, P. Wilkinson, J. Parkhill, N. Thomson, S. E. Reynolds, H. B. Bode, S. Dorus, and R. H. ffrench-Constant**. 2008. Rapid Virulence Annotation (RVA): identification of virulence factors using a bacterial genome library and multiple invertebrate hosts. Proc. Natl. Acad. Sci. 105:15967-15972.

189. **Weber, T., R. Baumgartner, C. Renner, M. A. Marahiel, and T. A. Holak**. 2000. Solution structure of PCP, a prototype for the peptidyl carrier domains of modular peptide synthetases. Structure Fold Des. 8:407-418.

190. **Wilkinson, B. and J. Micklefield**. 2007. Mining and engineering natural-product biosynthetic pathways. Nat. Chem. Biol. 3:379-386.

191. **Wilkinson, P., N. R. Waterfield, L. Crossman, C. Corton, M. Sanchez-Contreras, I. Vlisidou, A. Barron, A. Bignell, L. Clark, D. Ormond, M. Mayho, N. Bason, F. Smith, M. Simmonds, C. Churcher, D. Harris, N. R. Thompson, M. Quail, J. Parkhill, and R. H. ffrench-Constant**. 2009. Comparative genomics of the emerging human pathogen *Photorhabdus asymbiotica* with the insect pathogen *Photorhabdus luminescens*. BMC. Genomics 10:302.

192. **Williamson, J. M., E. Inamine, K. E. Wilson, A. W. Douglas, J. M. Liesch, and Albers-Schönberg**. 1985. Biosynthesis of the beta-lactam antibiotic, thienamycin, by *Streptomyces cattleya*. J. Biol. Chem. 260:4637-4647.

193. **Yang, X. M., Y. Z. Shimizu, J. R. Steiner, and J. Clardy**. 1993. Nostoclide I and II, extracelluarl metabolites from a symbiotic cyanobacterium, *Nostoc* sp., from the lichen *Peltigera canina*. Tetrahedron Lett. 34:761-764.

194. **Yang, Y. L., Y. Xu, R. D. Kersten, W. T. Liu, M. J. Meehan, B. S. Moore, N. Bandeira, and P. C. Dorrestein**. 2011. Connecting chemotypes and phenotypes of cultured marine microbial assemblages by imaging mass spectrometry. Angew. Chem. Int. Ed. 50:5839-5842.

195. **Yeh, E., R. M. Kohli, S. D. Bruner, and C. T. Walsh**. 2004. Type II thioesterase restores activity of a NRPS module stalled with an aminoacyl-S-enzyme that cannot be elongated. ChemBioChem 5:1290-1293.

196. **Yuhashi, K., N. Ichikawa, H. Ezura, S. Akao, Y. Minakawa, N. Nukui, T. Yasuta, and K. Minamisawa**. 2000. Rhizobitoxine production by *Bradyrhizobium elkanii* enhances nodulation and competitiveness on *Macroptilium atropurpureum*. Appl. Environ. Microbiol. 66:2658-2663.

197. **Zhang, W., I. Ntai, N. L. Kelleher, and C. T. Walsh**. 2011. tRNA-dependent peptide bond formation by the transferase PacB in biosynthesis of the pacidamycin group of pentapeptidyl nucleoside antibiotics. Proc. Natl. Acad. Sci. 108:12249-12253.

198. **Zhou, Q., A. Dowling, H. Heide, J. Wöhnert, U. Brandt, J. Baum, R. ffrench-Constant, and H. B. Bode**. 2012. Xentrivalpeptides A-Q: depsipeptide diversification in *Xenorhabdus*. J. Nat. Prod. 75:1717-1722.

Chapter 1

A new type of pyrrolidine biosynthesis is involved in the late steps of xenocoumacin production in *Xenorhabdus nematophila*

Daniela Reimer, Eva Luxenburger, Alexander O. Brachmann and Helge B. Bode

The article has been published in
ChemBioChem, Vol.10, Issue 12, 2009, pp 1997-2001

Author's effort

The author performed all feeding experiments, postulated the biosynthetic model and wrote the paper together with Helge B. Bode. The producer and mutant strains were also analyzed by the author via HPLC MS analysis. The generation of mutants were generated by the author under supervision of Alexander O. Brachmann. High-resolution MS was performed by Eva Luxenburger. The structures of the intermediates were elucidated by Helge B. Bode.

A new type of pyrrolidine biosynthesis is involved in the late steps of xenocoumacin production in *Xenorhabdus nematophila*

Daniela Reimer,[a, b] Eva Luxenburger,[b] Alexander O. Brachmann[a, b] and Helge B. Bode[a]

[a] *Molekulare Biotechnologie*
Institut für Molekulare Biowissenschaften
Goethe Universität Frankfurt
Max-von-Laue-Str. 9, 60438 Frankfurt am Main, Germany
Fax: (+) 49 (0)69 798 29527
E-mail: h.bode@bio.uni-frankfurt.de

[b] *Institut für Pharmazeutische Biotechnologie*
Universität des Saarlandes
P. O. Box 151150, 66041 Saarbrücken, Germany

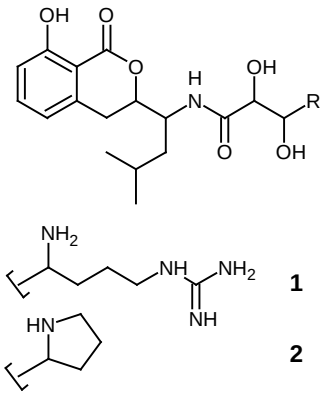

Feeding experiments have revealed that xenocoumacin I (**1**) is the precursor of xenocoumacin II (**2**), which was previously thought to be derived from the direct incorporation of proline. From mutational analyses of the biosynthesis gene cluster identified in the entomopathogenic bacterium *Xenorhabdus nematophila*, we propose that a desaturase (XcnN) and a saccharopine dehydrogenase-like enzyme (XcnM) are essential for this unusual transformation.

Bacteria of the genus *Xenorhabdus* live in symbiosis with nematodes of the genus *Steinernema*, and both form an entomopathogenic complex that is used commercially to kill several different insect larvae.[1-3] Briefly, the nematode carries the bacteria in the gut of its free-living state called infective juvenile (IJ). IJs actively search the soil for insect larvae. After an insect is identified, the nematode infects the insect and regurgitates the bacteria, which kill the insect within 24 h post-infection. The insect cadaver is then digested by the bacteria and the nematodes, and after several cycles of nematode development, new IJs are formed, which carry the bacteria in the gut and leave the now empty insect carcass to find new prey. As there have been hints in the literature that small molecules (e.g., secondary metabolites) produced by the bacterium are either involved in the pathogenesis against the insect or the symbiosis towards the nematode,[4] we have started to search for secondary metabolites produced by different *Xenorhabdus* species.

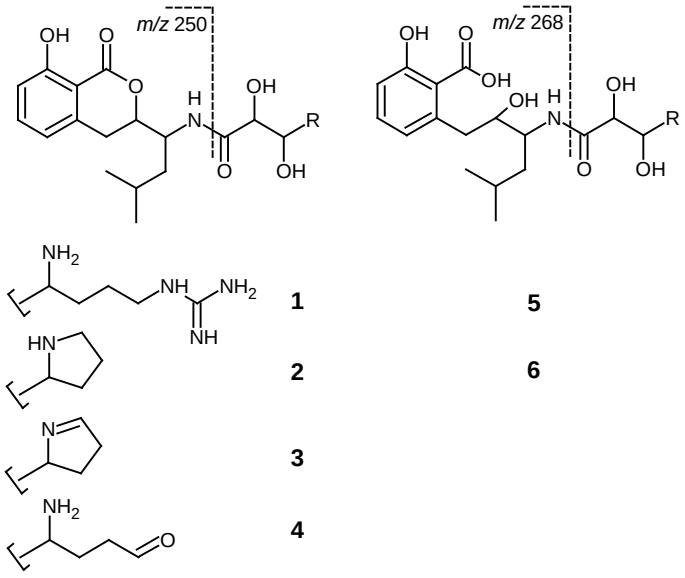

Scheme 1. Structures and characteristic fragmentation of XCN I–VI (**1**–**6**).

During this work, we could identify xenocoumacins (XCNs) I and II (**1** and **2**, respectively, in Scheme 1), which were isolated several years ago from different strains of *Xenorhabdus nematophila*.[5] Although both compounds show antibiotic activity, **1** is much more active and additionally shows good activity against different fungi.[5] Currently, both compounds are thought to be involved in killing bacteria living inside the insect gut, where these bacteria would compete with *Xenorhabdus* for food in the dead insect.[6] We could identify **1** and **2** in several *Xenorhabdus* strains by their characteristic fragmentation pattern in HRESI-MS (see below). Moreover, a detailed analysis of two different XCN producer strains, namely *X. nematophila* AN6/1 and *X. kozodoii* DSM 17907, under different cultivation conditions led to the identification of four new XCN derivatives named XCN III-VI (**3**-**6**). Whereas only traces of **3** and **4** are observed throughout the cultivation process in strain AN6/1, **5** and **6** start to accumulate in significant amounts after **1** and **2** have been formed (after 8 h); this indicates a structural relationship (Figure 1). Interestingly, only traces of **5** and **6** were observed in cultures grown with the adsorber resin Amberlite XAD-16, which seems to protect **1** and **2** from their transformation or degradation, as has also been observed for other secondary metabolites.[7] We performed detailed HRESI-MS and HRESI-MS-MS experiments in order to confirm this structural relationship as well as the structures of the new derivatives in general. Whereas **1**-**4** showed the expected fragment of 250 *m/z* $[M+H]^+$ ($C_{14}H_{20}NO_3$)

indicative of the benzopyran-1-one fragment (Scheme 1), an additional 268 *m/z* $[M+H]^+$ fragment could be observed for **5** and **6**, indicating the addition of water to these fragments ($C_{14}H_{22}NO_4$).

We also performed feeding experiments followed by MS analysis in order to confirm the proposed structures. All the XCNs were labeled between 12-30% after feeding with [5,5,5-D_3]leucine, and the expected mass shift of 3 Da was observed in the 250 and 268 *m/z* fragments, respectively. Encouraged by this result, we used an inverse feeding approach where compounds of natural abundance are fed to a culture of the bacterium grown in [U-^{13}C]medium (Table S2). An incorporation of the respective precursor can readily be seen by a shift to lower masses, reflecting the number of carbons introduced by the precursor.[8] Using this approach, we could confirm the incorporation of leucine into **1**-**6** in the benzopyrane-1-one fragment. Moreover, we could identify that arginine is not only incorporated into **1** and **5** but also into **2**, **4**, and **6** (**3** could not be analyzed due to very low production under the selected growth conditions). However, a mass decrease of only 5 Da was observed for the latter compounds in comparison to the 6 Da decrease in **1** and **5** after the feeding of arginine (Table S3). This indicates that **1** might be the precursor for all XCNs, as can also be concluded from the production curve since **1** is formed prior to all other XCNs (Figure 1 and S1). As a control experiment, we also fed proline to the growing cultures, but no incorporation into XCNs could be observed. as expected.

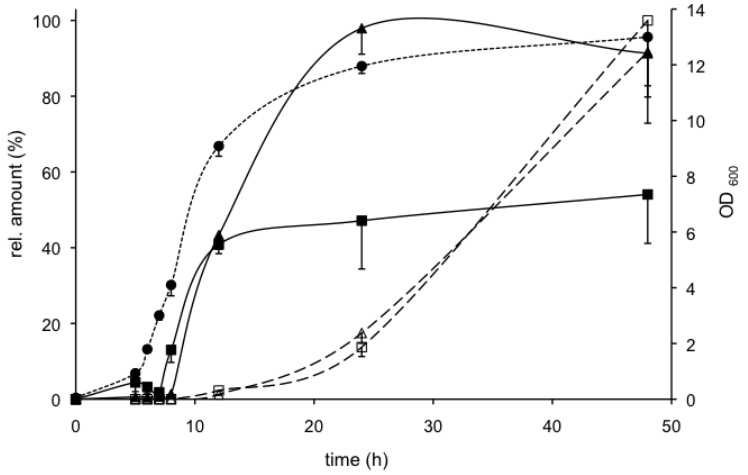

Figure 1. XCN production in cultures of strain AN6/1 without XAD-16. 100% refers to the maximum production of **2**. OD600 (●), 1 (■), 2 (▲), 5 (□), 6 (Δ). Results from triplicate experiments are shown. Compounds **3** and **4** are only produced in trace amounts and are not detectable.

As we were interested in the proteins involved in the transformation of **1** into **2**, we searched for the XCN biosynthesis gene cluster in the genome of *X. nematophila* ATCC19061, which was completely sequenced recently. "Retrobiosynthetic analysis" of the XCNs as well as the results from our feeding experiments strongly suggested their origin in a hybrid polyketide synthase (PKS)-nonribosomal polypeptide synthetase (NRPS) system. PKSs and NRPSs are gigantic multienzyme "assembly lines", which catalyze the sequential condensation of simple malonyl-CoA thioester and amino acid building blocks, respectively.[9, 10] A detailed annotation of all 16 biosynthesis gene clusters encoding PKSs and/or NRPSs led to the identification of a single gene cluster composed of 14 genes, which was postulated to be involved in

XCN biosynthesis (Figure 2, Table 1). Genes adjacent to the *xcn* gene cluster encode hypothetical proteins or proteins involved in flagellar biosynthesis, and therefore, were not thought to be involved in XCN biosynthesis (Table 1).

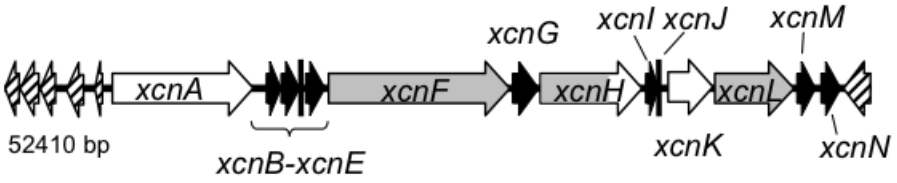

Figure 2. Organisation of the XCN (*xcn*) biosynthesis gene cluster in *Xenorhabdus nematophila* ATCC 19061; white (NRPS-encoding genes), gray (PKSencoding genes), black (other *xcn* genes), striped (non-*xcn* genes).

The inactivation of selected genes of this gene cluster confirmed its involvement in XCN biosynthesis and led to XCN-negative mutants. Plasmid insertion into *xcnA* and *xcnK* of the proposed PKS- or NRPS-encoding genes resulted in the total loss of XCN production (e.g., Figure 3C and data not shown). We named the genes in this biosynthesis gene cluster *xcnA–xcnN* (from XCN) and assigned functions to all proteins encoded by these genes by homology to known proteins using BLAST-P searches (Figure 2, Table 1).[13] In many systems of *Streptomyces* origin, the sequence of the biosynthetic proteins within the pathway directly correlates with the order of the genes within the cluster. However, this colinearity is not observed in the *xcn* cluster. Moreover, no order of proteins acting in the biosynthesis could be determined based on the docking of domains that mediate protein-protein interactions in these giant proteins, as was recently shown for DKxanthene biosynthesis.[14, 15] From a detailed analysis of the module and domain organization of the PKS and NRPS proteins encoded within the cluster (Figure S2–S8), we could not unambiguously deduce the biosynthesis pathway, as a few domains showed unusual amino acid residues and might, in fact, be inactive while some other domains are postulated to act in trans on neighboring modules. Our current model proposes the proteins acting in the order of XcnKHALF (Figure S9) with XcnK being the starting module due to its adenylation domain, which is proposed to be specific for arginine or glutamine. However, we might have missed some genes involved in XCN biosynthesis. Clearly, more work needs to be done to confirm the current biosynthesis model. Moreover, as the biosynthesis gene cluster consists of six transcriptional units, it is not clear how this complex system is regulated.[6] However, it was shown recently that the genes for the biosynthesis of isopropylstilbene—the major antibiotic in *Photorhabdus*, the sister taxa of *Xenorhabdus* with a very similar life style—are also not clustered but are scattered around 1.5 Mbp of the *Photorhabdus* genome.[16]

As our goal was to identify proteins involved in the proposed conversion of **1** into **2**, we concentrated on non-PKS and-NRPS-encoding genes present in the biosynthesis gene cluster. Genes *xcnB–E* encode all the enzymes required for the biosynthesis of the rare extender unit hydroxymalonyl-ACP,[11] and plasmid insertion into *xcnC* resulted in total loss of XCN production. Gene *xcnG* encodes a peptide transporter, which might be involved in the resistance mechanism. Gene *xcnI* encodes a type II thioesterase,[17] which might be involved in releasing misprimed intermediates from the PKS and NRPS enzymes, and *xcnJ* encodes a hypothetical protein. The most interesting genes with respect to the transformation of **1** into **2** are *xcnM* and *xcnN*, which encode proteins similar to saccharopine dehydrogenases and fatty acid desaturases, respectively.

Saccharopine dehydrogenases are involved in the biosynthesis of lysine in fungi by catalyzing the formation of lysine and aketoglutarate from 2-aminoadipate-6 semialdehyde and glutamate with saccharopine as the key intermediate,[18] whereas desaturases regiospecifically introduce double bonds into saturated fatty acids.[19] In order to elucidate the function of both enzymes for XCN biosynthesis, we constructed insertion mutants in *xcnM* and *xcnN* and a deletion mutant in *xcnM*, as the expression of both genes might be transcriptionally coupled.[6] Analysis of XCN production showed that **1** and also **5** (not shown) were produced in all mutants, whereas no other XCN derivative could be detected (Figure 3D and E). This clearly shows that XcnM and XcnN are involved in the conversion of **1** into **2**.

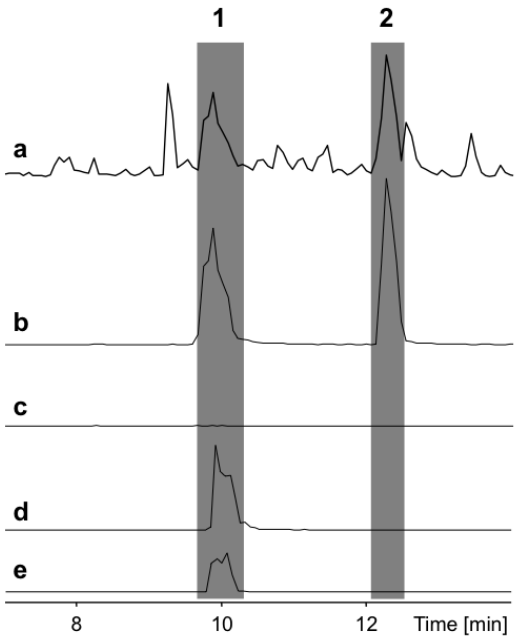

Figure 3. HPLC/MS analysis of the production of **1** and **2** in selected *xcn* mutants of *X. nematophila* HGB081. b)–e) Show extracted ion chromatograms specific for **1** (466 *m/z*) and **2** (407 *m/z*). a) basepeak chromatogram of HGB081 (WT), b) HGB081 (WT), c) *xcnA*::*cat*, d) *xcnN*::*cat*, e) Δ*xcnM*.

We propose that **1** is the terminal PKS/NRPS-derived product, which is oxidized by XcnN to XCN-464 (**7**), which has not yet been identified (Scheme 2). Intramolecular nucleophilic attack (Scheme 2 A) of the former arginine amino group of **7** and cleavage of the guanidinium group catalyzed by XcnM results in the formation of **3**, which is then reduced (probably also by XcnM) to **2**. According to this mechanism, **4** can be derived from **7** by simple hydrolysis (Scheme 2 B) or might be an intermediate of the XcnM-catalyzed conversion of **7** into **3** (Scheme 2 C). Alternatively, XcnM might catalyze the formation of **2** from **7** or **3** directly in an NADPH-dependent reaction.[18] In order to

investigate these possibilities, the heterologous expression of both proteins and *in vitro* experiments are currently underway in our group. As **5** and **6** are produced predominantly in the wild type when no XAD adsorber resin is added (Figure 1), we propose that they are nonspecific cleavage products of **1** and **2**, respectively.

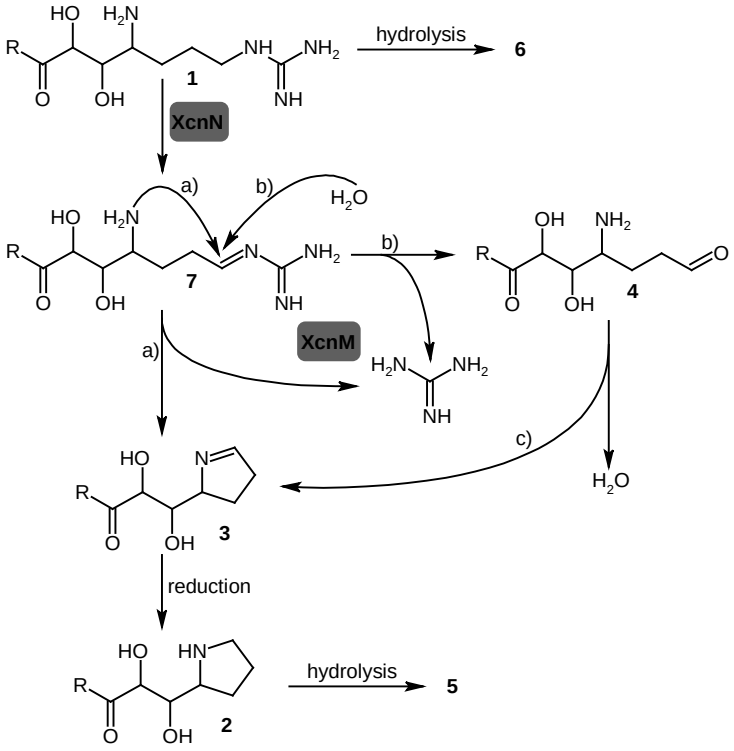

Scheme 2. Proposed biosynthesis of XCN II–VI (**2**-**6**) from XCN I (**1**). For details, see the main text and for R, see Scheme 1.

Experimental Section

Bacterial strains and culture conditions. *E. coli* strains were grown on solid or liquid Luria-Bertani (LB, pH7.0) medium at 37°C and 200 rpm. For plasmid selection in *E. coli*, chloramphenicol or ampicillin were added to a final concentration of 30µg mL^{-1} or 100 µg mL^{-1}, respectively. *X. nematophila* mutants were selected on LB containing rifampicin (40µg mL^{-1}) and chloramphenicol (30µg mL^{-1}) and cultivated at 30°C. Liquid cultures were grown at 200 rpm on a shaker in 250 mL Erlenmeyer flasks containing 50 mL LB medium, antibiotic and 2% (*v/v*) of XAD-16 (Sigma-Aldrich) each. These cultures were inoculated with 0.1% (*v/v*) of a 24 h preculture in the same medium without XAD-16. Cultures were harvested after 72 h, and XAD beads were separated from cells and supernatant by sieving. XAD beads were extracted with MeOH (25 mL) and the MeOH extract was concentrated to dryness on a rotary evaporator. The residue was redissolved in MeOH (1.5 mL) for HPLC/MS analysis.

Table 1. Proteins of the *xcn* cluster and and open reading frames adjacent to the *xcn* cluster, their proposed function, size and closest homologues.

Protein	Size [aa]	Proposed Function	Closest homologue Origin	Identities/ positives [%]	Accession number	NRPS/PKS Domains
XN_1716	275	hypothetical protein plu3102	*Photorhabdus luminescens subsp. laumondii* TT01	86/90	NP_930334.1	
XN_1715	357	hypothetical protein plu3103	*Photorhabdus luminescens subsp. laumondii* TT01	89/94	NP_930335.1	
XN_1714	295	hypothetical protein plu3104	*Photorhabdus luminescens subsp. laumondii* TT01	88/94	NP_930336.1	
XN_1713	309	hypothetical protein plu2652	*Photorhabdus luminescens subsp. laumondii* TT01	78/88	NP_929887.1	
XN_1712	110	no similarity found				
XcnA	673	NRPS	*Hahella chejuensis* KCTC 2396	52/66	YP_434622.1	*C*, *A*, *T*, *E*, C, A, T
XcnB[a]	286	3-hydroxybutyryl-CoA dehydrogenase	*Clostridium cellulolyticum* H10	51/69	ZP_01574038.1	
XcnC[a]	354	methoxymalonyl-ACP biosynthesis protein	*Bacillus pumilus* SAFR-032	52/73	YP_001485885.1	
XcnD[a]	86	hypothetical protein Plarl_10742	*Paenibacillus larvae* subsp. *larvae* BRL-230010	47/67	ZP_02328111.1	
XcnE[a]	384	Putative acyl-CoA dehydrogenase	*Bacillus cereus*	50/71	AAD40109.1	
XcnF	422	PKS	*Herpetosiphon aurantiacus* ATCC 23779	34/52	YP_001546725.1	KS, T, KS, AT, KR, T, KS, AT, T
XcnG	490	cyclic peptide transporter	*Bacillus cereus* AH1134	28/50	ZP_02525771.1	
XcnH	928	PKS/NRPS	*Bacillus cereus* AH1134	34/54	ZP_02525590.1	KS, AT, KR, T, *C*
XcnI	244	type II TE	*H. aurantiacus* ATCC 23779	34/54	YP_001545185.1	
XcnJ	108	hypothetical protein Mmwyl1_0491	*Marinomonas* sp. MWYL1	30/57	YP_001339362.1	
XcnK	358	NRPS	*B. pumilus* SAFR-032	36/56	YP_001485888.1	A, T
XcnL	488	PKS	*B. pumilus* ATCC 7061	34/54	ZP_03054477.1	KS, AT, KR, T
XcnM	362	saccharopine dehydrogenase	*Acaryochloris marina* MBIC11017	40/59	YP_001520361.1	
XcnN	361	fatty acid desaturase	*Burkholderia phymatum* STM815	36/56	YP_001863713.1	
XN_1697	502	hypothetical protein BACCOP_01733	*Bacteroides coprocola* DSM 17136	33/50	ZP_03009871.1	
XN_1696	44	no similarity found				
FliR	261	flagellar biosynthesis protein FliR	*Photorhabdus luminescens subsp. laumondii* TT01	70/86	NP_929203.1	
FliQ	90	flagellar biosynthesis protein FliQ	*Enterobacter s. 638*	76/92	YP_001177260.1	
FliP	273	flagellar biosynthesis protein FliP	*Photorhabdus luminescens subsp. laumondii* TT01	88/93	NP_929205.1	

[a] XcnBCDE show high similarity to ZmaGNDE which are involved in the proposed mechanism for hydroxymalonyl-ACP formation in the biosynthesis of Zwittermicin A in *Bacillus cereus*.[11, 12] Domains in italic might be inactive.

Plasmids and general DNA procedures. DNA isolation, plasmid preparation, restriction digests, PCR, gel electrophoresis and ligation reactions were conducted according standard methods.[20] PCR-amplified fragments were recovered from agarose gels with the Nucleo Spin Extract II Kit (Macherey & Nagel, Düren, Germany). For PCR experiments, Phusion Polymerase (Finnzymes, Espoo, Finland) was used according to the manufacturer's instructions.

Construction of mutants. For the construction of the *xcnA*, *xcnC*, *xcnK*, *xcnM*, and *xcnN* mutants, the genes were disrupted by plasmid integration as described previously.[21] Briefly, internal fragments of

the desired genes between 470-720 bp were amplified from genomic DNA using oligonucleotides listed in Table S1. After purification of the PCR product and restriction with *Sph*I and *Sac*I, the fragments were cloned into pDS132, carrying a chloramphenicol resistance gene.[22] The resulting plasmids were introduced into *E. coli* S17-1 λ pir by electroporation and then introduced into a rifampicin-resistant *X. nematophila* HGB081 strain[23] by biparental conjugation, yielding *X. nematophila* HGB081-*xcnA::cat*, HGB081-*xcnC::cat*, HGB081-*xcnK::cat*, HGB081-*xcnM::cat* and HGB081-*xcnN::cat*. The genotypes of all mutants were confirmed by PCR with the use of a plasmid-specific pair of primers— pDS132fw (5'-GAT CGA TCC TCT AGA GTC GAC CT-3') and pDS132rv (5'-ACA TGT GGA ATTGTG AGC GG-3')—and a genome-specific pair of primers listed in Table S1. The genome sequence of *X. nematophila* ATCC 19061 is available at the MaGe website (https://www.genoscope.cns.fr/agc/mage/wwwpkgdb/Login/log.php? pid=24).

For the construction of the *xcnM* deletion mutant, two fragments up- (945 bp) and downstream (722 bp) of the gene region encoding *xcnM* were amplified, and in a further step, fused together via complementary gene regions using oligonucleotides listed in Table S1. After purification, restriction with *Sph*I and *Sac*I, cloning into pDS132, electroporation into *E. coli* S17-1 λ pir and conjugation with HGB081, the HGB081-Δ*xcnM* mutant was constructed with an in-frame deletion of 876 bp via *sacB* counterselection as described previously.[21]

Phenotypic analysis. HPLC-MS analysis were performed with an Agilent 1100 series system with a photodiode array detector and coupled to a Bruker HCTplus mass spectrometer and a Luna C18/2.5 µm RP column (Phenomenex). Metabolites were eluted with a MeCN/0.1% formic acid in H_2O gradient ranging from 5% to 95% in 20 minutes at a flow rate of 0.4 mL min^{-1}. High-resolution MS were recorded with a Thermo LTQ Orbitrap Hybrid FT mass spectrometer and an X-Bridge C18/1.7 µm RP column (Waters) using a similar gradient.

Feeding experiments. Feeding experiments were carried out in 50 mL Erlenmeyer flasks containing 5 mL of ISOGRO-^{13}C (Sigma-Aldrich) medium or ISOGRO-^{15}N medium containing 10 mM K_2HPO_4, 10 mM KH_2PO_4, 8 mM $MgSO_4 \cdot 7H_20$ and 90 µM $CaCl_2 \cdot H_2O$. Feeding cultures were inoculated with 0.1% of a 24 h preculture grown in LB and washed with ISOGRO-^{13}C or ^{15}N medium, respectively. L-leucine, L-arginine, or L-proline (2mM) were added at 6, 24, and 48 h of incubation in three equal portions over three days leading to a final concentration of 6 mM. After 72 h of incubation at 30°C and 200 rpm, the compounds were extracted with ethyl acetate (5 mL). For further HPLC-MS and HRMS analysis, the extracts were evaporated to dryness and redissolved in MeOH (1.5 mL). Detailed results of all feeding experiments are shown in Table S2. No complete dataset could be observed for **3** due to the small amount of compound produced.

Acknowledgements

The authors are grateful to the *Xenorhabdus* genome consortium for access to the genome sequence prior to publication and especially to Steve Forst for useful discussions and sharing unpublished data. The authors would like to thank Kira Weissman for docking domain analysis and Rolf Müller for his general support. This work was funded by the Deutsche Forschungsgemeinschaft (DFG).

References

[1] H. Goodrich-Blair. *Curr. Opin. Microbiol.* **2007**, *10*, 225-230.

[2] E. E. Herbert, H. Goodrich-Blair. *Nat. Rev. Microbiol.* **2007**, *5*, 634-646.

[3] S. Forst, B. Dowds, N. E. Boemare, E. Stackebrandt. *Annu. Rev. Microbiol.* **1997**, *51*, 47-72.

[4] T. A. Ciche, S. B. Bintrim, A. R. Horswill, J. C. Ensign. *J. Bacteriol.* **2001**, *183*, 3117-3126.

[5] B. V. McInerney, W. C. Taylor, M. J. Lacey, R. J. Akhurst, R. P. Gregson. *J. Nat. Prod.* **1991**, *54*, 785-795.

[6] D. Park, K. Ciezki, R. van der Hoeven, D. Reimer, H. B. Bode, S. Forst. *J. Bacteriol.* **2009**, unpubslihed results.

[7] K. Gerth, S. Pradella, O. Perlova, S. Beyer, R. Müller. *J. Biotechnol.* **2003**, *106*, 233-253.

[8] A. O. Brachmann, S. Forst, G. M. Furgani, A. Fodor, H. B. Bode. *J. Nat. Prod.* **2006**, *69*, 1830-1832.

[9] C. T. Walsh. *Acc. Chem. Res.* **2007**, *41*, 4-10.

[10] K. J. Weissman, P. F. Leadlay. *Nat. Rev. Microbiol.* **2005**, *3*, 925-936.

[11] Y. A. Chan, M. T. Boyne, A. M. Podevels, A. K. Klimowicz, J. Handelsman, N. L. Kelleher, M. G. Thomas. *Proc. Natl. Acad. Sci. USA* **2006**, *103*, 14349-14354.

[12] E. A. B. Emmert, A. K. Klimowicz, M. G. Thomas, J. Handelsman. *Appl. Environ. Microbiol.* **2004**, *70*, 104-113.

[13] S. F. Altschul, T. L. Madden, A. A. Schaffer, J. H. Zhang, Z. Zhang, W. Miller, D. J. Lipman. *Nucleic Acids Res.* **1997**, *25*, 3389-3402.

[14] P. Meiser, K. J. Weissman, H. B. Bode, D. Krug, J. S. Dickschat, A. Sandmann, R. Müller. *Chem. Biol.* **2008**, *15*, 771-781.

[15] K. J. Weissman. *ChemBioChem* **2006**, *7*, 485-494.

[16] S. A. Joyce, A. O. Brachmann, I. Glazer, L. Lango, G. Schwär, D. J. Clarke, H. B. Bode. *Angew. Chem. Int. Ed.* **2008**, *47*, 1942-1945.

[17] E. Yeh, R. M. Kohli, S. D. Bruner, C. T. Walsh. *ChemBioChem* **2004**, *5*, 1290-1293.

[18] H. Xu, B. Andi, J. Qian, A. H. West, P. F. Cook. *Cell Biochem. Biophys.* **2006**, *46*, 43-64.

[19] P. H. Buist. *Nat. Prod. Rep.* **2004**, *21*, 249-262.

[20] J. Sambrook, E. F. Fritsch, T. Maniatis, *Molecular Cloning: A Laboratory Manual*, Cold Springer Harbor Press, New York, **1989**.

[21] A. O. Brachmann, S. A. Joyce, H. Jenke-Kodama, G. Schwär, D. J. Clarke, H. B. Bode. *ChemBioChem* **2007**, *8*, 1721-1728.

[22] N. Philippe, J. P. Alcaraz, E. Coursange, J. Geiselmann, D. Schneider. *Plasmid* **2004**, *51*, 246-255.

[23] S. S. Orchard, H. Goodrich-Blair. *Appl. Environ. Microbiol.* **2004**, *70*, 5621-5627.

Supporting Information

Analysis of the xcn biosynthesis gene cluster. In order to understand XCN biosynthesis we performed BLAST-P analysis of all 14 Xcn proteins (XcnA-XcnN) and thereby could assign functions to all but one protein (XcnJ). Overall five PKS and/or NRPS enzymes could be identified (XcnAFHKL), all enzymes required for the biosynthesis of the unusual extender unit hydroxymalonyl-ACP (XcnBCDE) [1, 2], a type II thioesterase (XcnI) and additional proteins listed in Table 1. PKS and/or NRPS proteins were analyzed as described previously [3] following a frame plot 2.3.2 analysis [4] and the PKS/NRPS analysis website (http://www.tigr.org/jravel/nrps). From a detailed analysis of the conserved and/or catalytic residues of these domains (Figures S2-S8) we can predict the following: Adenylation domain A1 in XcnA might be inactive as several conserved residues are missing [3]. Overall three adenylation domains have been identified and none shows the expected leucine specificity required for XCN production [5, 6]. From the specificity of XcnK which might activate glutamine or arginine one can postulate that XcnK is involved in loading of the arginine starting unit (Figure S2). Peptidyl and acyl carrier protein domains seem to be functional as all of them carry the conserved serine residue and most of the other conserved amino acids (Figures S3 and S4) [3, 7]. The same might hold true for the ketosynthase and acyltransferase domains (Figures S5 and S6) [8, 9]. However, not all amino acids for malonyl-CoA specificity could be detected for AT3 in XcnF and AT1 in XcnH [10, 11]. Unfortunately, it is not possible to postulate the stereochemistry of the OH groups accordingly to the ketoreductase sequence motifs. KR2 in XcnF and KR1 in XcnL lack the LDD motif (a hint for type A alcohol stereochemistry) but they also lack the conserved tryptophan. KR1 in XcnH shows the LDD motif for type B alcohol stereochemistry but lacks the additional PxxxN motif [12]. For the condensation domains it is also difficult to determine if they are active or not as similar to the adenylation domains several conserved amino acids are missing (Figure S8) [3]. Moreover, three condensation domains have been identified but only one would be needed in the XCN biosynthesis.

Additional analysis of docking domains involved in protein-protein interaction did not reveal a possible order of the PKS and NRPS enzymes involved in XCN biosynthesis (Kira Weissman, personal communication). However, from the assigned domains our current model suggests the order XcnKLAFH as depicted in Figure S9. But even in this model several unusual events must occur namely use of AT, and KR domains *in trans* or non-usage of KR domains, respectively. Clearly, much work has to be done in the future to prove the postulated biosynthesis pathway and we would like to

emphasize that the pathway shown in Figure S8 represents the best guess of our current "work-in-progress".

Table S1. Oligonucleotides used for the construction of mutants and their verification (v). *Sac*I restriction sites are shown in bold, *Sph*I restriction sites are underlined, complementary regions are in lower case.

Gene	Name	Sequence
xcnA	Xn8321fw	5'-TCATCT**GAGCTC**CTGGCTGTCCGTTTTATTTG-3'
xcnA	Xn8321rv	5'-TTTTGAGCATGCTGACGCAAAGTATCGTTGTG-3'
xcnA	vXn8321f	5'-ACACGACAGCAAGAAAATGA-3'
xcnA	vXn8321r	5'-TCTGCTTTTTGTTGTTCTGC-3'
xcnC	Xn12723fw	5'-CATTTA**GAGCTC**TCGAAATACCGGTAAAATGTA-3'
xcnC	Xn12723rv	5'-TCCTGAGCATGCTCTCTGCCTTCTTAATTTTG-3'
xcnC	vXn12723f	5'-CTGAAGATTGGTCGATTAAA-3'
xcnC	vXn12723r	5'-GATTGTTTCATCTGCAAGTT-3'
xcnK	Xn8346fw	5'-GATAAA**GAGCTC**CTATTTCTGGAAGAAAGTCA-3'
xcnK	Xn8346rv	5'-ATTCTCGCATGCATAATTTAAGGGTACTGAGC-3'
xcnK	vXn8346f	5'-GGATATGAGAAACACCCTTG-3'
xcnK	vXn8346r	5'-GGGTATGACCGAGTAACAAT-3'
xcnM	Xn8351fw	5'-TCCCAT**GAGCTC**GGGTTGTTGGGCATCAGGTT-3'
xcnM	Xn8351rv	5'-TGAATCGCATGCGACCGGCTTTATCCTGGGAA-3'
xcnM	vXn8351f	5'-AAATATAGATATTCCCATTG-3'
xcnM	vXn8351r	5'-AATAATTCTATAACGCACTT-3'
xcnM	xcnM_up-F	5'-ATGCAGCATGCTTATTATGGCGCCTATGGGCAA-3'
xcnM	xcnM_up-R	5'-gcttctcctaccataaaaatTCCGGCAATGATTAACTCCAGA-3'
xcnM	xcnM_down-F	5'-tctggagttaatcattgccggaATTTTTATGGTAGGAGAAGC-3'
xcnM	xcnM_down-R	5'-ATGC**GAGCTC**TTTGGCTAAAACATGATGAG-3'
xcnM	vxcnMDel-fw	5'-CTTCATGCTTTGCTTCAATC-3'
xcnM	vxcnMDel-rv	5'-GGAAGACTAAATGCCCAGATAA-3'
xcnN	Xn8354fw	5'-TCAAGT**GAGCTC**TAAGTTCAATATATCACGTA-3'
xcnN	Xn8354rv	5'-TTGCATGCATGCTTGATGACATAGTGTATAAA-3'
xcnN	vXn8354f	5'-TTTTATCCTAATTGGAGCTTGG-3'
xcnN	vXn8354r	5'-ATAAATATCCCGCCCCATAA-3'

Table S2. Incorporation rates of unlabelled precursors in XCNI, II, IV-VI (**1**, **2**, **4**-**6**).

Sample	Incorporation rates (%)				
	XCNI (**1**)	XCNII (**2**)	XCNIV (**4**)	XCNV (**5**)	XCNVI (**6**)
^{13}C + Arg	51	42	63	52	41
^{13}C + Leu	32	34	n.a.	n.a.	n.a.

n.a. = not analyzed.

Table S3. HRESI MS and MS^2 data of xenocoumacins XCNI-XCNVI (**1**-**6**).

XCNI (**1**)								
Sample	**1** *m/z* [M + H^+]	calc. *m/z* [M + H^+]	Δppm	Sum formula	BPF *m/z* [M + H^+]	calc. *m/z* [M + H^+]	Δppm	Sum formula
^{12}C	466.2658	466.2660	-0.435	$C_{22}H_{36}N_5O_6$	250.1438	250.1438	-0.008	$C_{14}H_{20}N_1O_3$
^{13}C	488.3398	488.3398	0.108	$^{13}C_{22}H_{36}N_5O_6$	264.1912	264.1907	0.840	$^{13}C_{14}H_{20}N_1O_3$
^{13}C + Arg	482.3193	482.3197	-0.722	$^{13}C_{16}C_6H_{36}N_5O_6$	264.1909	264.1907	0.450	$^{13}C_{14}H_{20}N_1O_3$
^{13}C + Pro	488.3395	488.3398	-0.571	$^{13}C_{22}H_{36}N_5O_6$	264.1908	264.1907	0.219	$^{13}C_{14}H_{20}N_1O_3$
^{13}C + Leu	482.3190	482.3197	-2.816	$^{13}C_{16}C_6H_{36}N_5O_6$	258.1704	258.1704	-0.887	$^{13}C_8C_6H_{20}N_1O_3$
XCNII (**2**)								
Sample	**2** *m/z* [M + H^+]	calc. *m/z* [M + H^+]	Δppm	Sum formula	BPF *m/z* [M + H^+]	calc. *m/z* [M + H^+]	Δppm	Sum formula
^{12}C	407.2153	407.2177	-5.878	$C_{21}H_{31}N_2O_6$	250.1436	250.1438	-0.618	$C_{14}H_{20}N_1O_3$
^{13}C	428.2869	428.2831	0.500	$^{13}C_{21}H_{31}N_2O_6$	264.1908	264.1907	0.335	$^{13}C_{14}H_{20}N_1O_3$
^{13}C + Arg	423.2715	423.2713	0.257	$^{13}C_{16}C_5H_{31}N_2O_6$	264.1908	264.1907	0.219	$^{13}C_{14}H_{20}N_1O_3$
^{13}C + Pro	428.2881	428.2881	-0.140	$^{13}C_{21}H_{31}N_2O_6$	264.1907	264.1907	-0.127	$^{13}C_{14}H_{20}N_1O_3$
^{13}C + Leu	422.2674	422.2685	-1.175	$^{13}C_{15}C_6H_{31}N_2O_6$	258.1705	258.1706	-0.534	$^{13}C_8C_6H_{20}N_1O_3$
XCNIII (**3**)								
Sample	**3** *m/z* [M + H^+]	calc. *m/z* [M + H^+]	Δppm	Sum formula	BPF *m/z* [M + H^+]	calc. *m/z* [M + H^+]	Δppm	Sum formula
^{12}C	405.2022	405.2020	0.485	$C_{21}H_{29}N_2O_6$	250.1439	250.1438	0.599	$C_{14}H_{20}N_1O_3$
^{15}N	407.1962	407.1961	0.355	$C_{21}H_{29}{}^{15}N_2O_6$	251.1407	251.1408	-3.148	$C_{14}H_{20}{}^{15}N_1O_3$
XCNIV (**4**)								
Sample	**4** *m/z* [M + H^+]	calc. *m/z* [M + H^+]	Δppm	Sum formula	BPF *m/z* [M + H^+]	calc. *m/z* [M + H^+]	Δppm	Sum formula
^{12}C	423.2127	423.2126	0.378	$C_{21}H_{31}N_2O_7$	250.1432	250.1438	-2.093	$C_{14}H_{20}N_1O_3$
^{13}C	444.2833	444.2830	-0.562	$^{13}C_{21}H_{31}N_2O_7$	264.1909	264.1907	0.453	$^{13}C_{14}H_{20}N_1O_3$
^{13}C + Arg	439.2664	439.2663	0.989	$^{13}C_{16}C_5H_{31}N_2O_7$	264.1912	264.1907	0.348	$^{13}C_{14}H_{20}N_1O_3$
^{13}C + Pro	444.2826	444.2830	-1.053	$^{13}C_{21}H_{31}N_2O_7$	n.m.	n.m.	n.m.	n.m.
^{15}N	425.2068	425.2066	0.263	$C_{21}H_{31}{}^{15}N_2O_7$	251.1409	251.1408	0.019	$C_{14}H_{20}{}^{15}N_1O_3$

XCNV (**5**)								
Sample	**5** *m/z* [M + H^+]	calc. *m/z* [M + H^+]	Δppm	Sum formula	BPF *m/z* [M + H^+]	calc. *m/z* [M + H^+]	Δppm	Sum formula
^{12}C	484.2763	484.2766	-0.556	$C_{22}H_{38}N_5O_7$	n.m.	n.m.	n.m.	n.m.
^{13}C	506.3496	506.3504	-1.525	$^{13}C_{22}H_{38}N_5O_7$	n.m.	n.m.	n.m.	n.m.
^{13}C + Arg	500.3298	500.3303	-0.905	$^{13}C_{16}C_6H_{38}N_5O_7$	n.m.	n.m.	n.m.	n.m.
^{13}C + Pro	506.3502	506.3504	-0.200	$^{13}C_{22}H_{38}N_5O_7$	282.2011	282.2013	-0.563	$^{13}C_{14}H_{22}N_1O_4$
XCNVI (**6**)								
Sample	**6** *m/z* [M + H^+]	calc. *m/z* [M + H^+]	Δppm	Sum formula	BPF *m/z* [M + H^+]	calc. *m/z* [M + H^+]	Δppm	Sum formula
^{12}C	425.2267	425.2282	-3.712	$C_{21}H_{33}N_2O_7$	268.1545	268.1543	0.768	$C_{14}H_{22}N_1O_4$
^{13}C	446.2982	446.2987	-1.187	$^{13}C_{21}H_{33}N_2O_7$	282.2011	282.2013	-0.789	$^{13}C_{14}H_{22}N_1O_4$
^{13}C + Arg	441.2817	441.2819	-0.310	$^{13}C_{16}C_5H_{33}N_2O_7$	282.2013	282.2013	0.077	$^{13}C_{14}H_{22}N_1O_4$
^{13}C + Pro	446.2981	446.2987	-0.627	$^{13}C_{21}H_{33}N_2O_7$	282.2011	282.2013	-0.577	$^{13}C_{14}H_{22}N_1O_4$

Feeding experiments in HGB081; calculated (calc.), benzopyran-1-one fragment (BPF), n.m.= not measurable.

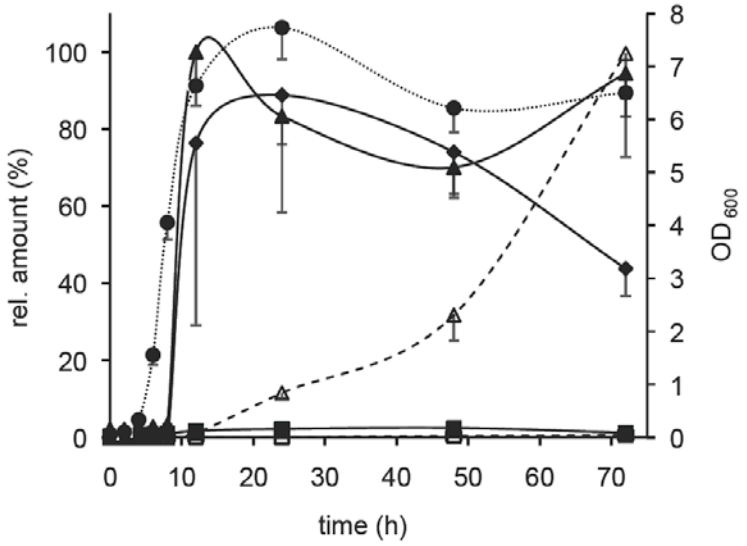

Figure S1. Xenocoumacin production in cultures of strain DSM 17907 without XAD-16. 100% refers to the maximum production of **2**. OD_{600} (filled circles), **1** (filled squares), **2** (filled triangles), **4** (filled diamonds), **5** (open squares), **6** (open triangles). Results from triplicate experiments are shown. DSM 17907 is an overproducer of **2**, which allows the detection of **4**. Compound **3** is only detectable in trace amounts.

	Core A1	Core A2	Core A3
		I	T
Consensus	**LSYxEL**	**LKAGxAYLVPLD**	**LAYxxYTSGSTGxPKG**
XcnK_A1 (214-747)	LNYIEL	LKIGAKYC-PFD	SAYIIFTSGSTGAPKG
XcnA_A2 (2027-2543)	ISNHEL	LFSGGSYC-YIN	EFYFIFTSGTTGTPKG
XcnA_A1 (468-1001)	LQWINP	LIENITVV-PAC	PAYILYTSGSTGEPKG

	Core A4	Core A5	Core A6
			L
Consensus	**FDxS**	**NxYGPTE**	**GELxIxGxGVARGYL**
XcnK_A1 (214-747)	FDAS	NAYGPTE	GEIAIAGKGLAKGYI
XcnA_A2 (2027-2543)	FDPS	NHYGPSE	GELWVGGRAVARGYT
XcnA_A1 (468-1001)	FDLT	NEYGPTE	GEIWIGGPVLADGYL

	Core A7	Core A8
Consensus	**YRTGDL**	**GRxDxQVKIRGxRIELGEIE**
XcnK_A1 (214-747)	YRTGDL	GRSDSQVKINGYRIELGEIE
XcnA_A2 (2027-2543)	YRTGDM	GRIDDQIKVNGVRIEPRELE
XcnA_A1 (468-1001)	YRTGDL	GRIDDEFKVRGYRIHPAEIE

	Core A9	Core A10
		I
Consensus	**LPxYMIP**	**NGKVDR**
XcnK_A1 (214-747)	LPSYMIP	SGKIDV
XcnA_A2 (2027-2543)	FPDTWLP	TGKIDR
XcnA_A1 (468-1001)	LPDAWMP	NGKVDT

Deduced specificity:

8 AA specificity for XcnK_A1:	D A Q D M G A V	MycB-M3-Gln
		PvdD-M2-Arg
8 AA specificity for XcnA_A1:	D L T K I G E V	MycC-M2-Asx
		TycC-M1-Asn
8 AA specificity for XcnA_A2:	D P E N I G H V	no hit

Figure S2. Detailed sequence analysis of adenylation domains in xenocoumacin biosynthesis gene cluster.[3]

	Ser Motif
	D I
Consensus	**DxFFxxLGGHSL**
XcnA_PCP2 (2559-2623)	TNFFE-AGGNSI
XcnK_PCP1 (763-829)	DNFFD-LGGSSY
XcnA_PCP1 (1051-1096)	TSFLE-QGGDSI

Figure S3. Detailed sequence analysis of peptidyl carrier protein domains in xenocoumacin biosynthesis gene cluster.[3]

	Ser Motif
	V
Consensus	**LGFDS**
XcnF_ACP3 (2995-3058)	ISLGGSS
XcnH_ACP1 (1399-1460)	FELGGNS
XcnF_ACP2 (1983-2047)	FELGANS
XcnL_ACP1 (1385-1449)	FDLGATS
XcnF_ACP1 (483-554)	FDVGASS

Figure S4. Detailed sequence analysis of acyl carrier protein domains in xenocoumacin biosynthesis gene cluster.[7]

		His motif I	His motif II
Consensus	**GPxxxxxTACSS**	**H**	**H**
XcnF_KS1 (10-431)	GPSVTIQTACST	IETHGTG	NVGHCDT
XcnF_KS3 (2088-2510)	GPSMVISTACSS	VETHGTG	NIGHLNF
XcnL_KS1 (21-443)	GPAVALQTACSS	IEAHGTA	ILGHLDS
XcnH_KS1 (7-429)	GPVMSVHTACST	IECHGTA	NIGHLDE
XcnF_KS2 (591-1020)	GPAVTVQSACSS	LEAHGTA	NLGHTDS

Figure S5. Detailed sequence analysis of β-ketoacyl carrier protein synthase domains in xenocoumacin biosynthesis gene cluster.[8,9]

	Ser motif	
Consensus	**GxSxG**	**HAFH**
XcnF_AT2 (1114-1410)	AMIGHSIGEY	ETSHAFHTAMMR
XcnF_AT3 (2609-2904)	AMIGHSLGEY	EIKRAFHTRYMD
XcnH_AT1 (524-816)	VLIGYSFGEL	KSKHAAHSSAMA
XcnL_AT1 (535-828)	ALFGHSLGEY	KTSHAFHSRAID

Deduced specificity:

specify for XcnF_AT2:	Malonyl
specify for XcnF_AT3:	Malonyl (?)
specify for XcnH_AT1:	Malonyl (?)
specify for XcnL_AT1:	Malonyl

Figure S6. Detailed sequence analysis of acyltransferase domains in xenocoumacin biosynthesis gene cluster.[10,11]

	NADP(H) binding motif	
Consensus	**GxGxxGxxxA**	**aSRrG**
XcnF_KR2 (1705-1902)	GLGDLGLLFAEY	VILSGRRELP
XcnH_KR1 (1126-1312)	GRGFIGHTFSQY	LVISSRSKYE
XcnL_KR1 (1117-1309)	GLGGIGLTLAES	LVLSSRSKFP

	Type A/B	Arg binding motif
Consensus	**LDD**	**PxxxN**
XcnF_KR2 (1705-1902)	AGVTEGDS	LGGLSFSAYS
XcnH_KR1 (1126-1312)	LAGLTDDA	LGGVGFYAYA
XcnL_KR1 (1117-1309)	AGSDAGAL	YGAYGQSAYV

Figure S7. Detailed sequence analysis of ketoreductase domains in xenocoumacin biosynthesis gene cluster.[7,12]

	Core C1	Core C2	Core C3 (His)
Consensus	**SxAQxRLYL**	**RHExLRTxF**	**HHxxxDGWS**
XcnA_C2 (1576-2018)	ATPQANGLLFH	SQPALRSIFVW	HHILMDGWS
XcnH_C1 (1480-1905)	SSGQRRLYLQQ	RHDSLRTSFVL	HHIISDGLS
XcnA_C1 (1-467)	SRSQQAVFKME	SMDIFHIGFET	HHAAMDGEG

	Core C4	Core C5
Consensus	**YxDYAVW**	**IGxFVNTL**
XcnA_C2 (1576-2018)	NYSQQLWQG	LGLFINTVP
XcnH_C1 (1480-1905)	YKDYTVWQQ	IGMFVNLLP
XcnA_C1 (1-467)	AEGEQNYEN	AAMAVAPVL

Figure S8. Detailed sequence analysis of condensation domains in xenocoumacin biosynthesis gene cluster.[3,13]

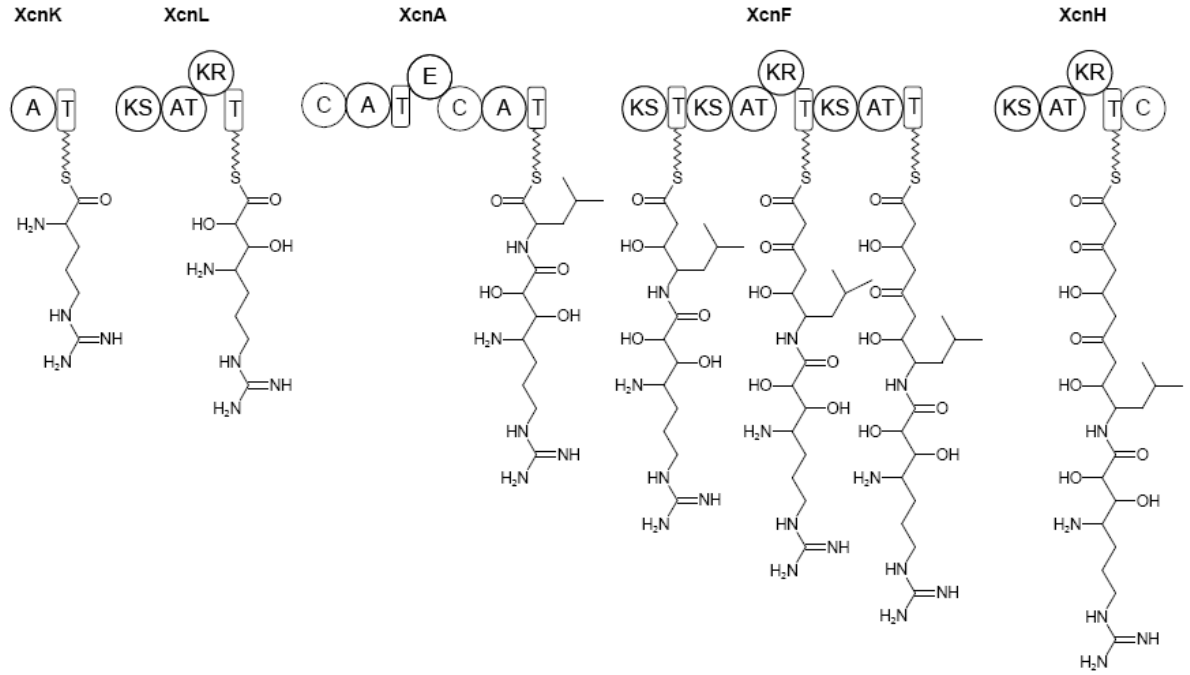

Figure S9. Proposed biosynthesis pathway for the formation of the polyketide/ peptide backbone of XCNI (**1**).

References

[1] E. A. B. Emmert, A. K. Klimowicz, M. G. Thomas, J. Handelsman. *Appl. Environ. Microbiol.* **2004**, *70*, 104-113.

[2] Y. A. Chan, M. T. Boyne, A. M. Podevels, A. K. Klimowicz, J. Handelsman, N. L. Kelleher, M. G. Thomas. *Proc. Natl. Acad. Sci. USA* **2006**, *103*, 14349-14354.

[3] D. Konz, M. A. Marahiel. *Chem. Biol.* **1999**, *6*, R39-R48.

[4] J. Ishikawa, K. Hotta. *FEMS Microbiol. Lett.* **1999**, *174*, 251-253.

[5] T. Stachelhaus, H. D. Mootz, M. A. Marahiel. *Chem. Biol.* **1999**, *6*, 493-505.

[6] G. L. Challis, J. Ravel, C. A. Townsend. *Chem. Biol.* **2000**, *7*, 211-224.

[7] L. Tang, Y. J. Yoon, C. Y. Choi, C. R. Hutchinson. *Gene* **1998**, *216*, 255-265.

[8] S. Donadio, M. J. Staver, J. B. McAlpine, S. J. Swanson, L. Katz. *Science* **1991**, *252*, 675-679.

[9] W. Huang, J. Jia, P. Edwards, K. Dehesh, G. Schneider, Y. Lindqvist. *EMBO J.* **1998**, *17*, 1183-1191.

[10] F. Del Vecchio, H. Petkovic, S. G. Kendrew, L. Low, B. Wilkinson, R. Lill, J. Cortes, B. A. Rudd, J. Staunton, P. F. Leadlay. *J. Ind. Microbiol. Biotechnol.* **2003**, *30*, 489-494.

[11] S. F. Haydock, J. F. Aparicio, I. Molnar, T. Schwecke, A. König, A. F. A. Marsden, I. S. Galloway, J. Staunton, P. F. Leadley. *FEBS Lett.* **1995**, *374*, 246-248.

[12] P. Caffrey. *ChemBioChem* **2003**, *4*, 654-657.

[13] T. A. Keating, C. G. Marshall, C. T. Walsh, A. E. Keating. *Nat. Struct. Biol.* **2002**, *9*, 522-526.

Chapter 2

Genetic analysis of xenocoumacin antibiotic production in the mutualistic bacterium *Xenorhabdus nematophila*

Dongjin Park, Kristin Ciezki, Ransome van der Hoeven, Swati Singh, Daniela Reimer, Helge B. Bode and Steven Forst

The article has been published in
Molecular Microbiology, Vol.73, Issue 5, 2009, pp 938-949

Author's effort

The author performed the quantification of xenocoumacin 1 and 2 production in wild type and mutant strains and wrote the respective parts in the manuscript together with Helge B. Bode. All other experiments were performed by the group of Steven Forst.

Genetic analysis of xenocoumacin antibiotic production in the mutualistic bacterium *Xenorhabdus nematophila*

Dongjin Park,[a] Kristin Ciezki,[b] Ransome van der Hoeven,[a] Swati Singh,[a] Daniela Reimer,[b] Helge B. Bode[b] and Steven Forst[a]

[a] *Department of Biological Sciences, University of Wisconsin, Milwaukee, WI 53201, USA*

[b] *Molekulare Biotechnologie, Institut für Molekulare Biowissenschaften, Goethe Universität Frankfurt, Frankfurt, Germany*

Summary

Xenocoumacin 1 (Xcn1) and xenocoumacin 2 (Xcn2) are the major antimicrobial compounds produced by *Xenorhabdus nematophila*. To study the role of Xcn1 and Xcn2 in the life cycle of *X. nematophila* the 14 gene cluster (*xcnA–N*) required for their synthesis was identified. Overlap RT-PCR analysis identified six major *xcn* transcripts. Individual inactivation of the nonribosomal peptide synthetase genes, *xcnA* and *xcnK*, and polyketide synthetase genes, *xcnF*, *xcnH* and *xcnL*, eliminated Xcn1 production. Xcn1 levels and expression of *xcnA–L* were increased in an *ompR* strain while Xcn2 levels and *xcnMN* expression were reduced. Xcn1 production was also increased in a strain lacking acetyl-phosphate that can donate phosphate groups to OmpR. Together these findings suggest that OmpR-phosphate negatively regulates *xcnA–L* gene expression while positively regulating *xcnMN* expression. HPLC-MS analysis revealed that Xcn1 was produced first and was subsequently converted to Xcn2. Inactivation of *xcnM* and *xcnN* eliminated conversion of Xcn1 to Xcn2 resulting in elevated Xcn1 production. The viability of the *xcnM* strain was reduced 20-fold relative to the wild type strain supporting the idea that conversion of Xcn1 to Xcn2 provides a mechanism to avoid self-toxicity. Interestingly, inactivation of *ompR* enhanced cell viability during prolonged culturing.

Introduction

Xenorhabdus nematophila, a member of the family *Enterobacteriaceae*, engages in a mutualistic association with the entomopathogenic nematode *Steinernema carpocapsae* and is also pathogenic towards different insect hosts (Poinar, 1979; Forst and Clarke, 2002; Herbert and Goodrich-Blair, 2007; Snyder *et al*., 2007). *X. nematophila* is transmitted by the infective juvenile stage (IJ) of the nematode into an insect host through natural openings such as the mouth or anus. The bacterial–nematode complex invades the insect's body cavity (haemocoel) and kills the host. The nematode subsequently reproduces in the haemocoel feeding on both *X. nematophila* and the nutrients derived from insect sources. With the depletion of nutrient supplies the nematodes develop into the IJ stage, which is colonized by its *Xenorhabdus* partner. The IJs emerge from the insect cadaver into the soil where they search for a new insect host.

As the IJ penetrates the intestinal wall to gain access to the nutrient-rich hemolymph microbial competitors derived from the insect gut enter the haemocoel (Isaacson and Webster, 2002; Walsh and Webster, 2003; Gouge and Snyder, 2006; van der Hoeven *et al*., 2008). Saprophytic microbes from the soil as well as bacteria adhering to the cuticle of the nematode represent other potential sources of competitors that can grow within the insect cadaver. It was recently shown that bacteria present in the insect gut appeared in the hemolymph soon after nematode invasion (Gouge and Snyder, 2006). These competitors were eliminated as *X. nematophila* became the dominant microbial species in the hemolymph.

To successfully compete for nutrient resources of the insect *X. nematophila* produces several water-soluble and non-polar antimicrobial compounds (Paul *et al*., 1981; Akhurst, 1982; McInerney *et al*., 1991; Sundar and Chang, 1993; Li *et al*., 1997; Webster *et al*., 2002), phage-derived bacteriocins (Thaler *et al*., 1995) and colicin E3-type killer proteins (Singh and Banerjee, 2008). The water-soluble peptide antimicrobial compounds, xenocoumacin 1 (Xcn1) and xenocoumacin 2 (Xcn2), are the major antibiotics produced in broth culture by *X. nematophila* strain All (McInerney *et al*., 1991). Both Xcn1 and Xcn2 were also shown to be produced in the haemocoel of *Xenorhabdus*-infected insect cadavers (Maxwell *et al*., 1994). Xcn1 is active against Gram-positive and Gram-negative bacteria and several fungal species while Xcn2 is less active against the bacteria and inactive towards the fungal species examined (McInerney *et al*., 1991).

Xcn1 and Xcn2 are composed of an arginine residue, a leucine residue and four acetate units creating a benzopyran-1-one (isocoumarin) ring structure (McInerney *et al*., 1991; Fig. 1A). As the xenocoumacins are hybrids of amino and carboxylic acid moieties, nonribosomal peptide synthetases (NRPSs) and polyketide synthtases (PKSs) (Crosa and Walsh, 2002; Finking and Marahiel, 2004) are most likely involved in their biosynthesis. These large enzyme complexes were originally found in *Bacillus* and *Streptomyces* species that are known for the production of a diverse array of secondary metabolites. Several other genera including Gram-negative bacteria such as *Burkholderia*, pseudomonads and myxobacteria have also been shown to be rich in these enzymes as can be deduced

from various genome sequencing projects. In contrast, NRPS and PKS enzymes in the Enterobacteriaceae are more often involved in the production of iron chelating siderophores and not in the biosynthesis of antibiotic compounds (Crosa and Walsh, 2002). Recently, a vibriobactin-like siderophore (photobactin) and a cytotoxic NRPS-derived peptide have been characterized in *Photorhabdus* species, the sister taxa to *Xenorhabdus* (Ciche *et al*., 2003; Waterfield *et al*., 2008).

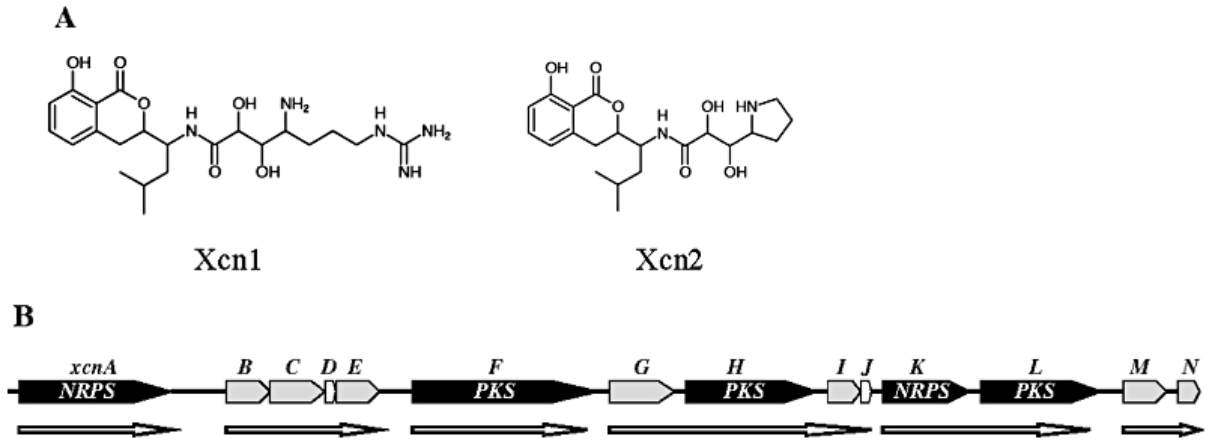

Figure 1. A. Structures of Xcn1 and Xcn2 (from McInerney *et al*., 1991). Xcn1 and Xcn2 are benzopyran structures derived from acetate units, a leucine residue and an arginine residue. Xcn1 contains a guanidinium group of arginine while this group is absent in Xcn2. B. Characterization of xenocoumacin cluster. Operon organization of the 14 *xcn* genes (*xcnA–N*) involved in Xcn1 and Xcn2 synthesis. NRPS and PKS genes are shown in black (see Table S1). Other annotated *xcn* genes are shown as grey boxes and unannotated genes are shown as white boxes. Six major transcriptional units identified by overlap RT-PCR are indicated by open arrows underneath the genes.

While antimicrobial compounds have been extensively used as therapeutic agents their role in the natural biology of the microbe producing them is not well understood. Although some of these compounds are clearly made to kill competitors, there is increasing evidence that some compounds might also serve as signalling molecules (Yim *et al*., 2007). The major antimicrobial compound, isopropylstilbene, produced by *Photorhabdus luminescens*, was shown to inhibit insect immune responses and also serve as a developmental signal for the infective juvenile nematode partner (Eleftherianos *et al*., 2006; Joyce *et al*., 2008). In this respect, insect–nematode–bacterial tripartite associations such as those involving *Xenorhabdus* species provide attractive systems for both discovery of new natural products and identification of novel compounds involved in interkingdom signalling.

During the investigation of the role of the master flagella regulator, FlhDC, in the co-ordinate regulation of motility, exoenzyme and antibiotic reproduction in *X. nematophila* we found that antibiotic production and expression of a NRPS gene (*xcnA*) located adjacent to a cluster of flagellar

genes were elevated by inactivation of either the response regulator gene, *ompR*, or the cognate histidine kinase gene, *envZ* (Park and Forst, 2006). Since xenocoumacin is the major antibiotic produced by *X. nematophila* these findings suggested that the NRPS encoded by *xcnA* may be involved in xenocoumacin synthesis. OmpR is a global response regulator involved in the regulation of outer membrane porin genes, various transporters, virulence genes, flagella and curli fibres (Mattison *et al*., 2002; Feng *et al*., 2003; Goh *et al*., 2004; Jubelin *et al*., 2005; Park and Forst, 2006; van der Hoeven and Forst, 2009).

Recent results from detailed feeding experiments revealed that the pyrrolidine ring of Xcn2 is formed from the guanidinium moiety of Xcn1 (Reimer *et al*., 2009). Initial genetic analysis also identified two NRPS genes (*xcnA* and *xcnK*) required for production of Xcn1 and two genes (*xcnM* and *xcnN*) involved in the conversion of Xcn1 to Xcn2 (Reimer *et al*., 2009). In the present study we show that individual inactivation of three PKS genes (*xcnF, xcnH* and *xcnL*) as well as the two NRPS genes *xcnA* and *xcnK* eliminated xenocoumacin synthesis and dramatically reduced total antibiotic activity. In contrast, inactivation of *xcnM* markedly increased Xcn1 production, eliminated Xcn2 production and reduced cell viability 20-fold suggesting that conversion of Xcn1 to Xcn2 provides a mechanism to avoid self-toxicity. The *xcn* genes were expressed on several separate monocistronic and polycistronic mRNA species. OmpR-phosphate was shown to negatively regulate *xcnA–L* and Xcn1 synthesis during exponential growth and positively regulate the conversion of Xcn1 to Xcn2 later in the growth phase. These findings represent the first example of regulation of secondary metabolism genes by OmpR.

Results

Identification of genes involved in xenocoumacin production. Xcn1 and Xcn2 (Fig. 1A) are major antibiotics produced by *X. nematophila* in broth culture (McInerney *et al*., 1991) and in insects (Maxwell *et al*., 1994). The NRPS gene, *xcnA*, previously designated *nrps1*, was shown to be highly expressed in an *ompR* strain that displayed a high level of antibiotic activity (Park and Forst, 2006). The genome of *X. nematophila* has been recently sequenced (http://www.genoscope.cns.fr/agc/mage/) allowing us to locate *xcnA* in a 39 kb region containing 14 genes (Fig. 1B and Table S1). Based on activities of characterized enzymes the 39 kb region contains two NRPS genes (*xcnA* and *xcnK*), three PKS genes (*xcnF, xcnH* and *xcnL*), three genes encoding enzymes predicted to be involved in hydroxymalonyl CoA synthesis (*xcnBCE*), a gene encoding a type II thioesterase (*xcnI*) that may be involved in clearing intermediates from misprimed NRPS and PKS enzymes and genes annotated as β-lactamase (*xcnG*), saccharopine dehydrogenase (*xcnM*) and fatty acid desaturase (*xcnN*). The *xcnD* and *xcnJ* genes are predicted to encode small proteins, 85 and 107 residues, respectively, of unknown function.

Distance tree analysis revealed that the closest orthologue of *xcnA* was found in a γ-proteobacterium (Table S1), the same taxonomic group as *X. nematophila*. The other *xcn* genes were

orthologous to genes from different phylogenetic lineages; *xcnB–L* (Firmicutes), *xcnM* (cyanobacteria) and *xcnN* (β-proteobacteria). The GC content of *xcnA* is 46%, the same as the *X. nematophila* genome, while the GC content for the *xcnB–N* genes ranges between 31% and 42% (Table S1). These findings suggest that the *xcnB–N* cluster is a mosaic of genes that *X. nematophila* acquired by lateral transfer.

Analysis of* xcn *gene expression. RT-PCR analysis was performed to assess whether all of the *xcn* genes were expressed in cells grown under LB broth conditions. Figure 2 shows that all *xcn* analysed were expressed under these conditions. To address the question of whether the *xcn* genes were encoded on a single polycistronic mRNA or several independently transcribed mRNAs, primers designed to span the region between the 3′ end of the upstream gene and the 5′ end of the adjacent downstream gene were used for RT-PCR analysis (Fig. 3). Prominent RT-PCR products were obtained for the *xcnB–C* and *xcnC–E* primer pairs indicating that a major polycistronic transcript was present for *xcnBCDE*. Prominent RT-PCR products were also obtained for the *xcnG–H* and *xcnH–I* primer pairs, the *xcnK–L* primer pair and *xcnM–N* primer pair. In contrast, RT-PCR products were barely detectable for the *xcnE–F* and *xcnF–G* primer pairs suggesting that *xcnF* is expressed as a monocistronic mRNA. Similarly, the RT-PCR product generated with the *xcnA–B* primer pair was present at very low levels suggesting that *xcnA* was predominantly expressed as a monocistronic mRNA. A transcript spanning *xcnL–M* was also detectable at low levels. Thus, it appears that the *xcn* cluster is expressed on several separate monocistronic and polycistronic mRNA species that encode different regions of the *xcn* cluster (Fig. 1B).

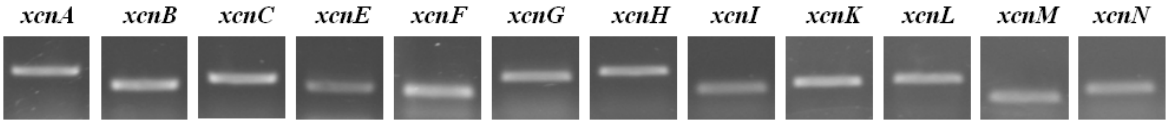

Figure 2. Analysis of *xcn* gene expression in the wild type strain. The transcript level of each *xcn* gene was determined by RT-PCR.

Insertional inactivation of* xcn *genes. To determine whether the *xcn* genes encoding NRPSs (*xcnA* and *xcnK*) and PKSs (*xcnF*, *xcnH* and *xcnL*) were involved in xenocoumacin production each of the five genes was disrupted by insertional inactivation. HPLC-MS analysis of cell-free culture supernatants revealed that Xcn1 and Xcn2 were not produced in any of the mutant strains (Fig. S1). Antibiotic activity was assessed using an overlay plate assay with *Micrococcus luteus* as the indicator strain (Fig. 4). All five *xcn* strains displayed a dramatic decrease in antibiotic activity relative to the parent strain. Residual antibiotic activity was presumably due to the production of non-xenocoumacin antibiotics. Furthermore, inactivation of *xcnB*, the first gene in the operon involved in the synthesis of hydroxymalonyl CoA, dramatically reduced antibiotic production (Fig. 4). Inactivation of *xcnI*

minimally affected antibiotic production indicating that the thioesterase encoded by *xcnI* was not required for cleavage of the final product from the enzyme complex (Fig. 4).

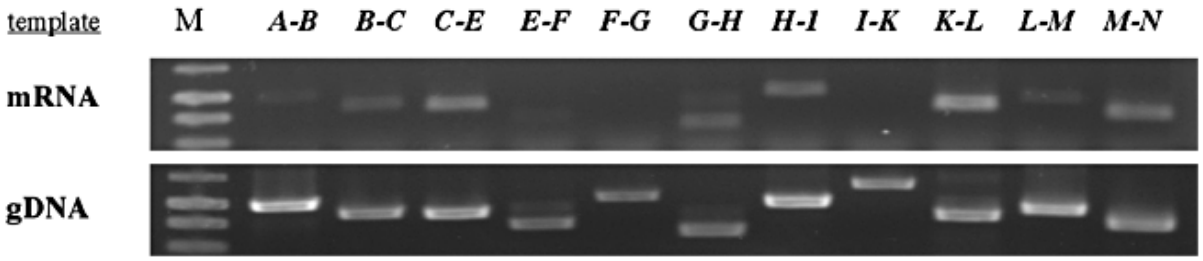

Figure 3. Analysis of transcriptional units in the *xcn* gene cluster by overlap RT-PCR. Primers were designed to span the intergenic region between two adjacent genes. The top gel shows RT-PCR product for each of the overlap primer sets. Control PCR products using *X. nematophila* genomic DNA as a template are shown below each RT-PCR reaction.

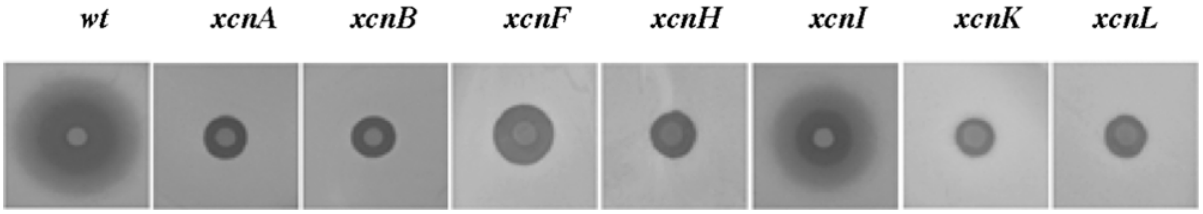

Figure 4. Antibiotic activities of wild type and *xcn*::Cm strains. Xcn activity was analysed in the respective *xcn*::Cm mutant strains by an overlay assay using *Micrococcus luteus* as the indicator. Activity is visible as zones of inhibition surrounding the colonies of the various *xcn* mutant strains.

The finding that *xcnA* and *xcnF* were primarily expressed as monocistronic mRNAs predicted that inactivation of these genes would not be polar on adjacent downstream genes. As expected, xcnB and *xcnG* were expressed in the *xcnA*::Cm and *xcnF*::Cm strains respectively (Fig. 5). In contrast, inactivation of *xcnH* in an operon of *xcnGHIJ* was polar on *xcnI*. Since antibiotic production was minimally affected in the *xcnI* strain absence of Xcn production in the *xcnH* mutant was due to inactivation of *xcnH* rather than a polar effect on *xcnI*. Inactivation of *xcnI* was not polar on *xcnK* as predicted by the overlap RT-PCR results. Finally, *xcnL* transcripts were detected in the *xcnK* strain suggesting that an internal promoter may be located in the 104 bp *xcnK–L* intergenic region and that the absence of Xcn1 production in the *xcnK* strain was likely due to the loss of the NRPS encode by *xcnK* rather than a polar effect on *xcnL*. Together, these findings indicate that NRPS and PKS genes of the *xcn* cluster as well as *xcnBCDE* are necessary for Xcn1 production and that xenocoumacin was the major antibiotic activity detected in the overlay assay.

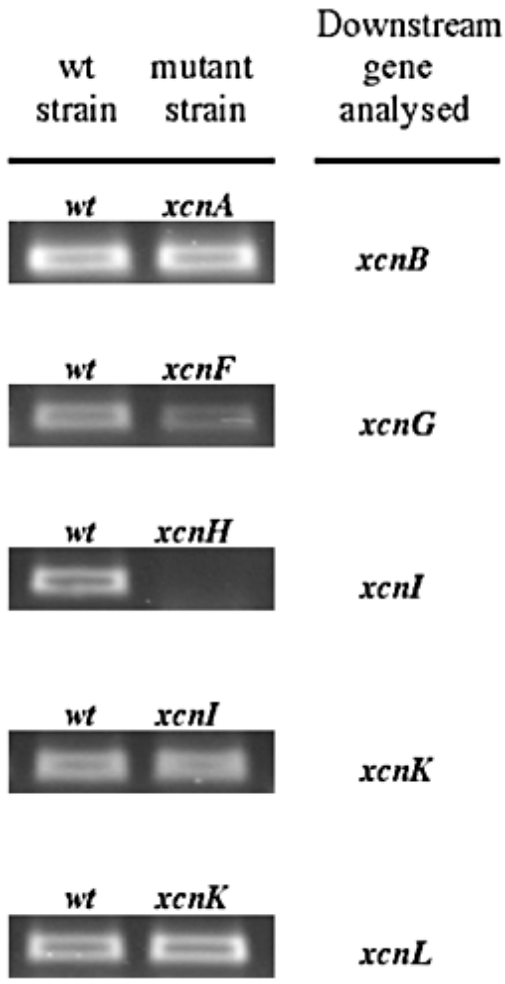

Figure 5. RT-PCR analysis of polar effects on downstream *xcn* genes. The mutant strain from which the RNA was derived is shown on the top of each panel. The downstream gene that was analysed is identified on the right side of the panel.

Analysis of Xcn1 and Xcn2 production. While the levels of Xcn1 and Xcn2 were determined previously in 48 h broth cultures (McInerney *et al*., 1991) their production during earlier stages of growth had not been studied. Furthermore, whether Xcn1 and Xcn2 were produced sequentially or simultaneously remained unknown. An HPLC-MS approach was taken to assess the temporal production of Xcn1 and Xcn2. In the wild type strain, Xcn1 levels were detectable during exponential growth (6 h), increased twofold during early stationary phase (12 h) and increased slightly (1.3-fold) during late stationary (24 h) phase (Table 1). In contrast, Xcn2 levels were barely detectable during exponential growth (6 h), increased ~10-fold during early stationary phase (12 h) and continued to increase (sixfold) during late stationary phase (24 h). These findings were consistent with the hypothesis that Xcn1 was produced initially and subsequently converted to Xcn2 later in the growth phase.

XcnMN is required for conversion of Xcn1 to Xcn2. During analysis of *xcn* genes we found that inactivation of *xcnM* and *xcnN* resulted in a marked increase in antibiotic activity (Fig. 6). In addition, quantitative RT-PCR (qRT-PCR) analysis of the expression of *xcnN* as a function of growth showed elevated expression during transition-phase and stationary-phase growth (D. Park, unpubl. data). To elucidate the role of *xcnMN* in Xcn1 and Xcn2 production culture supernatants of the *xcnM* strain were analysed by HPLC-MS. Xcn1 was produced at significantly higher levels than the wild type strain during stationary phase and Xcn2 was not produced in the *xcnM* strain (Table 1). These findings support the idea that the *xcnA–L* genes are responsible for Xcn1 production early in growth and the *xcnMN* genes are required for the subsequent conversion of Xcn1 to Xcn2. These findings also suggest that Xcn1 is the predominant antibiotic activity measured in overlay assay.

Table 1. Xcn1 and Xcn2 production in wild type, *xcnM* and *ompR* strains.

Strain	Time (h)	OD	Xcn1 Arbitrary units OD^{-1}	Xcn2 Arbitrary units OD^{-1}
wt	6	1.09	3.76 (0.58)	0.38 (0.12)
	12	5.81	7.66 (0.61)	3.11 (0.16)
	24	9.64	10.33 (1.82)	19.47 (3.12)
	48	8.58	8.82 (0.30)	15.47 (0.83)
xcnM	6	1.50	1.79 (0.68)	0.01 (0.01)
	12	6.63	10.0 (0.30)	0.03 (0.03)
	24	7.50	13.5 (1.52)	0.05 (0.01)
	48	5.97	16.7 (1.33)	0.26 (0.21)
ompR	6	1.00	7.36 (1.15)	0.19 (0)
	12	6.11	17.70 (1.45)	3.14 (0.31)
	24	8.59	23.00 (4.40)	5.11 (0.99)
	48	8.26	28.41 (4.45)	4.92 (0.76)

Experiments were performed in triplicate. Values represent mean and standard deviation in parentheses.

Increased production of Xcn1 in the* ompR *strain. The increased antibiotic activity of the *ompR* strain (Fig. 6; Park and Forst, 2006) suggested that Xcn1 was produced at elevated levels in this strain. To address this possibility Xcn1 and Xcn2 production in the *ompR* strain was measured by HPLC-MS. Xcn1 production was twofold higher during exponential growth (6 h) and 3.3-fold higher at 48 h in the *ompR* strain relative to the parent strain (Table 1). Xcn2 production was barely detectable during exponential growth and remained at significantly reduced levels relative to the parent strain over the 48 h growth period suggesting a lower rate of Xcn1 to Xcn2 conversion in the *ompR* strain.

We had previously shown that *xcnA* expression was elevated in the *ompR* strain grown for 6 h on 0.8% LB agar (Park and Forst, 2006). These conditions were found to be optimal for detection of negative regulation of *xcnA* by OmpR. To further analyse the role of OmpR in xenocoumacin production *xcn* transcript levels were compared in the parent and *ompR* strains grown on agar. RT-PCR analysis revealed that the level of mRNA for the *xcnA*–xcnL genes was significantly higher in the *ompR* strain (Fig. 7A). To assess the regulation of *xcnM* and *xcnN* by OmpR total RNA was extracted from cells grown to late exponential phase under standard LB broth conditions. RT-PCR analysis revealed that both *xcnM* and *xcnN* were expressed at lower levels in the *ompR* strain (Fig. 7B) suggesting these genes are either directly or indirectly positively regulated by OmpR. These finding were supported by qRT-PCR analysis showing that *xcnA* expression increased 64% while *xcnM* and *xcnN* expression decreased 1.9- and 2.5-fold, respectively, in the *ompR* strain (Table 2). Thus, the 3.3-fold increase in Xcn1 production in the *ompR* strain was likely due to the combined effect of elevated expression of the *xcnA–L* genes and reduced *xcnMN* expression.

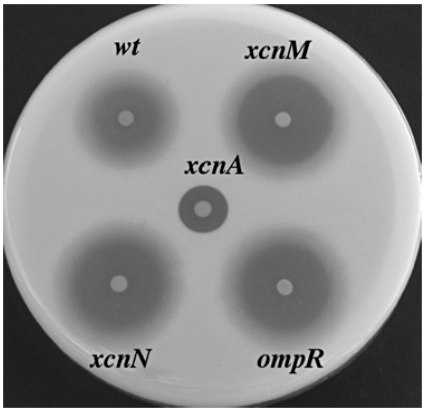

Figure 6. Antibiotic activities of the *xcnM*, *xcnN* and *ompR* strains. Xcn activity was analysed by an overlay assay using *Micrococcus luteus* as the indicator. Activity is visible as zones of inhibition surrounding the colonies of the various *xcn*::Cm mutant strains.

Role of OmpR-phosphate in* xcn *gene regulation. Antibiotic production was previously shown to be elevated in an *envZ* strain of *X. nematophila* (Park and Forst, 2006). Since EnvZ is the cognate histidine kinase that phosphorylates OmpR these findings suggested that OmpR-phosphate negatively regulates the *xcnA–L* genes. OmpR can also be phosphorylated by the small-molecular-weight phosphodonor, acetyl-phosphate (Shin and Park, 1995). Acetyl-phosphate is synthesized from acetyl-CoA and inorganic phosphate by phosphotransacetylase encoded by the *pta* gene and is converted to acetate and ATP by acetyl kinase encoded by *ackA*. Acetyl-phosphate levels can increase up to fivefold in an *ackA* strain and are eliminated in an *ackA-pta* strain (Klein *et al*., 2007; Keating *et al*., 2008). To assess the effect of acetyl-phosphate on the regulation of antibiotic production *ackA* and *ackA-pta* deletion strains were constructed. The zone of inhibition in the overlay assay was reduced in the *ackA* strain (20 mm) relative to the wild type strain (28 mm). Conversely, the zone of inhibition was elevated in the *ackA-pta* strain (32 mm) which lacks acetyl-phosphate. These findings are consistent with the hypothesis that acetyl-phosphate can donate phosphate to OmpR (Wolfe, 2005) and supports the idea that OmpR-phosphate negatively regulates Xcn1 production.

The* xcnM *strain displays reduced viability during prolonged growth. The above findings raised the question of the biological relevance of the conversion of Xcn1 to Xcn2. It was shown previously that Xcn1 was a more potent antibiotic than Xcn2 (McInerney *et al*., 1991). We considered the possibility that high concentrations of Xcn1 may negatively affect viability and induce self-toxicity. To assess this possibility we compared the growth rate, final cell density and viability during prolonged growth of the wild type and *xcnM* strains. The growth rate and final cell density of the *xcnM* strain after 18 h were indistinguishable from that of the wild type strain (data not shown). To assess whether prolonged incubation affected cell viability cultures were monitored over a 72 h time-course. The Cell viability of the *xcnM* strain incubated for 24 and 48 h was not significantly different from the wild type strain (Fig. 8A). However, after 60 h viability of the *xcnM* strain was 30% that of the wild type strain. At 72 h viability of the *xcnM* strain was reduced more than 20-fold relative to the wild type strain. In contrast, the cell viability of the *xcnA* strain during prolonged growth was not significantly different from the wild type strain (D. Park, S. Singh and S. Forst, unpubl. data). These findings suggested that

X. nematophila was sensitive to the higher levels of Xcn1 produced in the *xcnM* strain and that the conversion of Xcn1 to Xcn2 provides a mechanism to avoid self-toxicity.

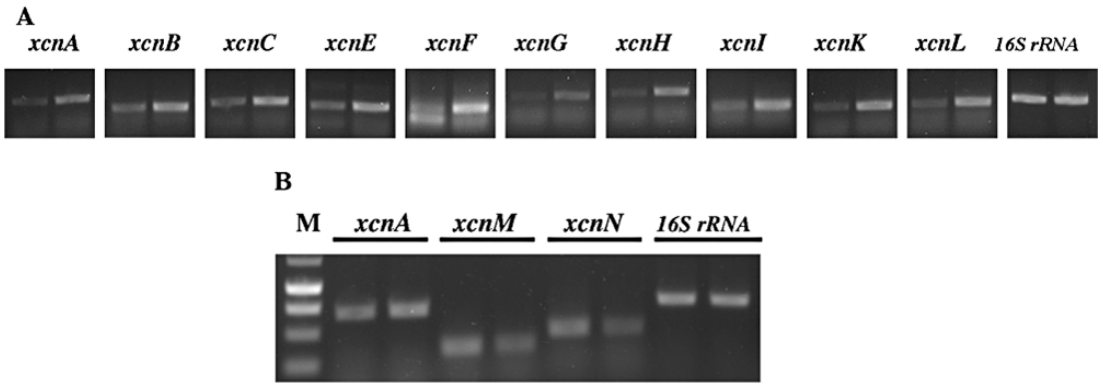

Figure 7. A. RT-PCR analysis of *xcn* genes in wild type and *ompR* strains. Total RNA was obtained from the wild type and *ompR* strains grown for 6 h on 0.8% LB agar plates. RT-PCR products from the wild type and *ompR* strains for each *xcn* gene are shown in the first and second lane respectively. B. RT-PCR analysis of *xcnM* and *xcnN* in the *ompR* strain. Total RNA was obtained from the wild type and *ompR* strains during exponential growth in LB broth. RT-PCR products from the wild type and *ompR* strains for each *xcn* gene are shown in the first and second lane respectively.

Table 2. *xcnA*, *xcnM* and *xcnN* expression in wild type and *ompR* strains.

	Ct		
Gene	***wt***	***ompR***	**Fold change (*ompR/wt*)**
xcnA	3.99 (0.22)[a]	3.28 (0.19)	1.64 (0.06)
xcnM	3.46 (0.25)	4.39 (0.09)	0.54 (0.08)
xcnN	2.62 (0.14)	3.92 (0.24)	0.39 (0.09)

a. Values represent mean and standard error in parentheses.

The *ompR* strain also produced high levels of Xcn1 but unlike the *xcnM* strain, still produced some Xcn2. To further address the question of whether elevated Xcn1 production affected viability, the *ompR* strain was cultured for 72 h as above. To assess the viability of a strain that produced elevated levels of Xcn1 but no Xcn2 an *xcnM-ompR* strain was constructed. During the first 48 h of culturing the viability of the *ompR* and *xcnM-ompR* strains was closely similar to the wild type strain (data not shown). By 60 h the viability of the *xcnM* strain had decreased 75% while the viability of both the *ompR* and *xcnM-ompR* strains was similar to the wild type strain (Fig. 8B). These differences were more dramatic at 72 h at which time the viability of the *xcnM* strain was 7% of the wild type strain while the viability of the *ompR* and *xcnM-ompR* strains was approximately 14-fold and 10-fold

greater than the wild type strain respectively. Thus, inactivation of *ompR* rescued the reduced viability of the *xcnM* strain and generally enhanced the viability of *X. nematophila* during prolonged culturing.

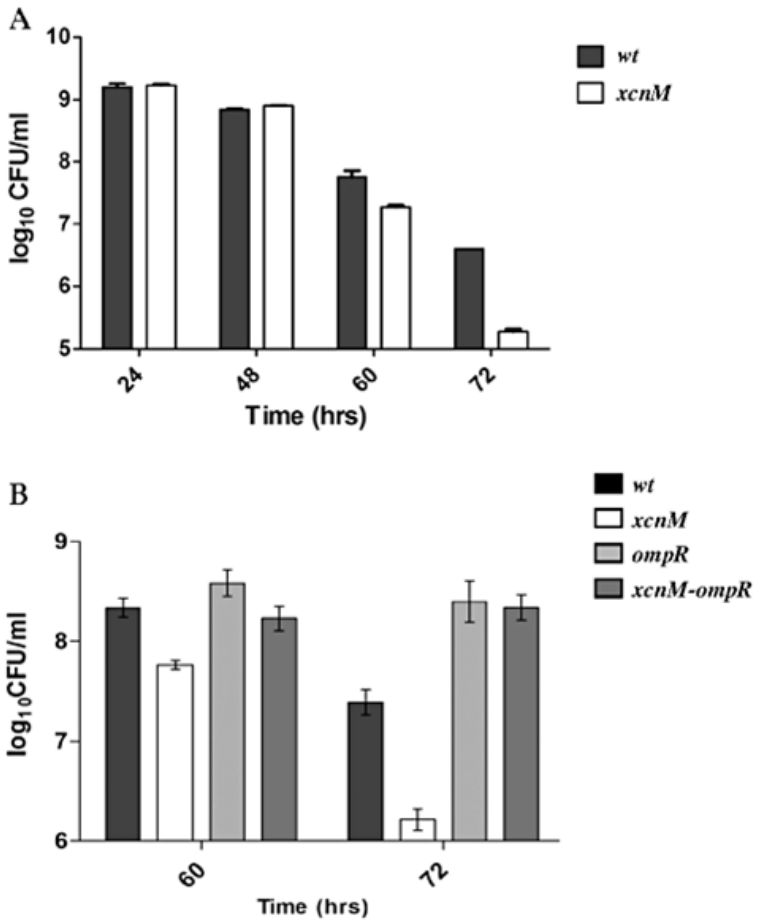

Figure 8. A. Comparison of cell viability of the wild type and *xcnM* strains during prolonged growth. The wild type strain (black bar) and *xcnM* strain (white bar) were grown in LB broth and cell viability as measured by colony-forming units (cfu) was determined in triplicate at the indicated time points. Regression analysis of the slopes derived from the 48, 60 and 72 h data indicated a significant difference (*P*-value < 0.001) between the wild type and *xcnM* strains. B. Comparison of cell viability of the wild type, *xcnM*, *ompR* and *xcnMompR* strains during prolonged growth. The wild type (black bar), *xcnM* (white bar), *ompR* (light grey bar) and *xcnMompR* (dark grey bar) strains were grown in LB broth and cell viability as measured by colony-forming units (cfu) was determined in triplicate at the indicated time points.

Discussion

To better understand the role of xenocoumacin in the life cycle of *X. nematophila* we identified and genetically analysed the 14 gene *xcn* cluster required for Xcn1 and Xcn2 synthesis. Inactivation of *xcnA*, *xcnK*, *xcnF* and *xcnL* eliminated production of Xcn1 and was not polar on downstream genes. Xcn1 production was also eliminated by disruption of *xcnH* that was polar on the downstream gene, *xcnI*. However, *xcnI* encodes a type II thioesterase that was not required for Xcn1 production. In addition, Xcn1 production was eliminated by inactivation of *xcnB* involved in the synthesis of

hydroxymalonyl CoA. In contrast, Xcn1 levels increased and Xcn2 production was eliminated in the *xcnM* strain. Similarly, Xcn1 production was increased in the *xcnN* strain. Together, these findings indicate that the *xcnA*, *B*, *F*, *H*, *K* and *L* genes are involved in the synthesis of Xcn1 while *xcnMN* are involved in the conversion of Xcn1 to Xcn2.

Overlap RT-PCR analysis revealed that six separate *xcn* transcripts and other minor transcripts were produced during late exponential growth. This transcriptional organization is distinct from NRPS–PKS biosynthetic clusters found in other γ-proteobacteria. For example, the pigment–antibiotic compound prodigiosin of *Serratia marcescens*, synthesized by the NRPS–PKS *pig* operon, is encoded on a major polycistronic transcript controlled by a single σ^{70} promoter (Williamson *et al*., 2006).

Xcn1 was shown to be produced at low levels during early exponential growth and increased as cells transitioned to late exponential phase. *xcnA* expression has also been found to increase later in the growth phase (D. Park, unpubl. data). In addition, *xcnA–L* expression was elevated in the *ompR* strain and Xcn1 production was increased in the *ompR*, *envZ* and *ackA-pta* strains while production was decreased in the *ackA* strain. Together, these findings support a model in which OmpR-phosphate either directly or indirectly negatively regulates *xcnA–L* during exponential growth. To further define the transcriptional organization of the *xcn* cluster 5′RACE analysis was carried out. A transcriptional start site and consensus σ^{70} promoter were identified 168 bp upstream of the AUG start codon of *xcnA* while start sites for other transcriptional units could not be established using this approach (D. Park, unpubl. data).

OmpR was previously shown to co-ordinately repress flagella synthesis and exoenzyme production in *X. nematophila* (Park and Forst, 2006) by negatively regulating the *flhDC* operon. FlhDC activates the class II flagella genes that includes *fliAZ* required for both flagellin and exoenzyme gene expression (Givaudan and Lanois, 2000; Park and Forst, 2006; Lanois *et al*., 2008). Unlike these functions, antibiotic production and *xcn* gene expression were not reduced in a *flhC* mutant strain (D. Park, unpubl. data) suggesting that OmpR may directly regulate the *xcn* genes. At present purified *X. nematophila* OmpR is not available to test this possibility. The repression of *xcn* genes in *X. nematophila* would represent the first example of regulation of secondary metabolite production by OmpR. During early stages of infection *X. nematophila* colonizes the connective tissue and musculature surrounding the insect midgut, proliferates and produces virulence factors (Morgan *et al*., 2001; Sicard *et al*., 2005). Co-ordinate repression of energy expensive processes such as flagella synthesis, exoenzyme and antibiotic production may confer an adaptive advantage during early stages of infection.

While OmpR differentially regulates more than 100 genes in *Escherichia coli* (Oshima *et al*., 2002), and controls virulence genes and stationary-phase acid tolerance genes in *Salmonella typhimurium* (Lee *et al*., 2000; Bang *et al*., 2002) it has not been shown to both positively and negatively regulate separate genes within a single biosynthetic cluster. In the present study, OmpR in *X. nematophila* was found to negatively regulate *xcnA–L* and positively regulate *xcnMN* expression.

OmpR usually functions as a repressor when it binds to sequences near the start of transcription and functions as an activator by binding to regions further upstream of the promoter (Feng *et al*., 2003; Goh *et al*., 2004; Rhee *et al*., 2008). One possible mechanism for the differential regulation of the *xcn* gene cluster is that OmpR binds near the start of transcription for the monocistronic and polycistonic mRNAs of the *xcnA–L* cluster and upstream of the promoter for *xcnMN*. Alternatively, OmpR may function indirectly by controlling a repressor that regulates the *xcnA–L* cluster and an activator that controls the expression of *xcnMN*. Purification of active *X. nematophila* OmpR and the mapping of the start of transcription and promoters for the *xcn* gene cluster will allow us to address these questions.

Inactivation of *xcnM* concomitantly elevated production of Xcn1, eliminated Xcn2 production and increased the zone of inhibition in the overlay assay. Together these findings support the idea that the increased antibiotic activity observed in the overlay assay was due to increased Xcn1 production. The contribution of Xcn2 to the antibiotic activity measured in the overlay assay is difficult to assess since it cannot be produced in the absence of Xcn1. Purified Xcn2 is less active than Xcn1 against the bacterial and fungal species tested to date (McInerney *et al*., 1991). The primary structural difference between Xcn1 and Xcn2 is the absence of the guanidinium group and presence of the pyrollidine ring in the latter structure which could effectively decrease its solubility relative to Xcn1. The higher solubility may in part account for higher antibiotic and antifungal activity of Xcn1 and its greater diffusibility in the overlay assay. In addition, Xcn1 may possess a higher intrinsic antimicrobial activity than Xcn2. The temporal regulation of Xcn1, which is produced earlier than Xcn2, together with the differences in the structural properties and biological activities of Xcn1 and Xcn2 suggests these antimicrobial compounds play distinct roles in the life cycle of *X. nematophila*.

Here we show that increased production of Xcn1 in the *xcnM* strain was correlated with a 20-fold loss in viability raising the possibility that elevated Xcn1 levels exceeded a threshold for resistance. This loss of viability of the *xcnM* strain during prolonged growth suggests that the conversion of Xcn1 to Xcn2 provides a mechanism to avoid self-toxicity. During early stages of infection bacteria derived from the insect gut predominate in the hemolymph. As *X. nematophila* proliferate to high levels the competitor population declines (Gouge and Snyder, 2006) presumably as a result of increased Xcn1 production. Thus, Xcn1 and Xcn2 production is balanced between the requirement to produce sufficient concentrations of Xcn1 for suppression of competitors and the need to maintain Xcn1 levels below a threshold of self-toxicity. The differential expression of the *xcnA–L* and the *xcnMN* genes may therefore be part of the adaptive response to optimize fitness during growth in the competitive haemocoelic environment. In addition, we found that inactivation of *ompR* rescued the reduced viability of the *xcnM* strain and enhanced viability of *X. nematophila* during prolonged culturing. Since OmpR positively regulates the outer membrane porins OpnP and OpnS inactivation of *ompR* could enhance viability during prolonged incubation by reducing outer membrane permeability to Xcn1. Alternatively, since OmpR functions as a global regulator, inactivation of *ompR* may alter adaptive responses that affect the sensitivity to Xcn1. Finally, how modulation of OmpR-phosphate

levels controls *xcn* gene expression remains to be determined. The question also arises whether Xcn2 possesses biological functions other than the antimicrobial activity already identified. The insect–nematode–*X. nematophila* model system will allow us to address these questions and help to further our understanding of the role of antimicrobial compounds in interspecies competition and the natural biology of microorganisms.

Experimental procedures

Bacterial strains, media and growth conditions. Strains and plasmids used in this study are listed in Table 3. Cells were routinely grown on Luria–Bertani (LB) broth (1.0% Bacto trypton, 0.5% yeast extract, 0.5% NaCl) supplemented with 0.01 mM $MgSO_4$, by shaking at 150 r.p.m. or on corresponding solid agar media (15 g l^{-1} agar). When required, ampicillin, chloramphenicol and kanamycin were added to a final concentration of 50, 25 and 30 μg ml^{-1} respectively. *X. nematophila* was cultured at 30°C, and *E. coli* was grown at 37°C. Unless otherwise noted, strains were initially grown overnight in 2 ml of LB selective broth, inoculated into 5–10 ml of fresh LB selective media in a 250 ml flask and incubated for desired period. Final bacterial cultures were normalized based on the optical density at 600 nm (OD_{600}) and used for further analysis. Graces insect culture medium (Volgyi *et al*., 1998) was prepared as described by the manufacturer (Gibco).

Construction of the* xcn *mutant strains. To construct mutant strains by insertional inactivation, primers for each gene were designed to amplify a 300–600 bp internal fragment located near the 5′ end of the gene. The amplified products were purified with PCR Clean Kit (Roche) and subsequently blunt end-ligated into the EcoRV site of pSTBlue-1 (Novagen). Ten recombinant colonies were selected and subsequently analysed by colony PCR using a T7 and SP6 primer pair from flanking region of EcoRV site of the vector to confirm the size of the cloned fragment. A colony having the desired plasmid was grown overnight and the recombinant plasmids were purified using spin column (Qiagen). A PstI–XbaI fragment containing either *xcnA*, *xcnB*, *xcnF*, *xcnH*, *xcnI*, *xcnK*, *xcnL*, *xcnM* or *xcnN* was gel-purified and ligated into the conjugal suicide vector pKnock-Cm (Alexeyev, 1999). The resultant plasmids were transformed into *E. coli* S17-*λpir* and conjugally transferred into the wild type strain of *X. nematophila*. In addition, the *xcnM* pKNOCK plasmid was conjugally transferred into the *ompR* deletion strain, ABR2, to create the *xcnMompR* mutant strain. Selection on ampicillin and chloramphenicol identified mutant cells in which the recombinant pKnock-Cm had integrated into the chromosome by single-cross-over homologous recombination. Gene disruption was confirmed by PCR. In addition, the absence of mRNA for the disrupted gene was verified by RT-PCR analysis using primers designed from the coding regions flanking the cloned region of each gene.

Table 3. Bacterial strains and plasmids used in this study

Strain or plasmid	Relevant genotype, phenotype or characteristic(s)	Reference or source
Strains		
X. nematophila		
AN6/1	Wild type, phase I variant; Amp	Laboratory stock
ABR2	AN6/1 *ompR*::Km	Forst & Boylan (2002)
ackA	AN6/1 Δ*ackA*::Km	R. van der Hoeven
ackA-pta	AN6/1 Δ*ackA-pta*::Km	R. van der Hoeven
xcnA::Cm	AN6/1 *xcnA*::Cm	This study
xcnB::Cm	AN6/1 *xcnB*::Cm	This study
xcnF::Cm	AN6/1 *xcnF*::Cm	This study
xcnH::Cm	AN6/1 *xcnH*::Cm	This study
xcnI::Cm	AN6/1 *xcn*I::Cm	This study
xcnK::Cm	AN6/1 *xcnK*::Cm	This study
xcnL::Cm	AN6/1 *xcnL*::Cm	This study
xcnM::Cm	AN6/1 *xcnM*::Cm	This study
xcnN::Cm	AN6/1 *xcnN*::Cm	This study
xcnM-ompR	AN6/1 *xcnM*::Cm *ompR*::Km	This study
E. coli		
XL-1 Blue MRF'	*recA1 endA1 gyrA96 thi-1 hsdR17 supE44 relA1 lac*[F'*proAB lacI*^{q}ZΔM15 Tn*10* (Tet)]	Stratagene
S17-λpir	*recA*, *thi*, *pro*, *hsdR*-M+. RP4-2Tc::Mu Km::Tn*7* in the chromosome	Laboratory stock
Plasmids		
pSTBlue-1	Cloning vector; Amp Km	Novagen
pUC19	Cloning vector; Amp	Laboratory stock
pKnock-Cm	Broad-host-range suicide vector; Cm RP4 *ori*T *ori*R6K	D. Saffarini
pKnock-*xcnA*	Internal fragment of *xcnA* cloned into pKnock-Cm	This study
pKnock-*xcnB*	Internal fragment of *xcnB* cloned into pKnock-Cm	This study
pKnock-*xcnF*	Internal fragment of *xcnF* cloned into pKnock-Cm	This study
pKnock-*xcnH*	Internal fragment of *xcnH* cloned into pKnock-Cm	This study
pKnock-*xcnI*	Internal fragment of *xcnI* cloned into pKnock-Cm	This study
pKnock-*xcnK*	Internal fragment of *xcnK* cloned into pKnock-Cm	This study
pKnock-*xcnL*	Internal fragment of *xcnL* cloned into pKnock-Cm	This study
pKnock-*xcnM*	Internal fragment of *xcnM* cloned into pKnock-Cm	This study
pKnock-*xcnN*	Internal fragment of *xcnN* cloned into pKnock-Cm	This study
pER2	p15A *ori*R6K *sacB* Mob^{+} Gm	D.Saffarini
pER2-Δ*ackA*:Km	*ackA* flaking regions with Km cloned into pER2	This study
pER2-Δ*ackA-pta*:Km	*ackA-pta* flaking regions with Km cloned into pER2	This study

Amp, ampicilin resistance; Km, kanamycin resistance; Cm, chloramphenicol resistance; Tet, tetracycline resistance; Gm, gentamicin resistance.

Construction of* ackA *and* ackA-pta *strains. Primers engineered with restriction sites (SacI and SphI) were used to PCR-amplify chromosomal fragments upstream and downstream of the *ackA* and *ackA-pta* genes. Fragments were cloned along with the kanamycin cassette into the SacI and SphI sites of cloning vector, pUC19. The resulting Δ*ackA*:Km and Δ*ackA-pta*:Km inserts were screened by PCR and cloned into the suicide vector pER2. These plasmids were transformed into *E. coli* S17-*λpir* and conjugally transferred into the wild type strain of *X. nematophila*. Allelic replacements creating Δ*ackA*:Km and Δ*ackA-pta*:Km were confirmed by PCR and RT-PCR using *ackA* and *pta* internal primers.

Overlay assay for antibiotic activity. For measurement of antibiotic activity, *Xenorhabdus* strains were initially grown overnight in 2 ml of LB selective broth, inoculated into 5–10 ml of fresh LB media in a 250 ml flask and incubated for 18–20 h. Final bacterial cultures were normalized based on the OD_{600}. Six-microlitre aliquots of *Xenorhabdus* culture were spotted onto LB agar plate and subsequently incubated for 15–24 h. The bacteria were then exposed to chloroform fumes for 30 min and air dried for 30 min. Five hundred microlitres of an overnight culture of either *M. luteus* or other indicator strains was added to 12 ml of top agar (0.7% agar) which was poured over the bacterial colonies (Akhurst, 1982; Volgyi *et al*., 1998). After incubation overnight, zones of growth inhibition surrounding bacterial colonies were observed. Experiments were performed in triplicates.

Quantification of Xcn1 and Xcn2. For quantification of Xcn1 and Xcn2 the following protocol was used: overnight cultures of all strains grown in LB with the required antibiotics were diluted to an OD_{600} of 0.05 in fresh LB (with antibiotics) in triplicates (10 ml in 50 ml flasks). After 6, 12, 24 and 48 h of cultivation at 30°C and 200 r.p.m., 1 ml of these cultures were taken, centrifuged to remove cells and the supernatant was diluted with MeOH to a final rate of 1:1 or 1:10 (supernatant/MeOH, v/v) following another centrifugation step in order to remove insoluble material. For the determination of Xcn1 and Xcn2 the ions *m/z*$[M+H]^+$ 466.3 and 407.3 were quantified, respectively, using a UPLC system (Themo Scientific) connected to a Nanomate ESI-source (Advion) followed by a LTQ Orbitrap (Thermo Scientific). HPLC separation was performed using an AQUITY RP18 column from Waters (1.7 μm) and a water/acetonitrile gradient (+ 0.1% formic acid) (gradient: 0–14 min, 5–95% acetonitrile, MS: positive mode between 200 and 2000 *m/z*, injection volume: 5 μl).

RNA purification. Standard conditions for isolating total RNA from cells grown in LB medium was as follows: *Xenorhabdus* strains were initially grown overnight in 2 ml of LB selective broth, inoculated into 5–10 ml of fresh LB selective media in a 250 ml flask and incubated to desired cell density. For RT-PCR analysis, exponentially growing cells were used to extract total RNA. To assess the regulation of *xcn* genes by OmpR growth on 0.8% LB agar for 6 h after inoculation was found to be optimal (Park and Forst, 2006). To prepare total RNA from cells grown on 0.8% agar plates, 6 μl of

18 h bacterial broth culture was spotted (~30 spots per plate) on the agar plate and grown for 6 h at 30°C. Bacterial colonies were collected using 2 ml of LB, pelleted and stored at −20°C. Total RNA was extracted with Trizol reagent (Sigma), following the standard protocol. Final RNA pellet was re-suspended with 100 µl of Nuclease-free distilled H_2O. RNA concentration was determined by optical density at 260 nm. Triple measurements were performed for each RNA sample and an average value was obtained as a final concentration. Total RNA was digested with the RNase-free DNase reagent (Promega). This RNA (100 ng μl^{-1} after the DNase digestion) was used in 5′RACE-PCR and RT-PCR. For every RNA preparation, DNA contamination was assessed by performing a control PCR reaction prior to RT-PCR analysis.

RT-PCR and qRT-PCR analysis

RT-PCR was performed using AccessQuick RT-PCR system (Promega). The RT-PCR reaction (25 µl) contained the following components: 300 µg of total RNA, 20 pmol each of forward and reverse primer and 1 unit of reverse transcriptase. cDNA synthesis was conducted at 52°C for 45 min. The following cycle condition was used for PCR reaction: 30 s at 94°C, 30 s at 55°C and 60 s at 72°C for extension. Annealing temperature varied depending on which primer was used. For RT-PCR analysis, 21–23 cycles of PCR reaction was used for all *xcn* genes. For overlap PCR analysis, 25 cycles was used. 16S rDNA was used as the internal control gene to confirm that equal amounts of total RNA was used in each reaction. Primers specific to a single 16S rDNA gene was used in this study to increase the sensitivity and 18 cycles of PCR reaction were performed. For the analysis of polarity effects, RNA was obtained from strains in which *xcn* genes were inactivated and primers internal to the downstream gene were used to assess expression by RT-PCR.

Quantitative RT-PCR was performed using SuperScript™ III Platinum Two-Step qRT-PCR Kit with SYBR® Green (Invitrogen). Equal amounts of DNase-treated total RNA (800 ng) were used to generate cDNA with random hexamer primers according to the manufacturer's protocol. The resultant cDNA was diluted eight times with Nuclease-free water. The diluted cDNA (2.5 µl) was subsequently used in 25 µl of qRT-PCR reaction, which was carried out in triplicate on cDNA with the SYBR Green master mix and DNA Engine Opticon® 2 thermal cycler. Sequences of primers used in qRT-PCR are shown in Table S2. As a negative control and a control to detect DNA contamination, water and DNase-treated RNA were used in place of cDNA template respectively. Cycle threshold (Ct) results and melting curve for each sample were generated by Opticon Monitor™ software, Version 1.0. The fold change in the amount of *xcnA*, *xcnM* and *xcnN* transcripts (target gene) relative to the *recA* transcripts (control gene) were determined by the following equation:

$$\textbf{Fold change} = 2^{-\Delta(\Delta Ct)}\textbf{; } \Delta Ct = Ct_{target} - Ct_{control}\textbf{; and}$$

$$\Delta(\Delta Ct) = \Delta Ct_{mutants} - \Delta Ct_{wt}\textbf{.}$$

Final mean values of Δ(ΔCt) and fold change were obtained from three independent RNA samples.

Cell viability assays. Strains were grown overnight in 2 ml of LB broth with selection. After 18 h of growth, cultures were diluted 1:5 in Graces media and normalized to equal absorbance (OD_{600}). Five millilitres of LB broth was inoculated with 100 µl of normalized culture and growth was monitored by turbidity. Dilutional plating was performed in triplicate at 24, 48, 60 and 72 h for each of the cultures and colony-forming units (cfu) ml^{-1} was calculated. The cell viability experiments were repeated three times yielding highly similar results.

Acknowledgements

We would like to thank Ransome van der Hoeven for construction of the *ackA* and *ackA-pta* deletion strains, Erika Buell for assistance in making the *xcnA*::Cm mutant strain, Dr Jane Witten for providing *Manduca sexta* larvae and Dr John Berges for assistance with statistical analyses. We are grateful to Dr A. Wolfe for his critically reading of and valuable suggestions on this manuscript, and to the members of the Forst laboratory for valuable discussions. This work was supported by a Research Growth Initiative (RGI) grant from the University of Wisconsin-Milwaukee.

References

Akhurst, R.J. (1982) Antibiotic activity of *Xenorhabdus* spp., bacteria symbiotically associated with insect pathogenic nematodes of the families *Heterorhabditidae* and *Steinernematidae*. *J Gen Microbiol* **128:** 3061–3065.

Alexeyev, M.F. (1999) The pKNOCK series of broad-hostrange mobilizable suicide vectors for gene knockout and targeted DNA insertion into the chromosome of gramnegative bacteria. *Biotechniques* **26:** 824–826, 828.

Bang, I.S., Audia, J.P., Park, Y.K., and Foster, J.W. (2002) Autoinduction of the *ompR* response regulator by acid shock and control of the *Salmonella enterica* acid tolerance response. *Mol Microbiol* **44:** 1235–1250.

Ciche, T.A., Blackburn, M., Carney, J.R., and Ensign, J.C. (2003) Photobactin: a catechol siderophore produced by *Photorhabdus luminescens*, an entomopathogen mutually associated with *Heterorhabditis bacteriophora* NC1 nematodes. *Appl Environ Microbiol* **69:** 4706–4713.

Crosa, J.H., and Walsh, C.T. (2002) Genetics and assembly line enzymology of siderophore biosynthesis in bacteria. *Microbiol Mol Biol Rev* **66:** 223–249.

Eleftherianos, I., Marokhazi, J., Millichap, P.J., Hodgkinson, A.J., Sriboonlert, A., ffrench-Constant, R.H., and Reynolds, S.E. (2006) Prior infection of *Manduca sexta* with nonpathogenic *Escherichia coli* elicits immunity to pathogenic *Photorhabdus luminescens*: roles of immune-related proteins shown by RNA interference. *Insect Biochem Mol Biol* **36:** 517–525.

Feng, X., Oropeza, R., and Kenney, L.J. (2003) Dual regulation by phospho-OmpR of *ssrA/B* gene expression in *Salmonella* pathogenicity island 2. *Mol Microbiol* **48:** 1131–1143.

Finking, R., and Marahiel, M.A. (2004) Biosynthesis of nonribosomal peptides. *Annu Rev Microbiol* **58:** 453–488.

Forst, S., and Boylan, B. (2002) Characterization of the pleiotropic phenotype of an *ompR* strain of *Xenorhabdus nematophila*. *Antonie van Leeuwenhoek* **81:** 43–49.

Forst, S., and Clarke, D.J. (2002) Bacteria-nematode symbiosis. In *Entomopathogenic Nematology*. Gaugler, R. (ed.). Wallingford, UK: CABI Publishing, pp. 57–77.

Givaudan, A., and Lanois, A. (2000) *flhDC*, the flagellar master operon of *Xenorhabdus nematophilus*: requirement for motility, lipolysis, extracellular hemolysis, and full virulence in insects. *J Bacteriol* **182:** 107–115.

Goh, E.B., Siino, D.F., and Igo, M.M. (2004) The *Escherichia coli tppB* (*ydgR*) gene represents a new class of OmpRregulated genes. *J Bacteriol* **186:** 4019–4024.

Gouge, D.H., and Snyder, J.L. (2006) Temporal association of entomopathogenic nematodes (Rhabditida: *Steinernematidae* and *Heterorhabditidae*) and bacteria. *J Invertebr Pathol* **91:** 147–157.

Herbert, E.E., and Goodrich-Blair, H. (2007) Friend and foe: the two faces of *Xenorhabdus nematophila*. *Nat Rev Microbiol* **5:** 634–646.

van der Hoeven, R., Betrabet, G., and Forst, S. (2008) Characterization of the gut bacterial community in *Manduca sexta* and effect of antibiotics on bacterial diversity and nematode reproduction. *FEMS Microbiol Lett* **286:** 249–256.

van der Hoeven, R., and Forst, S. (2009) OpnS, an outer membrane porin of *Xenorhabdus nematophila*, confers a competitive advantage for growth in the insect host. *J Bacteriol* **191:** 5471–5479.

Isaacson, P.J., and Webster, J.M. (2002) Antimicrobial activity of *Xenorhabdus* sp. RIO (*Enterobacteriaceae*), symbiont of the entomopathogenic nematode, *Steinernema riobrave* (Rhabditida: *Steinernematidae*). *J Invertebr Pathol* **79:** 146–153.

Joyce, S.A., Brachmann, A.O., Glazer, I., Lango, L., Schwär, G., Clarke, D.J., and Bode, H.B. (2008) Bacterial biosynthesis of a multipotent stilbene. *Angew Chem Int Ed Engl* **47:** 1942–1945.

Jubelin, G., Vianney, A., Beloin, C., Ghigo, J.M., Lazzaroni, J.C., Lejeune, P., and Dorel, C. (2005) CpxR/OmpR interplay regulates curli gene expression in response to osmolarity in *Escherichia coli*. *J Bacteriol* **187:** 2038–2049.

Keating, D.H., Shulla, A., Klein, A.H., and Wolfe, A.J. (2008) Optimized two-dimensional thin layer chromatography to monitor the intracellular concentration of acetyl phosphate and other small phosphorylated molecules. *Biol Proced Online* **10:** 36–46.

Klein, A.H., Shulla, A., Reimann, S.A., Keating, D.H., and Wolfe, A.J. (2007) The intracellular concentration of acetyl phosphate in *Escherichia coli* is sufficient for direct phosphorylation of two-component response regulators. *J Bacteriol* **189:** 5574–5581.

Lanois, A., Jubelin, G., and Givaudan, A. (2008) FliZ, a flagellar regulator, is at the crossroads between motility, hemolysin expression and virulence in the insect pathogenic bacterium *Xenorhabdus*. *Mol Microbiol* **68:** 516–533.

Lee, A.K., Detweiler, C.S., and Falkow, S. (2000) OmpR regulates the two-component system SsrA–ssrB in *Salmonella* pathogenicity island 2. *J Bacteriol* **182:** 771–781.

Li, J., Chen, G., and Webster, J.M. (1997) Nematophin, a novel antimicrobial substance produced by *Xenorhabdusnematophilus* (*Enterobactereaceae*). *Can J Microbiol* **43:** 770–773.

McInerney, B.V., Taylor, W.C., Lacey, M.J., Akhurst, R.J., and Gregson, R.P. (1991) Biologically active metabolites from *Xenorhabdus* spp., Part 2. Benzopyran-1-one derivatives with gastroprotective activity. *J Nat Prod* **54:** 785–795.

Mattison, K., Oropeza, R., Byers, N., and Kenney, L.J. (2002) A phosphorylation site mutant of OmpR reveals different binding conformations at *ompF* and *ompC*. *J Mol Biol* **315:** 497–511.

Maxwell, P.W., Chen, G., Webster, J.M., and Dunphy, G.B. (1994) Stability and activities of antibiotics produced during infection of the insect *Galleria mellonella* by two isolates of *Xenorhabdus nematophilus*. *Appl Environ Microbiol* **60:** 715–721.

Morgan, J.A., Sergeant, M., Ellis, D., Ousley, M., and Jarrett, P. (2001) Sequence analysis of insecticidal genes from *Xenorhabdus nematophilus* PMFI296. *Appl Environ Microbiol* **67:** 2062–2069.

Oshima, T., Aiba, H., Masuda, Y., Kanaya, S., Sugiura, M., Wanner, B.L., *et al.* (2002) Transcriptome analysis of all two-component regulatory system mutants of *Escherichia coli* K-12. *Mol Microbiol* **46:** 281–291.

Park, D., and Forst, S. (2006) Co-regulation of motility, exoenzyme and antibiotic production by the EnvZ–OmpR–FlhDC–FliA pathway in *Xenorhabdus nematophila*. *Mol Microbiol* **61:** 1397–1412.

Paul, V.J., Frautschy, S., Fenical, W., and Nealson, K.H. (1981) Antibiotics in microbial ecology, isolation and structure assignment of several new antibacterial compounds from the insect-symbiotic bacteria *Xenorhabdus* spp. *J Chem Ecol* **7:** 589–597.

Poinar, G.O. (1979) Biology and taxonomy of Steinernematidae and Heterorhabditidae. In *Entomopathogenic Nematodes in Biological Control*. Gaugler, R., and Kaya, H. (eds). Boca Raton, FL: CRC Press, pp. 270–280.

Reimer, D., Luxenburger, E., Brachmann, A.O., and Bode, H.B. (2009) A new type of pyrrolidine biosynthesis is involved in the late steps of xenocoumacin production in *Xenorhabdus nematophila*. *Chembiochem* **13:** 224–230.

Rhee, J.E., Sheng, W., Morgan, L.K., Nolet, R., Liao, X., and Kenney, L.J. (2008) Amino acids important for DNA recognition by the response regulator OmpR. *J Biol Chem* **283:** 8664–8677.

Shin, S., and Park, C. (1995) Modulation of flagellar expression in *Escherichia coli* by acetyl phosphate and the osmoregulator OmpR. *J Bacteriol* **177:** 4696–4702.

Sicard, M., Tabart, J., Boemare, N.E., Thaler, O., and Moulia, C. (2005) Effect of phenotypic variation in *Xenorhabdus nematophila* on its mutualistic relationship with the entomopathogenic nematode *Steinernema carpocapsae*. *Parasitology* **131:** 687–694.

Singh, J., and Banerjee, N. (2008) Transcriptional analysis and functional characterization of a gene pair encoding iron-regulated xenocin and immunity proteins of *Xenorhabdus nematophila*. *J Bacteriol* **190:** 3877–3885.

Snyder, H., Stock, S.P., Kim, S.K., Flores-Lara, Y., and Forst, S. (2007) New insights into the colonization and release processes of *Xenorhabdus nematophila* and the morphology and ultrastructure of the bacterial receptacle of ist nematode host, *Steinernema carpocapsae*. *Appl Environ Microbiol* **73:** 5338–5346.

Sundar, L., and Chang, F.N. (1993) Antimicrobial activity and biosynthesis of indole antibiotics produced by *Xenorhabdus nematophilus*. *J Gen Microbiol* **139:** 3139–3148.

Thaler, J.O., Baghdiguian, S., and Boemare, N. (1995) Purification and characterization of xenorhabdicin, a phage tail-like bacteriocin, from the lysogenic strain F1 of *Xenorhabdus nematophilus*. *Appl Environ Microbiol* **61:** 2049–2052.

Volgyi, A., Fodor, A., Szentirmai, A., and Forst, S. (1998) Phase variation in *Xenorhabdus nematophilus*. *Appl Environ Microbiol* **64:** 1188–1193.

Walsh, K.T., and Webster, J.M. (2003) Interaction of microbial populations in *Steinernema* (*Steinernematidae*, Nematoda) infected *Galleria mellonella* larvae. *J Invertebr Pathol* **83:** 118–126.

Waterfield, N.R., Sanchez-Contreras, M., Eleftherianos, I., Dowling, A., Wilkinson, P., Parkhill, J., *et al.* (2008) Rapid Virulence Annotation (RVA): identification of virulence factors using a bacterial genome library and multiple invertebrate hosts. *Proc Natl Acad Sci USA* **105:** 15967–15972.

Webster, J.M., Chen, G., Hu, K., and Li, J. (2002) Bacterial metabolites. In *Entomopathogenic Nematology*. Gaugler, R. (ed.). Wallingford, UK: CABI Publishing, pp. 99–114.

Williamson, N.R., Fineran, P.C., Leeper, F.J., and Salmond, G.P. (2006) The biosynthesis and regulation of bacterial prodiginines. *Nat Rev Microbiol* **4:** 887–899.

Wolfe, A.J. (2005) The acetate switch. *Microbiol Mol Biol Rev* **69:** 12–50.

Yim, G., Wang, H.H., and Davies, J. (2007) Antibiotics as signalling molecules. *Philos Trans R Soc Lond B Biol Sci* **362:** 1195–1200.

Supporting Information

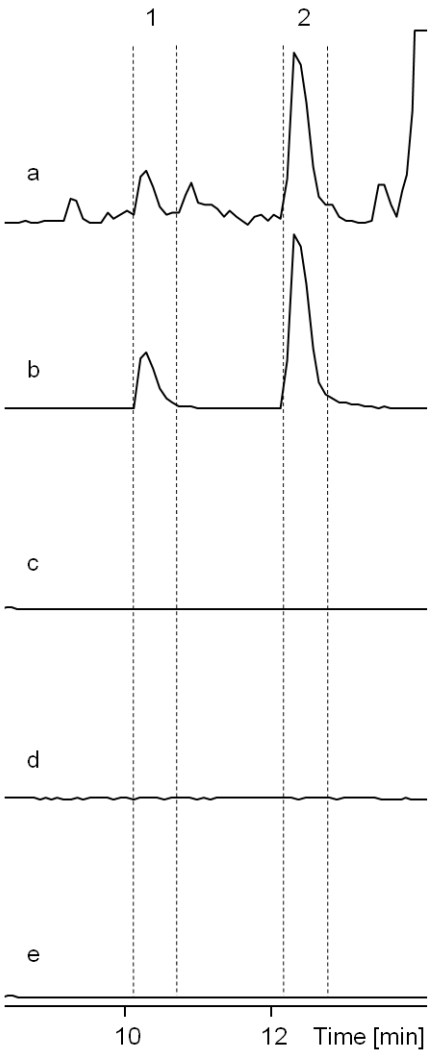

Fig. S1. HPLC-MS analysis of the production of Xcn1 and Xcn2 in *xcn* mutant strains of *X. nematophila*. a) basepeak chromatogram of AN6/1, b)-e) extracted ion chromatograms for Xcn1 (1) and Xcn2 (2), b) AN6/1, c) *xcnF*, d) *xcnH*, e) *xcnL*. The *xcnA* and *xcnK* mutant strains also did not produce Xcn1 and Xcn2 (data not shown).

Table S1. Annotations and orthologs of *xcn* genes

Gene	Gene annotation	No of aa	% G+C	Ortholog	% identity	Distance tree analysis
xcnA	NRPS	2672	46.3	*Hahella chejuensis*	52	γ-proteobacteria
xcnB	3-hydroxyacyl-CoA dehydrogenase	285	38.7	*Clostridium cellulolyticum*	51	Firmicute
xcnC	Methoxymalonyl-ACP biosynthesis	353	35.3	*Bacillus pumilus*	52	Firmicute
xcnD	unknown	85	32.2			
xcnE	Acyl-CoA dehydrogenase	383	43.1	*Bacillus cereus*	50	Firmicute
xcnF	PKS	3421	42.1	*Bacillus pumilus*	35	Firmicute
xcnG	Beta-lactamase	489	36.5	*Bacillus cereus*	28	Firmicute
xcnH	PKS	1927	39.0	*Bacillus cereus*	34	Firmicute
xcnI	Type II thioesterase	243	34.8	*Clostridium butyricum*	38	Firmicute
xcnJ	unknown	107	30.9			
xcnK	NRPS	857	36.6	*Bacillus pumilus*	36	Firmicute
xcnL	PKS	1487	39.5	*Bacillus pumilus*	34	Firmicute
xcnM	Saccharopine dehydrogenase	361	35.7	*Acaryochloris marina*	40	cyanobacteria
xcnN	Fatty acid desaturase	360	31.4	*Burkholderia phymatum*	36	β-proteobacteria

Table S2. List of primers used in this study

Primer	Sequence (5'----3')	Size of fragment
For cloning into pSTBlue-1		
xcnA-F1	TGAGTTGTCAAGATCACAGCAAG	
xcnA-R1	CTTCTTTCTCCAGAGCCTTCATC	479
xcnB-F1	GATAACCTGTGCTGCATATGGTC	
xcnB-R1	AGGTTTAATGTACGGTGTTATTGCTG	277
xcnF-F1	CGGCATTGAATGTCTCGGA	
xcnF-R1	CCGATTCCGTTCTCTCCG	423
xcnH-F3	GAATAAACAGTTCGCACCTACTCTG	
xcnH-R3	GATTCACCAAGATACTCTGAAGCC	593
xcnI-F1	TTCATCACGCTGGTGGATCTC	
xcnI-R1	CACAATGGATGAATACAACGTGTTTG	265
xcnK-F3	CATCCTTTGCCTCTCAGTTGTTAAG	
xcnK-R3	GGTACTATATGGAGGGTATGACCG	540
xcnL-F3	CTAAATCCATTCTCGGGCATCTTG	
xcnL-R3	CATACCCGGATATTGTGTTCCTTG	565
xcnM-F3	AATCAGTACGCTCCTCATCTGG	
xcnM-R3	AACAACACTTGCCATCCATGAAG	327
xcnN-F1	TGATTGCTAGTTTACGGGAGTTAAGG	
xcnN-R1	ATGTGCATGATGATACCTGACATGAG	314
For confirmation of xcn mutants		
xcnA-F2	CGAGTATTTAAACCATGAAGAAGACG	
xcnA-R2	CAGATTCCTGCCCGTTAATCAG	648
xcnF-F2	TAATGGGGTTGGCGTTGTTAC	
xcnF-R2	CGATTGGGCAGTTCCTGATAATTTAG	624
xcnH-F2	AAGCAATATCGGTCATTTAGACGAAG	
xcnH-R2	CTGCGCATATTGTGTCTGACTAAG	727
xcnK-F2	CACCCCTTACGTATCGCAG	
xcnK-R2	GAGTACAATCTGCAATATTGATGGCT	688
xcnL-F2	CCCTGAATACACTTTCCTGCTG	
xcnL-R2	GCAGGCAGTATCGCAATAGG	628
xcnM-F2	CTGTTTTATTAGTTGGAGGGTATGG	
xcnM-R2	CTGATATCAATACTCGTCACGTTCT	442
xcnB-F1	GATAACCTGTGCTGCATATGGTC	
xcnI-R1	CACAATGGATGAATACAACGTGTTTG	
xcnN-R1	ATGTGCATGATGATACCTGACATGAG	
pknock-R	CGTCACAGGTATTTATTCGGACACG	
For RT-PCR analysis		
xcnA-F3	CTGTCTGAAGATAAGCAGAGCTGG	
xcnA-R3	GGGAATTCGAATACCTTCCCAGAC	674
xcnB-F3	GTTCATATCGGATGCTGAAACCTG	
xcnB-R3	CCAGAAATGCTGCTTCGTTCATG	461
xcnC-F3	AAGTGACTTGCATTGATGCGTTG	
xcnC-R3	ACATTTGTCGATTACGAGGTGTACG	553

continued

xcnE-F3	ACAGTGCATACCAGTTTAGTCGG	
xcnE-R3	CCAGGCAATGCTGTAACGAC	471
xcnF-F3	GGAGCCGGTAATCAGTGGTCATGG	
xcnF-R3	CTCATCAAATACCCGTGTCTTGCCGTC	320
xcnG-F3	TCTTGCCAGAGCTCTCATTCTG	
xcnG-R3	AGTGTTAGGCTCCAGAATACGTTTC	524
xcnH-F3	GAATAAACAGTTCGCACCTACTCTG	
xcnH-R3	GATTCACCAAGATACTCTGAAGCC	593
xcnI-F3	AGTTCATTGCGATAGAGCTTCCTG	
xcnI-R3	TCAGTGAGTTCTTTGGTATCACCC	327
xcnK-F3	CATCCTTTGCCTCTCAGTTGTTAAG	
xcnK-R3	GGTACTATATGGAGGGTATGACCG	540
xcnL-F3	CTAAATCCATTCTCGGGCATCTTG	
xcnL-R3	CATACCCGGATATTGTGTTCCTTG	565
xcnM-F3	AATCAGTACGCTCCTCATCTGG	
xcnM-R3	AACAACACTTGCCATCCATGAAG	327
xcnN-F3	GATAGGTTCAACACAACGAGCATT	
xcnN-R3	CTATTGACTCATTGTTATCTCCAGCC	422
16S rDNA-F2	GGTAGTAAATGTTGGGGGATTTTCCC	
16S rDNA-R2	GACATCGTTTACAGCGTGGACTAC	715
For overlap RT-PCR/PCR analysis		
xcnAB-F	TCATCACCTTATTTGAACATCCGAC	
xcnAB-R	CAGGTTATCGCCGTGTCC	957
xcnBC-F	CGGATGCTGAAACCTGAATTCA	
xcnBC-R	AATATCATCACCTTCGGAAAGCAC	822
xcnCE-F	CCGGTATTACTTATAGCAGAGAACGA	
xcnCE-R	CTGCGGAGGGTCTTAATATGTTATC	792
xcnEF-F	CAATAATGCCGTTCAGGTCCTT	
xcnEF-R	TCTGCATCCGGATGATTAATTG	646
xcnFG-F	CGATTCCTGATGATTGCCAGATC	
xcnFG-R	CTTTATTTCTGACCGCAGGATCA	539
xcnGH-F	TCTTGGGATTCATTGATTATCTGGATG	
xcnGH-R	TCATGCAGTAACCGGCAC	562
xcnHI-F	GTATTGTTGCCTGCCCTGATA	
xcnHI-R	GGTCACTTCTGGATCATCTTTAGC	904
xcnIK-F	CATTGCGATAGAGCTTCCTGG	
xcnIK-R	TGGCTCATATTCATTAATGACTTTCTTCC	1197
xcnKL-F	GCAGCAGTGAGCTTGAAGT	
xcnKL-R	AACTACATTGATGCAGGTGTCTG	745
xcnLM-F	TAGACGTCTGGGAACATCAACT	
xcnLM-R	AACAACACTTGCCATCCATGAAG	848
xcnMN-F	TTGGCTGAGCATATTCAAGATCATC	
xcnMN-R	ATTGCTCGTTGTGTTGAACCTATC	680

continued

For qRT-PCR analysis		
xcnA-F4	TTGAGACATTGGACACGGTGAAAG	
xcnA-R4	GCAGGTTGTTCCGTACTATCGAC	103
xcnM-F4	GATTCGTATTGATGTTCATGGAGTTGATG	
xcnM-R4	ATGATCTTGAATATGCTCAGCCAACTG	148
xcnN-F4	ATCATCTGGTGCATCACCTGTATC	
xcnN-R4	ATGGTTTCTTGATGAGGATGCTGAC	148
recA-F4	TGATGAAGTTGTTGGTAGCGAAACG	
recA-R4	ACTCAGATCGATCAACTCTCCCAG	134
For ackA and ackA pta mutant construction		
ackA upstream-F	ACATGCATGCGTTAACAGGGGTCAGTAGAC	
ackA upstream-R	CGGAATTCAGTACCAGCTTACTTGACATG	1482
ackA downstream-F	CGGAATTCGCAACATGATCCTCAAACCG	
ackA downstream-R	CCGAGCTCAGCAGAAGTGACCAGCAAAG	1024
pta downstream-F	CGGAATTCGGTCACTACACATAGGGTATAGC	
pta downstream-R	CCGAGCTCTTCTGGAAGACGAGAAGGTTG	986
Km-F	CGGAATTCTAACTGTCAGACCAAGTTTACTC	
Km-R	CGGAATTCTCAAGAAGATCCTTTGATCTTTTC	1052
For ackA and ackA pta mutant confirmation		
ackA-F	GCGAAGCGTTGAACTTCATTG	
ackA-R	TGTATCAACACACTGACCGTTG	494
pta-F	AGCTGAGAGAGCGTATTGAAC	
pta-R	ACGGATCGAATCATCAATGGTG	509
For 5'RACE-PCR		
A. First strand cDNA synthesis		
xcnA-RACE-R2	CGATGTGAAATATATCCATTGAGTCC	
B. PCR amplification of dC-tailed cDNA		
xcnA-RACE-R3	CCATCCAGAGGAATACTGCC	
C. Colony PCR screen for5' RACE-product insert in pSTBlue-1		
xcnA-RACE-F2	TCGATGTTATCGGAACAGTATTGG	
xcnA-RACE-R3	CCATCCAGAGGAATACTGCC	256
D. Sequencing 5'RACE-product insert/pSTBlue-1		
T7	CTAATACGACTCACTATAGGG (forward sequencing)	
xcnA-RACE-R4	TTGGTGAAGAGCAGACACTAC (reverse sequencing)	

Chapter 3

A natural prodrug activation mechanism in nonribosomal peptide synthesis

Daniela Reimer, Klaas M. Pos, Marco Thines, Peter Grün and Helge B. Bode

The article has been published in
Nature Chemical Biology, Vol.7, Issue 12, 2011, pp 888-890

Author's effort

The author performed all experiments, except the isolation of amicoumacin, which was done by Peter Grün. Structure elucidation of the prexenocoumacins and writing of the paper was performed together with Helge B. Bode. Klaas M. Pos performed XcnG homology modeling and Marco Thines performed XcnA and XcnG phylogenetic analysis.

A natural prodrug activation mechanism in nonribosomal peptide synthesis

Daniela Reimer,[a] Klaas M. Pos,[b,c] Marco Thines,[d,e] Peter Grün[a] and Helge B. Bode[a]

[a] *Molecular Biotechnology, Institute for Molecular Biosciences, Goethe University Frankfurt, Frankfurt, Germany*

[b] *Institute of Biochemistry, Goethe University Frankfurt, Frankfurt, Germany*

[c] *Cluster of Excellence Frankfurt - Macromolecular Complexes, Goethe University Frankfurt, Frankfurt, Germany*

[d] *Biodiversity and Climate Research Center (BiK-F), Frankfurt, Germany*

[e] *Department of Biological Sciences, Institute of Ecology, Evolution and Diversity, Goethe University Frankfurt, Frankfurt, Germany*

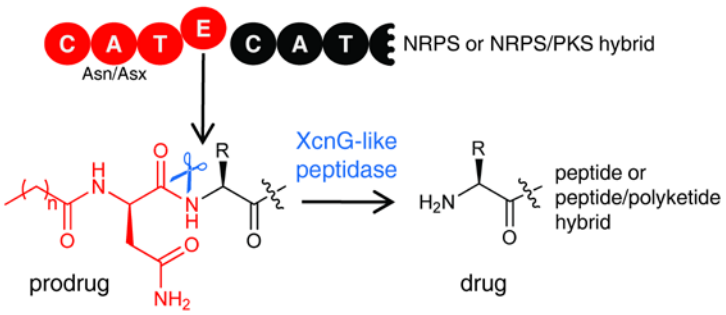

Cleavage of peptide precursors is well known for ribosomally produced sequences. Investigation of xenocoumacin biosynthesis now points to a similar function in nonribosomal peptide synthesis clusters, explaining one source of mismatches between genetic and chemical information.

We have identified a new mechanism for the cleavage and activation of nonribosomally made peptides and peptide-polyketide hybrids that are apparently operational in several different bacteria. This process includes the cleavage of a precursor molecule by a membrane-bound and D-asparagine-specific peptidase, as shown here in the biosynthesis of the antibiotic xenocoumacin from *Xenorhabdus nematophila*.

Activation of proteins by proteolytic cleavage is a common feature in biology: Signal peptides are used to sort proteins into different cellular compartments and are cleaved off the protein at its final location[1]. Proteases are activated by proteolytic cleavage enabling the 'on-demand' production of their active form, to allow very fast reactions to occur such as the blood coagulation cascade[2]. In the biosynthesis of ribosomal peptides, proteolytic cleavage also plays an important role as the bioactive peptides are often derived from much larger peptides or even small proteins[3,4]. However, this mechanism was not previously known to extend to nonribosomally synthesized peptides (NRP), the largest class of peptide natural products[5].

We recently identified the biosynthetic gene cluster for the production of the antibiotic xenocoumacin (XCN) (Fig. 1a) from *X. nematophila*[6]. *Xenorhabdus* live in symbiosis with *Steinernema* nematodes, and together they form entomopathogenic complexes that can infect and kill different insects[7,8]. Xenocoumacins are thought to be involved in clearing bacteria, such as insect gut microbes, from the infected insect, thereby removing food competitors and conferring benefits to the *Xenorhabdus-Steinernema* symbiosis. Our initial bioinformatics analysis of the XCN biosynthetic machinery could not fully assign functions to genes involved in the production of xenocoumacin-1 (**1**), which is the precursor of xenocoumacin-2 (**2**)[6]. Therefore, to gain insight into this pathway, we deleted genes in the biosynthetic gene cluster for which we could not predict roles within XCN biosynthesis (Supplementary Methods).

Deletion of *xcnG*, which encodes a protein with an N-terminal periplasmic peptidase domain (including a signal peptide sequence) and a C-terminal transmembrane domain, resulted in the complete loss of 1 and 2 production but led to the production of five newl compounds (Fig. 1b). As overlapping retention times prevented us from separating these compounds from another group of peptides, we inactivated the biosynthetic gene cluster responsible for the production of those peptides in a Δ*xcnG* background. This allowed us to isolate two compounds (**4** and **5**) that were detected in the Δ*xcnG* mutant and subsequently characterize them via NMR (Supplementary Results, Supplementary Table 3 and Supplementary Fig. 1) as well as degradation and derivatization according to the advanced Marfey's method[9] (Supplementary Fig. 2). The three other derivatives were identified using detailed labeling experiments followed by MS analyses developed previously[6] (Supplementary Tables 4 and 5). All five compounds represent derivatives of **1** extended at the N terminus by a D-asparagine carrying one of five different acyl chains (Fig. 1a). We named these five compounds prexenocoumacins (PXCN) A-E (**3**-**7**) and assumed they are the first products of the xenocoumacin biosynthetic machinery. With these new structures in hand, we were able to reconcile the predicted specificities of

the enzymes in the gene cluster with the compounds synthesized by the cluster (Supplementary Fig. 3). Disk diffusion assays revealed no antibiotic activity for **4** and **5** in contrast to the high activity of **1** (Supplementary Fig. 4). To directly show the cleavage of PXCN into **1**, we attempted to express XcnG in *Escherichia coli* for use in subsequent purification and *in vitro* tests of proteolytic activity against PXCN and other substrates. However, despite considerable efforts, XcnG could not be produced in *E. coli* in amounts suitable for *in vitro* characterization.

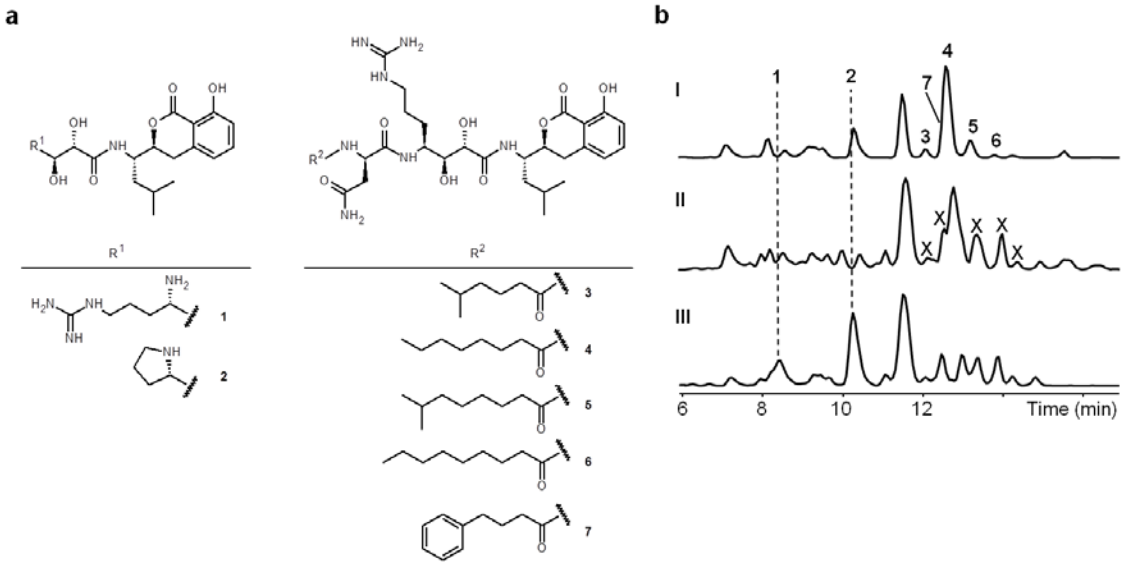

Figure 1. Xenocoumacins and prexenocoumacins produced from *Xenorhabdus nematophila.* (a) Structures of xenocoumacin-1 (**1**), xenocoumacin-2 (**2**) and prexenocoumacins A–E (**3**–**7**). (b) ESI-HPLC-MS analysis (base peak chromatograms) of (I) *X. nematophila* HGB081-Δ*xcnG.xnc1_2228*::*cat*, (II) HGB081-Δ*xcnG* and (III) wild type HGB081. The positions of **1**–**7** and of peptide masses (X) resulting from *xcn1_2228* are indicated. The peak at 11.4 min is xenortide A (ref. 22). All chromatograms are scaled to the same intensity.

Instead, expression of full-length *xcnG* in *E. coli* (Supplementary Fig. 5) and addition of **4** showed the expected decrease of **4** and the production of **1** (Fig. 2). However, only a small amount of **1** could be observed, most likely because of its antibiotic activity against an as-yet-unknown molecular target either on or in the *E. coli* cell, triggering the lysis of the culture. The isolated N-terminal peptidase domain of XcnG without the C-terminal transmembrane helices (XcnG^{-TMH}) was not able to cleave **4** in *E. coli* cells (Supplementary Fig. 5b); we conclude that the loss of the transmembrane helices caused inactivation of the protein rather than more severe disruptions in protein folding or trafficking as XcnG^{-TMH} was detected in the periplasmic fraction (Supplementary Fig. 5c). Heterologous expression in *E. coli* was also used to confirm the previously described conversion of **1** into **2** by the desaturase XcnM and the dehydrogenase XcnN[6]: Addition of **4** to an *E. coli* strain coexpressing *xcnG*,

xcnM and *xcnN* resulted in the production of **1** and **2,** as shown by MS analysis (Supplementary Fig. 6). This experiment therefore confirmed not only the peptidase function of XcnG but also the biochemical activity of XcnM and XcnN, which leads to pyrrolidine ring formation from the arginine moiety in **1**.

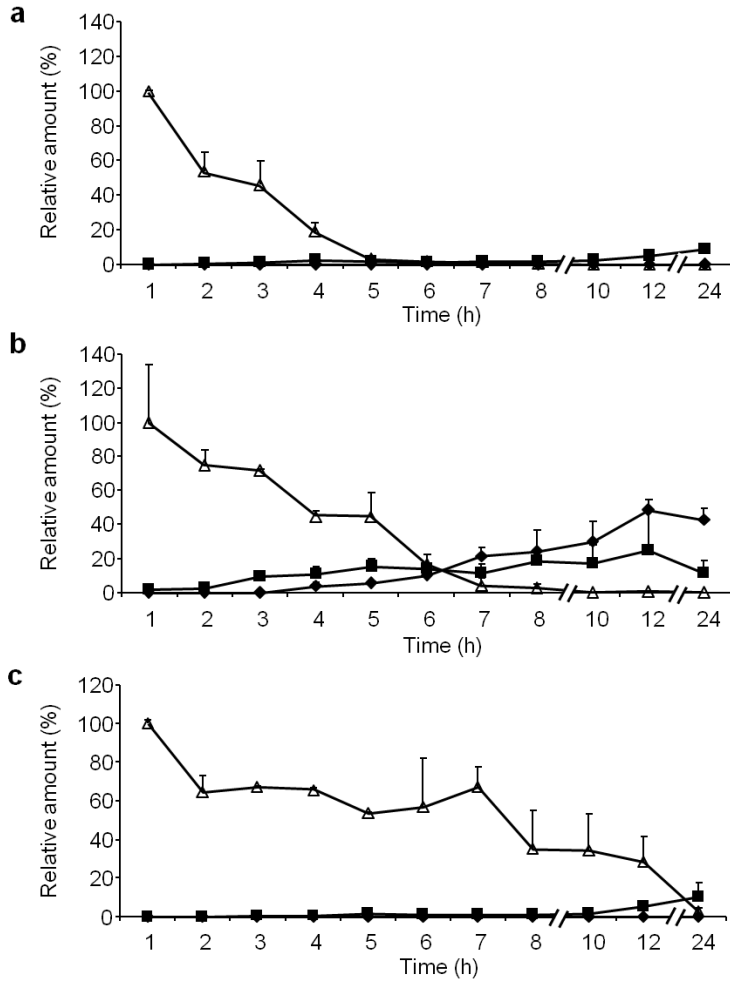

Figure 2. Transformation of prexenocoumacin B (**4**) by *E. coli*. Depicted are the relative amounts of **1** (black squares), **2** (black diamonds) and **4** (white triangles) in *E. coli* DH10B expressing (a) *xcnG*, (b) *xcnG* and *xcnMN* and (c) *xbJ1_2693*. Mean values and s.d. of two independent experiments are shown.

Although we initially we expected this complex activation mechanism to be rare in nature, we were able to identify at least seven other biosynthetic gene clusters encoding XcnG (Supplementary Table 6) and XcnA in different bacterial genera via homology searches[10], which form monophyletic groups with highly similar topologies in phylogenetic reconstructions and hint at a high degree of evolutionary conservation (Supplementary Fig. 7). Without exception, these clusters encode homologs of the xenocoumacin starting module that includes condensation, adenylation (specific to Asx), thiolation and epimerization domains as well as XcnG (Supplementary Figs. 8 and 9). Among these biosynthetic gene clusters are those coding for synthesis of amicoumacin[11], zwittermicin[12] (structures are listed in Supplementary Fig. 10) and colibactin[13,14], as well as several others for which no product or biological activity has been assigned yet (Supplementary Fig. 8). Notably, these biosynthetic gene clusters encode both polyketide synthase (PKS)-nonribosomal peptide synthetase (NRPS) hybrids, as in the case of xenocoumacin, and NRPS alone, as has been shown for *Clostridium botulinum*. Cleavage of an acylated D-asparagine might therefore be a widespread mechanism to produce active

natural products from prodrugs upon secretion. Indeed, a recent study provided complementary evidence that colibactin biosynthesis proceeds via this mechanism[15]. Intermediary acylation has also been identified in the saframycin biosynthesis[16], but in this case deacylation might occur via cytochrome P450-catalyzed hydroxylation as described in the myxothiazol biosynthesis[17]. We explored the generality of these enzymes by expressing the XcnG homologues *zmaM*, *xbJ1_2693* and *bpum_0630* from *Bacillus thuringiensis*, *Xenorhabdus bovienii* and *Bacillus pumilus*, respectively, in *E. coli*, and only *xbJ1_2693* showed activity (production of **1**), which occured when **4** was added (Fig. 2c, Supplementary Fig. 11). Although the natural product produced by the biosynthetic gene cluster in *X. bovienii* that encodes XbJ1_2693 is not known, the N terminus of the postulated natural product shows the highest similarity to prexenocoumacin as concluded from the amino acid specificity of the A domain in the second module (Supplementary Table 7).

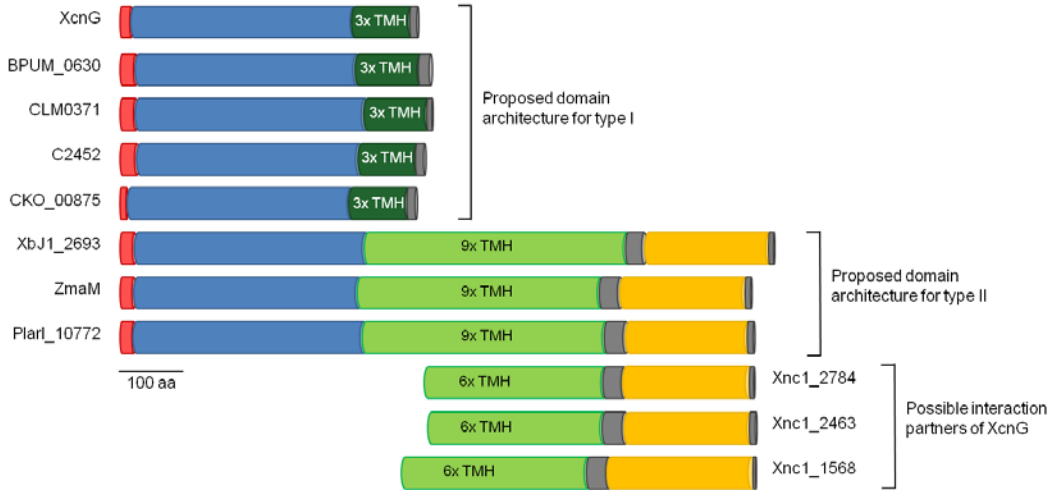

Figure 3. XcnG homologs and their domain architecture. Depicted are the domain architectures of XcnG (*X. nematophila*), the homologs Bpum_0630 (*B. pumilius* SAFR-032), CLM0371 (*C. botulinum* A2 strain Kyoto), C2452 (*E. coli* CFT073), CKO_00875 (*Citrobacter koseri* ATCC BAA-895), XbJ1_2693 (*X. bovienii* SS-2004), ZmaM (*Bacillus thuringiensis serovar Berliner* ATCC 10792) and Plarl_010100010772 (*Paenibacillus larvae* subsp. *larvae* BRL-230010), and possible interaction partners of XcnG in *X. nematophila*, which may supplement the ABC transporter function in the putative XcnG–ABC transporter complex. Peptidase homologs can be classified into two proposed domain architecture types. Type I consist of a signal sequence (red), specific for the transport of the protein into the periplasm, a peptidase domain (blue) and three *C*-terminal transmembrane helices (dark green). Type II consists of a signal sequence, a peptidase domain, nine transmembrane helices (light green) and an ABC transporter domain (yellow) located in the cytoplasm. TMH, transmembrane helices.

Domain architecture analysis of XcnG (Phyre server[18]) predicts a conserved β-lactamase/transpeptidase-like fold at the periplasmically located N terminus with distantly related protein family homology to D-alanyl-D-alanine carboxypeptidases. Its homology model structure (built by Phyre[18], Supplementary Fig. 12a) has a very strong superimposition[19] with the AmpC β-

lactamase from *E. coli* (Protein Data Base: 2FFY) that has an r.m.s. deviation of 2.15 Å, and it let us identify the catalytic triad comprising serine, lysine and tyrosine suggested for these peptidases (Supplementary Fig. 12b).

Domain architecture comparison of XcnG with its homologs led us to delineate two classes of these peptidases (Fig. 3). Whereas proteins such as XcnG (type I) comprise three transmembrane helices at the C-terminal end, larger homologs such as ZmaM from *B. thuringiensis* (type II) contain six additional transmembrane (nine total) helices and a C-terminal ABC-transporter nucleotide binding domain (NBD) (Fig. 3). However, three genes encoding candidate ABC transporters that have six transmembrane helices as well as nucleotide-binding-domain architecture have been identified in *X. nematophila* (Supplementary Table 8). Putatively, the XcnG architecture with three transmembrane helices together with on of these ABC transporters would resemble the domain architecture of ZmaM-like peptidases (Fig. 3).

Our combined results lead us to propose that the five different prexenocoumacins **3**-**7** are formed by the xenocoumacin biosynthetic machinery as inactive prodrugs that are secreted and synchronously cleaved into **1** by a XcnG-ABC transporter-TolC protein complex. TolC (Supplementary Table 9) has been shown to be involved in peptide-transporting ABC complexes[20]. Compound **1** then kills insect gut microbes or other bacterial food competitors during the infection cycle and nematode development. As **1** is also toxic to the producing strain *X. nematophila*[21] (Supplementary Fig. 4), detoxification by XcnMN by conversion of **1** into **2** occurs when **1** is taken up by *X. nematophila* (Supplementary Fig. 13). Furthermore, our data showed that this sort of peptidase-catalyzed prodrug activation and secretion mechanism is widespread among secondary metabolites of NRPS and PKS-NRPS-derived hybrids in different bacterial taxa and should be considered especially during the *in silico* analysis of secondary metabolite biosynthetic gene clusters and their predicted products during large-scale genome-mining approaches.

Acknowledgements

The authors thank A. Venneri for technical assistance. D.R., P.G. and H.B.B. are grateful to the Deutsche Forschungsgemeinschaft (DFG) for financial support. Work in H.B.B.'s lab is additionally supported by the Frankfurt Initiative for Microbial Sciences (FIMS), the European Community's Seventh Framework Programme (FP7/2007-2013) under grant agreement no. 223328 (GameXP), and by the research funding programme "LOEWE – Landes-Offensive zur Entwicklung Wissenschaftlich-ökonomischer Exzellenz" of Hessen's Ministry of Higher Education, Research, and the Arts. Support by the DFG-EXC115 (Cluster of Excellence Macromolecular Complexes at the Goethe-University Frankfurt), DFG-SFB807 (Transport and Communication across Biological Membranes) and FIMS is gratefully acknowledged by K.M.P. M.T. is financially supported by the LOEWE program of Hessen's Ministry of Higher Education, Research, and the Arts.

Author contributions

D.R. and H.B.B. designed experiments; D.R. and P.G. performed experiments; D.R. and H.B.B. analyzed experimental data, K.M.P. performed XcnG homology modeling; M.T. performed XcnA and XcnG phylogenetic analysis. D.R., K.M.P., M.T. and H.B.B. wrote the paper.

References

1. Tuteja, R. *Arch. Biochem. Biophys.* **441**, 107–111 (2005).
2. Green, D. *Hemodial. Int.* **10** Suppl 2, S2–S4 (2006).
3. Mylne, J.S. *et al. Nat. Chem. Biol.* **7**, 257–259 (2011).
4. Willey, J.M. & van der Donk, W.A. *Annu. Rev. Microbiol.* **61**, 477–501 (2007).
5. Finking, R. & Marahiel, M.A. *Annu. Rev. Microbiol.* **58**, 453–488 (2004).
6. Reimer, D., Luxenburger, E., Brachmann, A.O. & Bode, H.B. *ChemBioChem* **10**, 1997–2001 (2009).
7. Goodrich-Blair, H. *Curr. Opin. Microbiol.* **10**, 225–230 (2007).
8. Herbert, E.E. & Goodrich-Blair, H. *Nat. Rev. Microbiol.* **5**, 634–646 (2007).
9. Fujii, K. *et al. Anal. Chem.* **69**, 3346–3352 (1997).
10. Altschul, S.F., Gish, W., Miller, W., Myers, E.W. & Lipman, D.J. *J. Mol. Biol.* **215**, 403–410 (1990).
11. Hashimoto, M. *et al. J. Antibiot. (Tokyo)* **60**, 752–756 (2007).
12. Kevany, B.M., Rasko, D.A. & Thomas, M.G. *Appl. Environ. Microbiol.* **75**, 1144–1155 (2009).
13. Homburg, S., Oswald, E., Hacker, J. & Dobrindt, U. *FEMS Microbiol. Lett.* **275**, 255–262 (2007).
14. Nougayrède, J.P. *et al. Science* **313**, 848–851 (2006).
15. Dubois, D. *et al. J. Biol. Chem.* published online, doi:10.1074/jbc.M111.221960 (27 July 2011).
16. Koketsu, K., Watanabe, K., Suda, H., Oguri, H. & Oikawa, H. *Nat. Chem. Biol.* **6**, 408–410 (2010).
17. Silakowski, B. *et al. J. Biol. Chem.* **274**, 37391–37399 (1999).
18. Kelley, L.A. & Sternberg, M.J. *Nat. Protoc.* **4**, 363–371 (2009).
19. Krissinel, E. & Henrick, K. *Acta Crystallogr. D Biol. Crystallogr.* **60**, 2256–2268 (2004).
20. Holland, I.B., Schmitt, L. & Young, J. *Mol. Membr. Biol.* **22**, 29–39 (2005).
21. Park, D. *et al. Mol. Microbiol.* **73**, 938–949 (2009).
22. Lang, G., Kalvelage, T., Peters, A., Wiese, J. & Imhoff, J.F. *J. Nat. Prod.* **71**, 1074–1077 (2008).

Supplementary Information

Supplementary Methods

Bacterial strains and culture conditions. All *Xenorhabdus* strains used in this study, *Bacillus thuringiensis* DSM 2046^T and *Micrococcus luteus* were grown on solid and liquid Luria-Bertani (LB, pH 7.0) medium at 30 °C and 180 rpm at a rotary shaker. All *E. coli* strains used in this study were grown on solid LB medium at 37 °C and on liquid LB medium at 30 °C and 180 rpm on a rotary shaker. For plasmid selection in *E. coli*, chloramphenicol (34 μg mL^{-1}), ampicillin (100 μg mL^{-1}) or kanamycin (40 μg mL^{-1}) were added, respectively. *X. nematophila* and *X. bovienii* mutants were selected on LB containing rifampicin (40 μg mL^{-1}) or ampicillin (100 μg mL^{-1}). *Bacillus pumilus* SAFR-032 was grown on solid and liquid yeast tryptone (YT, pH 7.0) medium at 30 °C and 180 rpm on a rotary shaker.

General DNA and protein procedures. PCR, gel electrophoresis, restriction digestions, ligations, DNA transformations and SDS-PAGE were conducted according to standard methods[1]. DNA isolation and plasmid preparation were performed with GeneJET^{TM} Gel Extraction Kit (Fermentas) and Puregene Yeast/Bact. Kit B (Qiagen) according to manufacturer's instructions. All plasmids constructed were confirmed by sequencing (SeqIT GmbH, Germany, Kaiserslautern). Oligonucleotides used in this work were obtained from Sigma-Aldrich and are listed in Supplementary Table 1.

Construction of a *xcnG* deletion mutant. For the construction of the *xcnG* deletion mutant, fragments up- (936 bp) and downstream (733 bp) of the gene region encoding *xcnG* were amplified with primers xcnG_up-F, xcnG_up-R and xcnG_down-F, xcnG_down-R, fused together in an additional amplification step via complementary DNA regions and cloned into pDS132[2] via the *Sph*I and *Sac*I restriction site. Transformation into *E. coli* S17-1 λ pir, introduction into a rifampicin-resistant *X. nematophila* HG081 strain[3] by biparental conjugation and counterselection via *sacB* was performed as described previously[4], yielding the HGB081-Δ*xcnG* mutant with an in-frame deletion of 1,266 bp. The genotype of the mutant was confirmed by PCR using primers vxcnGDel-fw and vxcnGDel-rv lying outside the amplified region.

Construction of a prexenocoumacin production mutant. For the isolation of prexenocoumacin, *xnc1_2228* was disrupted via plasmid integration in the Δ*xcnG* mutant. An internal fragment of 537 bp was amplified with primers Xn2576fw and Xn2576rv and cloned into pDS132 via the *Sph*I and *Sac*I restriction site. The resulting plasmid was introduced into *E. coli* S17-1 λ pir by electroporation and conjugated into HGB081-Δ*xcnG*, yielding HGB081-Δ*xcnG-xnc1_2228*::*cat*. The genotype of the

mutant was confirmed by PCR using primers v2576f and v2576r lying outside the amplified region and two primers pDS132fw and pDS132rv specific for the vector backbone.

Phenotypic analysis. ESI HPLC MS analysis was performed with a Dionex UltiMate 3000 system coupled to a Bruker AmaZon X mass spectrometer and an Acquity UPLC BEH C18 1.7 µm RP column (Waters) using a MeCN/0.1 % formic acid in H_2O gradient ranging from 5 to 95 % in 22 min at a flow rate of 0.6 mL min^{-1}.High-resolution MS were performed with a Thermo LTQ Orbitrap Hybrid FT mass spectrometer and a XBridge C18 1.7 µm RP column (Waters) using a similar gradient in 20 min at a flow rate of 0.4 mL min^{-1} or a Thermo MALDI LTQ Orbitrap XL as described previously[5].

Feeding experiments for structure elucidation of prexenocoumacin. For structure elucidation feeding experiments were performed with DL-[2,3,4,4,4,5,5,5-D_8]valine, L-[5,5,5-D_3]leucine, 4-fluorophenylacetic acid, *p*-fluorophenylalanine and 4-chlorophenylacetic acid to LB medium as well as an inverse feeding approach with L-phenylalanine, L-leucine, L-valine, L-arginine, caprylic acid and decanoic acid to HGB081-Δ*xcnG* cultivated in [U-^{13}C]medium. Cultures were grown in 50 mL Erlenmeyer flasks containing 5 mL of ISOGRO-^{13}C (Sigma-Aldrich) or ISOGRO-^{15}N medium containing 10 mM K_2HPO_4, 10 mM KH_2PO_4, 8 mM $MgSO_4 \cdot 7H_2O$ and 90 µM $CaCl_2 \cdot H_2O$ or LB medium, respectively. Cultures were inoculated with 0.1 % of a preculture grown in LB and washed twice with the respective ISOGRO medium when required. All possible precursors were added at 4, 24 and 48 h after incubation in equal portions to a final concentration of 3 mM. Cultures were harvested after 72 h of incubation at 30 °C and 180 rpm, metabolites were extracted with 5 mL ethyl acetate and evaporated to dryness and redissolved in 1 mL MeOH.

Isolation of compounds. For the isolation of prexenocoumacin B (**4**) and C (**5**), *X. nematophila* HGB081-Δ*xcnG-xnc1_2228*::*cat* was cultivated in two 5 L Erlenmeyer flasks containing 2 L LB medium (pH 7.0) and 2 % (v/v) of Amberlite XAD-16 (Sigma-Aldrich) each. These cultures were inoculated with 0.1 % (v/v) of a 24 h preculture in the same medium without XAD-16. The cultures were harvested after 120 h and the XAD beads were separated from cells and supernatant by sieving. XAD beads were extracted with MeOH (3 × 200 mL, 1 × 100 mL, 1 × 50 mL) and concentrated to dryness on a rotary evaporator. The residue (2.97 g) was redissolved in 50 mL MeOH.

The crude extract was fractionated by a silica gel column chromatography (0.04 – 0.063 nm) using a hexane-chloroform-methanol gradient. The collected fractions were dried and checked for the presence of the substances by TLC (Silica gel/TLC-cards, Sigma-Aldrich) and HPLC MS. Pure compounds were isolated from enriched fractions by preparative RP HPLC MS (Waters 515 HPLC

Pump, Waters 2545 Binary Gradient Module, Waters 2998 Photodiode Array Detector, Waters SFO System Fluidics Organizer, Waters Selector Value, Waters 2767 Sample Manager coupled to a Waters 3100 mass detector; XBridge C18 5 μm RP column, Waters) using a 28 min gradient from 50-95% MeOH yielding pure prexenocoumacin B (**4**; Rt = 8.58 min; 5.7 mg L^{-1}) and prexenocoumacin C (**5**; Rt = 10.66 min; 1.5 mg L^{-1}). The pure fractions were dried and analyzed by HPLC MS prior to NMR analysis.

Amicoumacin A (**8**) was isolated as a reference compound for the advanced Marfey´s method for the structural assignment of compound **4**. Briefly, **8** was isolated from *B. pumilus* SAFR-032[6], which was cultivated in 5 L Erlenmeyer flasks (3 × 1 L) in YT medium (pH 7.0)[7] and 2 % (v/v) of Amberlite XAD-16. The cultures were harvested after 72 h, the XAD beads were extracted with MeOH (1 × 400 mL, 1 × 300 mL, 1 × 200 mL, 1 × 100 mL) and concentrated to dryness on a rotary evaporator. The crude extract (2.48 g) was fractionated using a silica gel column and fractions were tested for the presence of the compounds as described. Pure amicoumacin A (**8**; Rt = 10.58 min; 1.37 mg L^{-1}) was isolated by preparative RP HPLC MS using a 25 min gradient from 34-36% MeOH.

NMR analysis. ^{1}H, ^{1}H-^{1}H-COSY, ^{1}H-^{13}C-HSQC and ^{1}H-^{13}C-HMBC NMR spectra for **4**, **5** and **8** were recorded on a Bruker AV400 spectrometer (400 MHz) using MeOH-d_4 for all three substances and additionally DMSO-d_6 for **4** as solvent and internal standard (^{1}H-NMR: MeOH-d_4: δ = 3.31 ppm; DMSO-d_6: δ = 2.50 ppm; ^{13}C-NMR: MeOH-d_4: δ = 49.00 ppm; DMSO-d_6: δ = 39.52 ppm). ^{13}C NMR spectra were recorded on a Bruker AV300 (300 MHz).

Elucidation of amino acid configuration. Amino acid configurations of **4** and **8** were determined using the advanced Marfey's method[8-10]. The compounds (0.5 mg) were hydrolyzed in 6 M HCl at 110 °C overnight. The solution was evaporated to dryness and the residue was dissolved in 100 μL water and divided into two portions. Each portion was derivatized with 10 μL 1 M $NaHCO_3$ and 100 μL 1-fluoro-2,4-dinitrophenyl-5-L-leucinamide (L-FDLA) or D-FDLA for one hour at 40 °C in the dark. Addition of 10 μL 1 M HCl quenched the reaction and the dried solution was diluted with 400 μL MeOH. The stereochemistry was determined by comparison of the L-FDLA and L-/D-FDLA derivatized samples by ESI HPLC MS (**Supplementary Figure 2**).

Heterologous expression of *xcnG* and homologues in *E. coli*. For the construction of pUC18-XcnG, a plasmid containing the complete *xcnG* and the native promoter, a 1,968 bp fragment from genomic DNA from *X. nematophila* HGB081 using the primers xcnG_hetExp_PstI_fw and xcnG_hetExp_BamHI_rv was amplified and ligated via the *Pst*I and *BamH*I restriction site into pUC18 and transformed into *E. coli* DH10B, yielding DR001.

For a plasmid containing *xcnG*$^{-TMH}$ with the native promoter and without the *C*-terminal transmembrane helices pUC18-XcnG^{-TMH}, a fragment of 1,423 bp was amplified with the primers

pUC18-xcnG_oTMH_PstI_fw and pUC18-xcnG_oTMH_BamHI_rv, cloned into pUC18 via *Pst*I and *BamH*I and introduced into *E. coli* DH10B, yielding strain DR002.

A fragment of 1136 bp was amplified using the primers pET22b-xcnG_NcoI_fw and pET22b-xcnG_XhoI_rv for the construction of pET22b(+)-XcnG^{-TMH}, a plasmid containing *xcnG* without the *C*-terminal transmembrane helices and with a *C*-terminal Histag. Ligation was conducted via the *Nco*I and *Xho*I restriction site into pET22b(+) and transformed into *E. coli* DH10, and retransformed after sequencing into BL21 (DE3), yielding DR003.

For the construction of plasmids containing *xcnG* homologues from other organisms, fragments of 3,265 bp for *xbJ1_2693* (*Xenorhabdus bovienii* SS-2004) and of 1,621 bp for *pbum_0630* (*Bacillus pumilus* SAFR-032) were amplified using the primers pUC18-Xb2693_fw_PstI_T7A1_RBS and pUC18-Xb2693_rv_BamHI or pUC18-PbpX_fw_PstI_T7A1_RBS and pUC18-PbpX_rv_BamHI, respectively. The genes were amplified without the native promoter and an additional T7A1 promoter was cloned upstream of the genes. These fragments were ligated via the *Pst*I and *BamH*I restriction site into pUC18 and transformed into *E. coli* DH10B, yielding strains DR004 and DR005.

For the construction of the plasmid of the homologues ZmaM (*Bacillus thuringiensis* DSM 2046^{T}), a 3,106 bp fragment of *zmaM* without the native promoter was amplified with the primers ZmaM_pCK_T7A1_fw_BamHI_2 and ZmaM_pCK_T7A1_rv_XhoI, cloned via the *Bam*HI and *Xho*I restriction site into the plasmid pCK-T7A1[11] and introduced into *E. coli* DH10B, yielding strain DR006.

Heterologous expression of *xcnMN* in *E. coli* DH10B. For the construction of an *E. coli* strain containing the necessary genes for the cleavage of prexenocoumacin A-E (**3**-**7**) into xenocoumacin-1 (**1**) and the transformation into xenocoumacin-2 (**2**)[12] a 2,513 bp fragment containing *xcnMN* were amplified using the primers pCOLA_tacI_xcnMN_fw_NdeI and pCOLA_tacI_xcnMN_rv_XhoI. The fragment was cloned via *Nde*I and *Xho*I downstream of the *tac*I promoter into the plasmid pCOLA-*tac*I (Kegler, C., unpublished) carrying a kanamycin resistance cassette and transformed into *E. coli* DH10B. The plasmid pCOLA-*tac*I-XcnMN (**Supplementary Figure 14**) was introduced into *E. coli* DH10B pUC18-XcnG, yielding strain DR007.

Protein expression of XcnG without *C*-terminal transmembrane helices. Protein expression of XcnG with a *C*-terminal Histag and without the transmembran helices and isolation of the periplasmic fraction was conducted according to manufacturer's instructions (Novagen).

***In vivo* cleavage and resistance assay.** To study the cleavage of **4** into **1** by XcnG with and without the *C*-terminal transmembrane helices and the homologues XbJ1_2693, Bpum_0630 and ZmaM as well as the transformation of **1** into **2** by XcnMN[12] an *in vivo* assay in *E. coli* DH10 was performed.

The strains DR001, DR002 DR004-DR007 and as controls DR008-DR011 (**Supplementary Table 2**) were cultivated in duplicates in 250 mL Erlenmeyer flasks containing 20 mL LB medium, pH 7.0 each and antibiotic, respectively, at a rotary shaker at 30 °C and 180 rpm. These cultures were inoculated with a 16 h preculture up to an OD_{600} of 0.05. 0.2 mg of **4** dissolved in MeOH was added after three hours of cultivation, and strains containing pCOLA-*tac*I plasmids were induced with 0.1 mM IPTG. All cultures were cultivated for 72 h and samples of 350 µL were taken every hour for 8 h and after 10, 12 and 24 h. Optical density were measured directly after sampling with 100 µL and the remaining 250 µL of the samples was frozen at -20 °C. The samples were extracted with 200 µL of ethyl acetate at room temperature for 30 minutes, the organic layer was evaporated to dryness, redissolved in 75 µL MeOH and analyzed by ESI HPLC MS. Amounts of the metabolites **1**, **2** and **4** were analyzed using the program DataAnalysis 4.0 (Bruker Daltonics) and the "integrate only" command to find compounds in the selected extracted ion chromatogram trace.

Disk diffusion tests for antibiotic activity. Disk diffusion tests for antibiotic activity were carried out according to the Kirby-Bauer method[13]. Inoculums of *X. nematophila* HGB081, *xcnG*, *xcnM*, and *xcnK*::*cat*, *E. coli* DH10B and *M. luteus* with an OD_{600} of 0.5 were prepared from 24 h precultures in LB medium, pH 7.0. LB agar plates were overlaid with inoculums of the respective strains using a sterile swab, rotated several times and pressed firmly on the inside wall of the inoculum tubes. The swab was stricken over the agar surface three times, rotating for 60° each time.
Metabolites of 25 mL cultures of HGB081, *xcnG*, *xcnM* and *xcnK*::*cat* cultures were extracted after 48 h of incubation with ethyl acetate, evaporated to dryness and redissolved in MeOH. The obtained crude extract was diluted 1:50 for *E. coli* and *M. luteus* for antibiotic activity overlay assays and for *X. nematophila* overlays a fifth of the crude extracts were spotted on sterile filter paper discs with a 9 mm diameter, which were dried prior to their application on the inoculated agar surface. All agar plates were incubated for 48 h at 30 °C and inhibition zone diameters were measured thereafter.

Bioinformatic analyses. We performed BLAST-P[14] analysis of XcnG to find possible homologues being part of a polyketide synthase (PKS) and/or nonribosomal polypeptide synthetase (NRPS) biosynthetic gene cluster. PKS and NRPS proteins and their corresponding biosynthetic gene clusters were analyzed as described previously[15], following a frame plot 2.3.2 analysis[16] and the PKS/NRPS analysis website (http://nrps.igs.umaryland.edu/nrps/)[17]. Sequence alignments were constructed using ClustalW[18]. For the characterization of the transmembrane helices the TMHMM Server v. 2.0 (http://www.cbs.dtu.dk/services/TMHMM/)[19] and for prediction of signal peptide cleavage sites the SignalP 3.0 Server[20] was used.

The phylogenetic investigations were done as follows – Alignments were done using muscle[21] with default settings. Phylogenetic analyses were carried out using Mega (version 5.0)[22] for Minimum Evolution analysis and RAxML[23] with rapid bootstrapping as implemented on the RAxML

webservers[24] for Maximum Likelihood analysis. For both analyses the JTT model was used, other parameters were set to default values, and for both Minimum Evolution and Maximum Likelihood analyses 500 bootstrap replicates[25] were carried out.

Supplementary Table 1. Oligonucleotides used in this work. Restriction sites are marked in bold, complementary sequences used for overlap extension PCR are in lower case, inserted promoters and ribosomal binding sites are in lower case and underlined, respectively.

Gene	Oligonucleotide	(5'-3') Sequence
xcnG	xcnG_up-F	ATGCA**GCATGC**AGCGGAATATATAGAAAGACCG
xcnG	xcnG_up-R	gttgacattaacagcgttaaCAGTTGTTCCTTGAGTTCAGCA
xcnG	xcnG_down-F	tgctgaactcaaggaacaactgTTAACGCTGTTAATGTCAAC
xcnG	xcnG_down-R	ATGC**GAGCTC**CTATCCGGGTAATAACAGATTC
xcnG	vxcnGDel-fw	TGGCCTGCCTTAGATGACAGTT
xcnG	vxcnGDel-rv	AAGCGAGATCGCAATCACCA
xnc1_2228	Xn2576fw	ATGC**GAGCTC**TTATCGAACGTACCGCGCCT
xnc1_2228	Xn2576rv	TATGC**GCATGC**CATTCGGTAGCGGTTTGCCT
xnc1_2228	v2576f	CAGATAGTTTTTACGCTGGAGA
xnc1_2228	v2576r	GACTATAAGCAATCACCGCC
	pDS132fw	GATCGATCCTCTAGAGTCGACCT
	pDS132rv	ACATGTGGAATTGTGAGCGG
xcnG	xcnG_hetExp_PstI_fw	ATAT**CTGCAG**TCAACTTGAAAGTTCATTCTCTCT
xcnG	xcnG_hetExp_BamHI_rv	ATAT**GGATCC**GGGGTGTCGTTGCATCAGGA
xcnG	pUC18-xcnG_oTMH_PstI_fw	ATAT**CTGCAG**TCAACTTGAAAGTTCATTCTCTCT
xcnG	pUC18-xcnG_oTMH_BamHI_rv	ATAT**GGATCC**ATCAAACAACTCAATATCATTG
xcnG	pET22-xcnG_NcoI_fw	ATAT**CCATGG**CAAAAAATGAATCAACTGACCA
xcnG	pET22-xcnG_XhoI_rv	GGAT**CTCGAG**ATCAAACAACTCAATATCATTG
xcnMN	pCOLA_tacI_xcnMN_fw_NdeI	ATGC**CATATG**AAAAAGTTGTCTGTTTTAT
xcnMN	pCOLA_tacI_xcnMN_rv_XhoI	TATC**CTCGAG**TCAAATAGAAAGAAGATGTTTG
xbj1_2693	pUC18-Xb2693_fw_PstI_T7A1_RBS	ATAT**CTGCAG**atcaaaaagagtattgacttaaagtctaacctataggatacttacagcc atcgagaggGAAGACAATGAATAATACTGG
xbj1_2693	pUC18-Xb2693_rv_BamHI	ATTAT**GGATCC**TTAAGCATAACTCTCTCCCTT
bpum_0630	pUC18-PbpX_fw_PstI_T7A1_RBS	ATAT**CTGCAG**atcaaaaagagtattgacttaaagtctaacctataggatacttacagcc atcgagaggTATTTACATGAGGAAAAATCAG
bpum_0630	pUC18-PbpX_rv_BamHI	ATTAT**GGATCC**TTATAAGGATGAATGCCCGA
zmaM	ZmaM_pCK-T7A1_fw_BamHI_2	ATACG**GGATCC**ATGAAGTTAAACATATGGTT
zmaM	ZmaM_pCK-T7A1_rv_XhoI	ATTAT**CTCGAG**TCATGATAATGCCTCCTTTG

Homology modeling of the peptidase XcnG. The XcnG primary amino acid sequence was subjected to secondary and tertiary structure analysis via the Phyre Web Server[26] which resulted in a 3D homology model. The XcnG model showed excellent superimposition (rmsd: 2,15 Å) with the AmpC β-lactamase from *E. coli* (pdb:2FFY) using a secondary structure matching algorithm[27] and allowed the identification of the conserved catalytic Ser-Lys-Tyr triade as found in the family of β-lactamases/transpeptidases/carboxypeptidases. Moreover, XcnG function was also assessed *in silico*

by the automated protein function prediction method ConFunc[28] and returned the highest score for carboxypeptidase activity.

Supplementary Table 2. Plasmids and strains used.

Plasmid or strain	Genotype	Reference
Plasmids		
pUC18	pUC ori, *bla* (Ap^r)	Yanisch-Perron *et al*. (1985)[29]
pUC18-XcnG	pUC ori, *bla* (Ap^r), *xcnG* with native promoter region	This work, Supp. Fig. 14
pUC18-XcnG^{-TMH}	pUC ori, *bla* (Ap^r), *xcnG*$^{-TMH}$ without *C*-terminal transmembrane helices, with native promoter region	This work, Supp. Fig. 14
pUC18-T7A1-XbJ1_2693	pUC ori, *bla* (Ap^r), *xbj1_2693*, T7A1 promoter	This work, Supp. Fig. 14
pUC18-T7A1-Bpum_0630	pUC ori, *bla* (Ap^r), *pbum_0630*, T7A1 promoter	This work, Supp. Fig. 14
pCK-T7A att	pUC ori, *bla* (Ap^r), T7A1 promoter	Bode *et al.* (2009)[11]
pCK-T7A1-ZmaM	pUC ori, *bla* (Ap^r), *zmaM*, T7A1 promoter	This work, Supp. Fig. 14
pCOLA-tacI	pCOLA-Duet1 based vector, ColA ori, *kan* (Km^r), *tacI* promoter	C. Kegler, unpublished
pCOLA-tacI-XcnMN	pCOLA-Duet1 based vector, ColA ori, *kan* (Km^r), *xcnMN*, *tacI* promoter	This work, Supp. Fig. 14
pET22b(+)	ColE1 ori, *bla* (Ap^r),T7 lac, Histag, pelB signal sequence	Novagen
pET22b(+)-XcnG^{-TMH}	ColE1 ori, *bla* (Ap^r),T7 lac, Histag, pelB signal sequence, *xcnG*$^{-TMH}$ without *C*-terminal transmembrane helices	This work
Strains		
E. coli DH10B	F_ mcrA Δ (*mrr-hsd*RMS-mcrBC), 80*lac*Z Δ, M15, Δ *lac*X74 *rec*A1 *end*A1 *ara*D 139 Δ (*ara*, *leu*)7697 *gal*U *gal*K λ *rpsL* (*Str*^{r}) *nup*G	Grant *et al.* (1990)[30]
E. coli BL21 (DE3)	F^- *omp*T *gal dcm hsd*S_B (r_B-,m_B-) λ(DE3)	Novagen
DR001	DH10B::pUC18-XcnG, Ap^r	This work
DR002	DH10B::pUC18-XcnG^{-TMH}, Ap^r	This work
DR003	BL21 (DE3)::pET22b(+)-XcnG	This work
DR004	DH10B::pUC18-T7A1-XbJ1_2693, Ap^r	This work
DR005	DH10B::pUC18-T7A1-Bpum_0630, Ap^r	This work
DR006	DH10B::pCK-T7A1-ZmaM, Ap^r	This work
DR007	DH10B::pUC18-XcnG, pCOLA-tacI-XcnMN, Ap^r, Km^r	This work
DR008	DH10B::pUC18, Ap^r	This work
DR009	DH10B::pUC18, pCOLA-tacI, Ap^r,Km^r	This work
DR010	DH10B::pCK-T7A1, Ap^r	This work
DR011	DH10B::pUC18-XcnG, pCOLA-tacI, Ap^r, Km^r	This work

Supplementary Results

Supplementary Table 3. NMR data of prexenocoumacin B (**4**) and C (**5**). EAD (extended arginine derivative), BPF (benzopyran-1-one fragment).

			4 (D_6-DMSO)		**4 (CD_3OD)**		**5 (CD_3OD)**
subunit	position	δ_C	δ_H, mult. (*J* in Hz)	δ_C	δ_H, mult. (*J* in Hz)	δ_C	δ_H, mult. (*J* in Hz)
Acyl	1	172.5		176.4		176.5	
	2	35.0	2.07, t (7.3)	36.9	2.24, t (7.4)	36.9	2.24, t (7.5)
	3	24.8	1.44, m	26.8	1.58, m	26.9	1.58, m
	4	28.3	1.21, m	n.d.		30.6	1.29, m
	5	21.8	1.21, m	23.7	1.28, m	28.3	1.30, m
	6	24.8	1.46, m	30.2	1.28, m	25.8	1.72, m
	7	30.9	1.21, m	32.9	1.28, m	29.1	1.51, m
	8	13.7	0.83, t (7.1)	14.4	0.88, d (6.8)	23.0	0.86, d (6.6)
	9					23.0	0.86, d (6.6)
D-Asn	1	171.3		173.6		173.6	
	2	49.8	4.48, q (7.0)	52.0	4.63, t (6.6)	52.0	4.62, m
	2-NH		8.02, d (7.6)		-		-
	3	37.3	2.48, dd (15.6, 5.8)	37.8	2.65, dd (15.5, 6.7)	37.7	2.73, dd (15.3, 6.6)
			2.38, dd (15.2, 7.8)		1.73, m		2.66, dd (15.7, 6.8)
	4	n.d.		n.d.		n.d.	
	4-NH_2		7.39, br s[a]		-		-
EAD	1	173.0		174.8		174.8	
	2	71.1	3.88, d (6.6)	73.3	4.11, d (5.4)	73.3	4.10, d (5.2)
	3	74.5	3.50, t (5.0)	76.3	3.71, t (5.6)	76.3	3.71, t (5.7)
	4	49.3	3.95, m	51.9	4.05, m	51.9	4.08, m
	4-NH		7.56, d (9.2)		-		-
	5	24.8	1.32, m	27.6	1.77, m; 1.50, m	27.7	1.50, m
	6	23.8	1.63, m	26.3	1.60, m	26.3	1.60, m
	7	48.8	3.16, m	42.2	3.10, m	42.2	3.10, m
	7-NH						-
	8	n.d.		158.5		158.5	
	8-NH		6.89, br s[a]		-		-
BPF	1	169.4		171.1		171.2	
	2	108.4		109.4		109.4	
	3	161.0		163.2		163.2	
	4	115.1	6.84, d (8.4)	116.7	6.83, d (8.4)	116.7	6.83, d (8.4)
	5	136.3	7.46, t (7.9)	137.5	7.43, t (7.9)	137.5	7.44, t (8.0)
	6	118.4	6.80, d (7.4)	119.5	6.77, d (7.3)	119.5	6.77, d (7.3)
	7	140.9		141.8		141.8	
	8	28.8	3.08, dd (16.2, 13.1)	30.3	3.15, dd (16.7, 13.0)	31.1	3.14, dd (16.2, 12.5)
			2.82, br d (14.4)		2.89, dd (16.7, 2.7)		2.89, dd (16.4, 2.6)
	9	81.0	4.67, br d (12.6)	82.9	4.65, m	82.3	4.67, m
	10	48.0	4.19, m	50.5	4.33, dt (10.0, 2.7)	50.5	4.32, dt (10.4, 2.7)
	10-NH		7.89, d (9.2)		-		-
	11	38.7	1.66, m	40.9	1.82, m	40.9	1.82, m
			1.35, m		1.45, m		1.45, m
	12	24.0	1.66, m	25.8	1.73, m	25.8	1.74, m
	13	23.0	0.89, d (6.4)	23.8	0.97, d (6.6)	23.8	0.97, d (6.6)
	14	21.3	0.85, d (6.3)	22.1	0.94, d (6.5)	22.1	0.94, d (6.6)

n.d. (not detected); [a] might be exchangeable.

Supplementary Table 4. Structure elucidation of prexenocoumacin A-E (**3**-**7**). **a.** HRMS analysis of **3**-**7**. **b.** Typical fragmentation pattern of prexenocoumacin derivatives. Positions of fragmentations are colored in blue.

a.

Compound	measured m/z $[M + H]^+$	calc. m/z $[M + H]^+$	Δppm	Sum formula
3	692.3981	692.3978	0.52	$C_{33}H_{54}O_9N_7$
4	706.4119	706.4134	2.10	$C_{34}H_{56}O_9N_7$
5	720.4274	720.4291	2.32	$C_{35}H_{58}O_9N_7$
6	734.4431	734.4447	2.14	$C_{36}H_{60}O_9N_7$
7	726.3827	726.3821	0.82	$C_{36}H_{52}O_9N_7$

b.

Fragment	measured m/z $[M + H]^+$	calc. m/z $[M + H]^+$	Δppm	Sum formula
563 (**a**)	563.2853	563.2824	5.22	$C_{26}H_{39}O_8N_6$
466 (**1**)	466.2679	466.2660	4.03	$C_{22}H_{36}O_6N_5$
449 (**b**)	449.2412	449.2395	6.94	$C_{22}H_{33}O_6N_4$
BPF (**c**)	250.1442	250.1438	1.64	$C_{14}H_{20}O_3N$

BPF (benzopyran-1-one fragment)

Supplementary Table 5. Structure elucidation of prexenocoumacin A-E (**3**-**7**) resulting from feeding experiments in HGB081-Δ*xcnG*.

compound	labeling experiment	m/z [M + H^+]	Sum formula	BPF m/z [M+H^+]	Sum formula
3	^{12}C	692.5	$C_{33}H_{54}O_9N_7$	250.1	$C_{14}H_{20}O_3N$
	^{12}C + $^{2}H_3$-leu	698.6	$C_{33}H_{48}{}^{2}H_6O_9N_7$	n.d.	n.d.
	^{13}C	725.6	$^{13}C_{33}H_{54}O_9N_7$	264.3	$^{13}C_{14}H_{20}O_3N$
	^{13}C + arg	n.d.	n.d.	n.d.	n.d.
	^{13}C + leu	719.4	$^{13}C_{27}C_6H_{54}O_9N_7$	n.d.	n.d.
	^{13}C + leu	714.2	$^{13}C_{22}C_{11}H_{54}O_9N_7$	n.d.	n.d.
	^{15}N	699.4	$C_{33}H_{54}O_9{}^{15}N_7$	251.1	$C_{14}H_{20}O_3{}^{15}N$
4	^{12}C	706.5	$C_{34}H_{56}O_9N_7$	250.2	$C_{14}H_{20}O_3N$
	^{12}C + $^{2}H_3$-leu	709.5	$C_{34}H_{53}{}^{2}H_3O_9N_7$	253.2	$C_{14}H_{17}{}^{2}H_3O_3N$
	^{13}C	740.6	$^{13}C_{34}H_{56}O_9N_7$	264.2	$^{13}C_{14}H_{20}O_3N$
	^{13}C + arg	734.6	$^{13}C_{28}C_6H_{56}O_9N_7$	264.2	$^{13}C_{14}H_{20}O_3N$
	^{13}C + leu	734.6	$^{13}C_{28}C_6H_{56}O_9N_7$	258.3	$^{13}C_8C_6H_{20}O_3N$
	^{13}C + caprylic acid	732.6	$^{13}C_{26}C_8H_{56}O_9N_7$	264.3	$^{13}C_{14}H_{20}O_3N$
	^{13}C + decanoic acid	734.6	$^{13}C_{28}C_6H_{56}O_9N_7$	264.3	$^{13}C_{14}H_{20}O_3N$
	^{15}N	713.4	$C_{34}H_{56}O_9{}^{15}N_7$	251.1	$C_{14}H_{20}O_3{}^{15}N$
5	^{12}C	720.5	$C_{35}H_{58}O_9N_7$	250.2	$C_{14}H_{20}O_3N$
	^{12}C + $^{2}H_3$-leu	726.6	$C_{35}H_{52}{}^{2}H_6O_9N_7$	253.2	$C_{14}H_{17}{}^{2}H_3O_3N$
	^{13}C	755.7	$^{13}C_{35}H_{58}O_9N_7$	264.3	$^{13}C_{14}H_{20}O_3N$
	^{13}C + arg	749.1	$^{13}C_{29}C_6H_{58}O_9N_7$	n.d.	n.d.
	^{13}C + leu	749.5	$^{13}C_{29}C_6H_{58}O_9N_7$	258.2	$^{13}C_8C_6H_{20}O_3N$
	^{13}C + leu	744.6	$^{13}C_{24}C_{11}H_{58}O_9N_7$	258.2	$^{13}C_8C_6H_{20}O_3N$
	^{15}N	727.4	$C_{35}H_{58}O_9{}^{15}N_7$	251.1	$C_{14}H_{20}O_3{}^{15}N$
6	^{12}C	734.5	$C_{36}H_{60}O_9N_7$	250.2	$C_{14}H_{20}O_3N$
	^{12}C + $^{2}H_3$-leu	737.5	$C_{36}H_{57}{}^{2}H_3O_9N_7$	n.d.	n.d.
	^{13}C	770.6	$^{13}C_{36}H_{60}O_9N_7$	264.1	$^{13}C_{14}H_{20}O_3N$
	^{13}C + arg	764.7	$^{13}C_{30}C_6H_{60}O_9N_7$	264.1	$^{13}C_{14}H_{20}O_3N$
	^{13}C + leu	764.5	$^{13}C_{30}C_6H_{60}O_9N_7$	258.1	$^{13}C_8C_6H_{20}O_3N$
	^{13}C + caprylic acid	762.8	$^{13}C_{28}C_8H_{60}O_9N_7$	n.d.	n.d.
	^{13}C + decanoic acid	760.6	$^{13}C_{26}C_{10}H_{60}O_9N_7$	n.d.	n.d.
	^{15}N	741.4	$C_{36}H_{60}O_9{}^{15}N_7$	251.1	$C_{14}H_{20}O_3{}^{15}N$
7	^{12}C	726.5	$C_{36}H_{52}O_9N_7$	250.1	$C_{14}H_{20}O_3N$
	^{12}C + $^{2}H_3$-leu	729.3	$C_{36}H_{49}{}^{2}H_3O_9N_7$	n.d.	n.d.
	^{12}C + 4-F-phenylacetic acid	744.8	$C_{36}H_{51}O_9N_7F_1$	250.2	$C_{14}H_{20}O_3N$
	^{12}C + *p*-F-phe	744.8	$C_{36}H_{51}O_9N_7F_1$	250.2	$C_{14}H_{20}O_3N$
	^{12}C + 4-Cl-phenylacetic acid	760.4	$C_{36}H_{51}O_9N_7Cl_1$	250.1	$C_{14}H_{20}O_3N$
	^{13}C	762.5	$^{13}C_{36}H_{52}O_9N_7$	264.3	$^{13}C_{14}H_{20}O_3N$
	^{13}C + arg	756.6	$^{13}C_{30}C_6H_{52}O_9N_7$	264.3	$^{13}C_{14}H_{20}O_3N$
	^{13}C + leu	756.6	$^{13}C_{30}C_6H_{52}O_9N_7$	258.3	$^{13}C_8C_6H_{20}O_3N$
	^{13}C + phe	754.6	$^{13}C_{28}C_8H_{52}O_9N_7$	264.1	$^{13}C_{14}H_{20}O_3N$
	^{15}N	733.4	$C_{36}H_{52}O_9{}^{15}N_7$	251.1	$C_{14}H_{20}O_3{}^{15}N$

n.d. (not detected), BPF (benzopyran-1-one fragment)

Supplementary Table 6. XcnG homologues, their accession number and identities/positives of the full length protein and the peptidase domain.

Protein	Identities/ Positives of the complete protein [%]	Identities / Positives of the peptidase domain [%]	Accession number
Bpum_0630	30/51	33/54	YP_001485882.1
CLM0371	29/52	34/57	YP_002802626.1
C2452	28/49	30/52	NP_754344.1
CKO_00875	28/49	30/52	YP_001452461.1
XbJ_2693	27/46	29/49	YP_003468581.1
ZmaM	30/51	34/53	ZP_04105327.1
Plarl_010100010772	31/50	33/53	ZP_02328117.1

Supplementary Table 7. Amino acid specificities of adenylation domains in the second module following the XcnA homologue. Presented are the 8 amino acid code[31] and known incorporated amino acids. The second module of *X. nematophila*, *B. pumilus* and *B. thuringiensis* is deduced from the known structures. In *P. larvae* no conclusion is possible due to the incomplete biosynthesis gene cluster. In *C. koseri* and *E. coli* two different modules as a second module are possible. In all other cases co-linearity in the biosynthesis machinery is assumed.

Strain	Compound	Specificity of the A-domain in the first module	Incorporated amino acid	Specificity of the A-domain in the second module	Incorporated amino acid
X. nematophila HGB081	xenocoumacin	Asx (DLTKIGEV)	Asn	no hit (DPENIGHV)	Arg
B. pumilus SAFR-032	amicoumacin	Asx (DLTKIGEV)	unknown	Asx (DLTKIGEV)	Asp
B. thuringiensis DSM2046^T	zwittermicin	Asx (DLTKIGEV)	unknown	Thr (DMWNTGMV)	Ser
C. botulinum A2 str. Kyoto	unknown	Asx (DLTKIGEV)	unknown	no hit (VAWELTAD)	unknown
C. koseri ATCC BAA-895	colibactin	Asn (DLTKVGEV)	unknown	no hit (DILQVALI) Val (DVFXTGGI)	unknown unknown
E. coli CFT073	colibactin	Asn (DLTKVGEV)	unknown	no hit (DILQVALI) Val (DVFXTGGI)	unknown unknown
P. larvae ssp. larvae BRL-230010	unknown	Asx (DLTKIGEV)	unknown	-[a]	-[a]
X. bovienii SS-2004	unknown	Asx (DLTKIGEV)	unknown	no hit (DPENWFHV)	unknown

[a]no conclusion possible.

Supplementary Table 8. Possible ABC-transporter in bacteria containing XcnG-like peptidase domain architecture.

Organism	Protein	Identities/ Positives of the ABC transporter region [%]	Accession number	Possible function
X. nematophila HGB081	Xnc1_2784	28/48	YP_003712977.1	Putative ATP-binding protein
	Xnc1_2463	29/50	YP_003712685.1	Putative transport protein (Multidrug resistance protein)
	Xnc1_1568	25/43	YP_003711829.1	Lipid A transporter
B. pumilus SAFR-032	Bpum_3517	23/41	YP_001488725.1	ABC transporter ATP-binding protein
	Bpum_0919	21/44	YP_001486163.1	ABC transporter ATP-binding protein involved in Fe-S cluster assembly
	Bpum_0918	22/43	YP_001486162.1	ABC transporter ATP-binding protein involved in cytochrom bd biosynthesis
	Bpum_3516	23/43	YP_001488724.1	ABC transporter ATP-binding protein involved in cytochrom bd biosynthesis
C. botulinum A2 str. Kyoto	CLM_0726	26/46	YP_002802962.1	Putative ABC transporter, ATP-bindung protein/permease protein
	CLM_1206	22/44	YP_002803417.1	Lipid A transporter
	CLM_2586	21/43	YP_002804740.1	Putative ABC transporter, ATP-bindung protein/permease protein
	CLM_1843	20/41	YP_002804021.1	ABC transporter, ATP-bindung protein/permease protein
E. coli CFT073	C2752	31/50	NP_754638.1	Multidrug transporter membrane component/ATP-binding component (Microcin peptide J25)
	C2422	27/44	NP_754314.1	Permease and ATP-binding protein of yersiniabactin-iron ABC transporter
	C1054	25/46	NP_752981.1	Lipid A transporter
	C1024	25/43	NP_752953.1	Cysteine + glutathione transporter
C. koseri ATCC BAA-895	CKO_00563	33/51	YP_001452154.1	Multidrug transporter membrane component/ATP-binding component (Microcin peptide J25)
	CKO_00913	27/43	YP_001452499.1	Permease and ATP-binding protein of yersiniabactin-iron ABC transporter
	CKO_02156	24/45	YP_001453716.1	Lipid A transporter
	CKO_02185	26/43	YP_001453745.1	Cysteine + glutathione transporter
E. coli DH10B	ECDH10B_2368	31/50	YP_001731151.1	Multidrug transporter membrane component/ATP-binding component (Microcin peptide J25)
	ECDH10B_0984	25/46	YP_001729892.1	Lipid A transporter
	ECDH10B_0957	25/43	YP_001729865.1	Cysteine + glutathione transporter

Supplementary Table 9. Possible TolC proteins in Gram-negative bacteria forming complexes with XcnG- and ZmaM-like peptidases.

Organism	Protein	Identities/ Positives of TolC (AP_003585.1) [%]	Accession number	Possible function
X. nematophila HGB081	Xnc1_4077	59/77	YP_003714188.1	Outer membrane channel (tolerance to colicin E1)
	Xnc1_4021	26/46	YP_003714134.1	Alkaline protease secretion protein aprF
X. bovienii SS-2004	XbJ1_1814	61/77	YP_003467720.1	Outer membrane channel (tolerance to colicin E1)
	XbJ1_0487	26/46	YP_003466432.1	Alkaline protease secretion protein aprF
E. coli CFT073	C3781	99/99	NP_755652.2	Outer membrane channel
	C1765	22/39	NP_753669.1	Partial outer membran channel
C. koseri ATCC BAA-895	CKO_04427	90/96	YP_001455919.1	Outer membrane channel
	CKO_02835	23/42	YP_001454377.1	Hypothetical protein

Supplementary Figure 1. NMR analysis of prexenocoumacin B (**4**, D_6-DMSO) and C (**5**, CD_3OD) showing selected COSY (bold lines) and HMBC (arrows) correlations.

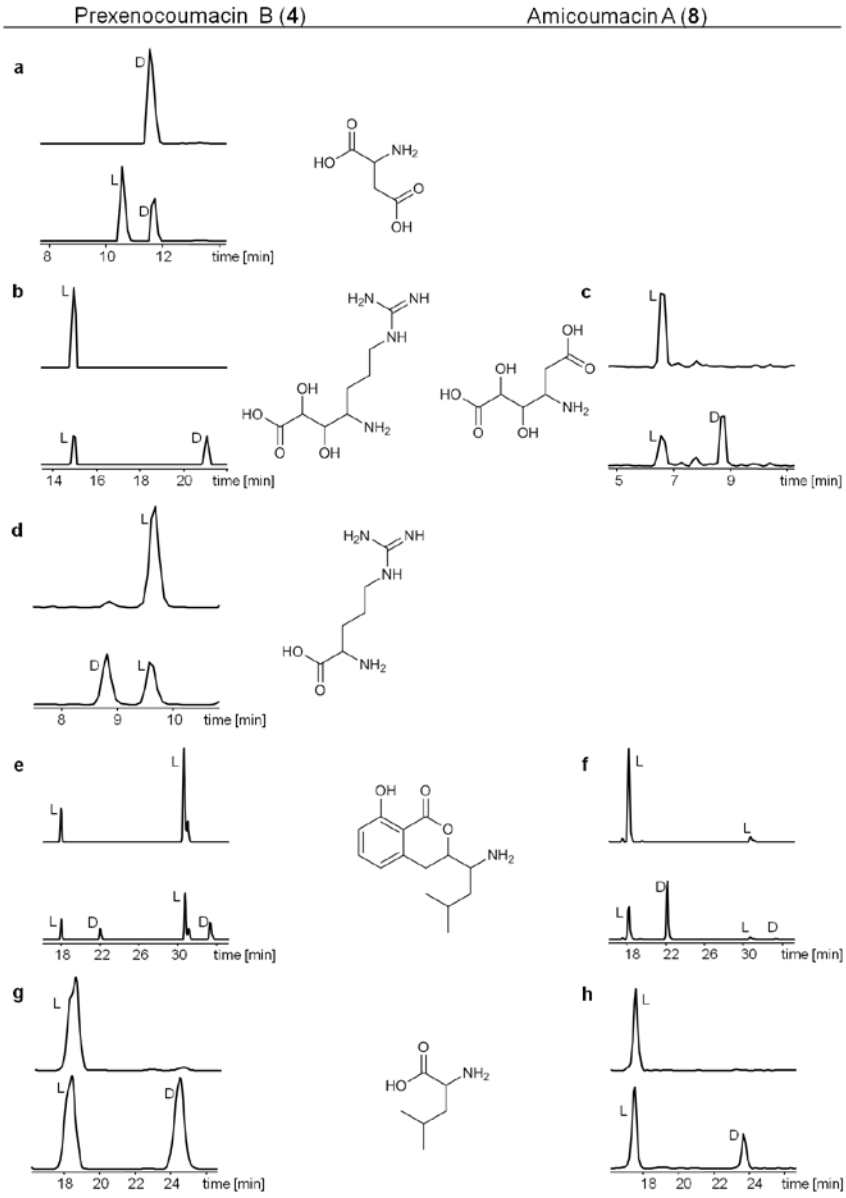

Supplementary Figure 2. ESI HPLC MS analysis of prexenocoumacin B (**4**) and amicoumacin A (**8**) hydrolyzed and derivatized with FDLA. Depicted are extracted ion chromatogram traces of derivatized amino acids or their corresponding building blocks in the polyketide-peptide structure with L-FDLA (top) and L-/D-FDLA (bottom), (**a**) aspartic acid, (**b**) 4-amino-7-guanidinium-2,3-dihydroxy-heptanoic acid, (**c**) 4-amino-2,3-dihydroxy-hexanedioic acid, (**d**) arginine, (**e, f**) 3-(1-amino-3-methylbutyl)-8-hydroxy-3,4-dihydro-1*H*-isochromen-1-one and (**g, h**) leucine. The stereochemistry is determined by the elution order of the derivatized amino acids or the building blocks. Based on the hydroxylation of asparagine to aspartic acid, only traces for the L-FDLA derivatized D-aspartic acid eluting later to the L-enantiomer in **4**, could be detected. L-FDLA derivatized L-arginine in **4** elutes later than the D-enantiomer and L-FDLA derivatized L-4-amino-7-guanidinium-2,3-dihydroxy-heptanoic acid in **4** elutes earlier. Hydroxylation of asparagine to aspartic acid could also detected in **8** resulting in the L-FDLA derivatized L-4-amino-2,3-dihydroxy-hexanedioic acid eluting prior to the D-enantiomer. L-FDLA derivatized L-leucine elutes prior to its D-enantiomer. As a result of the L-FDLA derivatization of 3-(1-amino-3-methylbutyl)-8-hydroxy-3,4-dihydro-1*H*-isochromen-1-one the leucine side chain is more hydrophilic than the isocoumarine ring and the L-derivative elutes earlier. D-FDLA derivatized amino acids or building blocks behave inversely. All chromatograms are scaled in the same intensity.

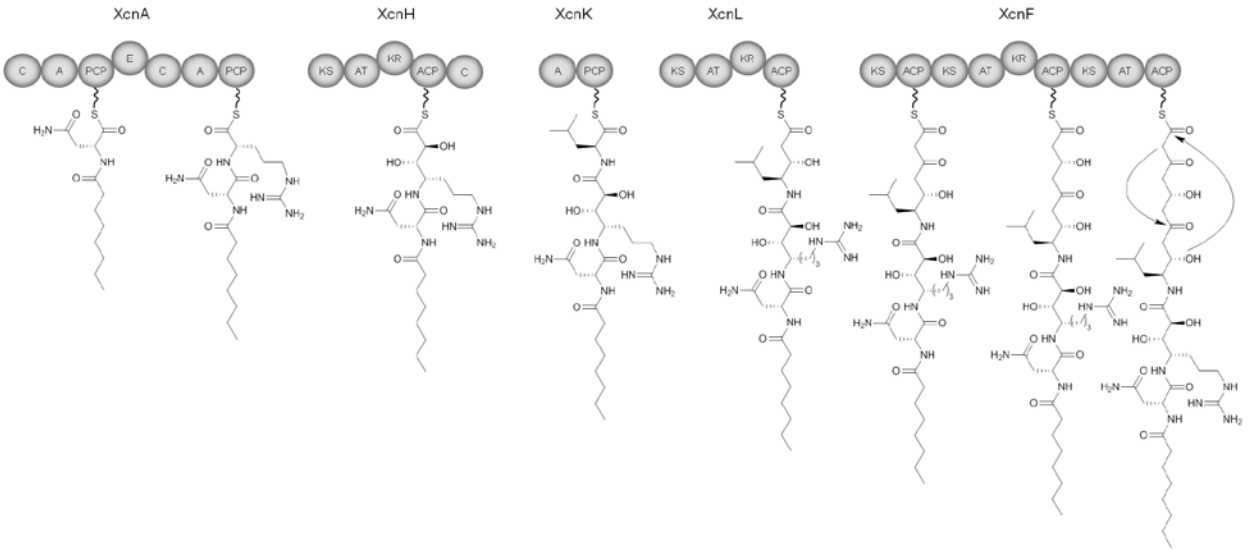

Supplementary Figure 3. Proposed biosynthesis pathway for the formation of the polyketide-peptide backbone of prexenocoumacin B (**4**), which allowed a correction of the proposed biosynthesis of xenocoumacin published earlier[12]. Our new model suggests the order XcnAHKLF as depicted and the new biosynthetic gene order fits perfectly to the elucidated structure of the prexenocoumacin. A: adenylation domain, C: condensation domain, E: epimerization domain, PCP: peptidyl carrier protein domain, AT: acyltransferase domain, ACP: acyl carrier protein domain, KS: β-ketoacyl carrier protein synthase domain, KR: ketoreductase domain.

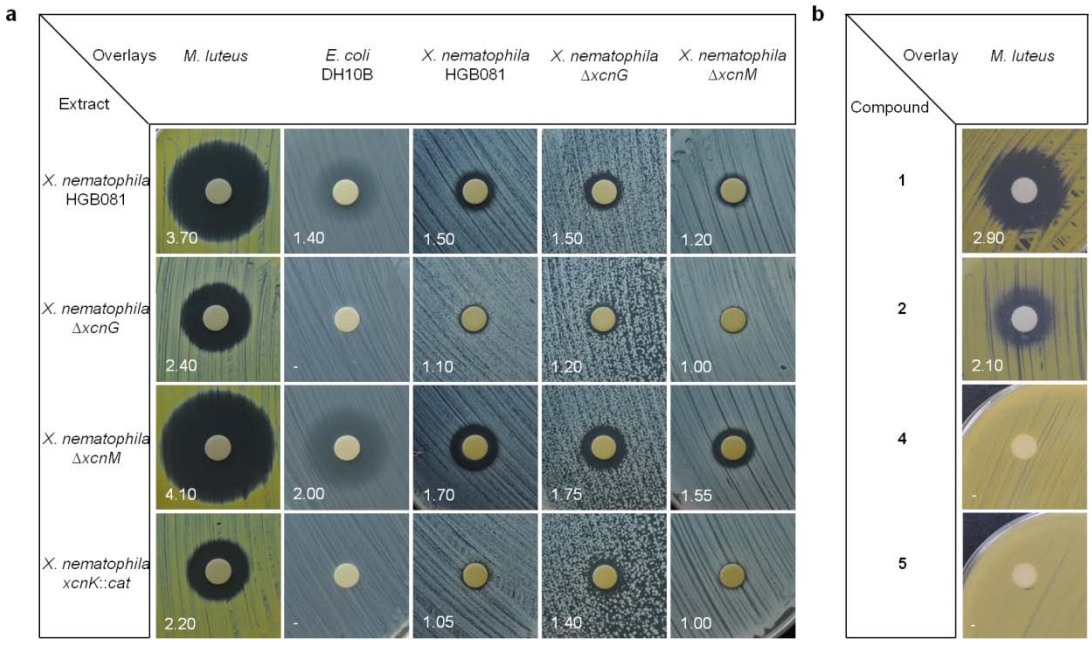

Supplementary Figure 4. a. Results from disk diffusion assays of extracts from different *X. nematophila* strains against selected microorganisms. Shown are the inhibition zones after 48 h of incubation. The known strong activity of **1**[32] could be detected against all strains tested. The strains Δ*xcnG* (producing **3**-**7**) and *xcnK*::*cat* (producing neither xenocoumacin nor prexenocoumacin) show a clearly smaller inhibition zone than the wild type HGB081 (producing **1** and **2**) and Δ*xcnM* (producing only **1**). The previously described sensitivity of *X. nematophila* towards **1** could also be detected. **b.** Results from disk diffusion assays of compounds **1**, **2**, **4** and **5** against *M. luteus*. Prexenocoumacins (**4**, **5**) show no activity, xenocoumacin-1 (**1**) shows a much larger inhibition zone than **2**. Diameters (in cm) of inhibition zones are stated in the figure.

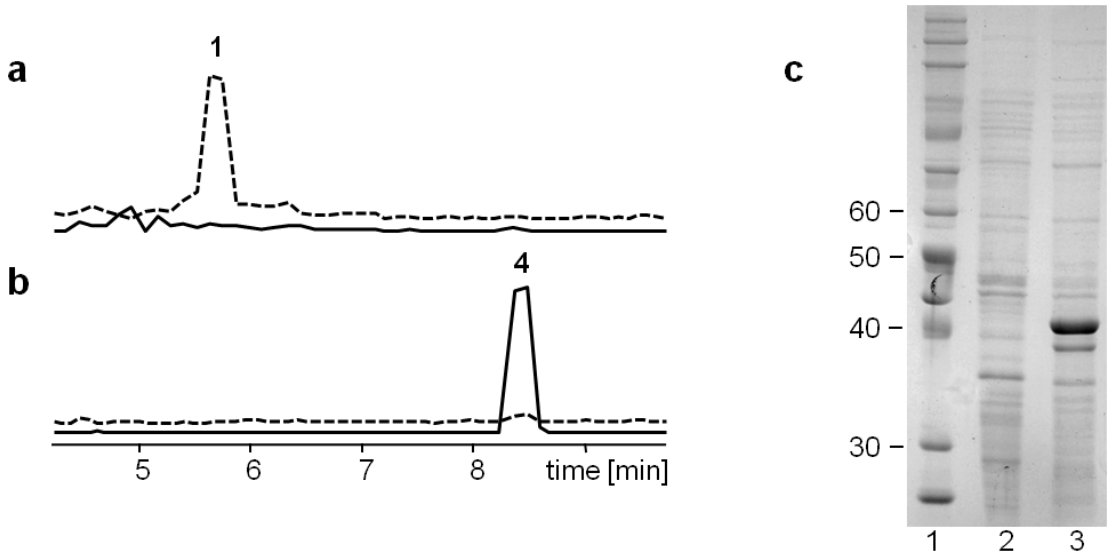

Supplementary Figure 5. MS analysis of xenocoumacin-1 (**1**) resulting from prexenocoumacin B (**4**) cleavage by *E. coli* grown for 24h. Depicted are extracted ion chromatogram traces of **1** (dashed lines) and **4** (continuous lines) in an *E. coli* strain expressing full length *xcnG* (**a**) and *xcnG*$^{-TMH}$ without transmembrane helices (**b**). The positions of **1** and **4** are indicated. All chromatograms are scaled in the same intensity. **c.** 10 % SDS-PAGE of the *E. coli* periplasmic fractions expressing XcnG^{-TMH} without transmembrane helices. Lane 1: molecular weight marker, lane 2: uninduced BL21 (DE3) pET22b(+)-XcnG^{-TMH}, lane 3: IPTG-induced BL21 (DE3) pET22b(+)-XcnG^{-TMH} expressing XcnG with a C-terminal Histaq and without C-terminal transmembrane helices (40.580 kDa).

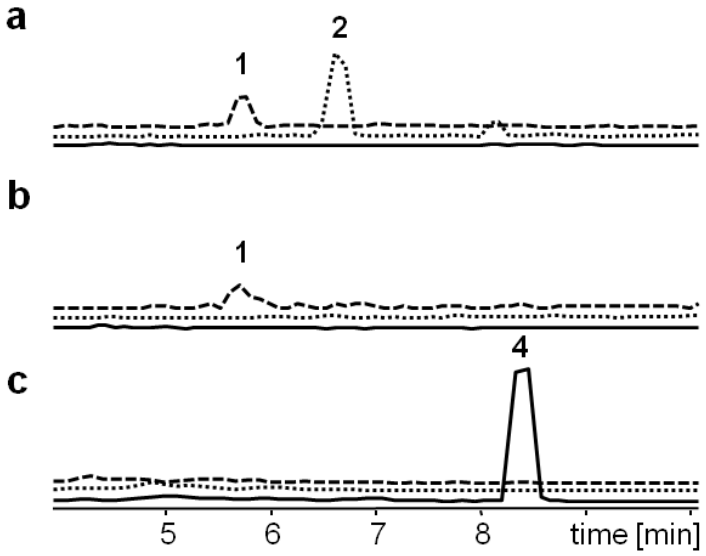

Supplementary Figure 6. MS analysis of xenocoumacin 1 (**1**) and 2 (**2**) resulting from prexenocoumacin B (**4**) cleavage by *E. coli* grown for 24h. Depicted are extracted ion chromatogram traces of **1** (dashed lines), **2** (dotted lines) and **4** (continuous lines) in *E. coli* strains expressing (**a**) *xcnG* and *xcnMN*, (**b**) *xcnG* only and as a control an *E. coli* strain with an empty plasmid (**c**). The positions of **1**, **2** and **4** are indicated. All chromatograms are scaled in the same intensity.

a

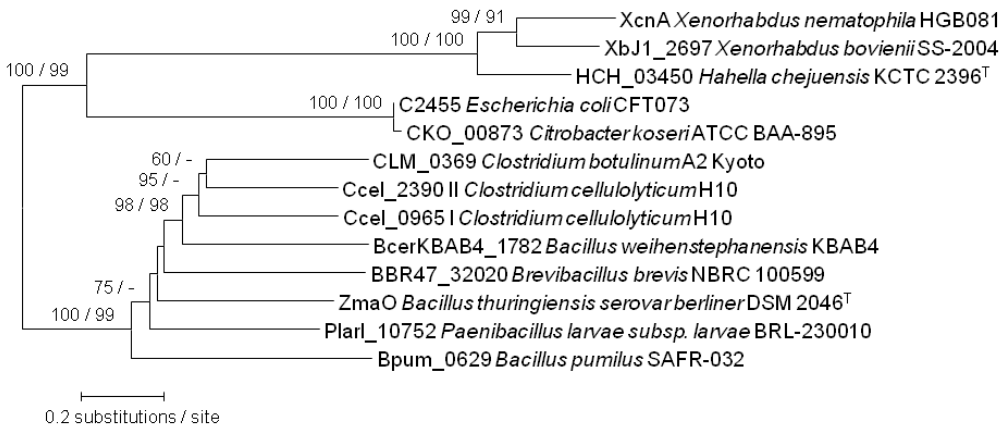
99 / 91
100 / 100
100 / 99
100 / 100
60 / -
95 / -
98 / 98
75 / -
100 / 99
XcnA Xenorhabdus nematophila HGB081
XbJ1_2697 Xenorhabdus bovienii SS-2004
HCH_03450 Hahella chejuensis KCTC 2396T
C2455 Escherichia coli CFT073
CKO_00873 Citrobacter koseri ATCC BAA-895
CLM_0369 Clostridium botulinum A2 Kyoto
Ccel_2390 II Clostridium cellulolyticum H10
Ccel_0965 I Clostridium cellulolyticum H10
BcerKBAB4_1782 Bacillus weihenstephanensis KBAB4
BBR47_32020 Brevibacillus brevis NBRC 100599
ZmaO Bacillus thuringiensis serovar berliner DSM 2046T
PlarI_10752 Paenibacillus larvae subsp. larvae BRL-230010
Bpum_0629 Bacillus pumilus SAFR-032
0.2 substitutions / site

b

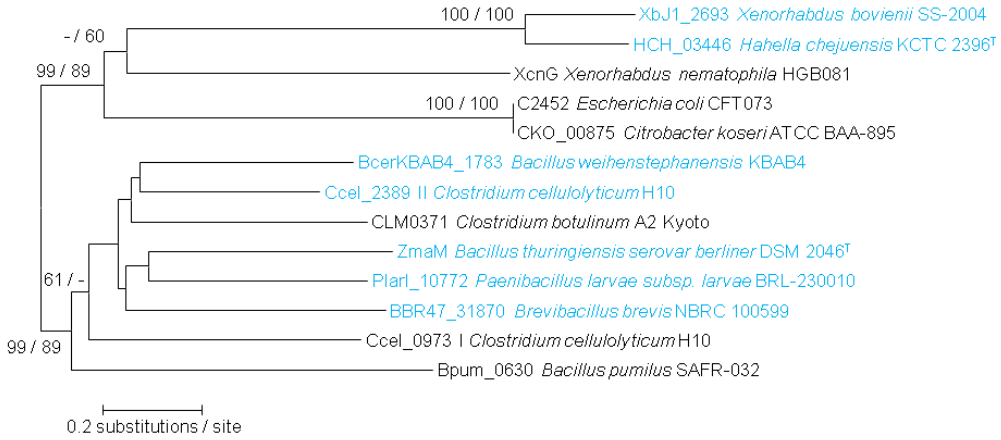
100 / 100
- / 60
99 / 89
100 / 100
61 / -
99 / 89
XbJ1_2693 Xenorhabdus bovienii SS-2004
HCH_03446 Hahella chejuensis KCTC 2396T
XcnG Xenorhabdus nematophila HGB081
C2452 Escherichia coli CFT073
CKO_00875 Citrobacter koseri ATCC BAA-895
BcerKBAB4_1783 Bacillus weihenstephanensis KBAB4
Ccel_2389 II Clostridium cellulolyticum H10
CLM0371 Clostridium botulinum A2 Kyoto
ZmaM Bacillus thuringiensis serovar berliner DSM 2046T
PlarI_10772 Paenibacillus larvae subsp. larvae BRL-230010
BBR47_31870 Brevibacillus brevis NBRC 100599
Ccel_0973 I Clostridium cellulolyticum H10
Bpum_0630 Bacillus pumilus SAFR-032
0.2 substitutions / site

c

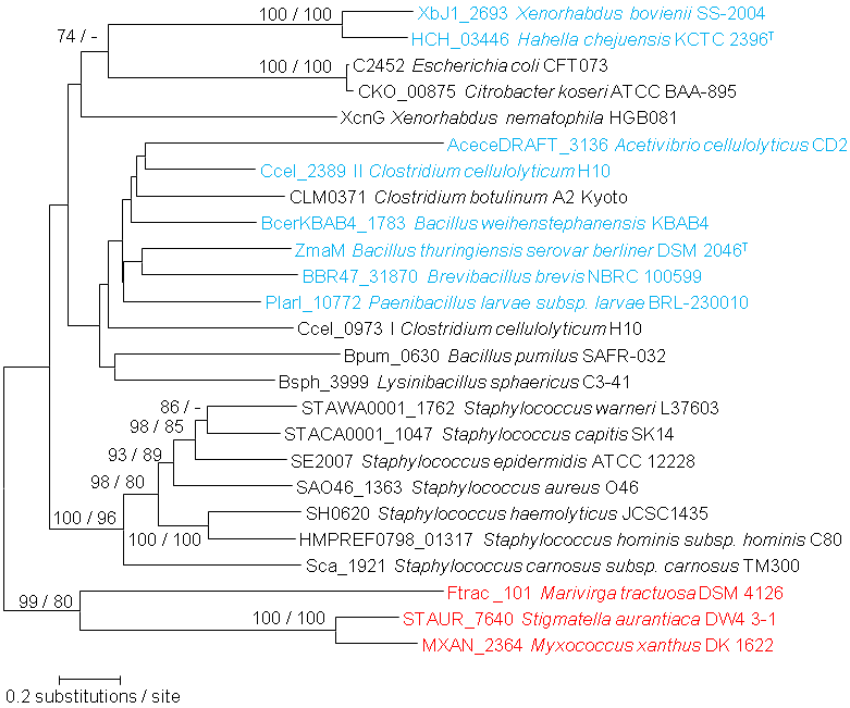
100 / 100
74 / -
100 / 100
86 / -
98 / 85
93 / 89
98 / 80
100 / 96
100 / 100
99 / 80
100 / 100
XbJ1_2693 Xenorhabdus bovienii SS-2004
HCH_03446 Hahella chejuensis KCTC 2396T
C2452 Escherichia coli CFT073
CKO_00875 Citrobacter koseri ATCC BAA-895
XcnG Xenorhabdus nematophila HGB081
AceceDRAFT_3136 Acetivibrio cellulolyticus CD2
Ccel_2389 II Clostridium cellulolyticum H10
CLM0371 Clostridium botulinum A2 Kyoto
BcerKBAB4_1783 Bacillus weihenstephanensis KBAB4
ZmaM Bacillus thuringiensis serovar berliner DSM 2046T
BBR47_31870 Brevibacillus brevis NBRC 100599
PlarI_10772 Paenibacillus larvae subsp. larvae BRL-230010
Ccel_0973 I Clostridium cellulolyticum H10
Bpum_0630 Bacillus pumilus SAFR-032
Bsph_3999 Lysinibacillus sphaericus C3-41
STAWA0001_1762 Staphylococcus warneri L37603
STACA0001_1047 Staphylococcus capitis SK14
SE2007 Staphylococcus epidermidis ATCC 12228
SAO46_1363 Staphylococcus aureus O46
SH0620 Staphylococcus haemolyticus JCSC1435
HMPREF0798_01317 Staphylococcus hominis subsp. hominis C80
Sca_1921 Staphylococcus carnosus subsp. carnosus TM300
Ftrac_101 Marivirga tractuosa DSM 4126
STAUR_7640 Stigmatella aurantiaca DW4 3-1
MXAN_2364 Myxococcus xanthus DK 1622
0.2 substitutions / site

Supplementary Figure 7. Phylogenetic analysis for XcnA and XcnG in Minimum Evolution. Numbers at the branches denote bootstrap support in Minimum Evolution and Maximum Likelihood analyses, in the respective order. Only support values greater 60% are given. The phylogram **a** (XcnA homologues) and **b** (XcnG homologues from biosynthesis gene clusters encoding both XcnA and XcnG) highlight the high degree of similarity of XcnA and XcnG evolution. Phylogram **c** (XcnG homolouges) additionally includes sequences of both Gram-positive and Gram-negative bacteria containing only XcnG. Noteably, sequences of species containing both XcnG and XcnA are clustering together. Only the orphan XcnG homologues from *Acetivibrio cellulolyticus* and *Lysinibacillus sphaericus* cluster together with the XcnA associated XcnG homologues pointing to a potential loss of XcnA. However, in *A. cellulolyticus* the small contig size limits the identification of a closely clustered XcnA encoding gene. Referring to Fig. 3 peptidase domain architecture type I is shown in black and type II in blue, XcnG homologues without any transmembrane helices are shown in red.

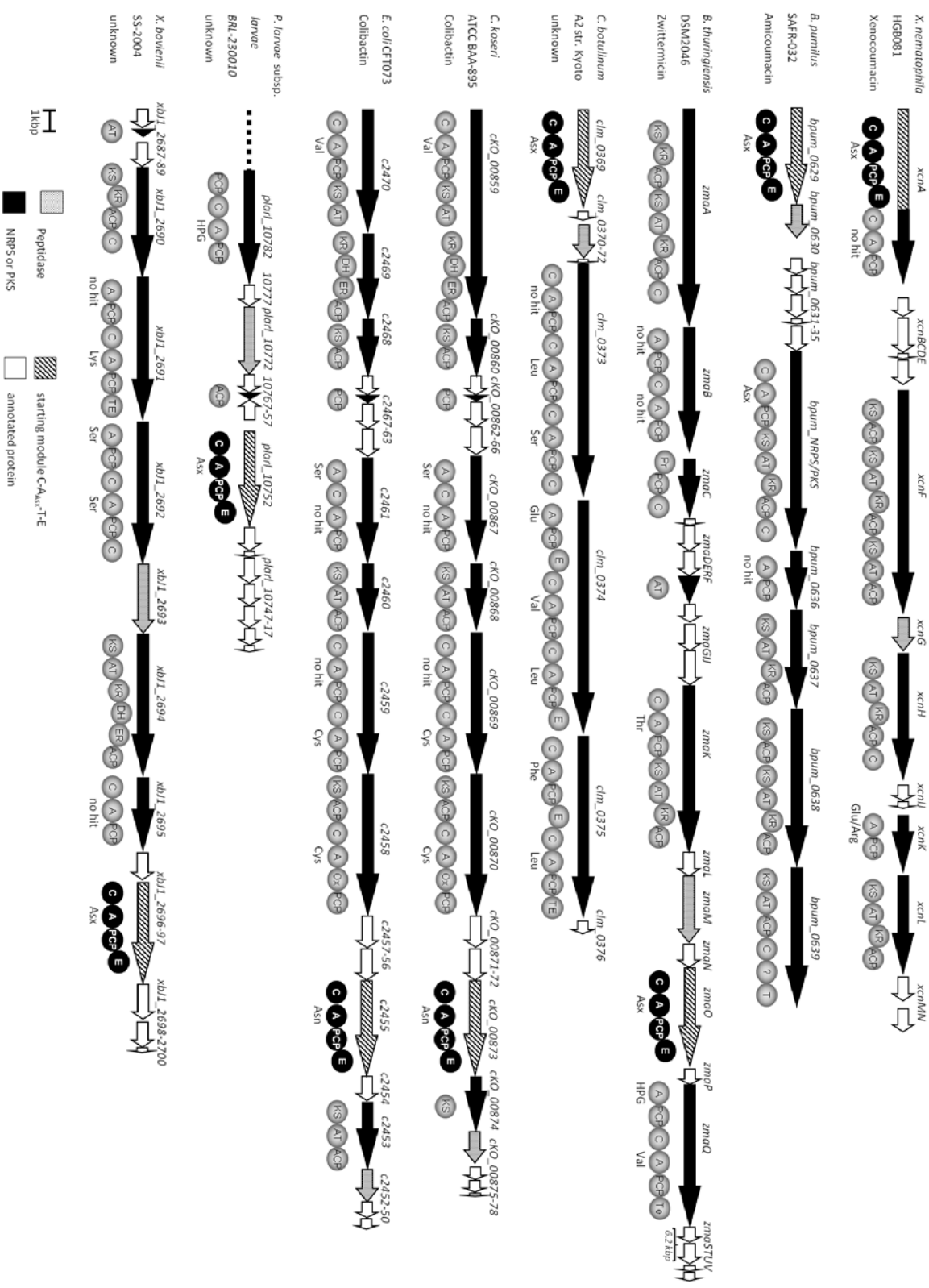

Supplementary Figure 8. Selected biosynthesis gene clusters from other bacteria highlighting the peptidase XcnG (grey) and XcnA homologues with the typical C-A_{Asx}-T-E starting module (hatched). PKS and NRPS encoding genes are shown in black. A: adenylation domain, C: condensation domain, E: epimerization domain, PCP: peptidyl carrier protein domain, AT: acyltransferase domain, ACP: acyl carrier protein domain, KS: b-ketoacyl carrier protein synthase domain, KR: ketoreductase domain, DH: dehydratase domain, ER: enoylreductase domain, Ox:

oxidation domain, TE: thioesterase, PR: C39A protease. One unassigned gene in *B. pumilus* SAFR-032 was named *bpum_NRPS/PKS*. Due to unassigned ORFs in *B. thuringiensis* DSM2046, zwittermicin biosynthesis genes were named according to the gene names in the literature[33]. Gene names in the *P. larvae* subsp. *larvae* BRL-230010 biosynthesis gene cluster are shortened from *plarl_0101000107xx* to *plarl_107xx* for clarity and it might be that the biosynthesis gene cluster is larger than depicted as it was localized at the end of one contig.

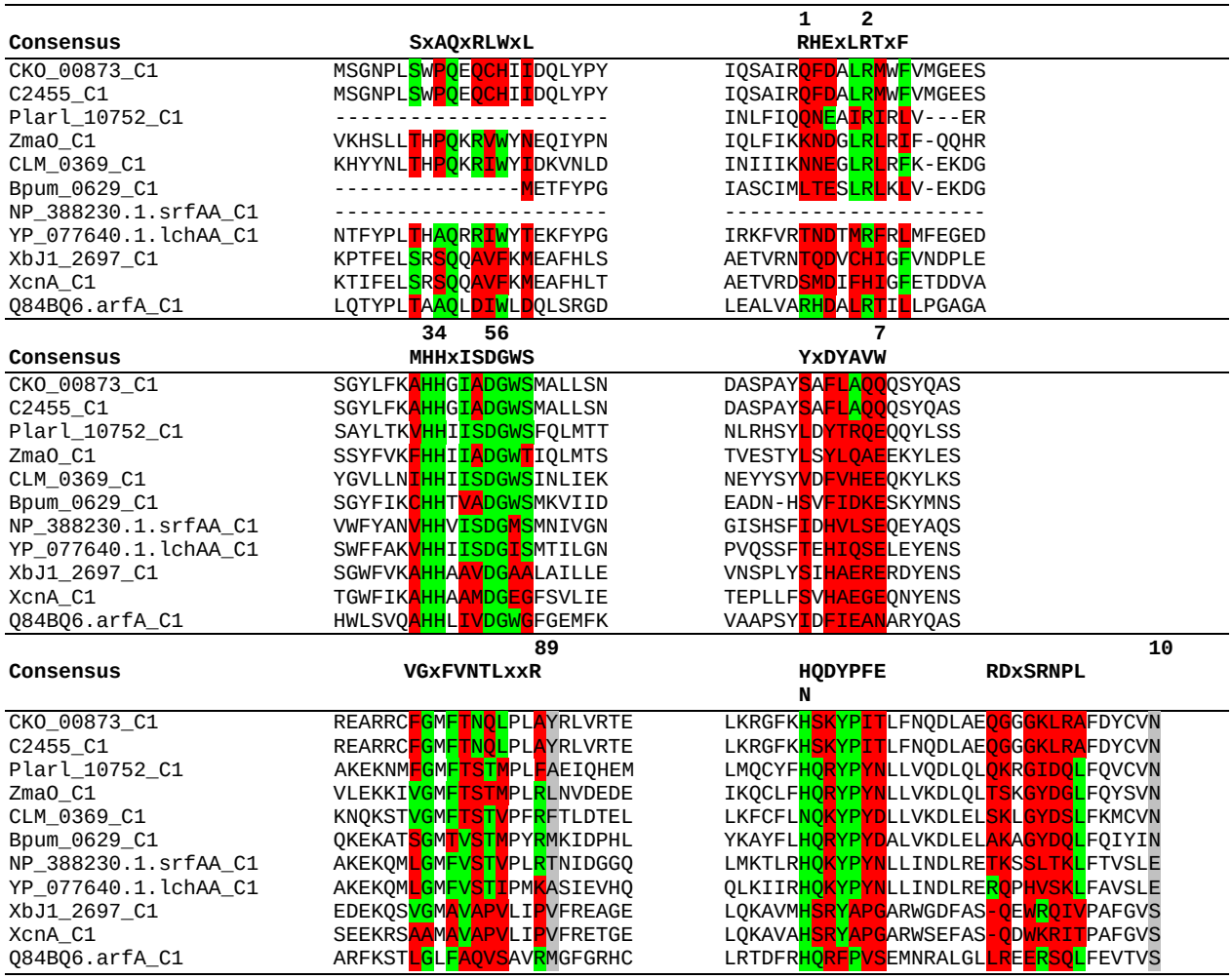

Supplementary Figure 9. Conserved core motives for the lipo-initiation of all starter condensation domains identified in this study including the domains for the lipopetides surfactin[33], lichenysin[35] and arthrofactin[36]. Catalytic residues in the motifs C1 – C7 were characterized as described in literature[15,37]. Conserved residues within the consensus regions indicated are colored in green, non-conserved residues in red. Numbers above the residues indicate residues of functional and structural importance as described by Rausch *et al.*[38]. As expected for starter domains, residues 2 (Arg, folding), 3 (His, folding), 4 (His, catalytic activity), 6 (Gly, catalytic activity) and 8 (Arg, structure) are mostly or highly conserved.

Supplementary Figure 10. Structures of amicoumacin A (**8**) and zwittermicin A (**9**).

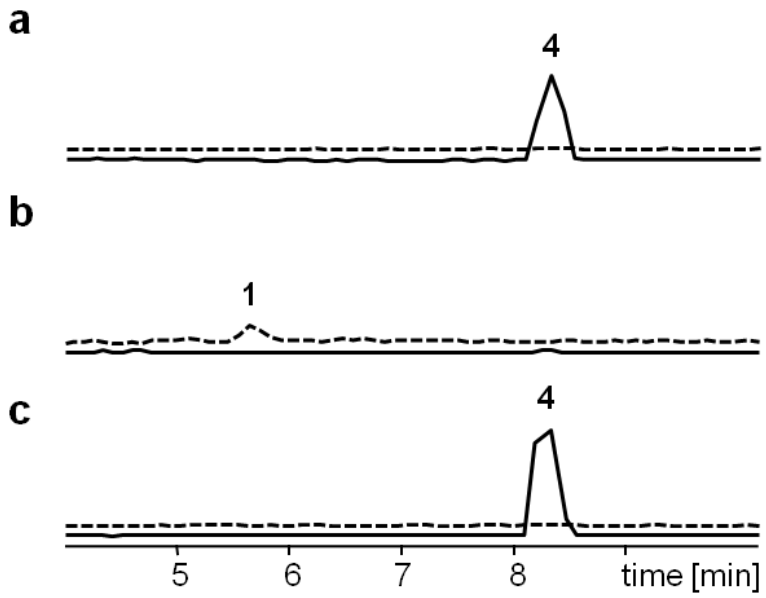

Supplementary Figure 11. Addition of prexenocoumacin B (**4**) to *E. coli* DH10B cells expressing *bpum_0630*, *xbJ1_2693* and *zmaM*. MS analysis of **1** and **4** are shown. Depicted are extracted ion chromatogram traces of **1** (dashed lines) and **4** (continuous lines) in an *E. coli* strain expressing (**a**) *bpum_0630*, (**b**) *xbJ1_2693* and (**c**) z*maM* 24 h after incubation. The positions of **1** and **4** are indicated. All chromatograms are scaled in the same intensity.

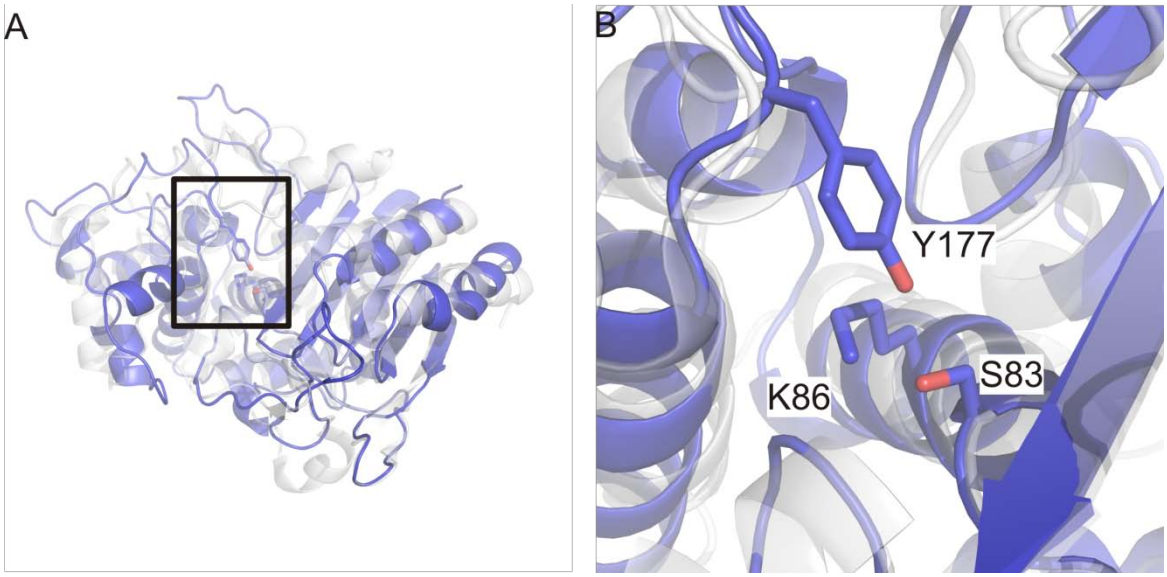

Supplementary Figure 12. XcnG homology model structure derived by analysis of the primary XcnG amino acid structure by Phyre[26]. **A)** Superimposition of the AmpC β-lactamase from *E. coli* (pdb:2FFY) in transparent grey cartoon representation and the XcnG homology model (cartoon representation in blue). In the boxed region is the putative catalytic triad (identified via analysis using ConFunc[28] consisting of Ser83, Lys86 and Tyr177 (blue sticks) with an enlarged view displayed in **B).**

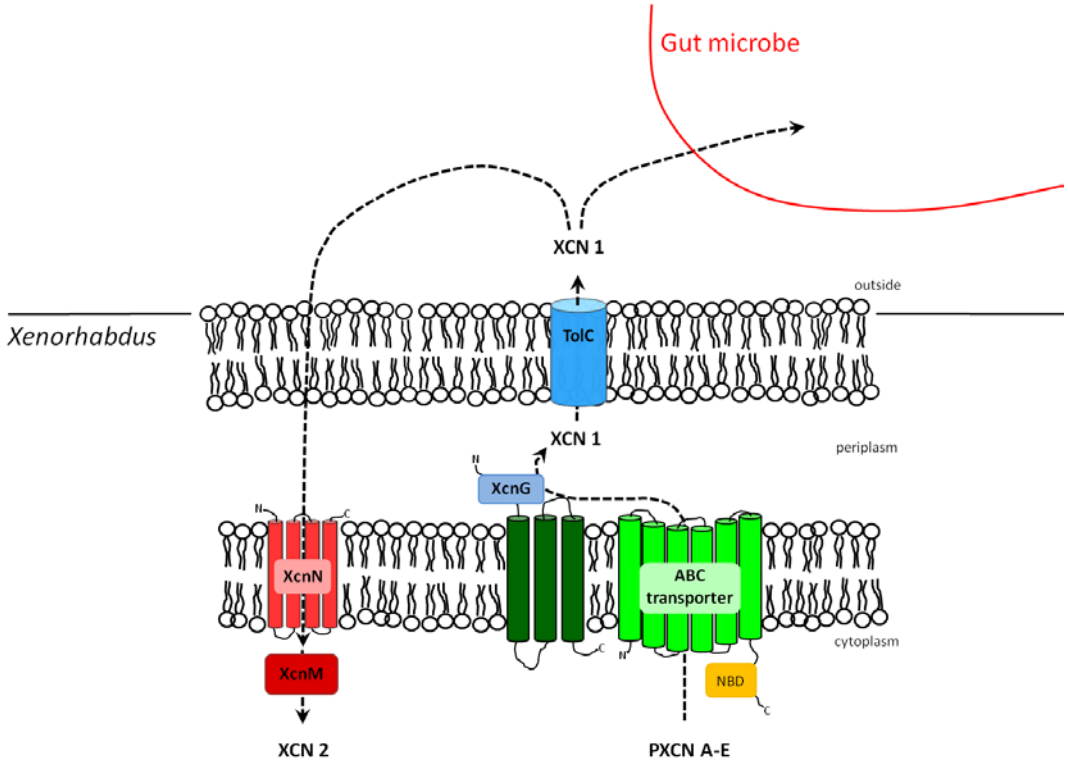

Supplementary Figure 13. Schematic model for the postulated prexenocoumacin and xenocoumacin biosynthesis and resistance. Depicted is *Xenorhabdus* outer and inner membrane with necessary proteins for the prexenocoumacin cleavage and secretion and xenocoumacin-1 resistance. Prexenocoumacins A-E (**3**-**7**) are formed as inactive prodrugs and cleaved into xenocoumacin-1 (**1**) by a XcnG/ABC transporter/TolC protein complex. **1** kills insect gut microbes and as it is also toxic to *X. nematophila* it is converted into xenocoumacin-2 (**2**) by XcnMN.

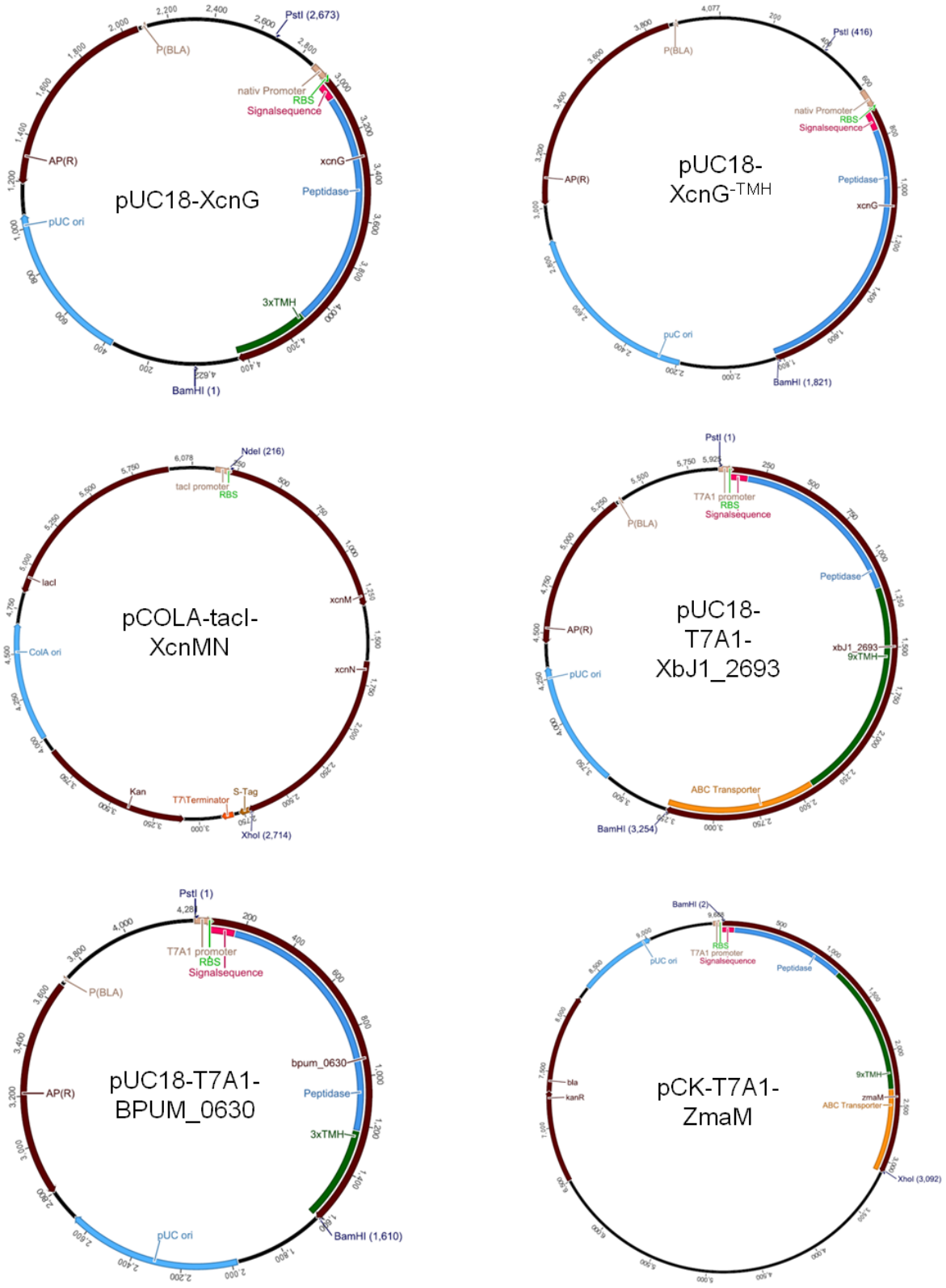

Supplementary Figure 14. Maps of plasmids pUC18-XcnG (4,622 bp), pUC18-XcnG-TMH (4,077 bp), pCOLA-tacI-XcnMN (6,078 bp), pUC18-T7A1-XbJ1_2693 (5,925 bp), pUC18-T7A1-Bpum_0630 (4,281 bp) and pCK-T7A1-ZmaM (9,688 bp), used in the *in vivo* cleavage and resistance assays.

References

1. Sambrook, J., Fritsch, E.F. & Maniatis, T. *Molecular cloning: A laboratory manual* (Cold Spring Harbor Laboratory Press, Cold Spring Harbor, NY, 1989).
2. Philippe, N., Alcaraz, J.P., Coursange, E., Geiselmann, J. & Schneider, D. *Plasmid* **51**, 246-255 (2004).
3. Orchard, S.S. & Goodrich-Blair, H. *Appl. Environ. Microbiol.* **70**, 5621-5627 (2004).
4. Brachmann, A.O. *et al*. *ChemBioChem* **8**, 1721-1728 (2007).
5. Fuchs, S.W., Proschak, A., Jaskolla, T.W., Karas, M. & Bode, H.B. *Org. Biomol. Chem* **9**, 3130-3132 (2011).
6. Gioia, J. *et al. PLoS ONE* **2**, e928 (2007).
7. Miller, J.H. *Experiments in molecular genetics*(Cold Spring Harbor Laboratory, Cold Spring Harbor, NY, 1972).
8. Fujii, K. *et al. Anal. Chem.* **69**, 3346-3352 (1997).
9. Fujii, K., Shimoya, T., Ikai, Y., Oka, H. & Harada, K. *Tetrahedron Lett.* **39**, 2579-2582 (1998).
10. Nozawa, Y., Sakai, N., Arai, K., Kawasaki, Y. & Harada, K. *J. Microbiol. Methods* **70**, 306-311 (2007).
11. Bode, H.B. *et al. ChemBioChem* **10**, 128-140 (2009).
12. Reimer, D., Luxenburger, E., Brachmann, A.O. & Bode, H.B. *ChemBioChem* **10**, 1997-2001 (2009).
13. National Committee for Clinical Laboratory Standards. *Methods for Dilution Antimicrobial Susceptibility Tests for Bacteria that Grow Aerobically: Approved Standards - Sixth Edition. NCCLS Document M7-A6 and MIC Testing Supplemental Tables, M100-S13.* (NCCLS, Wayne, PA, USA, 2003).
14. Altschul, S.F., Gish, W., Miller, W., Myers, E.W. & Lipman, D.J. *J. Mol. Biol.* **215**, 403-410 (1990).
15. Konz, D. & Marahiel, M.A. *Chem. Biol.* **6**, R39-R48 (1999).
16. Ishikawa, J. & Hotta, K. *FEMS Microbiol. Lett.* **174**, 251-253 (1999).
17. Bachmann, B.O. & Ravel, J. *Methods Enzymol.* **458**, 181-217 (2009).
18. Thompson, J.D., Higgins, D.G., & Gibson, T.J. *Nucleic Acids Res.* **22**, 4673-4680 (1994).
19. Krogh, A., Larsson, B., von Heijne, G. & Sonnhammer, E.L.L. *J. Mol. Biol.* **305**, 567-580 (2001).
20. Bendtsen, J.D., Nielsen, H., von Heijne, G. & Brunak, S. *J. Mol. Biol.* **340**, 783-795 (2004).
21. Edgar, R.C. *Nucleic Acids Res.* **32**, 1792-1797 (2004).
22. Tamura, K. *et al. Mol. Biol. Evol.*(2011).
23. Stamatakis, A. *Bioinformatics.* **22**, 2688-2690 (2006).
24. Stamatakis, A., Hoover, P. & Rougemont, J. *Syst. Biol.* **57**, 758-771 (2008).

25. Felsenstein, J. *Evolution* **39**, 783-791 (1985).
26. Kelley, L.A. & Sternberg, M.J. *Nat. Protoc.* **4**, 363-371 (2009).
27. Krissinel, E. & Henrick, K. *Acta Crystallogr. D. Biol. Crystallogr.* **60**, 2256-2268 (2004).
28. Wass, M.N. & Sternberg, M.J. *Bioinformatics.* **24**, 798-806 (2008).
29. Yanisch-Perron, C., Vieira, J. & Messing, J. *Gene* **33**, 103-119 (1985).
30. Grant, S.G., Jessee, J., Bloom, F.R. & Hanahan, D. *Proc. Natl. Acad. Sci. USA* **87**, 4645-4649 (1990).
31. Stachelhaus, T., Mootz, H.D. & Marahiel, M.A. *Chem. Biol.* **6**, 493-505 (1999).
32. McInerney, B.V., Taylor, W.C., Lacey, M.J., Akhurst, R.J. & Gregson, R.P. *J. Nat. Prod.* **54**, 785-795 (1991).
33. Kevany, B.M., Rasko, D.A. & Thomas, M.G. *Appl. Environ. Microbiol.* **75**, 1144-1155 (2009).
34. Arima, K., Kakinuma, A. & Tamura, G. *Biochem. Biophys. Res. Commun.* **31**, 488-494 (1968).
35. Horowitz, S. & Griffin, W.M. *J. Ind. Microbiol.* **7**, 45-52 (1991).
36. Morikawa, M. *et al. J. Bacteriol.* **175**, 6459-6466 (1993).
37. Marahiel, M.A., Stachelhaus, T. & Mootz, H.D. *Chem. Rev.* **97**, 2651-2674 (1997).
38. Rausch, C., Hoof, I., Weber, T., Wohlleben, W. & Huson, D.H. *BMC Evol. Biol.* **7**, 78-92 (2007).

Annex

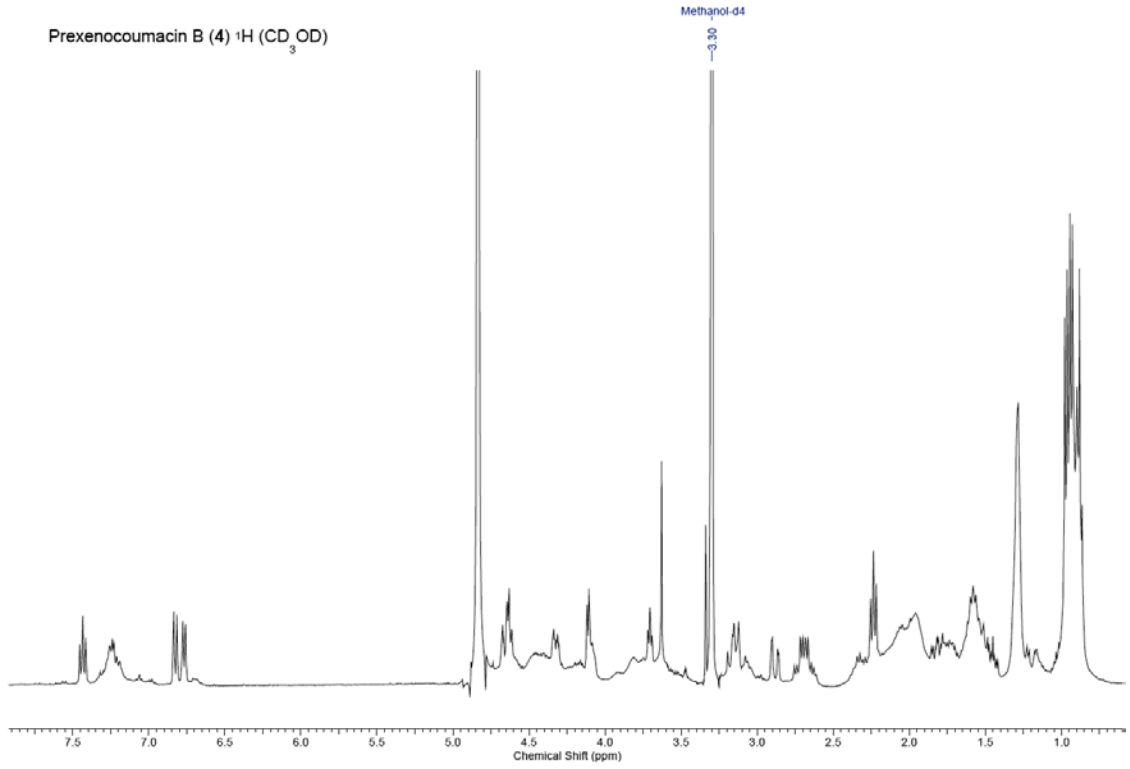
Prexenocoumacin B (4) 1H (CD3OD)
Methanol-d4
3.30
7.5
7.0
6.5
6.0
5.5
5.0
4.5
4.0
3.5
3.0
2.5
2.0
1.5
1.0
Chemical Shift (ppm)

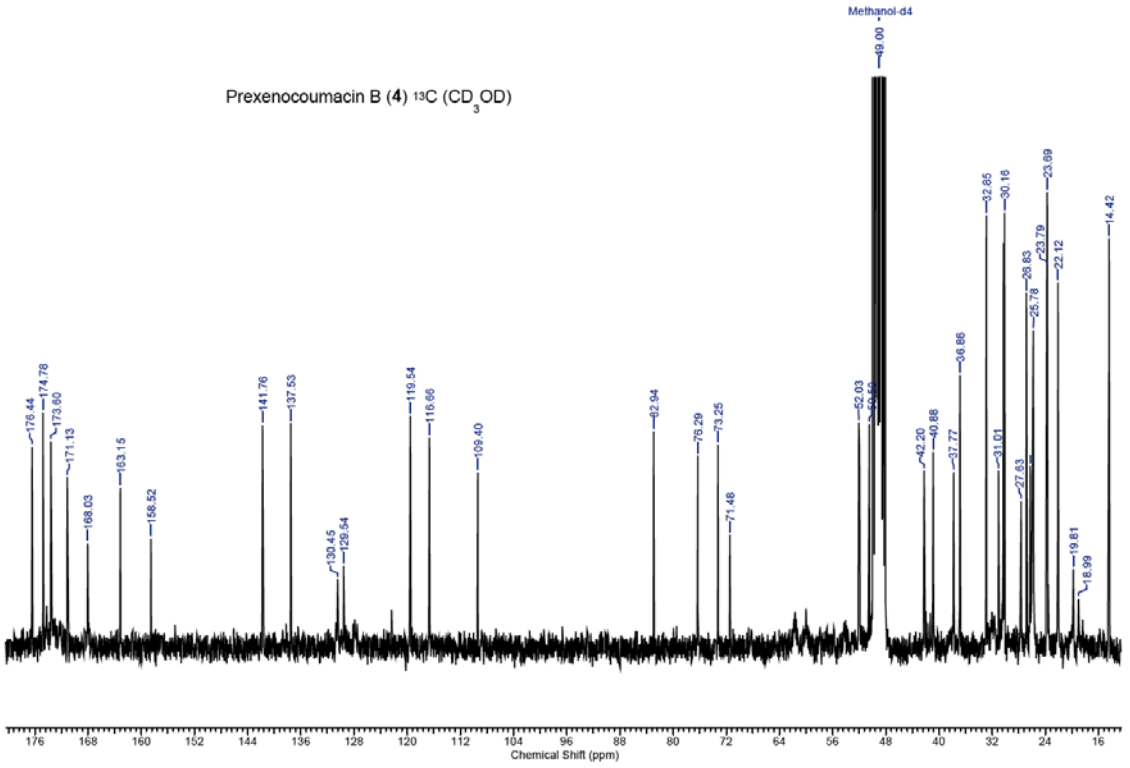
Prexenocoumacin B (4) 13C (CD3OD)
Methanol-d4
49.00
176.44
174.78
173.60
171.13
168.03
163.15
158.52
141.76
137.53
130.45
129.54
119.54
116.66
109.40
82.94
76.29
73.25
71.48
52.03
42.20
40.88
37.77
36.86
32.85
31.01
30.16
28.63
27.83
25.78
23.89
23.79
22.12
19.61
18.99
14.42
176
168
160
152
144
136
128
120
112
104
96
88
80
72
64
56
48
40
32
24
16
Chemical Shift (ppm)

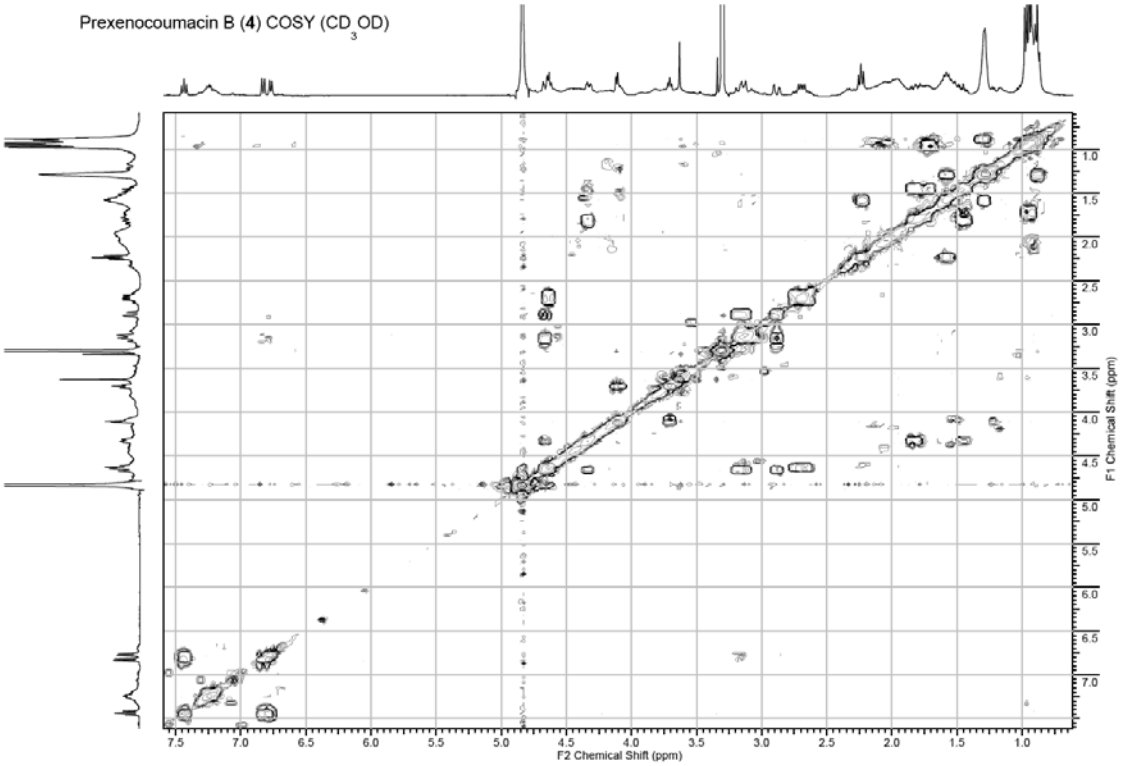
Prexenocoumacin B (4) COSY (CD3OD)
F2 Chemical Shift (ppm)
F1 Chemical Shift (ppm)

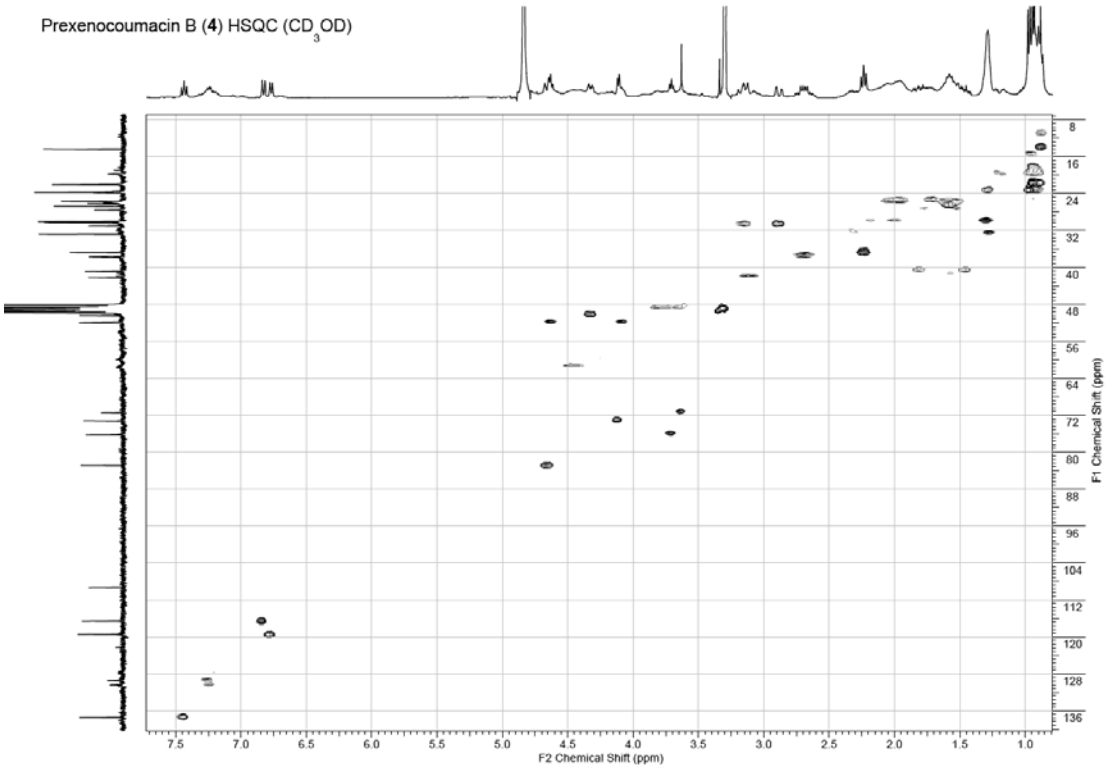
Prexenocoumacin B (4) HSQC (CD3OD)
F2 Chemical Shift (ppm)
F1 Chemical Shift (ppm)

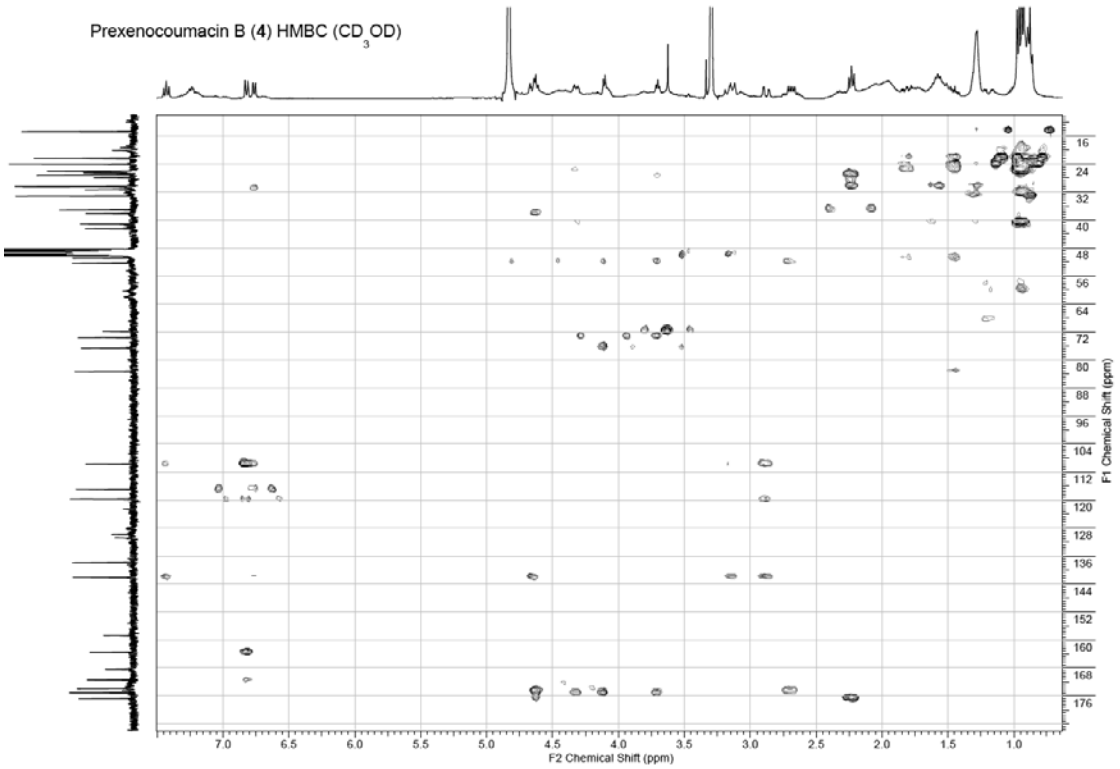
Prexenocoumacin B (4) HMBC (CD3OD)
F2 Chemical Shift (ppm)
F1 Chemical Shift (ppm)

Chapter 4

Determination of the absolute configuration of peptide natural products by using stable isotope labeling and mass spectrometry

Helge B. Bode, Daniela Reimer, Sebastian W. Fuchs, Ferdinand Kirchner, Christina Dauth, Carsten Kegler, Wolfram Lorenzen, Alexander O. Brachmann and Peter Grün

The article has been published in
Chemistry - a European Journal, Vol.18, Issue 8, 2012, pp 2342-2348

Author's effort

The author generated the *X. nematophila* transaminase mutant strains and performed all feeding experiments in *Xenorhabdus* wild type and transaminase mutant strains. Detailed HPLC-MS analysis of all transaminase mutants followed by manual MS fragmentation of GameXPeptide was additionally performed by the author with the help of Helge B. Bode. Furthermore, the author annotated the GameXPeptide biosynthetic gene cluster. Feeding experiments in *Photorhabdus* and the generation of *Photorhabdus* transaminase mutants were carried out by Alexander O. Brachmann and Ferdinand Kirchner. Compounds were isolated by Peter Grün and GC/MS analysis performed by Wolfram Lorenzen. Christina Dauth, synthesized GameXPeptide. Carsten Kegler analyzed the transaminases in the genome and Sebastian W. Fuchs performed MALDI MS analysis and *P. entomophila* experiments. The structures of the GameXPeptides were elucidated by Helge B. Bode.

Determination of the absolute configuration of peptide natural products by using stable isotope labeling and mass spectrometry

Helge B. Bode, Daniela Reimer, Sebastian W. Fuchs, Ferdinand Kirchner, Christina Dauth, Carsten Kegler, Wolfram Lorenzen, Alexander O. Brachmann and Peter Grün[a]

[a] *Molekulare Biotechnologie*
Institut für Molekulare Biowissenschaften
Goethe Universität Frankfurt
Max-von-Laue-Str. 9, 60438 Frankfurt am Main, Germany
Fax: (+) 49 (0)69 798 29527
E-mail: h.bode@bio.uni-frankfurt.de

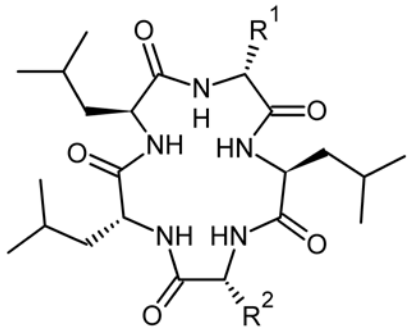

GameXPeptide A $R^1 = {}^i\text{Pr}$, $R^2 = \text{Bn}$
GameXPeptide B $R^1 = {}^i\text{Bu}$, $R^2 = \text{Bn}$
GameXPeptide C $R^1 = {}^i\text{Pr}$, $R^2 = {}^i\text{Bu}$
GameXPeptide D $R^1 = {}^i\text{Bu}$, $R^2 = {}^i\text{Bu}$

Game over—structure solved: A combination of labeling experiments with mass spectrometry results in the reliable determination of the sum formula, the nature of the building blocks, and for peptide natural products also the determination of the absolute configuration as exemplified for the novel natural products GameXPeptide A–D (see scheme).

Abstract

Structure elucidation of natural products including the absolute configuration is a complex task that involves different analytical methods like mass spectrometry, NMR spectroscopy, and chemical derivation, which are usually performed after the isolation of the compound of interest. Here, a combination of stable isotope labeling of *Photorhabdus* and *Xenorhabdus* strains and their transaminase mutants followed by detailed MS analysis enabled the structure elucidation of novel cyclopeptides named GameXPeptides including their absolute configuration in crude extracts without their actual isolation.

Introduction

An important and time-consuming step in natural product research is the structural elucidation of novel compounds. Usually a crude extract from the producer of a natural product is analyzed by HPLC/UV or HPLC/MS to clarify whether the respective peak in the chromatogram represents a compound that is worth its isolation. In that case, the compound of interest must be purified and its structure subsequently elucidated by means of NMR spectroscopic analysis.[1] Today, high-resolution mass spectrometry allows the determination of the mass of the respective compound to such accuracy that a sum formula can be predicted, which can be used for database searches for rapid identification of novel compounds. Whereas the possible compositions for protein-derived peptides or normal lipids would allow only a certain number of possible sum formulae due to their known building-block composition,[2,3] this is different for natural products, which can be built from very unusual precursors and thus increase the number of possible sum formulae. To address this problem and to speed up the identification and structure elucidation of natural products especially from microorganisms, one can apply an isotope-labeling strategy followed by mass spectrometry. This approach allows the reliable determination of the correct sum formula and has been used extensively for metabolomics in plants and bacteria.[4–8] Here we describe the application and further development of this simple and robust approach for the structure elucidation of natural products from entomopathogenic bacteria, applied to four novel cyclopeptides. The approach allows for differentiation between isobar building blocks such as leucine or isoleucine, as well as the determination of the absolute configuration in the case of amino acids.

Results and Discussion

Sum formula determination. Entomopathogenic bacteria of the genus *Xenorhabdus* and *Photorhabdus* were analyzed because these bacteria are usually multiproducers of several different natural products simultaneously.[9] Additionally, highly similar compounds have been observed in different strains, and thus a method was needed to differentiate these compounds. When *Photorhabdus luminescens* strain TT01 was grown in standard growth medium, the sum formulas of all peaks that

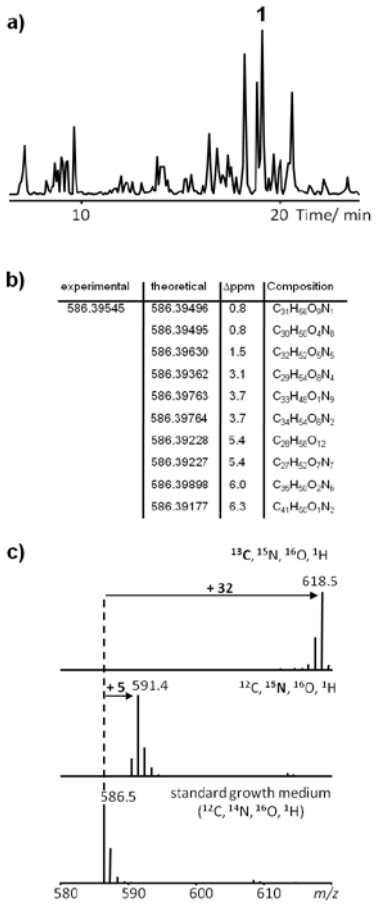

Figure 1. a) HPLC/MS analysis (base peak chromatogram) of *P. luminescens* TT01 highlighting compound **1** (arrow). b) Sum formula prediction for **1** using HRESI-MS data. c) Determination of the number of carbon and nitrogen atoms for **1** as determined from growth of strain TT01 in standard growth medium, or medium fully labeled with ^{15}N or ^{13}C.

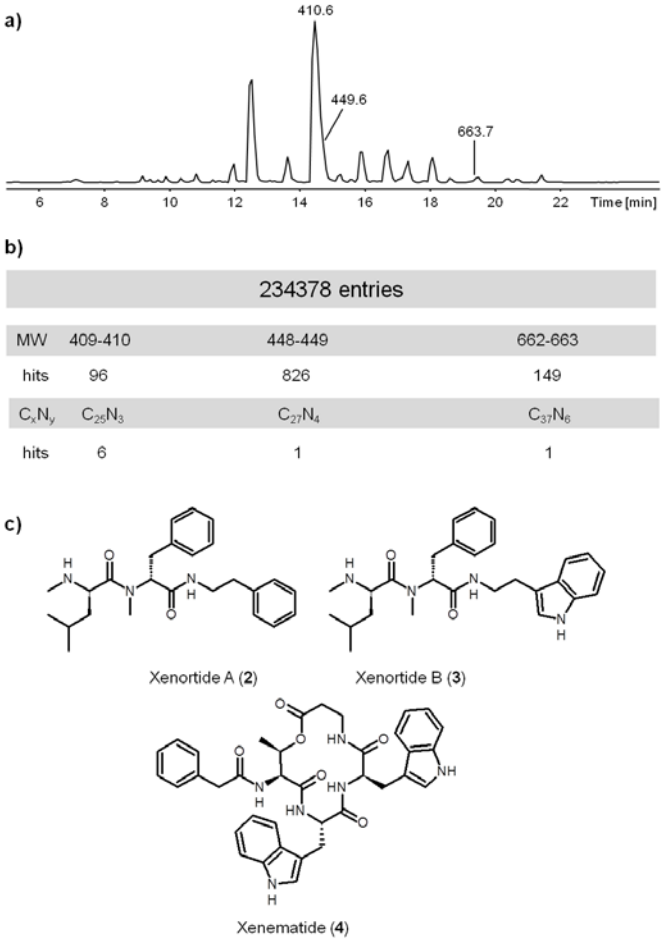

Figure 2. a) HPLC/MS analysis of *X. nematophila* HGB081 indicating the positions of compounds **2**–**4**. b) Identification of **2**–**4** in the Dictionary of Natural Products (http://dnp.chemnetbase.com/dictionary-search.do?method=view&id=2265390&struct=start&props=&&si=last accessedon November 3, 2011) based on the mass range and the number of carbon and nitrogen atoms identified from labeling experiments. c) Structures of xenortide A (**2**), xenortide B (**3**), and xenematide (**4**).[7]

appeared in an HPLC/MS analysis (Figure 1a) could be predicted from high-resolution MS analysis, as exemplified by compound **1** with *m/z* 586.39545 (Figure 1b). However, because usually several sum formulae are chemically and biologically possible, it is often difficult to find the correct one. It was previously shown that the number of possible chemical formulae can be significantly reduced by taking into account the isotope pattern of ultrahigh-resolution MS data.[10] Similarly, growing bacteria in culture media fully labeled with ^{13}C drastically reduces the number of possible sum formulae for lipids[11] and therefore we have applied this approach to *Photorhabdus luminescens*. When comparing HPLC/MS analyses of strain TT01 grown in standard growth medium (natural abundance of all isotopes), ^{15}N or ^{13}C medium allowed the rapid identification of the correct sum formula as the number

of nitrogen and carbon atoms can be easily determined from the mass shifts of **1** in the different growth media (Figure 1c). Despite its simplicity, this approach is also cheap as culture volumes as little as 1 mL can be used (media costs are around 1 €mL^{-1}). Moreover, the sum formulae for all compounds produced under the selected growth conditions (even produced in minute amounts) can be determined in parallel (Table S3 in the Supporting Information) as has also been described in metabolome experiments in different organisms.[4–8] Indeed, the approach is so powerful that it works even without HRMS data. Analysis of *Xenorhabdus nematophila* HGB081 led to the identification of compounds **2**–**4** with *m/z* 410.6, 449.6, and 663.7. A database search in the Dictionary of Natural Products with a total of 234 378 entries using the number of carbon and nitrogen atoms ($C_{25}N_3$, $C_{27}N_4$, and $C_{37}N_6$) as determined by labeling experiments and the molecular-weight range (409–410, 448–449, and 662–663) resulted in only six, one, and one hit, respectively, and thus led to the identification of xenortide A (**2**) and xenortide B (**3**), and xenematide (**4**), which were already known from another *Xenorhabdus* strain (Figure 2).[12]

Building-block determination. Similarly, this labeling approach can be used to identify building blocks of natural products such as amino acids. Here, labeled precursors (^{13}C, ^{2}H, ^{15}N) are usually added to a producing culture and their incorporation would confirm the involvement of the precursor in the natural product biosynthesis. Again, MS-based detection allows for the analysis of compounds produced in minute amounts. However, because not all possible precursors are available for a reasonable price, one can also add a [^{12}C/^{14}N] precursor with natural abundance to a culture grown in a fully labeled ^{13}C or ^{15}N medium as described above. Precursor incorporation in such an 'inverse' labeling experiment is easily visible by a shift to lower masses. In the case of compound **1**, its composition was determined to be cyclo(FLLLV) or a positional isomer thereof, as shown by inverse labeling experiments with valine (Val), leucine (Leu), and phenylalanine (Phe) in ^{13}C medium (Figure 3). The connectivity of these building blocks can be determined easily from MS-MS experiments as shown for **1** (Figure S1 in the Supporting Information), which was demonstrated to be cyclo(VLFLL) and named GameXPeptide A (**1**). This approach additionally facilitates the differentiation of isobar building blocks as leucine, isoleucine, and *N*-methyl valine, which are often found in peptides from entomopathogenic bacteria.

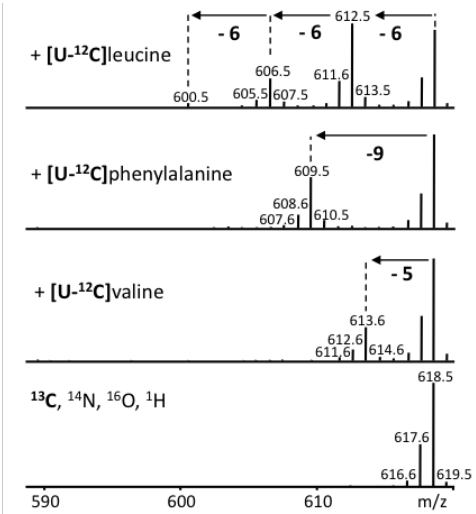

Figure 3. Determination of building blocks of **1** derived from growth of strain TT01 in fully labeled ^{13}C medium without (bottom) or with the addition of different L-^{12}C amino acids (natural abundance).

To demonstrate this, the method was applied to entolysin A (**5**) from *Pseudomonas entomophila* for which previous structure-elucidation efforts could not differentiate between leucine and isoleucine.[13] From labeling experiments with deuterated [$^2H_9$]leucine followed by tandem MS analysis, the correct peptide sequence was determined (Figure 4). This could have been done for the entolysin isotopologue that exhibited the incorporation of all four expected deuterated leucine residues. However, since the fully labeled isotopologue is usually present in minute amounts, the positional analysis was performed with the isotopologue carrying only one labeled leucine. If the random incorporation of one [$^2H_9$]leucine into one of the four possible positions of each fragmented molecule is considered, the ratio of individual sequence ions (in this case, b ions) with and without the incorporated [$^2H_9$]leucine residue would change in a predictable manner. As one isoleucine (Ile) and four Leu residues are present in **5** as deduced from the buildingblock analysis (data not shown), the following expectations for ratios of labeled and unlabeled b ion isotopologues can be made for **5** labeled with one [$^2H_9$]leucine: Every b ion that results from fragmentation at the *N*-terminal position of

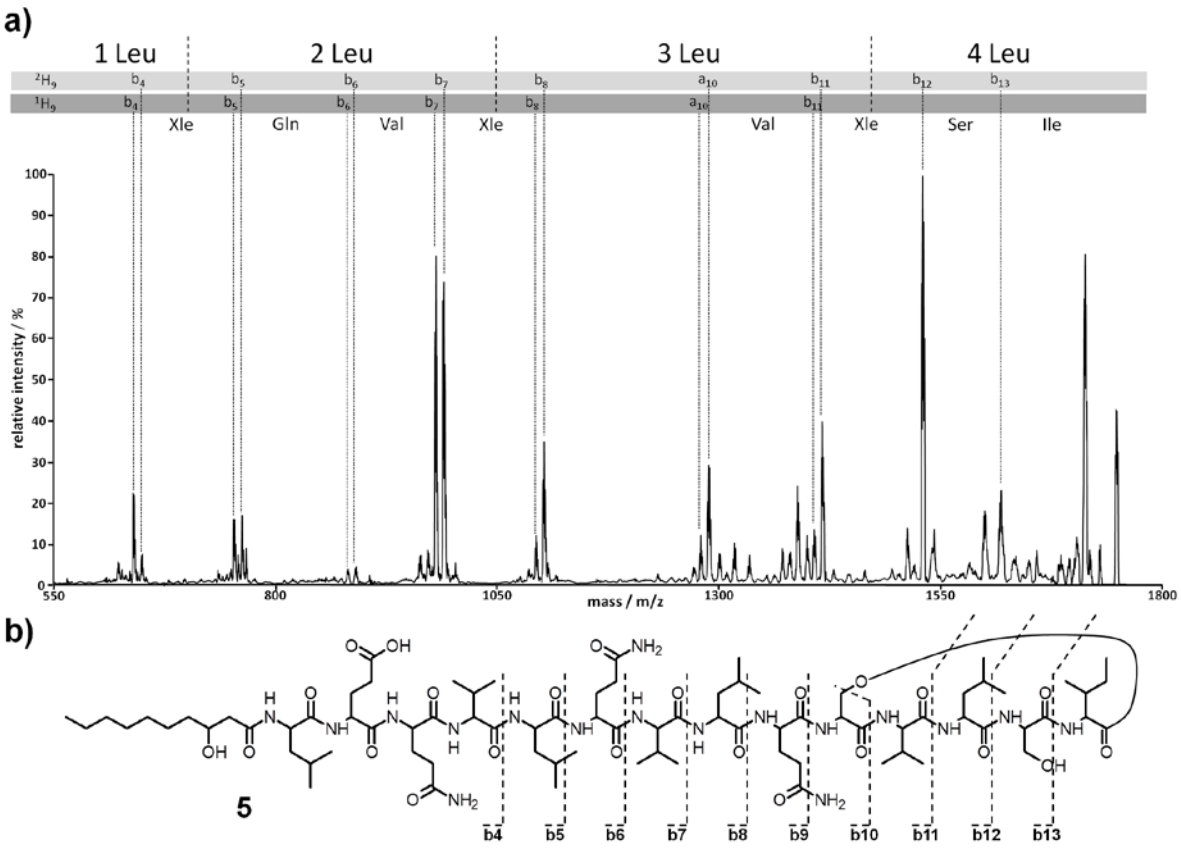

Figure 4. Structure of entolysin A (**5**) and determination of the position of leucine and isoleucin residues in **5**. Depicted is an MS^2 resulting from **5** carrying one [$^2H_9$]leucine; b ions are labeled with dotted lines highlighting deuterated (light gray) and nondeuterated (dark gray) isotopologues.

Leu should exhibit an altered ratio of the b ion isotopologues ([$^2H_9$]/[$^1H_9$]) in comparison to the b_{+1} ion isotopologues, which still contain the Leu, in which the relative amount of the unlabeled b ion ([$^1H_9$])

would increase. Therefore b ions that harbor 3 of 4, 2 of 4, and 1 of 4 Leu should exhibit ratios of unlabeled to labeled isotopologues [$^1H_9$]/[$^2H_9$] of 1:3 (b_{11}/b_8), 1:1 (b_7/b_5), and 3:1 (b_4), respectively, as was indeed the case (Figure 2). The b_{13} ion could exclusively be detected as its labeled isotopologue, thereby indicating that the *C*-terminal amino acid residue of entolysin is isoleucine (Figure 4).

Determination of amino acid configuration. The absolute configuration of the amino acid building blocks still needs to be determined. Peptides like **1**–**5** are usually derived from nonribosomal peptide synthetases (NRPS).[14] These multifunctional giant multienzyme complexes consist of single domains for amino acid activation: adenylation (A domain), condensation (C domain) of two amino acids as peptidyl carrier protein, or thiotemplate (T domains) for covalent binding of peptide intermediates. All domains necessary for the incorporation of a single amino acid are grouped into modules and thus the number of modules usually reflects the number of amino acids in the final natural product and vice versa. In most cases in which D-amino acids are present in the natural product, epimerization (E) domains or mixed C/E domains are present at the corresponding position in the NRPS. These E domains racemize the enzyme-bound L-amino acid or the bound L-peptide intermediate, and subsequently only the D derivative is further processed. During this process, the amino acid is converted to the corresponding enolate anion and vice versa.[15] Thus, by using an amino acid with a ^2H label at the a position, the presence of an E domain can be probed indirectly: Is the label found in the final product? Then the amino acid at this position must be L due to a missing or nonfunctional E domain. Is the label lost? Then it has been exchanged against ^1H from the culture medium by means of E-domain-catalyzed racemization, and the amino acid at this position must be D (Figure 5a) if no other factor contributes to the peptide configuration. Unfortunately, in wild type strains, this approach cannot be used because of the catalytic activity of transaminases in the cells, which convert amino acids into the corresponding 2-keto carboxylic acids and vice versa and that are involved in the last step in amino acid biosynthesis and the first step in amino acid degradation[16] (Figure 5b). In Gram negative bacteria, these transaminases are encoded by *ilvE*, *tyrB*, and *aspC*, which show specificities to different sets of amino acids. These genes are highly conserved and could be identified easily in the genome of *P. luminescens*. When fully labeled [$^2H_8$]valine, [$^2H_{10}$]leucine, or [$^2H_8$]phenylalanine were added to *P. luminescens* wild type cultures, the percentage of the fully labeled amino acids decreased to 34, 20, and 11% in favor of [$^2H_7$]valine, [$^2H_9$]leucine, or [$^2H_7$]phenylalanine, respectively (Figures S2 and S3 in the Supporting Information). As expected, a deletion of *ilvE* resulted in 95% preservation of [$^2H_{10}$]leucine after 24 h and a deletion of *tyrB* in full preservation of [$^2H_8$]phenylalanine.

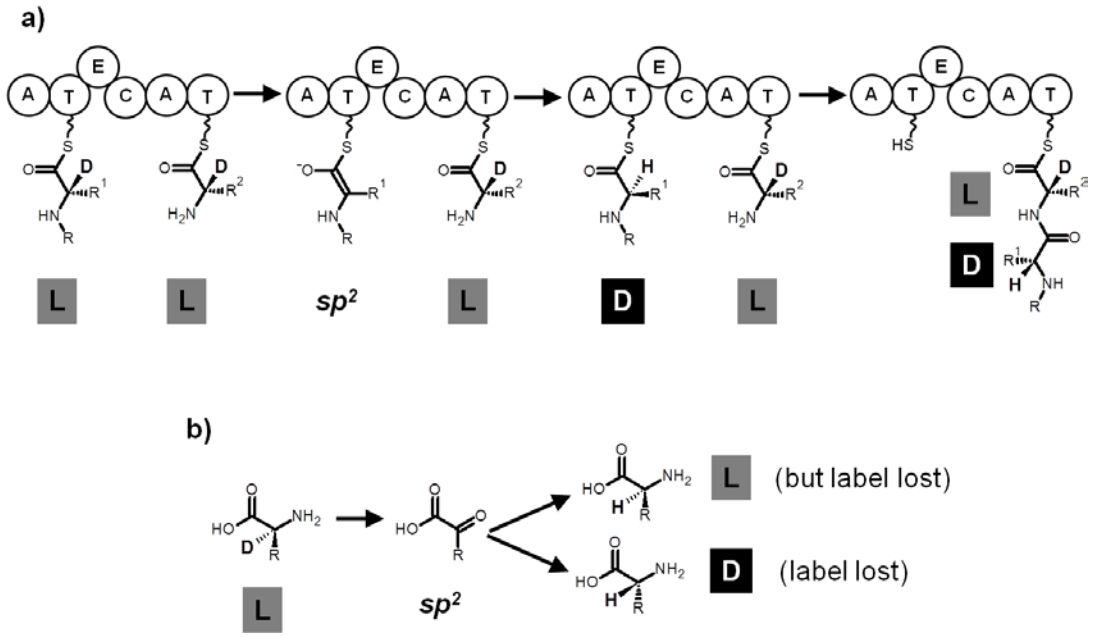

Figure 5. a) Epimerization-domain-catalyzed conversion of L- into D-amino acids based on ^{2}H-labeled amino acids. Adenylation (A), peptidyl carrier protein (PCP), epimerization (E), and condensation (C) domains are indicated. b) Transaminase-catalyzed loss of label from ^{2}H-labeled amino acids.

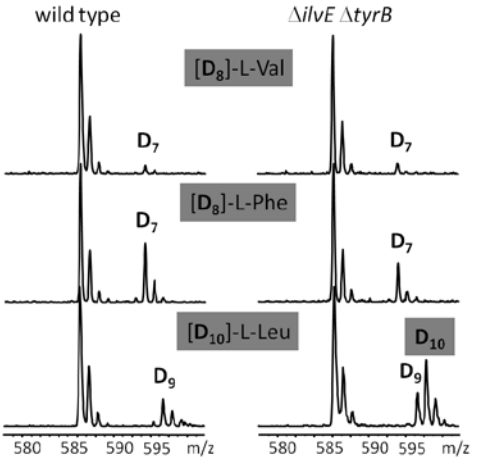

Figure 6. Labeling of GameXPeptide A (**1**) with [$^{2}H_8$]valine, [$^{2}H_{10}$]leucine, or [$^{2}H_8$]phenylalanine in wild type and a Δ*ilvE*Δ*tyrB* mutant of *P. luminescens.*

Unfortunately, the loss of label from deuterated valine could not be decreased further in Δ*ilvE*, Δ*tyrB*, or Δ*ilvE*Δ*tyrB* mutants, and we have not been able to construct an *ilvE*/*tyrB*/*aspC* mutant. When we tested the incorporation of [$^{2}H_8$]valine and [$^{2}H_8$]phenylalanine into compound **1** in Δ*ilvE* or Δ*ilvE*Δ *tyrB* mutants, we could only observe isotopes of **1** that showed the loss of one deuterium for valine and phenylalanine (*m/z* 593.4) as expected for the incorporation of [$^{2}H_7$]valine or [$^{2}H_7$]phenylalanine, respectively. In the case of leucine, we could observe signals from isotopes at *m/z* 595.4 and 596.4 in a ratio of 1:2, thereby indicating the incorporation of [$^{2}H_9$] leucine and [$^{2}H_{10}$]leucine (Figure 6). Thus, **1** is composed out of D-Val, D-Phe, D-Leu, and two L- Leu, and therefore the configuration of all amino acids has been identified. Subsequently, MS^{3} fragmentation experiments of the isotope that was carrying one [$^{2}H_9$]leucine and one [$^{2}H_{10}$]leucine (*m/z* 605.4) to determine the L- and D-leucine positions were performed. Fragmentation of *m/z* 458.4 (loss of phenylalanine; Figure 7a) showed a [$^{2}H_9$]leucine-derived fragment, whereas for *m/z* 506.5

(loss of valine; Figure 7b), *m/z* 492.4 (loss of leucine; Figure 7c), and *m/z* 483.4 (loss of [$^2H_9$]leucine; Figure 7d), only [$^2H_{10}$]leucine-derived fragments were observed. Fragmentation of *m/z* 482.4 (loss of [$^2H_{10}$]leucine; Figure 7e) showed the expected loss of valine. For comparison, unlabeled **1** was also fragmented similarly (Figure 7f–h). Thus, from the different connections of the five different building blocks as determined in Figure 7a–e and summarized in Figure 7i, the absolute configuration of **1** was determined to be cyclo(VLFLL). We confirmed the structure of **1** by solid-phase synthesis and could show that synthetic **1** has indeed the same retention time (Figure S4 in the Supporting Information) and identical NMR spectroscopic data (Table S4 in the Supporting Information) as the natural compound. Furthermore a small amount of **1** was isolated and subjected to Marfey's advanced analysis which also indicated the correct configuration of the amino acids (Figure S5 in the Supporting Information).

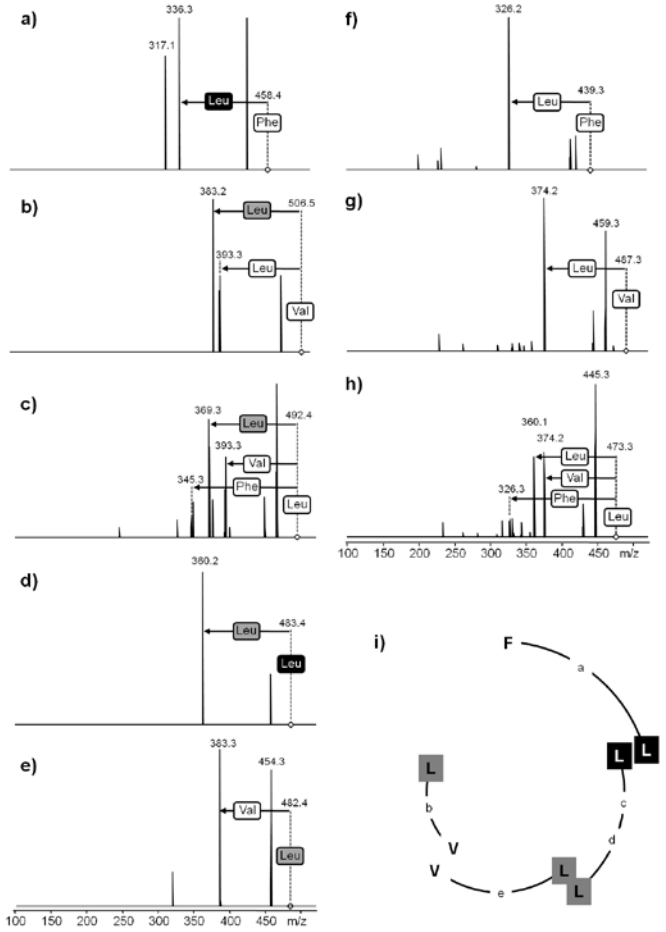

Figure 7. MS^3 spectra of **1** isolated from *P. luminescens* Δ*ilvE*Δ*tyrB* a–e) labeled with [$^2H_{10}$]leucine and [$^2H_9$]leucine (*m/z* 605.5) and f–h) nonlabeled **1** as control. The parent MS^2 ions are labeled with a diamond. Amino acid labels in white boxes refer to unlabeled amino acids; [$^2H_{10}$]leucine is shown in gray boxes and [$^2H_9$]leucine in black boxes. i) The assignment of the stereochemistry as concluded from the spectra in (a)–(e).

In addition, we identified the gene encoding of the GameXPeptide NRPS *gxpS* by plasmid integration and the expected loss of production of **1** when compared to the wild type (Figure S4 in the Supporting Information). A detailed analysis of GxpS allowed the prediction of all required domains for GameXPpetide biosynthesis including three C/E domains at the positions determined by the labeling experiments (Figure 8a, Figure S6 in the Supporting Information). A detailed analysis of the *P. luminescens* extract revealed the presence of three additional derivatives of **1** named GameXPeptide B–D (6–8, Figure 8b), the structure of which was elucidated similarly (Table S3 in the Supporting Information) and which all were lost in the *gxpS* mutant. Their structural variability

results from the exchange of Val[1] and/ or Phe[3] against Leu. As the presence of [$^2H_7$]valine in **1** could not fully differentiate between the incorporation of [$^2H_8$]valine followed by epimerization-domain-catalyzed loss of one deuterium and the incorporation of [$^2H_7$]valine that resulted from residual transamination activity in the bacterial culture, we analyzed another novel peptide named mevalagmapeptide (**9**) from strain TT01 (Figure 9a) that is composed of L-valine exclusively as determined by Marfey's advanced analysis (Figure 9b) after the isolation of **9**. Here, the presence of [$^2H_7$] valine but also of [$^2H_8$]valine was detected almost in a 1:1 ratio in the wild type (Figure 9c, bottom line), which is in contrast to the exclusive [$^2H_7$]valine-derived isotopomer observed for **1** (Figure 6), thus confirming the **l** configuration and indicating that even a presence of 66% of fully deuterated valine (see Figure S3 in the Supporting Information) is sufficient for a stereochemical analysis. Similarly, the configuration of leucine in **2**, **3**, and xenocoumacin-1,[17] and phenylalanine in **3** was determined in transaminase mutants of *X. nematophila* HGB081. Comparison of the labeling results from the *ilvE* or *tyrB* mutants with the wild type allowed the differentiation between D- and L-amino acids and confirmed that all analyzed amino acids are L in these compounds (Figures S7 and S8 in the Supporting Information) as described previously.[12,18] As the three transaminases are highly conserved at the protein but also at the DNA level in *Xenorhabdus* and *Photorhabdus* and other bacteria (data not shown), their corresponding genes can probably be disrupted or deleted even by means of homologous recombination based on sequences of closely related strains, thus enabling the determination of absolute configuration in similar peptides also in strains in which no genome sequence is available.

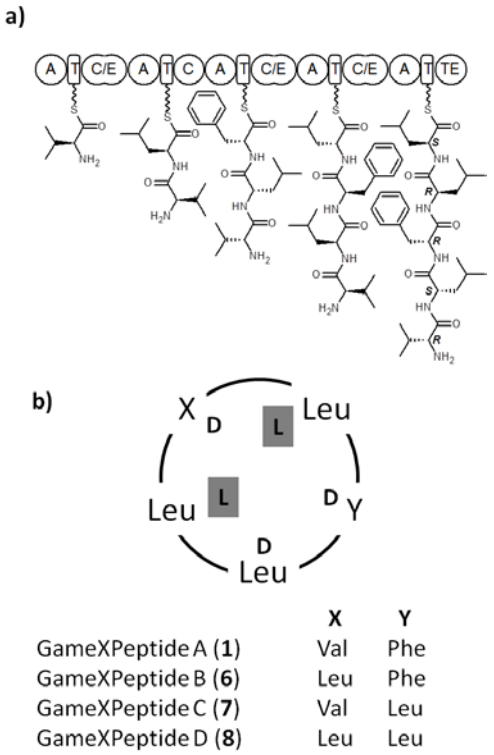

	X	Y
GameXPeptide A (**1**)	Val	Phe
GameXPeptide B (**6**)	Leu	Phe
GameXPeptide C (**7**)	Val	Leu
GameXPeptide D (**8**)	Leu	Leu

Figure 8. a) Domain organization of GxpS responsible for the biosynthesis of **1** (enzyme-bound intermediates are shown) and **6**–**8**. b) Structures of GameXPeptides A–D (**1** and **6**–**8**).

Conclusion

In summary, we have shown that a combination of labeling experiments of wild type and transaminase mutants with MS analysis allows 1) the correct determination of sum formulas; 2) the rapid and reliable identification of building blocks, and especially amino acids; and 3) the determination of the absolute configurations of these amino acids. Our approach is especially useful for peptides because

they can often be synthesized more easily than they are isolated. In particular, when several different derivatives are produced by microorganisms, with some of them present only in trace amounts, our approach might enable the structure elucidation of the derivatives, which can then be synthesized and subsequently tested for their bioactivity following their synthesis.

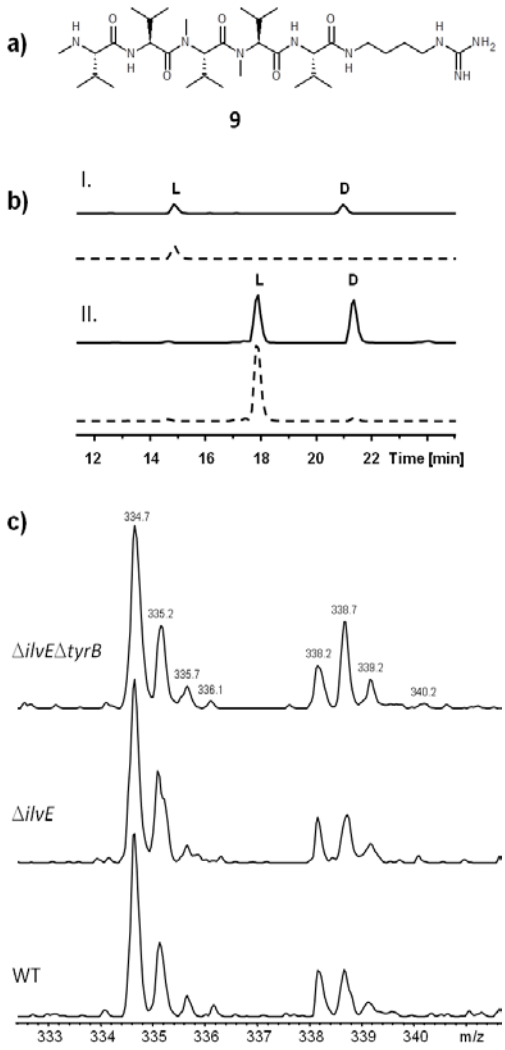

Figure 9. a) Structure results from Marfey's advanced analysis showing the D,Ll-FDLA derivatives (continuous lines) and the L-FDLA derivatives (dashed lines) of *N*-methylvaline (*m/z* 426.2, I), and valine (*m/z* 412.2, II) in b) the positive mode, and results from labeling experiments with c) [$^2H_8$]valine of mevalagmapeptide (**9**) produced by *P. luminescens* TT01. Mevalagmapeptide **9** (*m/z* 334.7, $C_{33}H_{67}O_5N_9$) is detected as a double-charged ion, thus incorporation of [$^2H_7$]valine and [$^2H_8$]valine led to *m/z* 338.2 (+3.5) and 338.7 (+4.0), respectively.

Acknowledgements

This work was supported by the Deutsche Forschungsgemeinschaft (DFG) and the European Community's Seventh Framework Programme (FP7/2007–2013) under grant agreement no. 223328. Work in the author's laboratory is additionally supported by the Bundesministerium für Bildung und Forschung (BMBF) and the Frankfurt Initiative for Microbial Sciences (FIMS).

References

[1] S. Donadio, S. Maffioli, P. Monciardini, M. Sosio, D. Jabes, J. *Antibiot.* **2010**, *63*, 423 – 430.

[2] V. An Thieu, D. Kirsch, T. Flad, C. Müller, B. Spengler, Angew. Chem. **2006**, 118, 918; *Angew. Chem. Int. Ed*. **2006**, *45*, 904.

[3] B. Spengler, J. Am. Soc. *Mass Spectrom*. **2004**, *15*, 703 – 714.

[4] P. Giavalisco, K. Kohl, J. Hummel, B. Seiwert, L. Willmitzer, *Anal. Chem.* **2009**, *81*, 6546 – 6551.

[5] P. Giavalisco, Y. Li, A. Matthes, A. Eckhardt, H. M. Hubberten, H. Hesse, S. Segu, J. Hummel, K. Kohl, L. Willmitzer, *Plant J.* **2011**, *68*, 364 – 376.

[6] P. Giavalisco, J. Hummel, J. Lisec, A. C. Inostroza, G. Catchpole, L. Willmitzer, *Anal. Chem.* **2008**, *80*, 9417 –9425.

[7] L. Feldberg, I. Venger, S. Malitsky, I. Rogachev, A. Aharoni, *Anal. Chem.* **2009**, 81, 9257 – 9266.

[8] R. Baran, B. P. Bowen, N. J. Bouskill, E. L. Brodie, S. M. Yannone, T. R. Northen, *Anal. Chem.* **2010**, *82*, 9034 –9042.

[9] H. B. Bode, Curr. Opin. *Chem. Biol.* **2009**, *13*, 224 – 230.

[10] N. Stoll, E. Schmidt, K. Thurow, J. Am. Soc. *Mass Spectrom.* **2006**, *17*, 1692 –1699.

[11] R. P. Rodgers, E. N. Blumer, C. L. Hendrickson, A. G. Marshall, *J. Am. Soc. Mass Spectrom.* **2000**, *11*, 835 –840.

[12] G. Lang, T. Kalvelage, A. Peters, J. Wiese, J. F. Imhoff, *J. Nat. Prod.* **2008**, *71*, 1074 –1077.

[13] I. Vallet-Gely, A. Novikov, L. Augusto, P. Liehl, G. Bolbach, M. Pechy-Tarr, P. Cosson, C. Keel, M. Caroff, B. Lemaitre, Appl. *Environ. Microbiol.* **2010**, *76*, 910 – 921.

[14] R. Finking, M. A. Marahiel, *Annu. Rev. Microbiol.* **2004**, *58*, 453 – 488.

[15] T. Stachelhaus, C. T. Walsh, *Biochemistry* **2000**, *39*, 5775 –5787.

[16] G. Michal, Biochemical Pathways, *Spektrum Akad. Verlag*, Heidelberg **1999**.

[17] D. Reimer, E. Luxenburger, A. O. Brachmann, H. B. Bode, *ChemBioChem* **2009**, *10*, 1997-2001.

[18] D. Reimer, K. M. Pos, M. Thines, P. Grün, H. B. Bode, *Nat. Chem. Biol.* **2011**, *7*, 888 – 890.

Supporting Information

Material and Methods. *Photorhabdus luminescens* subsp. *laumondii* TT01 (rifampicin resistant strain), *Xenorhabdus nematophila* HGB081 (rifampicin resistant strain) and mutants, *Xenorhabdus cabanillasii* DSM17905[1] were cultivated in Luria-Bertani (LB) broth (pH 7.0) at 30°C and 180 rpm on rotary shaker. *E. coli* S17-1λ*pir* (Tp^r Sm^r *recA thi hsdR* RP4-2-Tc::Mu-Km::Tn7, λ *pir* phage lysogen) was used for conjugation. Appropriate antibiotics were added to LB liquid and agar cultures when necessary at following concentrations: ampicillin 100 µg/mL, kanamycin 50 µg/mL, rifampicin 50 µg/mL and chloramphenicol 34 µg/mL. Feeding experiments were performed as follows: L-[2,3,4,4,4,5,5,5-D_8]valine, L-[2,3,3,4,5,5,5,5´,5´,5´-$^2H_{10}$]leucine, L-[2,3,3,5,5´,6,6´,7-$^2H_{10}$] phenylalanine, and L-[*methyl*-$^2H_3$]methionine were fed to LB medium with 2% XAD-16 and leucine, valine, isoleucine, phenylalanine, tryptophane, and methionine were also added in an inverse feeding approach to bacterial cultures grown in [U-^{13}C]medium. Cultures were grown in 50 mL Erlenmeyer flasks containing 5 mL of ISOGRO-^{13}C (Sigma-Aldrich) or ISOGRO-^{15}N medium containing 10 mM K_2HPO_4, 10 mM KH_2PO_4, 8 mM $MgSO_4 \cdot 7H_2O$ and 90 mM $CaCl_2 \cdot H_2O$ also containing XAD-16.

Cultures were inoculated with 0.1 % of a preculture grown in LB and washed twice with the respective ISOGRO medium when required. All possible precursors were added at 4, 24 and 48 h after incubation in equal portions to a final concentration of 3 mM. Cultures were harvested after 72 h of incubation at 30 °C and 180 rpm. Metabolites were identified in crude extracts obtained from MeOH extraction of XAD-16 resin using HPLC/MS. All production cultures were made in 5 L-Erlenmeyer flasks containing 500 mL LB and inoculated with a 24 h preculture of the same medium (0.1 %, v/v) if not noted otherwise. *P. entomophila*[2] was cultivated in LB medium which was supplemented with 2 mM L-[2,3,3,4,5,5,5,5´,5´,5´-$^{2}H_{10}$]leucine and DL-[2,3,4,4,4,5,5,5-$^{2}H_{8}$]valine, respectively.

Isolation of compounds 1 and 9. For the isolation of GameXPpetide A (**1**), cultures of *P. luminescens* TT01 (6 x 1 L in 5 L Erlenmeyerflasks) in LB medium with 2% XAD-16 (Sigma-Aldrich, Deisenhofen, Germany) was grown for three days and then the XAD was harvested by sieving and extracted with MeOH (3 x 500 mL). The crude extract was fractionated using a silica gel column with a stepwise gradient of hexane, hexane/$CHCl_3$ (1:1), $CHCl_3$, $CHCl_3$/MeOH (99:1, 9:1, 8:2, 7:3, 6:4, 1:1), and MeOH. Fractions containing **1** were identified by HPLC/MS analysis and further purified by preparative HPLC/MS using a AcCN/H2O gradient (0.1% formic acid) yielding 1.5 mg pure **1**. Similarly, mevalagmapeptide (**9**) was isolated from TT01 but only using separation of the crude extract by preparative HPLC. Full structure elucidation of **9** will be given elsewhere.

MS analysis. ESI HPLC/MS and MS^n analysis was performed with a Dionex UltiMate 3000 system coupled to a Bruker AmaZon X mass spectrometer and an Acquity UPLC BEH C18 1.7 µm RP column (Waters) using a MeCN/0.1 % formic acid in H_20 gradient (gradient: 5-95 % MeCN in 22 min, flowrate: 0.6 mL min^{-1}, MS: alternating positive and negative ionization mode between 100-1200 m/z). Fragmentation of labeled compounds with [$^{2}H_{8}$]valine, [$^{2}H_{8}$]phenylalanine and [$^{2}H_{10}$]leucine was performed using a manual isolation and fragmentation mode with an isolation width of 0.5 m/z to guarantee the isolation of the isotope of interest and to differentiate between isotopes resulting of incorporation and racemisation and isotopes of natural abundance. Fragmentation patterns were verified up to MS^5 using the described isolation method. HRESI MS was performed as described previously[3].

For the structure elucidation of entolysin, a culture supernatant of *P. entomophila* grown with labeled leucine or valine was diluted 1:4 in 0.1 % trifluoroacetic acid (TFA) and loaded onto Strata C18E solid phase extraction (SPE)-cartridges (Waters, Eschborn, Germany), which were handled according to the manufacturer's instructions. After washing with 0.1 % TFA, 30 % Acetonitril (ACN)/0.1 % TFA and 50 % ACN/0.1 % TFA, entolysin was eluted with 99.9 % ACN/0.1 % TFA. After evaporation to dryness with a vacuum evaporator, entolysin was linearized by means of NH_4OH according to the protocol of Vallet-Gely[4]. The reaction was stirred at 40°C for 14 h and dried in a vacuum concentrator. The resulting samples samples were dissolved with 30 % ACN/0.1 % TFA,

mixed 1:2 with 1 µl of a 20 mM 4-chloro-α-cyanocinnamic acid (ClCCA)5, 6 in 70 % ACN onto a polished stainless steel target and air-dried. MS analysis was performed with a MALDI LTQ Orbitrap XL (Thermo Fisher Scientific, Inc., Waltham, MA) equipped with a nitrogen laser at 337 nm and used in the ion trap mode. The following instrument parameters were used: laser energy, 28 µJ; automatic gain control, on; auto spectrum filter, off; scan mode, full; plate motion, survey CPS. MS/MS analysis was performed using the following parameters: wide band activation, on; precursor width range, optimized for every single precursor with regard to complete isolation; normalized collision energy, 40. Spectra were analyzed using Qual Browser (version 2.0.7; Thermo Fisher Scientific, Inc., Waltham, MA). For graphical depiction, spectra were opened as ASCI-files in the Data Explorer 4.9 software (Applied Biosystems, Darmstadt, Germany) and the following modifications were conducted: Gaussian smooth, 5; noise removal, 2.

GC/MS analysis. Supernatants of the bacterial cultures were analysed for their content of [$^2H_8$]valine, [$^2H_7$]valine, [$^2H_{10}$]leucine, [$^2H_9$]leucine, [$^2H_8$]phenylalanine, [$^2H_7$]phenylalanine and their respective non deuterated derivatives by complete hydrolysis, silylation of the resulting amino acids and subsequent GC-MS analysis: 50 µl of cell free media was hydrolysed by the addition of 800 µl of 6N HCl and subsequent incubation for 24 h at ~100°C. Afterwards, samples were dried in a 5301 Concentrator (Eppendorf, Hamburg, Germany) under reduced pressure at 60°C. 150 µl of a 2:1 mixture of Acetonitrile/MSTFA (*N*-Methyl-*N*-Trimethylsilyl-Trifluoroacetamide) was added to each dried sample and incubated at 56°C over night in order to derivatise and redissolve the amino acids. The resulting N,O-trimethylsilyl derivatives of the amino acids were subjected to GC-MS analysis.

All analysis were conducted on a 7890A model gas chromotagraph (Agilent, Waldbronn, Germany) equiped with a CTC PAL Combi XT autosampler and coupled to Series 5975C mass selective detector (Agilent, Waldbronn, Germany). A DB5ht column (Agilent, Waldbronn, Germany) with a length of 30 m, an inner diameter of 0.25 mm and a column film of 0.1 µm in strength was used for the separation of the silylated amino acids. Helium was used as the carrier gas at a constant flow rate of 1 ml/min. The method parameters were as follows: Injection volume: 2 µl; inlet temperature: 300°C; injection mode: Split, ratio 10:1/25:1 depending on the sample concentration; oven temperature program for the analysis of valine and phenylalanine: starting temperature 35°C, then 8°C/min to 250°C, 120°C/min to 30°C for 0 min; oven temperature program for the analysis of leucine: starting temperature 35 °C, then 20°C/min to 250°C and 120°C/min to 30 °C for 0 min. The temperature of the transfer line was held constant at 280°C. The ion sources temperature of the MSD was 230°C, the quadrupol temperature 150°C. Ionisation of the analyte molecules were carried out by electron impact ionisation at 70keV. The "Automated Mass Deconvolution and Identification Software" (AMDIS) version 2.64 was used for the identification and relative quantification of the various deuterated and non-deuterated amino acid species. The overall intensities of the deconvoluted mass spectra of the respective amino acid species were the basis of all calculations. The Software

DataAnalysis Version 4.0 SP1 (Bruker Daltonics, Bremen, Germany) was used to create Base Peak (BP) and Extracted Ion Chromatograms (EIC).

Construction of a gxpS and transaminase mutants. All deletion and insertion mutants in this work were generated by using the conjugatable suicide vector pDS132, carrying a chloramphenicol resistance gene (*cat*). For a markerless deletion of *tyrB* in *P. luminescens laumondii* TT01 two fragments were amplified flanking the region of *tyrB*. The 502 bp upstream fragment was amplified with primers TyrB_up_Fw (containing a *Sac*I restriction site) and TyrB_up_Rv and the 411 bp downstream fragment with primers TyrB_down_Fw and TyrB_down_Rv (containing a *Pae*I restriction site). A 10 base complementary sequence, introduced by the primers TyrB_up_RV and Tyr_down_Fw, was used to fuse the upstream and downstream PCR fragments. In a second PCR, the resulting product was used as a template with primers TyrB_up_Fw and TyrB_up_Rv to yield the desired deletion fragment. The fragment was subcloned into vector pJET1.2 (Thermo Scientific, Fermentas) and subsequently digested with restriction endonucleases *Sac*I and *Pae*I (both Thermo Scientific, Fermentas), vector pDS132 was digested similarly. The fragment was introduced into vector pDS132 yielding pDS4357Del and transformed by electroporation into *E. coli* S17-1 λ*pir*. The appropriate construct was delivered into TT01 rif by conjugation. For conjugation, cultures of *E. coli* S17-1λ*pir* carrying pDS4347Del and TT01 were grown to an OD of 0.6-0.8 and spotted onto a LB agar plate in a ratio of 1:3. Agar plates were incubated at 37°C for 3 h, following 30°C overnight. The next day the cells were harvested with an inoculating loop and resuspended in 3 ml LB medium. Different volumes of the resuspension (50 µl, 100 µl, 200 µl) were spread on LB agar plates containing rifampicin and chloramphenicol to select for TT01 colonies with acquired chloramphenicol resistance. Single colonies were grown in LB medium overnight without selection marker and spread onto agar plates containing rifampicin and 6% sucrose and incubated at 30°C. Deletion mutants were verified with primers VTyrB_Fw and TyrB_down_Rv, yielding fragments of approx. 1100 bp for a deletion mutant and approx. 2200 bp for a wild type strain. For an insertion mutant a partial sequence of *plu4357* was amplified with modified primers 4357KO_Fw (containing a *Sac*I restriction site) and 4357KO_Rv (containing a *Pae*I restriction site) yielding a product of 482 bp. The construction of the pDS132 vector construct and generation of a mutant strain was carried out accordingly to the procedure described before. The same approach was applied for the generation of *aspC*, *ilvE* and *tyrB* insertion mutants in *X. nematophila*. For *aspC* an internal fragment of 824 bp (*xnc1_1585*) was amplified with primers Xn_aspC_ko_for and Xn_aspC_ko_rv, subcloned into vector pJet1.2 and cloned into pDS132 via the *PstI* and *Sac*I restriction site, yielding pDSXnaspCKO. The resulting plasmid was introduced into *E. coli* S17-1 λ*pir* by electroporation and conjugated into HGB081. For *ilvE*, an internal fragment of 691 bp and for *tyrB* a fragment of 812 bp was amplified and the plasmids pDSXnilvEKO, pDSXbtyrBKO and mutants were generated as described before. Genomic DNA of all single mutants were isolated and correct plasmid insertion was confirmed by PCR using one genomic-

specific primer pair listed in Table S1 inclosing the binding sites of the afore amplified DNA region and one plasmid-specific primer pair inclosing the multiple cloning site of pDS132. TT01 Δ*ilvE* was generated accordingly. Disruption of *gxpS* (*plu3263*) was done as previously described using the primers plu3263-1 and plu3263-2 for amplification of an *gxpS* internal fragment that was cloned into pDS132 resulting in plasmid pDS132_plu3263, which was finally used to disrupt *gxpS* in strain TT01. The *gxpS* disruption phenotype was confirmed as described above using the loci specific primers plu3263-3, plu3263-4, and the pDS132 specific primers (Table S1).

GxpS analysis and annotation. GameXPeptide NRPS proteins (GxpS) of the corresponding biosynthetic gene cluster responsible for the production of **1** were analyzed as described previously,[7] following a frame plot 2.3.2 analysis[8] and the PKS/NRPS analysis website (http://nrps.igs.umaryland.edu/nrps/).[9] A detailed sequence analysis of the NRPS domains was performed using ClustalW for the construction of sequence alignments.[10] All conserved and catalytic residues of the adenylation domains[7], condensation and dual epimerization/condensation domains[7,11] respectively were characterized as described in literature. Specificities of amino acids for the incorporation into **1** were predicted based on the eight amino acid code described by Stachelhaus *et al.*[12,13]

Synthesis of GameXPeptide A (1). For the synthesis of GameXPeptide A (**1**) the linear precursor was received *via* microwave-enhanced solid phase synthesis using Wang resin and Fmoc protection. The cyclisation of the linear pentapeptide was conducted by a microwave-assisted HATU/DIPEA protocol from Cini *et al.*[14].

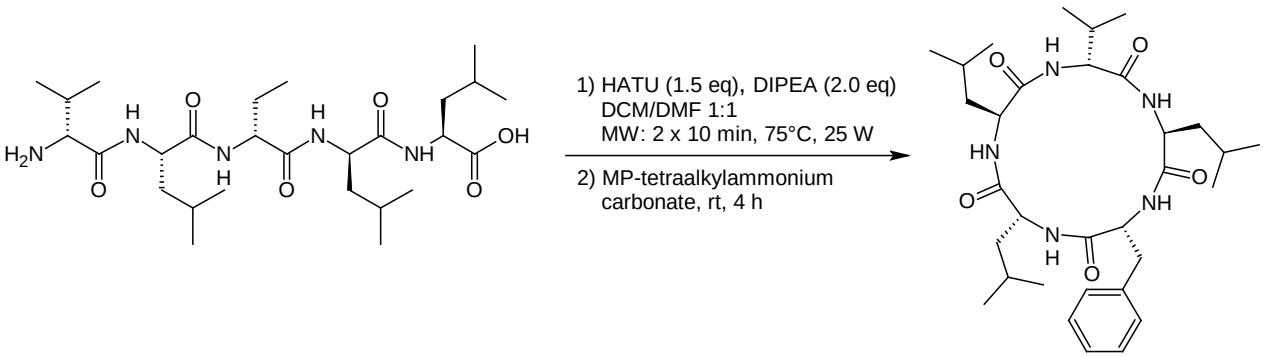

Purification of the cyclic pentapeptide was achieved by the addition of polymer-bound MP tetraalkylcarbonate[15] for scavenging the formed HOAt and for neutralization of the DIPEA salt. Fmoc-L-Leu-Wang, Fmoc-D-Leu, Fmoc-D-Phe, Fmoc-L-Leu, Fmoc-D-Val-OH and HBTU were purchased from *Iris Biotech GmbH* and DIPEA, MP-tetraalkylammonium carbonate, DCM (over molecular sieves) and DMF p.a. from *Sigma Aldrich*. The linear pentapeptide was built up by microwave-assisted solid phase synthesis using a *Discovery* microwave system from *CEM*. Fmoc-L-Leu-Wang

(100 μmol) was successively coupled with Fmoc-D-Leu, Fmoc-D-Phe, Fmoc-L-Leu and Fmoc-D-Val by using the following single coupling protocol:

step	reagents	MW conditions
1	20 % piperidine in DMF	75°C, 35 W, 30 s
2	20 % piperidine in DMF	75°C, 35 W, 3 min
3	20 % piperidine in DMF	75°C, 35 W, 3 min
4	Fmoc-AA (0.2 M in DMF, 6.0 eq) HBTU (0.5 M in DMF, 5.0 eq) DIPEA (2 M in NMP, 10 eq)	75°C, 25 W, 10 min (Leu, Phe) 75°C, 20 W, 10 min (Val)

Fmoc deprotection oft the resin-bound pentapeptide was achieved by applying steps 1-3 of the single coupling protocol. The peptide was cleaved from the Wang resin with TFA 95% (6 ml) under the following microwave conditions: 30°C, 20 W, 18 min. The TFA was evaporated with a light air stream over night and the oily residue was evaporated three times with DCM. The crude linear pentapeptide was received quantitatively as a pure white foam. The crude linear pentapeptide (30.2 mg, 50 μmol) was dissolved in a mixture of DMF p.a. (6 ml) and dry DCM (6 ml). After the addition of HATU (1.5 eq) and DIPEA (2.0 eq), the reaction mixture was subjected to the following microwave conditions: 1. 75°C, 25 W, 10 min; 2. 60°C, 0 W, 2 min; 3. 75°C, 25 W, 10 min. MP-tetraalkylammonium carbonate (12 eq) was added and the reaction mixture was lightly stirred at room temperature for 4 hours. The resin was removed by filtration and was washed three times with DMF. After evaporation of the solvents the cyclic pentapeptide (20.0 mg, 34.2 μmol, 68%) was received in pure form as a white solid. GameXPeptide B-D (**6-8**) were synthesized accordingly.

Table S1. Oligonucleotides

TyrB_up_Fw	GAGCTCACGGCCGTGGATTTTAACC
TyrB_up_Rv	GGTTGACGCCACCAGCATAAGCATCAACATTC
TyrB_down_Fw	TTATGCTGGTGGCGTCAACCATCGTAATGT
TyrB_down_Rv	GCATGCGGACTGAGTTCCCTCCAAGTG
VTyrB_Fw	AGGTGTAAGGCCGGAAGATGC
4357KO_Fw	GAGCTCTGATGCTTATGCTGGTGATCCGATTC
4357KO_Rv	GCATGCCACTGAATTTTACCCCTTTGGTCTGTGT
V4357_Fw	GTGGGATCTGGGTCAGTGAACGTG
V4357_Rv	CCGCCATACAGACTCGGCCATTAC
pDS132_Fw	GATCGATCCTCTAGAGTCGACCT
pDS132_Rv	ACATGTGGAATTGTGAGCGG
Xn_aspC_ko_for	CCGGCAGACCCTATTCTTGG
Xn_aspC_ko_rv	ACAATGGATTTTGCCTGACTG
vXn_aspC_fw	TTGACGGCCTGAACTTTGCT
vXn_aspC_rv	TGGGACATGAACGGAAAACCA
Xn_ilvE_ko_for	ATGGAGAAATGGTACCTTGGG
Xn_ilvE_ko_rv	GCACTTCCAGACCCAGATC
vXn_ilvE_fw	AAGGCTTAGGTGCTGCGGATTT
vXn_ilvE_rv	ATGTTGCGGCCATGTGTTGT
Xn_tyrB_ko_for	ATCCTATCCTGTCG
Xn_tyrB_ko_rv	CCAAGACATGTTCTGC
vXn_tyrB_fw	TTGAGGCGGCAGATTTACCTGTT
vXn_tyrB_rv	GCGGCGGACAATGTGATGATAA
plu3263-1	ATGCGCATGCGGATACCCTTGAACAGGCCC
plu3263-2	ATGCGAGCTCATCACGTAGGCTAGGTGGCG
plu3263-3	CTCTGCTGAATGATCGTCTA
plu3263-4	CCAACCGAGCTTCAATTTCT

Table S2. Plasmids used in this work.

Plasmid	Genotype	Source / Reference
pDS132	R6Kγori oriT *sacB* Cm^R	Philippe *et al*. (2004)[16]
pDS4357Del	R6Kγori oriT *sacB* Cm^R Δ*plu4357*	This work
pDS4357KO	R6Kγori oriT *sacB* Cm^R *plu4357´*	This work
pDSXnaspCKO	R6Kγori oriT *sacB* Cm^R *xnc1_1585´*	This work
pDSXnilvEKO	R6Kγori oriT *sacB* Cm^R *xnc1_0370´*	This work
pDSXntyrBKO	R6Kγori oriT *sacB* Cm^R *xnc1_3918´*	This work
pJet1.2/blunt	*rep* Amp^r *eco47IR*	Fermentas GmbH
pDS132_plu3263	R6Kγori oriT *sacB* Cm^R *plu3263*	This work

Table S3. Sum formulae of compounds identified in *P. luminescens* strain TT01. Compound identification (see comments) was based on MS-fragmentation data and/or retention time similarity with known compounds.

R_t	m/z	C_xN_y	$[M+H]^+$	comments
3.59	334.76294^{2+}	$C_{33}N_9$	$C_{33}H_{67}O_5N_9$	mevalagmapeptide (**9**)
3.75	341.77057^{2+}	$C_{34}N_9$	$C_{34}H_{69}O_5N_9$	derivative of **9**
3.99	422.18255	$C_{22}N_5$	$C_{22}H_{24}O_4N_5$	
4.20	388.21225	$C_{22}N_1$	$C_{22}H_{30}O_5N$	
4.58	402.22768	$C_{23}N_1$	$C_{23}H_{32}O_5N$	
5.31	287.12823	$C_{17}N_0$	$C_{17}H_{19}O_4$	isopropylstilbene derivative[17]
6.40	285.07474	$C_{17}N_0$	$C_{17}H_{17}O_4$	
6.52	285.07571	$C_{16}N_0$	$C_{16}H_{13}O_5$	anthraquinone[18]
6.56	255.13730	$C_{17}N_0$	$C_{17}H_{19}O_2$	isopropylstilbene[19]
6.93	215.21220	$C_{12}N_2$	$C_{12}H_{27}ON_2$	
7.02	523.38507	$C_{28}N_4$	$C_{28}H_{51}O_5N_4$	
7.08	426.26144	$C_{19}N_1$	$C_{19}H_{41}O_7NP$	*lyso*-phospatidyl ethanolamine (PE)
7.21	452.27679	$C_{21}N_1$	$C_{21}H_{43}O_7NP$	*lyso*-PE
7.22	440.27674	$C_{20}N_1$	$C_{20}H_{43}O_7NP$	*lyso*-PE
7.27	229.22708	$C_{13}N_2$	$C_{13}H_{29}ON_2$	
7.42	552.41077	$C_{29}N_5$	$C_{29}H_{54}O_5N_5$	GameXPeptide C (**7**)
7.48	466.29219	$C_{22}N_1$	$C_{22}H_{45}O_7NP$	*lyso*-PE
7.55	586.39545	$C_{32}N_5$	$C_{32}H_{52}O_5N_5$	GameXPeptide A (**1**)
7.71	281.21139	$C_{17}N_0$	$C_{17}H_{29}O_3$	
7.82	566.42596	$C_{30}N_5$	$C_{30}H_{56}O_5N_5$	GameXPeptide D (**8**)
7.88	243.24326	$C_{14}N_2$	$C_{14}H_{31}ON_2$	
7.92	600.41010	$C_{32}N_5$	$C_{32}H_{54}O_5N_5$	GameXPeptide B (**6**)
8.04	295.22670	$C_{18}N_0$	$C_{18}H_{31}O_3$	
8.28	257.25760	$C_{15}N_2$	$C_{15}H_{33}ON_2$	
8.59	309.24228	$C_{19}N_0$	$C_{19}H_{33}O_3$	
8.86	323.25757	$C_{20}N_0$	$C_{20}H_{35}O_3$	

Table S4. NMR data of isolated and synthetic GameXPeptide A (**1**).

		isolated		synthetic	
subunit	position	δ_C	δ_H, mult. (*J* in Hz)	δ_C	δ_H, mult. (*J* in Hz)
D-Val[1]	1	171.9		171.4	
	2	57.2	4.13, dd (9.1, 6.7)	57.0	4.14, dd (9.2, 6.9)
	3		1.80, m	30.7	1.81, dqq(6.9, 6.7, 6.7)
	4	19.1	0.82, d (7.0)	19.1	0.83, d (6.7)
	5	17.9	0.79, d (7.0)	17.8	0.80, d (6.7)
	NH		7.58, d (9.0)		7.58, d (9.2)
L-Leu[2]	1	171.8		171.5	
	2	52.1	4.08, dt (9.4, 6.7)	52.0	4.09, ddd (9.4, 6.7, 6.7)
	3	38.7	1.31, m 1.13, m	38.6[a]	1.15, m 1.32, m
	4	21.4	0.88, d (6.7)	23.7	0.89, m
	5	21.7	0.71, d (6.7)	21.8	0.72, d (6.4)
	6	22.7	0.62, d (6.4)	22.7	0.64, d (6.5)
	NH		8.48, br s		8.50. d (6.7)
D-Phe[3]	1	170.9		170.7	
	2	55.8	4.22, ddd (11.6, 8.5, 3.0)	55.8	4.23, ddd (12.0, 8.0, 3.2)
	3	36.8	2.75, dd (13.7, 12.2) 3.09, dd (13.7, 3.3)	36.5	2.76, dd (13.7, 12.0) 3.01, dd (13.7, 3.2)
	4	138.9		138.3	
	5	128.5	7.22, m	128.9	7.22, m
	6	128.5	7.22, m	128.0	7.22, m
	7	126.9	7.17, m	126.1	7.19, m
	NH		8.81, d (8.0)		8.83, d (8.0)
D-Leu[4]	1	171.1		170.7	
	2	52.1	4.30, m	52.0	4.31, m
	3	40.4	1.38, m 1.65, m	40.2[a]	1.40, m 1.66, m
	4	36.4	1.43, m	24.9	1.40, m
	5	22.4	0.85, d (6.0)	23.1	0.86, d (6.9)
	6	21.4	0.88, d (6.7)	21.7	0.89, d (6.3)
	NH		7.27, d (7.0)		7.27, d (6.8)
L-Leu[5]	1	172.0		171.6	
	2	49.9	4.35, m	50.0	4.36, m
	3	36.4	1.50, m	36.4	1.45, m 1.50, m
	4	36.4	1.57, m	24.1	1.54, m
	5	21.4	0.78, d (6.4)	21.4	0.79, d (6.3)
	6	22.8	0.86, d (6.7)	22.8	0.87, d (6.6)
	NH		8.83, d (8.0)		8.85, d (8.0)

[a] ^{13}C signal was overlaid by DMSO signal, the chemical shift was estimated by HSQC correlations.

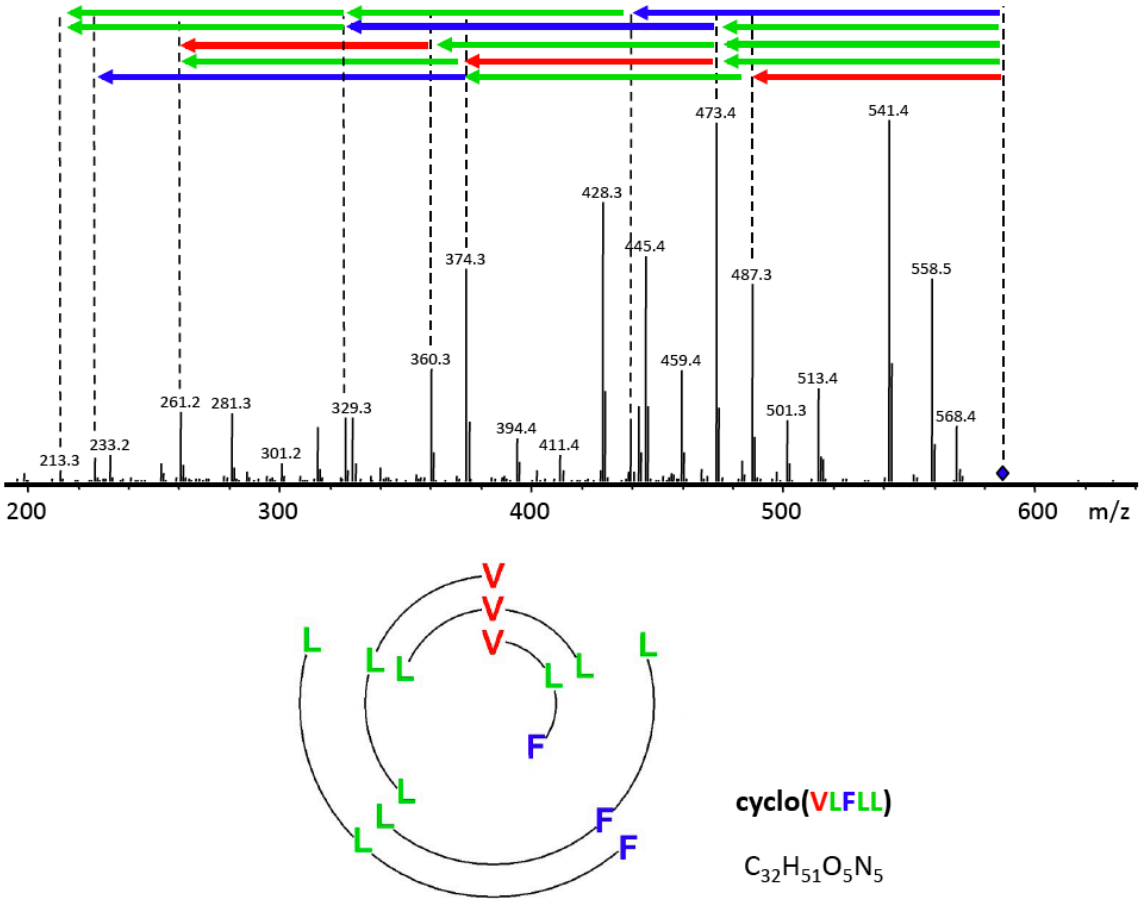

Figure S1. MS/MS analysis of compound **1**. The fragmentation profile has been confirmed by MS^3 and MS^4 experiments of the respective masses.

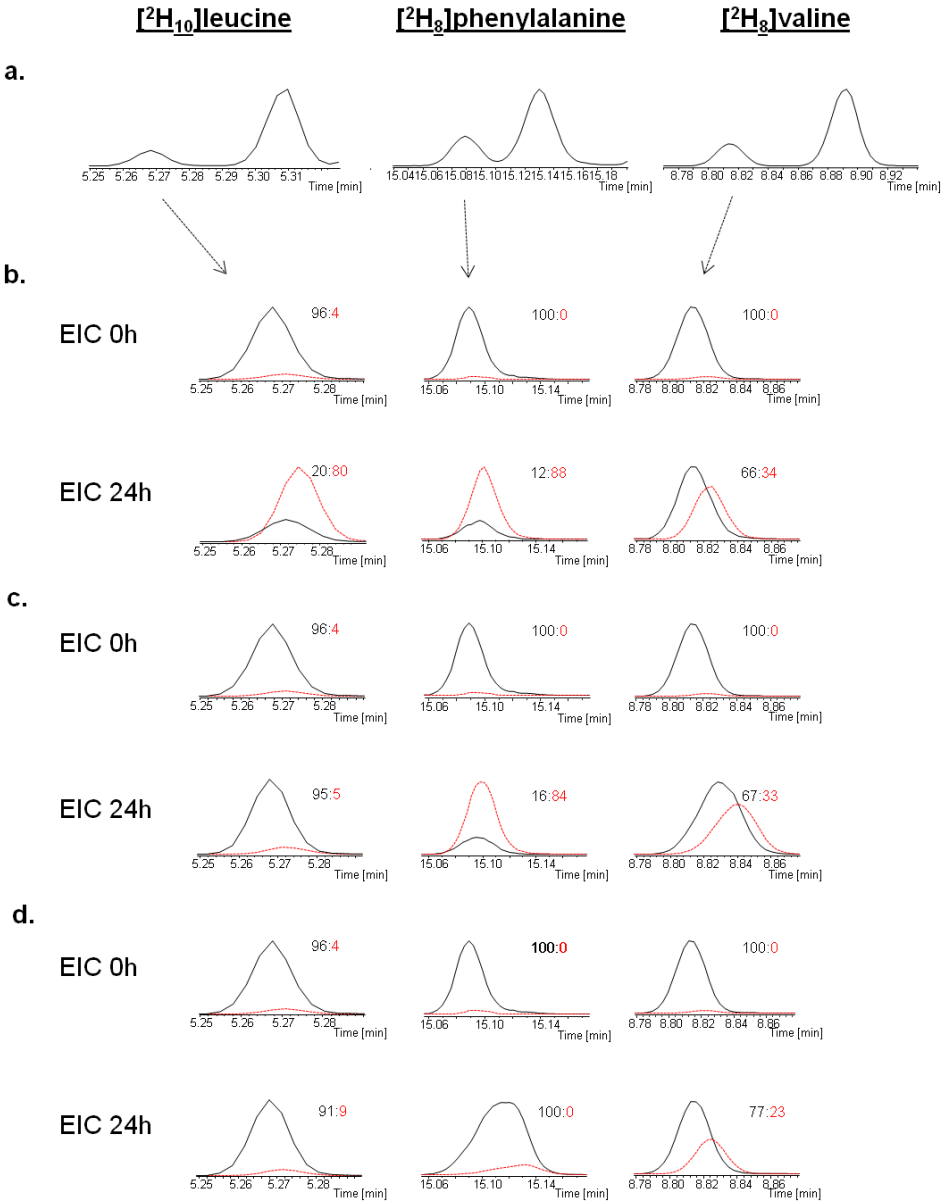

Figure S2. GC/MS analysis for stability of deuterated amino acids in *P. luminescens*. Base Peak Chromatograms of the deuterated and non-deuterated amino acid **(a)**, Extracted Ion Chromatograms (EIC) of the prominent fragment (depicted in **Figure S3**) of the respective fed deuterated [^{2}Hx] amino acids (black, continuous) and due to transamination occurring [^{2}Hx-1] amino acids (red, dashed) of *Photorhabdus luminescens* TT01 **(b)**, Δ*ilvE* **(c)** and Δ*ilvE*/Δ*tyrB* **(d)** with ratios of the integrated EIC signals.

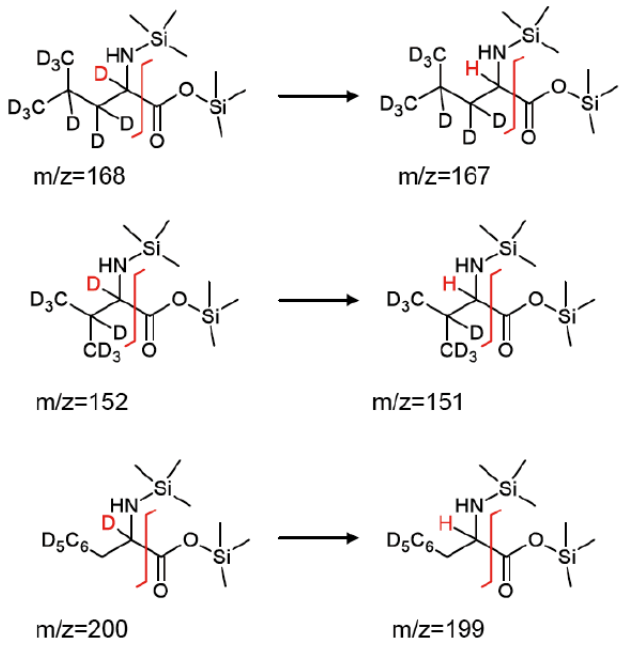

Figure S3. Respective most prominent fragment in die EI-MS spectra of [$^2H_8$]/[$^2H_7$]valine, [$^2H_{10}$]/[$^2H_9$]leucine and [$^2H_8$]/[$^2H_7$]phenlyalanine used for EICs in **Figure S2**.

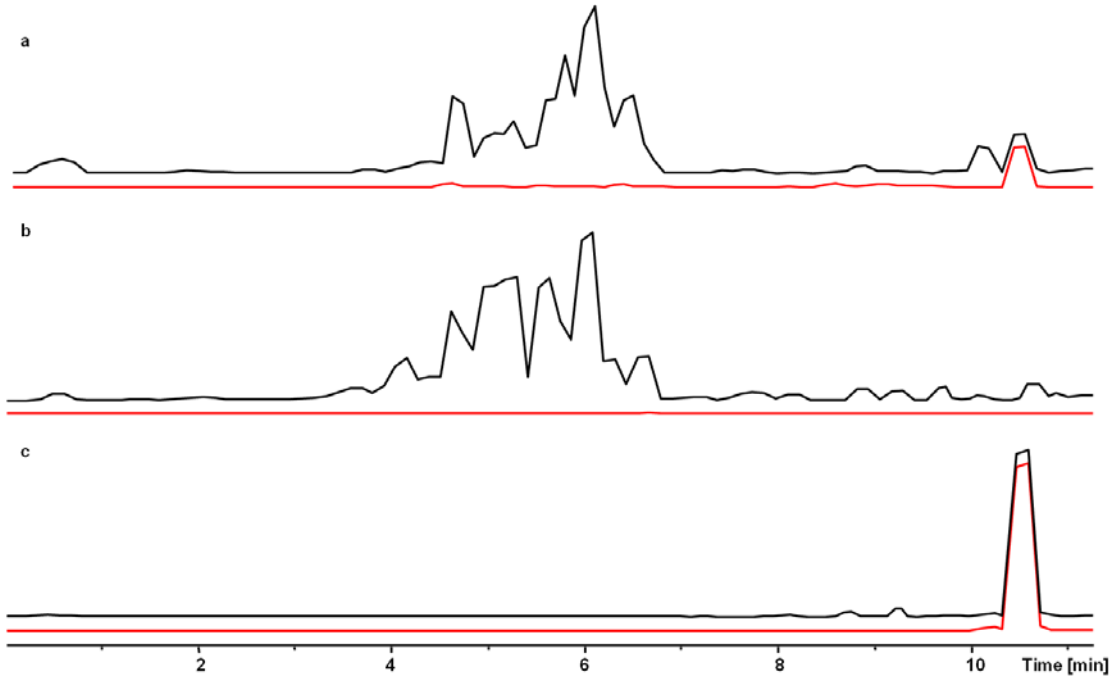

Figure S4. HPLC/MS EIC analysis of *P. luminescence* TT01 (**a**), a *gxpS* knock-out mutant (**b**), and synthetic **1** (**c**). Depicted are the base peak chromatograms (black lines) and extracted ion chromatograms of *m/z* 586.4 (red lines) in the positive mode.

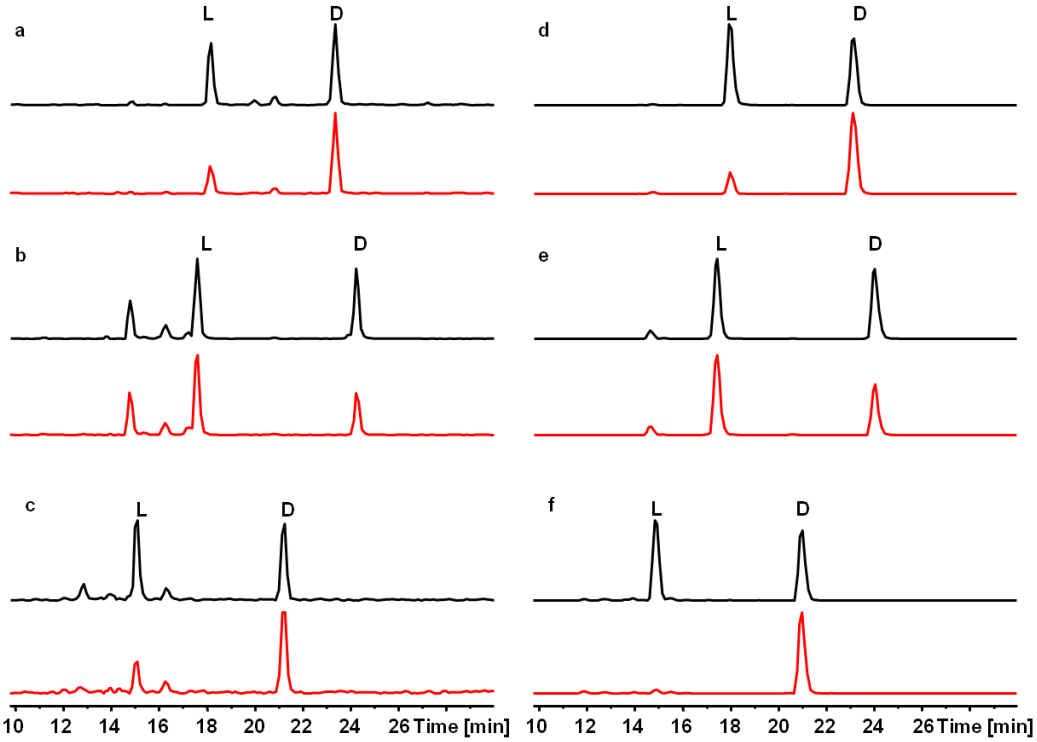

Figure S5. Results from Marfey´s advanced method applied to hydrolyzed isolated **1** (**a**-**c**) and to hydrolyzed synthesized **1** (**d**-**f**). Depicted are the extracted ion chromatograms of the DL-FDLA derivatives (black lines) and the L-FDLA derivatives (red lines) of phenylalanine *m/z* 460.2 (**a**, **d**), leucine *m/z* 426.2 (**b**, **e**), and valine *m/z* 412.2 (**c**, **f**) in the positive mode.

a.

Motif	C1	Dual E/C	C2	C3 (His)
		HHLxxxxGD		
Consensus	**SxAQxRLWxL**		**RHExLRTxF**	**MHHxISDGWS**
Plu3263 C2	SPLQDGILFHHLLAKEGDPY		RHDILRTAF	QHHLIGDHTT
Plu3263 C3	SFGQQRLWFLAQFEGVSDTY		RHEALRSVF	QHHIISDAWS
Plu3263 C4	SPLQDGILFHHLLANEGDPY		RHDILRTAF	LHHLIGDHTT
Plu3263 C5	SPLQDGILFHHLLADEGDPY		RHDILRTAF	MHHLIGDHTA

Motif	C4	C5	C6
Consensus	**YxDYAVW**	**IGxFVNTLxxR**	**HQDYPFE**
Plu3263 C2	FRNLVAQ	MGLFINTLPLR	HASLALA
Plu3263 C3	YPDYAAW	LGFFVNTLALR	HQDLPFE
Plu3263 C4	FRHLVAQ	MGLFINTLPLR	HASLALA
Plu3263 C5	FRNLVAQ	MGLFINTLPLR	YASLALA

b.

Motif	8 AA Code	Specificity
Plu3263 A1	D A F W I G A T	TycC-M4-Val
Plu3263 A2	D A W C I G A V	Cdal-M3-Trp
Plu3263 A3	D A W C I A A V	TycA-M1-D-/L-Phe
Plu3263 A4	D A W C I G A V	Cdal-M3-Trp
Plu3263 A5	D A W C I G A V	Cdal-M3-Trp

Figure S6. Analysis of GxpS. **a.** Depicted are conserved motifs for condensation and dual epimerization/condensation domains. Consensus sequences of condensation domains are highlighted in green and motifs for dual epimerization/condensation domains in blue. **b.** Depicted are the specificities for the amino acids of the adenylation domains based on the eight amino acid code.

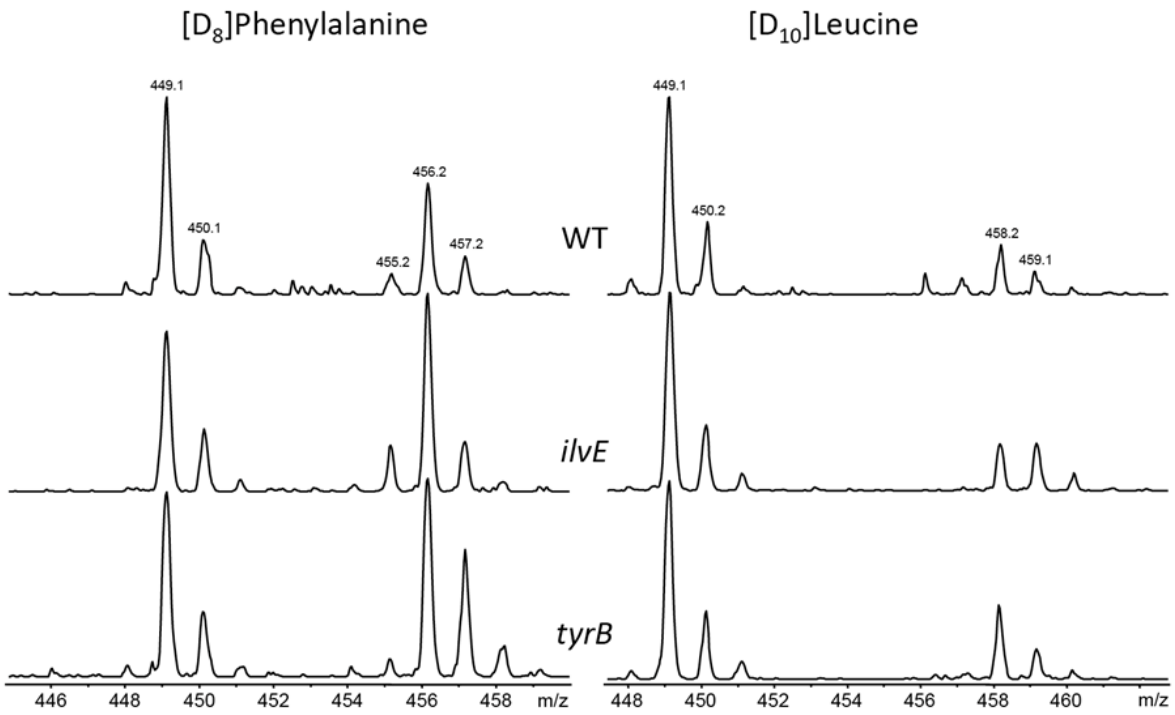

Figure S7. Labeling of xenortide B (**3**) with [$^{2}H_{8}$]phenylalanine and [$^{2}H_{10}$]leucine in WT cells and transaminase insertion mutants in *X. nematophila* HGB081.

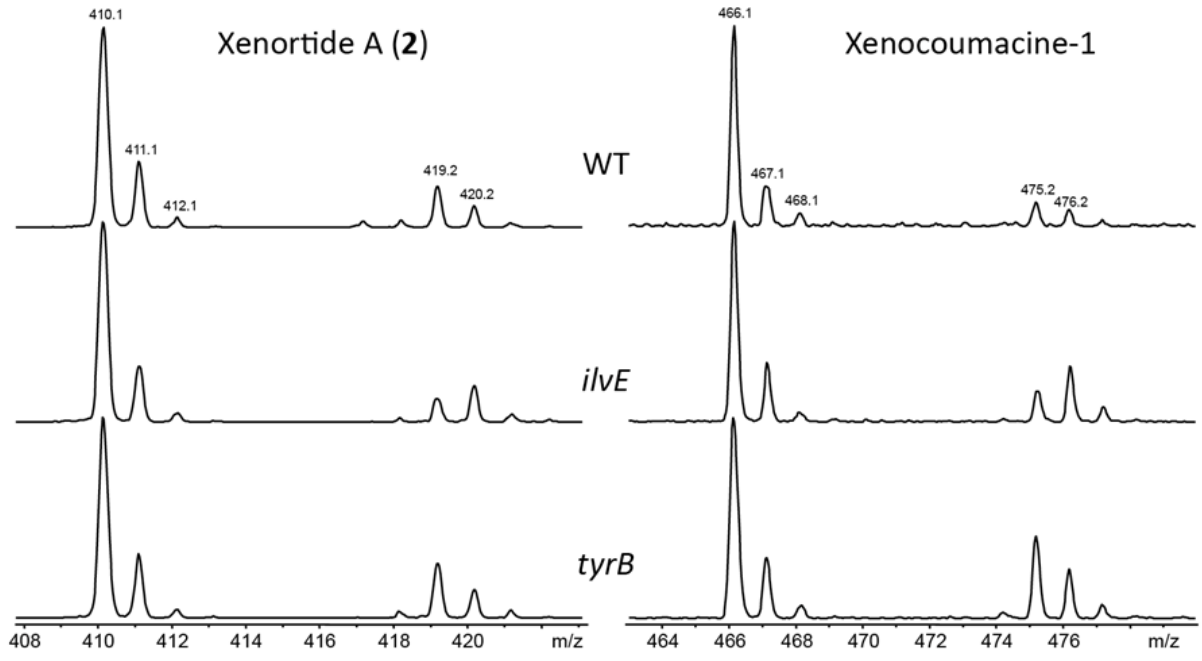

Figure S8. Labeling of xenortide A (**2**) and xenocoumacin-1 with [$^{2}H_{10}$]leucine in WT cells and transaminase insertion mutants in *X. nematophila* HGB081.

References

1. Tailliez, P., Pages, S., Ginibre, N., & Boemare, N. *Int. J. Syst. Evol. Micr.* **56**, 2805-2818 (2006).
2. Vodovar, N. *et al. Nat. Biotechnol.* **24**, 673-679 (2006).
3. Reimer, D., Pos, K.M., Thines, M., Grün, P., & Bode, H.B. *Nat. Chem Biol.*(2011) doi: 10.1038/nchembio.688.
4. Vallet-Gely, I. *et al. Appl. Environ. Microbiol.* **76**, 910-921 (2010).
5. Joskalla, T., Fuchs, B., Karas, M., & Schiller, J. *J. Am. Soc. Mass Spectrom.* **20**, 867-874 (2009).
6. Joskalla, T.W., Lehmann, W.D., & Karas, M. *Proc. NatI. Acad. Sci. USA* **105**, 12200-12205 (2008).
7. Konz, D. & Marahiel, M.A. *Chem. Biol.* **6**, R39-R48 (1999).
8. Ishikawa, J. & Hotta, K. *FEMS Microbiol. Lett.* **174**, 251-253 (1999).
9. Bachmann, B.O. & Ravel, J. *Methods Enzymol.* **458**, 181-217 (2009).
10. Thompson, J.D., Higgins, D.G., & Gibson, T.J. *Nucleic Acids Res.* **22**, 4673-4680 (1994).
11. Balibar, C.J., Vaillancourt, F.H., & Walsh, C.T. *Chem. Biol.* **12**, 1189-1200 (2005).
12. Stachelhaus, T., Mootz, H.D., & Marahiel, M.A. *Chem. Biol.* **6**, 493-505 (1999).
13. Challis, G.L., Ravel, J., & Townsend, C.A. *Chem. Biol.* **7**, 211-224 (2000).
14. Cini, E., Botta, M., Rodriguez, M., & Taddei, M. *Tetrahedron Lett.* **50**, 7151-7161 (2009).
15. Parlow, J.S., Naing, W., South, M.S., & Flynn, D.L. *Tetrahedron Lett.* **38**, 7959-7962 (2011).
16. Philippe, N., Alcaraz, J.P., Coursange, E., Geiselmann, J., & Schneider, D. *Plasmid* **51**, 246-255 (2004).
17. Kontnik, R., Crawford, J.M., & Clardy, *J. ACS Chem Biol.* **5**, 659-665 (2010).
18. Brachmann, A.O. *et al. ChemBioChem* **8**, 1721-1728 (2007).
19. Joyce, S.A. *et al. Angew. Chem. Int. Ed.* **47**, 1942-1945 (2008).

Chapter 5

Rhabdopeptides from entomopathogenic bacteria as examples for insect-associated secondary metabolites

Daniela Reimer, Kimberly N. Cowles, Friederike I. Nollmann, Heidi Goodrich-Blair and Helge B. Bode

The article has been submitted to

ChemBioChem, 2013

.

Author's effort

The author generated the mutants necessary for the identification of the rhabdopeptides, performed all feeding experiments as well as the structure elucidation and wrote most of the paper. HPLC MS analysis was conducted by the author and high-resolution MS with the help of Eva Luxenburger. Moreover, the author annotated the biosynthetic gene cluster and performed the analysis of produced compounds in the *in vivo* system in *G. mellonella*. Friederike I. Nollmann synthesized the rhabdopeptides and Kimberly N. Cowles performed the IVET screen and analyzed IVET screen mutants phenotypically.

Rhabdopeptides from entomopathogenic bacteria as examples for insect-associated secondary metabolites

Daniela Reimer,[a] Kimberly N. Cowles,[b] Friederike I. Nollmann,[a] Heidi Goodrich-Blair[b] and Helge B. Bode[a]

[a] *Merck Stiftungsprofessur für Molekulare Biotechnologie*
Fachbereich Biowissenschaften
Goethe Universität Frankfurt
Max-von-Laue-Str. 9, 60438 Frankfurt am Main, Germany
Fax: (+) 49 (0)69 798 29527
E-mail: h.bode@bio.uni-frankfurt.de

[b] *Department of Bacteriology*
University of Wisconsin-Madison
1550 Linden Dr., Madison, WI, 53706, USA

Abstract

Six novel linear peptides named rhabdopeptides have been identified in the entomopathogenic bacterium *Xenorhabdus nematophila* after the identification of the corresponding *rdp* gene cluster using a promoter trap strategy for the detection of insect inducible genes. The structures of these rhabdopeptides were deduced exclusively from labeling experiments combined with detailed MS analysis and their structures were confirmed by chemical synthesis. Detailed analysis of a *rdp* mutant revealed that these compounds participate in virulence towards insects and are produced upon bacterial infection of a suitable insect host.

Introduction

The bacterium *Xenorhabdus nematophila* is pathogenic against numerous insects and is a mutually beneficial symbiont of the entomopathogenic nematode *Steinernema carpocapsae*.[1,2] In response to environmental changes *X. nematophila* regulates the transition between mutualism and pathogenesis and adapts to its two hosts.[3,4] Within the insect, *X. nematophila* produces multiple compounds, such as toxins, enzymes and small molecules that bring about insect death (typically within 48 h) and help protect the insect cadaver from various competitors.[5-8] Several classes of diverse secondary metabolites representing a broad spectrum of antibacterial, antifungal, insecticidal, nematicidal and cytotoxic activities from *X. nematophila* and related *Xenorhabdus* strains are isolated and described.[5,9-13] Many secondary metabolites are produced by multienzyme thiotemplate mechanisms like the nonribosomal peptide synthetases (NRPS) and the fatty acid synthase-related polyketide synthases.[14-17] Here, we describe a method to identify *X. nematophila* virulence-associated small molecules using the example of the linear nonribosomally-produced rhabdopeptides.

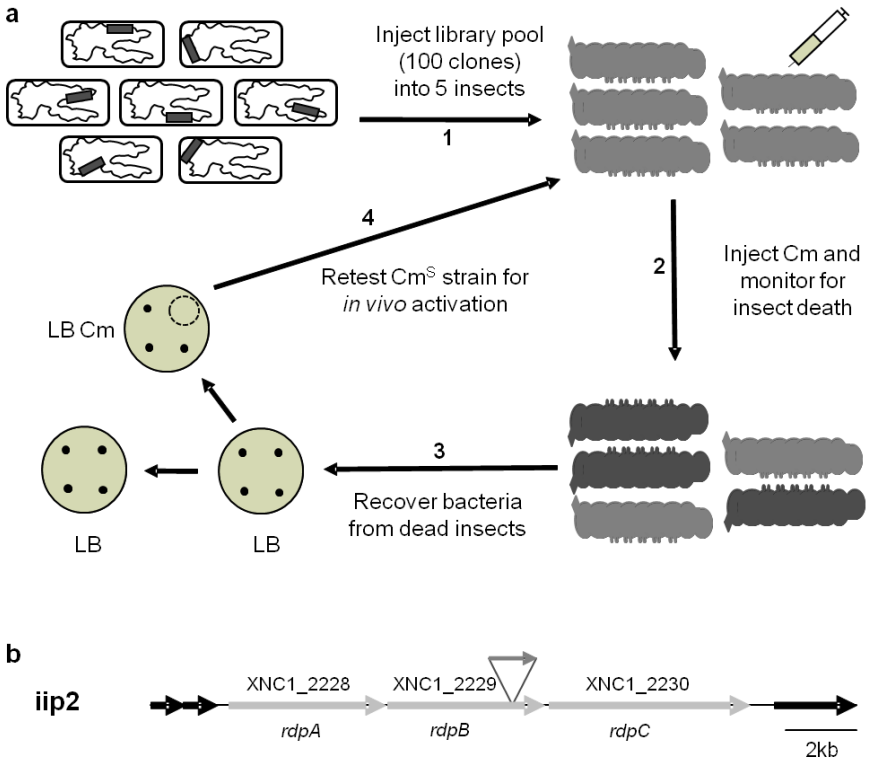

Figure 1. Schematic representations of the *X. nematophila* IVET protocol and iip2 locus. (**a**) Using the IVET protocol, 3,600 clones were tested for insect-inducibility; steps are shown in numerical order. *X. nematophila* strains carrying an integrated promoter-*cat* fusion (dark gray rectangles) were pooled and injected into living *M. sexta* insects (light gray) (1). 1 h post-injection Cm was injected additionally into *M. sexta* and monitored for insect death (2). Bacteria were recovered from dead insects (dark gray) 24-48 h post-injection and plated onto selective media (3). *In vitro* Cm sensitive strains (Cm^S) (circled colony) were retested individually for *in vivo* promoter activation (4). The eight clones that passed this retesting procedure were classified as iip (insect-inducible promoters). (**b**) *X. nematophila* iip2 locus. Light gray arrows indicate the locus (RdpA-RdpC) interrupted by IVET plasmid integration, with the insertion site and *cat* gene orientation represented by the triangle in XNC1_2229 and the associated dark gray arrow respectively. Black arrows denote flanking genes.

Results and Discussion

Identification of rhabdopeptide biosynthesis gene cluster using IVET. The gene XNC1_2229 (hereafter referred to as *rdpB*), predicted to be part of a rhabdopeptide biosynthetic gene cluster, was identified in a promoter trap strategy. In this strategy, *in vivo* expression technology (IVET) was employed to reveal genes upregulated during and therefore potentially important for *X. nematophila* infection of *Manduca sexta* insects.[18,19] Insect-inducible promoters (iip) were identified from a library of 3,600 clones using a promoterless chloramphenicol acetyl transferase (*cat*) gene as a reporter of promoter expression. Only those strains carrying an active promoter fused to *cat* were resistant to the antibiotic chloramphenicol (Cm) inside the insect and thus able to proliferate and kill the insect host (Figure 1a). Bacteria were collected from dead insects and tested for *in vitro* Cm resistance. Strains with constitutive promoters were Cm resistant both *in vivo* and *in vitro* while the iip were Cm sensitive *in vitro*. The *in vitro*-Cm-sensitive strains were retested individually to confirm the resistance to Cm during infection, yielding eight iip strains (iip1-8). Sequencing of the *X. nematophila* DNA cloned upstream of the *cat* reporter revealed genes putatively upregulated *in vivo*. For iip2 the promoter-*cat* fusion integrated such that the *cat* reporter was fused to XNC1_2229 (*rdpB*) and was oriented in the same transcriptional direction of this and the other genes encoded in the region (Figure 1b). The other iip loci with *cat* fusions in the same transcriptional orientation as the surrounding genes were iip3 (putative transposase), iip4 (putative lipoprotein associated with genes predicted to encode LPS modification enzymes), iip6 (putative oxidoreductase), and iip7 (putative CRISPR-associated sequence gene *casE*) (Figure S1). These were not characterized further in this study.

Identification of rhabdopeptides and structure elucidation by labeling. To gain insight into the products of the iip2 locus, we constructed mutants in the corresponding gene cluster. Analysis of a plasmid insertion mutant of XNC1_2228 (*rdpA*) led to the identification of six new compounds, named rhabdopeptides, that were no longer produced in the mutant strain (Figure 2a-c, Figure S2a-c). HR MS analysis of the identified compounds allowed the determination of the molecular formulae for **1** – **6** (Table 1). As these rhabdopeptides were only produced in small amounts in *X. nematophila* HGB081 cultivated in LB medium under standard lab conditions and as isolation of these compounds via preparative RP HPLC MS was difficult due to overlapping peaks with other compounds produced, we elucidated the structures of all compounds without their isolation or their NMR analysis but only based on MS techniques as described for other peptides.[20] Thus, a combination of labeling experiments and detailed ESI HPLC MS and high-resolution mass spectrometry (HR MS) analysis as previously described by our group was used.[21,22] In inverse labeling experiments, possible building blocks of natural abundance, e.g. amino acids like L-leucine, L-valine, L-phenylalanine, were fed to the wild type strain *X nematophila* HGB081 cultivated in [U-^{13}C] medium. An incorporation of the carbons incorporated. Alternatively, deuterated amino acids were added to HGB081 grown in standard LB medium resulting in an increased mass depending on the number of hydrogen atoms**.**

Table 1. High-resolution MS analysis of rhabdopeptides 1 - 6 (**1** – **6**) produced in *Xenorhabdus nematophila.*

No	Sum formula $[H]^+$	*m/z* calc. $[M+H]^+$	*m/z* det. $[M+H]^+$	Δppm
1	$C_{32}H_{56}N_5O_4$	574.4327	574.4313	2.458
2	$C_{33}H_{58}N_5O_4$	588.4483	588.4469	2.433
3	$C_{38}H_{67}N_6O_5$	687.5167	687.5158	1.361
4	$C_{39}H_{69}N_6O_5$	701.5324	701.5312	1.719
5	$C_{44}H_{78}N_7O_6$	800.6008	800.6000	0.961
6	$C_{45}H_{80}N_7O_6$	814.6165	814.6154	1.276

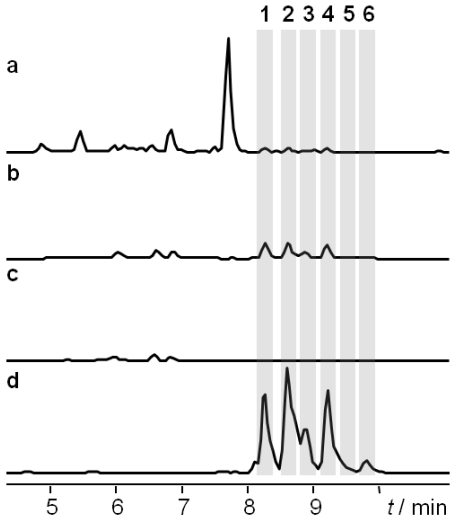

Figure 2. HPLC MS analysis of rhabdopeptides 1 - 6 (**1**-**6**) in *X. nematophila* strains. Base peak chromatograms (BPC) and extracted ion chromatograms (EIC) traces specific for **1** (*m/z* 574 $[M+H]^+$), **2** (*m/z* 588 $[M+H]^+$), **3** (*m/z* 687 $[M+H]^+$), **4** (*m/z* 701 $[M+H]^+$), **5** (*m/z* 800 $[M+H]^+$) and **6** (*m/z* 814 $[M+H]^+$) are shown. Depicted are (**a**) BPC of HGB081 wild type after 3 days of incubation in LB medium (**b**) EIC of HGB081 wild type cultivated in LB medium, (**c**) EIC of *rdpA*::*cat* cultivated in LB medium, (**d**) EIC of HGB081wild type injected into *G. mellonella*. All chromatograms are scaled in the same intensity.

For rhabdopeptide 1 (**1**) a mass decrease of 6 Da in the labeling experiment with $[^{12}C_6]$leucine to X. nematophila cultivated in [U-^{13}C]medium and 15 Da (3 x 5 Da) for $[^{12}C_5]$valine indicated as building blocks one leucine and three valines (Figure 3a). The methylation of leucine and/or leucine was confirmed by a +9 Da mass shift in a culture with L-[methyl-D_3]methionine, Figure 3a). Moreover, a mass decrease of 8 Da instead of an expected mass decrease of 9 Da for the feeding with $[^{12}C_9]$phenylalanine indicated phenylethylamine as *C*-terminal building block as it is the case for xenortide A[9] (Figure 3a). Once the predicted molecular formula was in agreement with the incorporated building blocks, the sequential order of the building blocks in **1** was assigned by analysis of MS^2 and MS^n fragmentation patterns.[21] Based on the MS^2 fragmentation pattern, we could not reveal the position of the leucine as leucine and methylvaline show both the same mass shift of 113 *m/z*. To clarify this point, we combined the MS^2 fragmentation pattern of all labeling experiments with their MS^n fragmentation pattern to identify leucine as *N*-terminal building block in **1** (Figure 3b, Table S1). As depicted in Figure 3b an incorporation of $[^{12}C_6]$leucine at this position could be observed by a mass decrease of 6 Da to *m/z* 129 in comparison to *m/z* 135 for the respective fragment of completely ^{13}C labeled **1** or with $[^{12}C_5]$valine labeled **1**. Furthermore, this comparison also allowed the identification of the correct position of the unmethylated valine. Thus, **1** is composed of phenylethylamine with *N*-methylleucine and two *N*-methylvalines and one non-methylated valine (Figure 3, Figure 4).

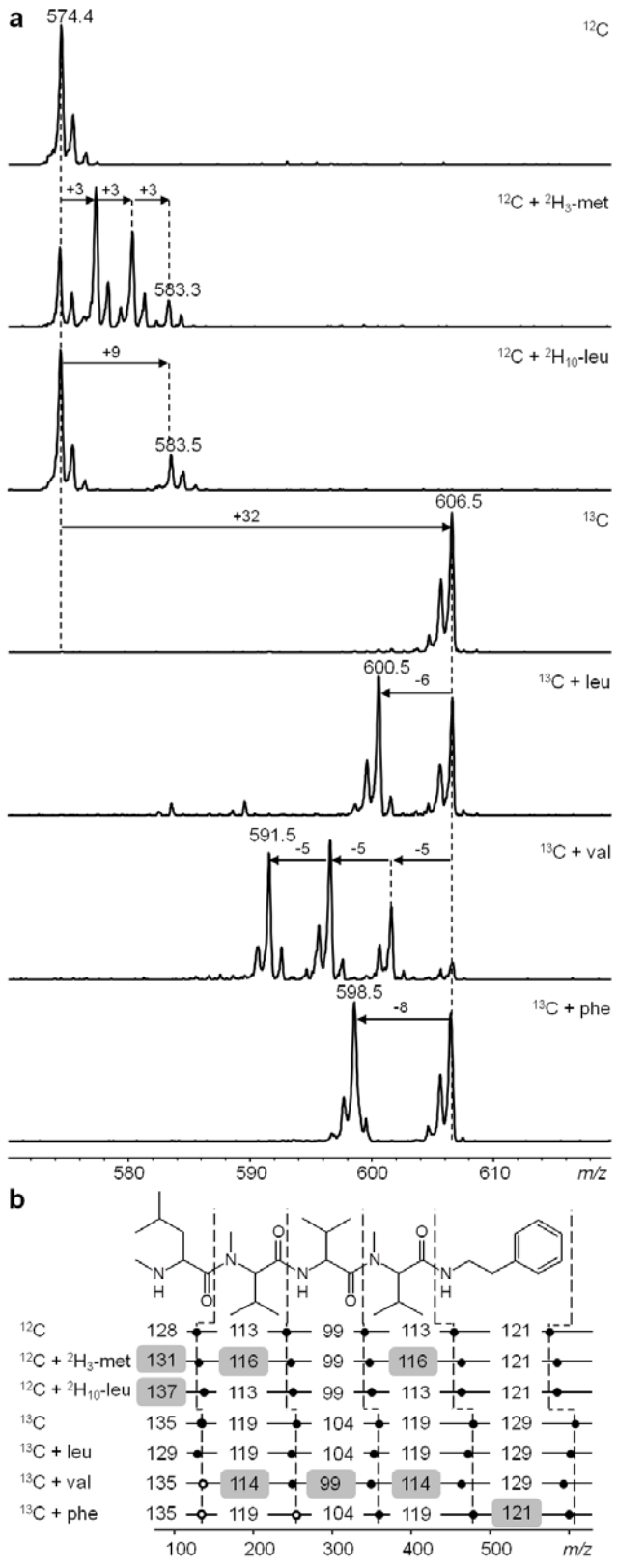

Figure 3. Structure elucidation of rhabdopeptide 1 (**1**) via fragmentation pattern and feeding experiments. *X. nematophila* was cultivated in ^{12}C LB medium supplemented with L-[methyl-D_3]methionine, L-[2,3,3,4,5,5,5,6,6,6-D_{10}]leucine and for an inverse feeding approach in [U-^{13}C] medium, supplemented with L-leucine, L-valine and L-phenylalanine (from top to bottom). (**a**) MS feeding experiments data of **1**. Identified mass shifts are indicated by arrows. (**b**) MS^2 fragmentation pattern of **1**. Positions of the possible b-ion MS^2 fragmentation sites are indicated with dashed lines. Precursor ion masses (filled circle on the right) and identified fragmentation ions *m/z* $[M+H]^+$ are indicated by a filled circle. Fragmentation b-ions that could not be detected in this experiment but could be concluded from other results are indicated with an open circle. Masses of fragments predicting the incorporated amino acid are highlighted in boxes.

The structures of rhabdopeptides 2 – 6 (**2**–**6**) were elucidated similarly (see Supporting Information, Table S1, Figure S3). In summary, rhabdopeptides are composed of five to seven amino acids (valine, leucine) and phenylethylamine. Two different series of rhabdopeptides have been identified differing in the building block composition and the methylation pattern (compounds **1**, **3**, **5** and compounds **2**, **4**, **6**) (Figure 4). Synthesis and comparison of retention times and MS2 data as for example shown for **2** (Figure S4) confirmed the proposed structures of the rhabdopeptides. Additionally, from the comparison of the synthetic all-L **2** with the natural **2** the absolute configuration of the amino acids were revealed, which is in agreement with the analysis of the biosynthesis enzymes (see below).

Biosynthesis of rhabdopeptides by nonribosomal peptide synthetase. Detailed bioinformatic analysis of the postulated biosynthesis gene cluster allowed the prediction of a three module NRPS system (RdpABC) (Figure 1b, Table S2). RdpABC show high homology to NRPS from *Photorhabdus luminescens*, the sister taxa of *X. nematophila*. From *P. luminescens*, a similar compound named mevalagmapeptide is known but the corresponding biosynthetic gene cluster is still unknown.[21] Each protein is a single module and responsible for the loading, incorporation and processing of one amino acid. RdpA, B, and C are each typical extender modules consisting of condensation (C), adenylation (A), methlytransferase (MT) and thiolation (T) domains and RdpC harbors an additional *C*-terminal C-domain (Figure 5). Such a terminal C-domain was already identified in acinetobactin[23], pseudomonine[24] and fimsbactin[25] and characterized biochemically in pseudomonine biosynthesis.[26] In rhabdopeptide biosynthesis, it might be involved in the condensation of a decarboxylated amino acid (e.g., phenylethylamine) with the peptide intermediate during the release mechanism (Figure 5).

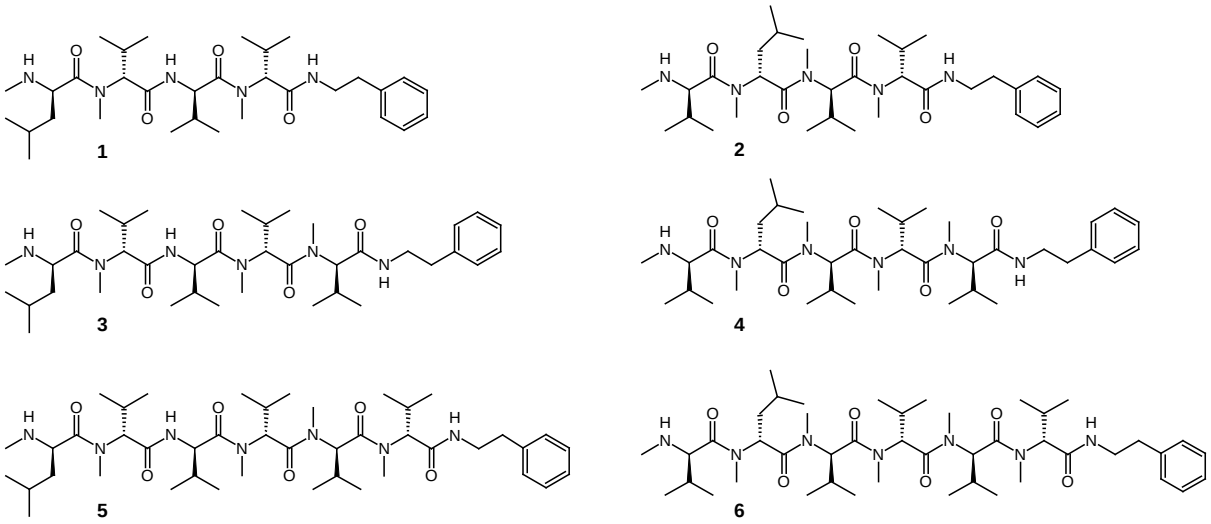

Figure 4. Structures of rhabdopeptides 1 - 6 (**1**-**6**) produced by *X. nematophila* HGB081.

Indeed, we could identify a decarboxylase which plays a role in providing the necessary amine for the rhabdopeptides as in the mutant strain a complete loss of the production could be observed (data not shown). The downstream gene XNC1_2233 encoding a fourth NRPS module seemed not to be involved in the production of the rhabdopeptides as no change in production of **1**–**6** could be identified in a XNC1_2233 deletion mutant (Figure S2d). All adenylation (A) domains of RdpABC harbor an additional *S*-adenosylmethionine-dependent *N*-methyltransferase (MT) domain nested between the $A_{1\text{-}8}$ and $A_{9\text{-}10}$ A-domain motifs. The highly conserved GxGxG amino acid sequence, being part of motif I of *N*-methyltransferases and also present in all MT domains, indicate their functionality.[27,28] Using the 10 amino acid code of Stachelhaus and the NRPSpredictor2[29,30] the amino acid specificity for the RdpABC A domains were predicted to activate L-2,3-diaminopropane

with all three A domains having an identical amino acid code (DALVLAVSIK). We have observed previously, that the prediction of A domain specificities using the standard codes[29,30] is not always correct in *Photorhabdus* and *Xenorhabdus*.[21] As no separate epimerization domain or dual condensation/epimerization domain could be detected in the gene cluster, the rhabdopeptides might have all L-configuration, as confirmed by their total synthesis (Figure S4). Due to the presence of four to six amino acids in the rhabdopeptides and the corresponding gene cluster encoding only three modules, an iterative usage of one or more modules must be assumed as has been proposed previously for coelichelin,[31] fuscachelin[32] and thalassospiramide.[33] To illustrate a possible biosynthesis of **1**, we propose that RdpB might act iteratively and the growing peptide is translocated backwards to incorporate *N*-methylvaline or valine (Figure 5).

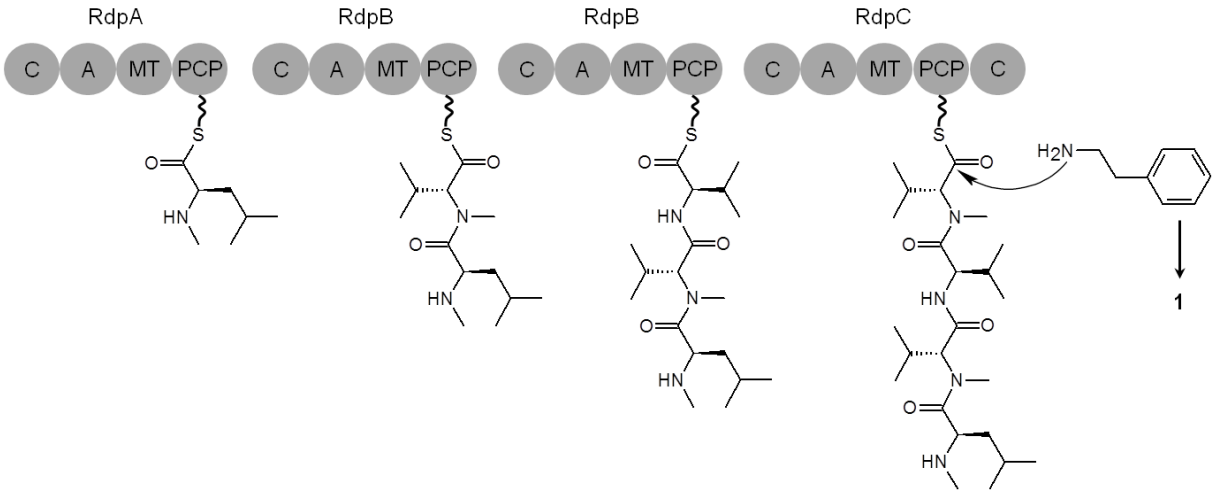

Figure 5. Domain organization of the biosynthetic gene cluster corresponding to the production of the rhabdopeptides in *X. nematophila*. A proposed biosynthesis of **1** with enzyme bound intermediates via an iterative usage of the second module RdpB and a possible termination mechanism catalyzed by the *C*-terminal C-domain of RdpC are shown. C: condensation domain, A: adenylation domain, MT: methyltransferase domain, PCP: peptidyl carrier protein domain.

Other structural related highly *N*-methylated nonpolar linear peptides are reported in diversity in marine-derived organisms including the almiramides[34] and dragonamides[35] produced by the cyanobacterium *Lyngbya majuscula*, pterulamides[36] from a Malaysian fungus *Pterula* sp. and the RHMs[37] from a marine sponge-derived *Acremonium* fungus. These peptides are composed by a variety of nonpolar amino acids and harbor partially unusual *N*- and *C*-terminal modifications (e.g., free amides, cinnamoyl groups, (2*R*)-methyloct-7-ynoic acids or methylamides). However, rhabdopeptides are clearly different from the mentioned peptides by the presence of a *C*-terminal amine.

Rhabdopeptides are expressed at late stages of insect infection. To analyze the biological function of the rhabdopeptides, an *X. nematophila rdpB::km* insertion mutant was compared to the wild type for virulence in *M. sexta* insects and *S. carpocapsae* nematode colonization. Although a slight attenuation in virulence was reproducibly observed for the *rdpB::km* mutant relative to wild type, this difference was not significant (students t-test, p=0.34 for 72 h time point) (Figure 6a). Also, no difference in nematode colonization could be observed (data not shown). Similarly the *rdpB::km* mutant displayed wild type phenotypes in a number of other assays (Table S3).

To study the amount of the Rdp-synthesized rhabdopeptides in an *in vivo* insect host model, relative amounts of **1**–**6** were analyzed after injection of *X. nematophila* in *Galleria mellonella*. Here, **2**, **4** and **6** are produced in higher amounts than **1**, **3** and **5**, respectively similar to their production in LB medium (Figure 6b, Figure S5). Maximum production for **1** and **2** is reached after 10 days post infection in contrast to all other rhabdopeptides, which are only produced in small amounts. Between 2 and 14 days post injection the relative amount e.g. for **5** and **6** is only doubled and for **2** it is four-fold higher (Figure 6b). These results suggested **2** as the main produced rhabdopeptide. It is interesting to note the high production after four days post infection as the insect is killed within 48-72 h post infection, despite the fact that iip2 was selected based on its upregulation 1 h post-injection. It may be that *rdp* genes are initially upregulated upon infection, then further upregulated after insect death. Alternatively, metabolite availability

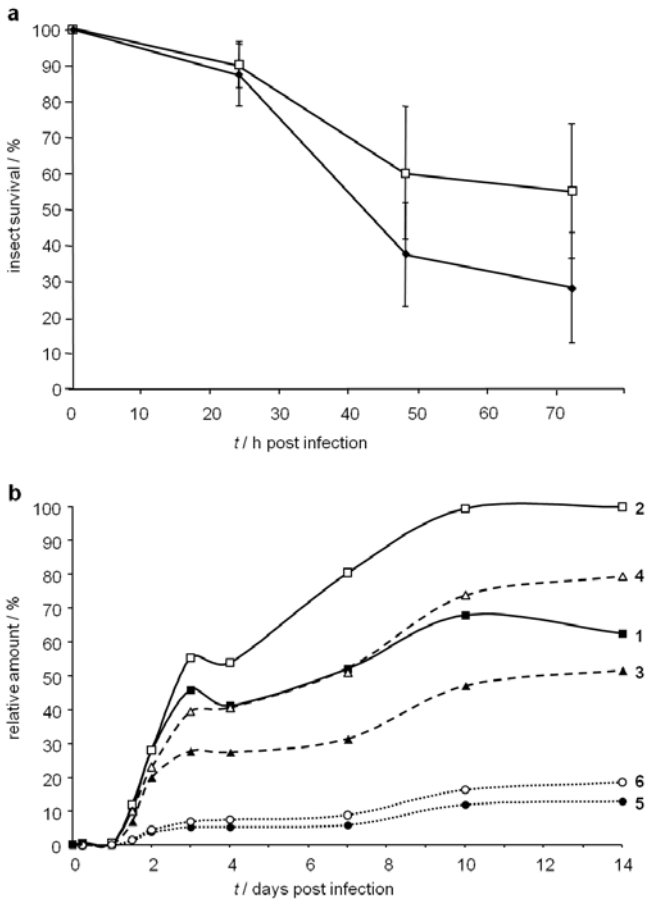

Figure 6. *In vivo* activity and production of rhabdopeptide. (**a**) an *rdpB::km* mutant is slightly attenuated in full virulence towards *M. sexta* insects. Stationary phase wild type *X. nematophila* HGB007 (filled diamonds) and the *rdpB*::*km* mutant (open squares) were injected into 4th instar *M. sexta* insects at ~2000-4000 cfu/insect. Insect survival was monitored for 72 h post infection. Error bars represent standard deviation (n=4). (**b**) Rhabdopeptide (**1** - **6**) production of *X. nematophila* injected into *G. mellonella* in days post infection. 100% refers to the maximum production of **2**. **1** (filled squares), **2** (open squares), **3** (filled triangles), **4** (open triangles), **5** (filled circle) and **6** (open circle).

or other regulatory control may limit *rdp* gene product activity and rhabdopeptide synthesis until after insect death. Regardless, the facts that the *rdpB::km* mutant did not display a severe virulence defect and rhabdopeptides were most abundant after insect death, suggest these molecules function during the insect bioconversion and nematode reproduction phases of the *Xenorhabdus* life cycle (Figure 6).

Biological activity. Compound **2** was tested for biological activity against the parasites *Trypanosoma brucei rhodesiense*, *Trypanosoma cruzi* and *Plasmodium falciparum* which are the causative agents of neglected tropical diseases[38] like sleeping sickness, chagas disease and malaria, respectively. Weak activities against *T. b. rhodesiense* (IC_{50} 3.97 µg mL^{-1}), *T. cruzi* (IC_{50} 5.11 µg mL^{-1}) and *P. falciparum* (IC_{50} 3.02 µg mL^{-1}) could be observed. A much weaker cytotoxicity against rat skeletal myoblasts (L6 cells) was obtained (IC_{50} 19.3 µg mL^{-1}).

Conclusion

The results of this work have shown that IVET can be used successfully to identify factors expressed in insects. Eight iip loci were identified in *X. nematophila*, including the iip2 encoding the rhabdopeptide biosynthesis gene cluster. Consistent with the IVET data, rhabdopeptides were synthesized. The IVET screen described in this work was not saturating for the *X. nematophila* genome, and therefore additional factors with potential activity against insects await identification. Furthermore, the timing of the screen could be altered to detect promoters that are regulated at different points in infection. The genetic loci identified in this study were upregulated within one hour after entry into the insect host, but a different set of factors could be expressed later in infection as well. Despite the success of this initial IVET screen, future characterization of *X. nematophila in vivo* expression will benefit from the availability of multiple *Xenorhabdus* genomes that will allow comparative genomic analyses,[39] RNAseq technologies to identify global transcriptional changes occurring *in vivo*, and fluorescence reporters to monitor *in vivo* gene expression. In addition to xenortides[9,40] the structures of the linear, highly methylated nonribosomally produced rhabdopeptides represent a new class of *N*-methylated peptides carrying a decarboxylated amino acid. These compounds reveal interesting starting points to study their probably iterative biosynthesis in more detail. In summary, this approach could not only be used to identify new secondary metabolites but also their true natural function in their ecological niche.

Acknowledgements

Work in the Bode lab was supported by the DFG. The authors are grateful to Eva Luxenburger and Rolf Müller for HR-ESI MS data.

References

[1] S. Forst, B. Dowds, N. E. Boemare, E. Stackebrandt, *Annu. Rev. Microbiol.* **1997,** *51,* 47-72.

[2] H. Goodrich-Blair, *Curr. Opin. Microbiol.* **2007,** *10,* 225-230.

[3] U. Hentschel, M. Steinert, J. Hacker, *Trends Microbiol.* **2000,** *8,* 226-231.

[4] G. R. Richards, H. Goodrich-Blair, *Cell Microbiol.* **2009,** *11,* 1025-1033.

[5] H. B. Bode, *Curr. Opin. Chem. Biol.* **2009,** *13,* 224-230.

[6] J. M. Park, M. Kim, J. Min, S. M. Lee, K. S. Shin, S. D. Oh, S. J. Oh, Y. H. Kim, *J. Agric. Food Chem.* **2012,** *60,* 4053-4059.

[7] J. J. Sheets, T. D. Hey, K. J. Fencil, S. L. Burton, W. Ni, A. E. Lang, R. Benz, K. Aktories, *J. Biol. Chem.* **2011,** *286,* 22742-22749.

[8] G. R. Richards, E. E. Herbert, Y. Park, H. Goodrich-Blair, *J. Bacteriol.* **2008,** *190,* 4870-4879.

[9] G. Lang, T. Kalvelage, A. Peters, J. Wiese, J. F. Imhoff, *J. Nat. Prod.* **2008,** *71,* 1074-1077.

[10] A. O. Brachmann, S. Forst, G. M. Furgani, A. Fodor, H. B. Bode, *J. Nat. Prod.* **2006,** *69,* 1830-1832.

[11] S. W. Fuchs, A. Proschak, T. W. Jaskolla, M. Karas, H. B. Bode, *Org. Biomol. Chem.* **2011,** *9,* 3130-3132.

[12] A. Proschak, K. Schultz, J. Herrmann, A. J. Dowling, A. O. Brachmann, R. ffrench-Constant, R. Müller, H. B. Bode, *ChemBioChem* **2011,** *12,* 2011-2015.

[13] D. Reimer, K. M. Pos, M. Thines, P. Grün, H. B. Bode, *Nat. Chem. Biol.* **2011,** *7,* 888-890.

[14] M. A. Marahiel, T. Stachelhaus, H. D. Mootz, *Chem. Rev.* **1997,** *97,* 2651-2674.

[15] M. Strieker, A. Tanovic, M. A. Marahiel, *Curr. Opin. Struct. Biol.* **2010,** *20,* 234-240.

[16] C. Hertweck, *Angew. Chem. Int. Ed.* **2009,** *48,* 4688-4716.

[17] J. Staunton, K. J. Weissman, *Nat. Prod. Rep.* **2001,** *18,* 380-416.

[18] M. J. Mahan, J. M. Slauch, P. C. Hanna, A. Camilli, J. W. Tobias, M. K. Waldor, J. J. Mekalanos, *Infect. Agents Dis.* **1993,** *2,* 263-268.

[19] G. M. Young, V. L. Miller, *Mol. Microbiol.* **1997,** *25,* 319-328.

[20] R. D. Kersten, Y. L. Yang, Y. Q. Xu, P. Cimermancic, S. J. Nam, W. Fenical, M. A. Fischbach, B. S. Moore, P. C. Dorrestein, *Nat. Chem. Biol.* **2011,** *7,* 794-802.

[21] H. B. Bode, D. Reimer, S. W. Fuchs, F. Kirchner, C. Dauth, C. Kegler, W. Lorenzen, A. O. Brachmann, P. Grün, *Chem. Eur. J.* **2012,** *18,* 2342-2348.

[22] D. Reimer, E. Luxenburger, A. O. Brachmann, H. B. Bode, *ChemBioChem* **2009,** *10,* 1997-2001.

[23] S. Yamamoto, N. Okujo, Y. Sakakibara, *Arch. Microbiol.* **1994,** *162,* 249-254.

[24] J. Mercado-Blanco, K. M. van der Drift, P. E. Olsson, J. E. Thomas-Oates, L. C. van Loon, P. A. Bakker, *J.Bacteriol.* **2001,** *183,* 1909-1920.

[25] A. Proschak, P. Lubuta, P. Grün, F. Loehr, G. Wilharm, V. De Berardinis, H. B. Bode, *ChemBioChem* **2013**, *14*, 633-638.

[26] E. S. Sattely, C. T. Walsh, *J. Am. Chem. Soc.* **2008,** *130,* 12282-12284.

[27] M. Z. Ansari, J. Sharma, R. S. Gokhale, D. Mohanty, *BMC Bioinformatics.* **2008,** *9,* 454.

[28] C. Hacker, M. Glinski, T. Hornbogen, A. Doller, R. Zocher, *J. Biol. Chem.* **2000,** *275,* 30826-30832.

[29] M. Röttig, M. H. Medema, K. Blin, T. Weber, C. Rausch, O. Kohlbacher, *Nucleic Acids Res.* **2011,** *39,* W362-W367.

[30] T. Stachelhaus, H. D. Mootz, M. A. Marahiel, *Chem. Biol.* **1999,** *6,* 493-505.

[31] S. Lautru, R. J. Deeth, L. M. Bailey, G. L. Challis, *Nat. Chem. Biol.* **2005,** *1,* 265-269.

[32] E. J. Dimise, P. F. Widboom, S. D. Bruner, *Proc. Natl. Acad. Sci.* **2008,** *105,* 15311-15316.

[33] A. C. Ross, Y. Xu, L. Lu, R. D. Kersten, Z. Shao, A. M. Al-Suwailem, P. C. Dorrestein, P. Y. Qian, B. S. Moore, *J. Am. Chem. Soc.* **2013,** *135,* 1155-1162.

[34] L. M. Sanchez, D. Lopez, B. A. Vesely, T. G. Della, W. H. Gerwick, D. E. Kyle, R. G. Linington, *J. Med. Chem.* **2010,** *53,* 4187-4197.

[35] M. J. Balunas, R. G. Linington, K. Tidgewell, A. M. Fenner, L. D. Urena, G. D. Togna, D. E. Kyle, W. H. Gerwick, *J. Nat. Prod.* **2010,** *73,* 60-66.

[36] G. Lang, M. I. Mitova, A. L. Cole, L. B. Din, S. Vikineswary, N. Abdullah, J. W. Blunt, M. H. Munro, *J. Nat. Prod.* **2006,** *69,* 1389-1393.

[37] C. M. Boot, K. Tenney, F. A. Valeriote, P. Crews, *J. Nat. Prod.* **2006,** *69,* 83-92.

[38] N. Feasey, M. Wansbrough-Jones, D. C. Mabey, A. W. Solomon, *Br. Med. Bull.* **2010,** *93,* 179-200.

[39] J. M. Chaston, G. Suen, S. L. Tucker, A. W. Andersen, A. Bhasin, E. Bode, H. B. Bode, A. O. Brachmann, C. E. Cowles, K. N. Cowles, C. Darby, L. de Leon, K. Drace, Z. J. Du, A. Givaudan, E. E. H. Tran, K. A. Jewell, J. J. Knack, K. C. Krasomil-Osterfeld, R. Kukor, A. Lanois, P. Latreille, N. K. Leimgruber, C. M. Lipke, R. Y. Liu, X. J. Lu, E. C. Martens, P. R. Marri, C. Medigue, M. L. Menard, N. M. Miller, N. Morales-Soto, S. Norton, J. C. Ogier, S. S. Orchard, D. Park, Y. Park, B. A. Qurollo, D. R. Sugar, G. R. Richards, Z. Rouy, B. Slominski, K. Slominski, H. Snyder, B. C. Tjaden, R. van der Hoeven, R. D. Welch, C. Wheeler, B. S. Xiang, B. Barbazuk, S. Gaudriault, B. Goodner, S. C. Slater, S. Forst, B. S. Goldman, H. Goodrich-Blair, *PLoS ONE* **2011,** *6,* e27909.

[40] J. M. Crawford, C. Portmann, R. Kontnik, C. T. Walsh, J. Clardy, *Org. Lett.* **2011,** *13,* 5144-5147.

Supporting Information

Supplementary Results

Structure elucidation of rhabdopeptide 2. As in the case of **1**, also for **2** a mass decrease of 6 Da for the feeding with [$^{12}C_6$]leucine and 15 Da (3 x 5 Da) for [$^{12}C_5$]valine could be observed. These mass

shifts indicated one leucine and three valines for **2** (Figure S3a). The methylation of all building blocks was suggested by an observed mass shift of +12 Da according to four methylations in **2**. Additionally, the mass decrease of -8 Da for phenylethylamine as the *C*-terminal building block occurred. Thus, **2** is composed of phenylethylamine with *N*-methylleucine and three *N*-methylated valines (Figure S3a). Based on the MS^2 and MS^n fragmentation pattern in all feeding experiments, we could identify methylleucine as the second *N*-terminal building block in **2** (Table S1, Figure S3b). This incorporation of [$^{12}C_6$]leucine could be verified by a mass decrease in the respective fragment of 6 Da to *m/z* 128 in comparison to *m/z* 134 for completely ^{13}C labeled **2**. A mass shift of +3 Da from *m/z* 113 to *m/z* 116 indicated the methylation (Figure S3b).

Structure elucidation of rhabdopeptide 3-6. **3, 4** and **5, 6** showed the same incorporation pattern as **1** and **2** extended with one and two more *N*-methylated valines for each, respectively (Figure 4, Table S1). Due to technical limitations resulting from very low amounts of fragment ions, the two *N*-terminal residues of compounds **5** and **6** could not be identified in ESI and HR MS analysis and were concluded from **1**, **3** and **2**, **4**, respectively. All predicted structures were verified by synthesis as described for **10** and their synthesis will be published elsewhere.

Supplementary Experimental Procedures

Bacterial strains and culture conditions. *E. coli* strains were grown on solid Luria-Bertani (LB, pH 7.0) medium at 37 °C and on liquid LB medium at 30 °C and 180 rpm at a rotary shaker. Except where noted, for plasmid selection in *E. coli*, chloramphenicol (Cm) (34 µg mL^{-1}) or ampicillin (100 µg mL^{-1}) were added, respectively. All *Xenorhabdus* strains were cultivated on solid and liquid LB medium at 30 °C if not noted otherwise. *X. nematophila* HGB081 mutants were selected on LB containing rifampicin (40 µg mL^{-1}) and chloramphenicol (Cm) (34 µg mL^{-1}) at 30°C. *X. nematophila* HGB007 *rdpB::km* was selected on LB containing kanamycin (50 µg mL^{-1}).

Insect hosts. *Manduca sexta* insect eggs were obtained from Walt Goodman (UW-Madison, Department of Entomology) and were reared on Gypsy Moth Wheat Germ Diet (MP Biomedicals, Aurora, OH) as previously described.[1] *Galleria mellonella* insect larvae were obtained from PetShop Haindl (Frankfurt am Main, Germany).

Plasmid and general DNA procedures. Plasmid isolation, PCR, restriction digests, ligations, gel electrophoresis and DNA transformations were conducted according to standard methods.[2] Agarose gel extraction of amplified PCR fragments and DNA isolation were performed with GeneJET™ Gel Extraction Kit (Fermentas) and Puregene Yeast/Bact. Kit B (Qiagen) according to manufacturer's instructions. All plasmids and strains constructed were listed in Table S4. All oligonucleotides used in this work are listed in Table S5.

Optimization of IVET technique. First, the appropriate level of Cm was determined for use as a selective agent in the *X. nematophila*-insect system. During the IVET screen, insects were injected with a pool of *X. nematophila* clones carrying promoter-*cat* fusions. After 1 h, insects were injected with Cm-succinate. Cm-succinate is soluble in water and therefore less likely to cause damage to the insect host than Cm dissolved in ethanol. Only those strains carrying an active promoter fused to *cat* were resistant to Cm inside the insect and thus able to kill the insect host (Figure 1a). The optimal dose of Cm would allow Cm resistant strains to thrive while preventing Cm sensitive strains from surviving. A too high a dosage would inhibit even those strains expressing *cat* from killing the insect while a too low a dosage could allow inactive-promoter clones to pass through the screen as false positives. Insects were injected with wild type *X. nematophila* (HGB007) cells in combination with varying concentrations of Cm. The *X. nematophila* Tn*10* Cm mutant, designated D11, from an unrelated study (G. Templeton, unpublished data) was used as a positive control for Cm resistance. The results of multiple injections showed that 200 μg μL^{-1} of Cm prevented HGB007 from killing insects while having no effect on D11 virulence (Figure S6).

The second optimization step was to determine the appropriate pool size for the IVET screen. One advantage of IVET is its high throughput capacity; many clones can rapidly be tested for insect-inducibility. Large pool size could increase the speed of the screening process but the presence of too many clones in a pool could prevent even a Cm resistant clone from passing through the screen. For example, in the *X. nematophila*-insect system, if there is a single clone carrying an active promoter in an individual pool, then there must also be enough of those cells present to retain the ability to kill the insect. Thus, determining pool size is an important aspect of IVET optimization. To establish the optimal number of clones for the screen, HGB007 and the Cm-resistant D11 mutant were mixed at different ratios and injected into insects in the presence of 200 μg μL^{-1} Cm. At least 60% of the insects were reproducibly killed only when $\geq$1% of the injected population was Cm resistant (Figure S7). Additionally, bacteria recovered from dead insects were all Cm resistant, demonstrating that Cm sensitive cells (HGB007) were unable to survive the infection process even in the presence of Cm resistant strains. From these results, it was concluded that pools of 100 clones were optimal for this system.

Construction of IVET library. The plasmid used in the IVET screen (pGY2) was acquired from Virginia Miller (Washington University, St. Louis).[3] This plasmid contains a promoterless chloramphenicol resistance gene (*cat*), mobilization functions, an ampicillin resistance marker, and a streptomycin resistance marker. To allow for counter-selection against the *E. coli* donor during conjugations into *X. nematophila*, the ampicillin resistance cassette was removed from pGY2 using *Apa*LI to create the IVET plasmid, pKJN102 (Table S4; Figure S8). *X. nematophila* chromosomal DNA was partially digested with *Sau*3AI and gel-extracted fragments ranging in size from ~500-2,500 bp were cloned into the *Bgl*II site immediately upstream of the promoterless *cat* gene of pKJN102.

Inserts were observed in 80% of the library clones tested and found to be different in size (data not shown). Library clones were grown overnight in LB medium in pools of 100 clones. Each pool was separately conjugated into *X. nematophila* HGB007 and stored at –80°C. Thirty-six *X. nematophila* pools were made in this manner.

IVET screen. The IVET protocol used for the *X. nematophila*-insect system is outlined in Figure 1a. Briefly, stationary phase cultures of individual pools (each with 100 clones) were injected into the first proleg of 5 fourth-instar *M. sexta* larvae. After 1 h, 10 µL of 200 µg μL^{-1} Cm were injected into the opposite proleg. Dead insects were bled 24-48 h post-injection, and dilutions of recovered bacteria were plated on LB pyruvate (0.1%) ampicillin (75 µg μL^{-1}) streptomycin (25 µg μL^{-1}) plates. Isolated colonies were then patched to the same medium with or without Cm (30 µg μL^{-1}). Cm sensitive clones were retested individually for Cm resistance in insects. Eight clones were found to be Cm resistant *in vivo* and Cm sensitive *in vitro*. These clones were designated at iip1 – iip8 and initially sequenced using arbitrary PCR with primers ARB1 and either ArbCat2 (for upstream of the cat gene insertion) or Arb102out (for downstream sequence). In the second PCR, ARB2 was used with CatUp (for upstream sequence) or Arb102in (for downstream sequence). CatUp and Arb102in were then used to sequence the final product.[4,5] Further information regarding these loci and flanking sequences were acquired from the *X. nematophila* genome sequence.[6]

The *cat* gene was integrated into the chromosome in the opposite orientation for three of the eight iip loci (iip1, iip5, and iip8). One possible explanation for this result is that a promoter for an as-yet unidentified antisense RNA is driving expression of *cat* in an insect-inducible manner. A second possibility is that a promoter from a flanking gene is causing *cat* transcription. For example, the divergently transcribed putative thiamine binding protein could have a promoter that extends into the upstream transposase-like gene in iip5. Alternatively, these three iip may be false positives from the screen. The remaining five iip loci each contain an appropriately oriented promoter-*cat* fusion where the gene at the integration site is transcribed with *cat*. iip3 (putative transposase), iip4 (putative lipoprotein associated with an operon with homology to the *Salmonella enterica* Typhimurium *pmrH* LPS modification operon),[7] iip6 (putative dehydrogenase), and iip7 (CRISPR associated sequence homolog *casE*) were not characterized further in this study (Figure S1).

Construction of X. nematophila mutant strains. For the construction of an *rdpA* mutant, XNC1_2228 was disrupted via plasmid integration. An internal fragment of 537 bp was amplified with primers Xn2576fw and Xn2576rv and cloned into pDS132[8] via the *Sph*I and *Sac*I restriction site. The resulting plasmid was introduced into *E. coli* S17-1 λ *pir* by electroporation and introduction into a rifampicin-resistant *X. nematophila* HGB081 strain[9] by biparental conjugation, yielding *rdpA*::*pDS132*. The genotype of the mutant was confirmed by PCR using primers v2576f and v2576r

lying outside the amplified region and two primers pDS132fw and pDS132rv specific for the vector backbone.

For the construction of the *rdpB::km* mutant (XNC1_2229) a 12,973-bp *Eco*RI fragment containing the iip2 locus was identified from a library of chromosomal fragments in pBluescript II SK+. Using this plasmid, pBlueNRPS as a target, the GeneJumper transposon insertion kit (Invitrogen) was used to generate kanamycin resistance insertions in the *iip* locus, according to the manufacturer's instructions. One mutagenized plasmid, pBlueNRPSkan, with an insertion in *rdpB* (at nt 3,151 of the 4,665 nt ORF) was selected and a 5-kb *Sph*I fragment containing the *rdpB*::*km* insertion was subcloned into the suicide vector pKR100 to create pKR100NRPSkan. This plasmid was conjugated from S17-1 λ *pir* into *X. nematophila* HGB007. A kanamycin resistant, chloramphenicol-sensitive candidate was confirmed as an *rdpB::km* mutant by Southern and PCR analysis.

For the construction of the XNC1_2233 deletion mutant, fragments up- (517 bp) and downstream (732 bp) of the gene region encoding XNC1_2233 were amplified with primers DelXn2564_up-F_SphI, DelXn2564_up-R and DelXn2564_down-F, DelXn2564_down-R_SacI, fused together in an additional amplification step via complementary DNA regions and cloned into pDS132 via the *Sph*I and *Sac*I restriction site. Transformation into *E. coli* S17-1 λ *pir*, conjugation into HGB081 and counter selection via *sacB* was performed as described previously,[10] yielding the ΔXNC1_2233 mutant with an in-frame deletion of 4122 bp. The genotype of the mutant was confirmed by PCR using primers for the verification listed in Table S5 lying outside the amplified region.

Phenotypic analysis of mutants. To analyze the relative produced amounts of **1** - **6** in the wild type strain HGB081 and in the mutant strains *rdpA*::*pDS132*, ΔXNC1_2233, all strains were cultivated at a rotary shaker at 30 °C and 200 rpm in duplicates in Erlenmeyer flasks (50 mL) containing LB medium (5 mL) with Amberlite XAD-16 (2%, v/v, Sigma-Aldrich) each and antibiotic, respectively. The cultures were inoculated with an overnight preculture up to an OD_{600} of 0.1. XAD beads were harvested after 77 h of cultivation, separated by sieving and extracted with MeOH (5 mL). These extracts were diluted 1:1 with MeOH and analyzed in positive ionization mode by ESI HPLC MS with a rate of three injections per sample to minimize the error rate of the machine.

Various phenotypes of the *rdpB::km* mutant were compared to the wild type parent strain HGB007. To monitor virulence in *M. sexta* overnight cultures of bacteria inoculated from -80˚C glycerol stocks were subcultured 1:100 into fresh LB broth then incubated for 24 h shaking at 30˚. Cells were pelleted, washed and diluted in sterile PBS. Approximately 15 min before injection, individual fourth-instar insect larvae were incubated on ice. For each of 10 insects per treatment per experiment, 10 µl of the diluted culture was injected into the first proleg using a 30-gauge syringe (Hamilton, Reno, NV).[11] Insects were monitored for 72 h post injection. Dilution plating of bacterial cultures was used to determine the cfu that had been injected into each insect (generally 1000-5000).

Control insects injected with PBS alone did not die within the 72 h assay period (data not shown).

To monitor pigment production, cultures of HGB007 wild type and *rdpB::km* mutant cells were each pelleted after 48 h of growth at 30˚C in LB. Supernatants were transferred to a new tube and 2X volume of acetone was added. After mixing and pelleting the supernatant was transferred to a new tube and the process was repeated. The acetone was evaporated and the resulting pellet was resuspended in 10 µl H_2O, of which 5 µl, in 1 µl aliquots, were spotted onto a Silica Gel 150 Å thin layer chromatography plate, with drying in between applications. The plate was placed in water, and after migration pigment was visible with the naked eye.

To measure oral toxicity of *X. nematophila* supernatants, cultures were grown for 72 h in LB at 30˚C, pelleted and passed through a 0.2 micron filter (Millipore). For each strain a 100 kDa Centricon filter was used to concentrate the supernatant 10-15 fold. Fifty microliters of each concentrate were spotted onto a 1-cm piece of insect diet, and LB was used as a negative control. One 2nd instar larva was placed onto each cube of food, with 5 cubes per treatment. Insects were monitored for 72 h for signs of growth and development. Insects reared on *Xenorhabdus* treatments (wild type or the *rdpB::km* mutant) did not develop, while those on the LB control did.

To observe siderophore production, bacterial cultures were spotted onto CAS agar plates supplemented with 0.2% glucose and 0.5% casamino acids. After 2 d incubation at 30˚C the size of the orange halo surrounding the bacterial colony was measured.

For growth curves, hemolymph was extracted from *M. sexta* insects as described previously.[9] Other phenotypes shown in Table S3 were assayed as previously described.[12]

Structure elucidation by feeding experiments and MS experiments. Structure elucidation of compounds **1 - 6** was done by using a method combining feeding and inverse feeding experiments following detailed ESI HPLC MS and HR MS analysis as already described previously in detail by our group.[13,14] For structure elucidation, feeding experiments with L-[methyl-D_3]methionine, L-[2,3,4,4,4,5,5,5-D_8]valine, L-[2,3,3,4,5,5,5,6,6,6-D_{10}]leucine and L-[2,3,3,5,6,7,8,9-D_8]phenylalanine to LB medium and for an inverse feeding approach with L-leucine, L-valine, L-phenylalanine and L-phenylethylamine (PEA) to *X. nematophila* cultivated in [U-^{13}C]medium were performed. Cultures were inoculated with 0.1 % (v/v) of a preculture grown overnight in LB medium, washed twice with the final cultivation medium and grown at 30 °C and 180 rpm in Erlenmeyer flasks containing ISOGRO-^{13}C (5 mL, Sigma-Aldrich) or ISOGRO-^{15}N medium containing K_2HPO_4 (10 mM), KH_2PO_4 (10 mM), $MgSO_4 \cdot 7H_2O$ (8 mM) and $CaCl_2 \cdot H_2O$ (90 µM) or LB medium, respectively. All possible precursors were added at 4, 24 and 48 h after inoculation in equal portions to a final concentration of 3 mM. All cultures were harvested after 72 h of cultivation, metabolites were extracted with ethyl acetate (5 mL) and evaporated to dryness, redissolved in MeOH (1 mL) and diluted 1:10 for detailed ESI HPLC MS and HR MS analysis. The structures of the linear peptides were elucidated by analysis of the MS^2 fragmentation patterns in positive ionization mode $[M+H]^+$ and

the identified mass shifts resulting from incorporation of the amino acids as structure building blocks. All fragmentation pathways were confirmed with additional MS^n experiments to differentiate between fragments resulting from the fragmentation of the peptide backbone and fragments resulting from splitting off additional functional groups or "wrong" fragmentation pathways. Sum formula of the compounds and as well of the identified fragments were verified by HR MS analysis.

Phenotypic analysis. ESI HPLC MS and MS^n analysis were performed with a Dionex UltiMate 3000 system coupled to a Bruker AmaZon X mass spectrometer and an Acquity UPLC BEH C18 1.7 µm RP column (Waters). Metabolites were eluted using a MeCN/0.1 % formic acid in H_20 gradient ranging from 5 to 95 % MeCN in 22 min with a flowrate of 0.6 mL min^{-1} (MS: positive ionization mode between 100-1200 m/z). Fragmentation of compounds of interest was performed using a manual isolation and fragmentation mode. High-resolution MS were recorded on a Thermo LTQ Orbitrap Hybrid FT mass spectrometer and a X-Bridge C18/1.7 µm RP column (Waters) using a similar gradient in 20 min at a flow rate of 0.4 mL min^{-1}.

Insect in vivo system. To study the production of **1 - 6** in an *in vivo* system, *X. nematophila* was injected into *G. mellonella* insect larvae. *X. nematophila* HGB081 was cultivated over night in LB medium (30 °C, 180rpm) at a rotary shaker and diluted to an optical density (OD_{600}) of 1.0 in fresh LB medium. Prior to injection, *G. mellonella* insect larvae were kept on ice. Ten larvae for every time point of analysis were treated with diluted bacteria culture (5 µL) by injection of the bacteria into the first proleg of each insect. All larvae were held at room temperature up to 14 days post-infection. Sets of 10 larvae were taken out for analysis after 6, 24, 36 and 48 h, as well after 3, 4, 7, 10 and 14 d post-infection, frozen in liquid nitrogen and stored up to 14 d at -80 °C. For analysis, sets of larvae were pulverized under the usage of liquid nitrogen and cells were extracted with MeOH and acetone (1:1 v/v, 50 mL) for one hour at room temperature. Extracts were concentrated to dryness on a rotary evaporator, redissolved in MeOH (3 mL) and diluted 1:10 for ESI HPLC MS analysis with a rate of three injections per sample to minimize the error rate of the machine.

Biological activity testing. Bioactivity against the protozoan parasites *P. falciparum* NF54, *T. cruzi* Tulahuen C4, *T. b. rhodesiense* STIB900 and against rat skeletal myoblasts (L-6 cells) for cytotoxicity assessment was determined as previously described.[15]

Synthesis of N-methyl-L-valine-N-methyl-L-leucine-N-methyl-L-valine-N-methyl-L-valine–phenyl-ethylamine. The assembly of the peptide sequence and the cleavage of the fully protected peptide fragment were conducted following standard protocols. Then the peptide was permethylated with 10.0 eq iodomethane and 6.3 eq sodium hydride in a mixture of 0.4 mL/mmol tetrahydrofuran and 0.2 mL/mmol *N,N*-dimethylformamide at 0°C while stirring and warmed to room temperature within

18h**.** The reaction's progress was monitored using thin layer chromatography (0.2 mm silica gel with fluorescent indicator pre-coated polyester sheets; eluent: 90% chloroform, 10% methanol). After completion of the reaction the solvents were removed under reduced pressure. The residue was dissolved in water, washed with n-hexane, acidified to pH 1 with 1 M hydrochloric acid, diluted with satured brine and extracted with ethyl acetate. The organic phases were combined, dried with Na_2SO_4 and the solvents removed under reduced pressure. This was followed by an ester saponification with lithium hydroxide solution (6.0 eq, 0.4 M in water) in a mixture of 5 mL/mmol methanol and 15 mL/mmol tetrahydrofuran. After completion of the reaction the reaction mixture was dissolved with saturated $NaHCO_3$ and extracted with diethyl ether. The organic phases were combined, dried with Na_2SO_4 and the solvents removed under reduced pressure. 1.1 eq of phenylethylamine was dissolved in 10 mL/mmol dry dichloromethane and cooled to -10°C, then 1.1 eq 2-Bromo-1-ethyl-pyridinium tetrafluoroborate and 3.2 eq *N*,*N*-diisopropylethylamine together with 1.0 eq of the prior permethylated peptide**.** The reaction mixture was stirred at -10°C for 30 min and then slowly warmed to room temperature within 18 h. The reaction's progress was monitored using thin layer chromatography (0.2 mm silica gel with fluorescent indicator pre-coated polyester sheets; eluent: 90% chloroform, 10% methanol). Then the organic solvent was removed under reduced pressure and the *N*-terminal protecting group cleaved according to standard protocol, followed by a HPLC-ESI-MS purification.

Bioinformatic analysis and biosynthetic gene cluster annotation. Identification of possible candidates of biosynthetic gene clusters responsible for the production of the NRPS derived xenortides and rhabdopeptides was done by *in silico* analysis of all identified NRPS biosynthetic gene clusters in *X. nematophila* ATCC 19061.[6] Verification of involvement of these gene clusters in the production was done by construction of insertion and deletion mutants. Biosynthetic gene clusters were analyzed as described previously,[16] following a frame plot 4.0beta analysis[17] and the PKS/NRPS analysis website (http://nrps.igs.umaryland.edu/nrps/).[18] For the analysis of all NRPS domains, sequence alignments were constructed using ClustalW[19] and all conserved and catalytic residues were characterized as described in literature.[16,20,21] Amino acid specificity of adenylation domains were predicted on the basis of the 10 amino acid code using the NRPSpredictor2.[22]

Table S1. Structure elucidation of rhabdopeptides 1 - 6 (**1** – **6**) resulting from feeding experiments in HGB081 following ESI and HR MS^n fragmentation analysis**.** The structures of **1** - **6** are listed resulting from the identified b-fragmentation ion s. Structure elucidation is started at the *C*-terminal amine. The *N*-terminal residues of **5** and **6** which could not be detected in this study could be concluded from **1**, **3** and **2**, **4** respectively. MeVal (*N*-methylvaline), MeLeu (*N*-methylleucine), PEA (phenylethylamine), n.d. (not detected), det. (detected), calc. (calculated). [a] fragmentation ions detected in ESI MS only.

Rhabdopeptide 1 (1)	**MeLeu – MeVal – Val – MeVal – PEA**			**MeLeu – MeVal – Val – MeVal**		
labeling experiment	**m/z det. (calc.) $[M+H]^+$**	**Sum formula $[H]^+$**	**Δppm**	**m/z det. (calc.) $[M+H]^+$**	**Sum formula $[H]^+$**	**Δppm**
^{12}C	574.4313 (574.4327)	$C_{32}H_{56}N_5O_4$	2.458	453.3423 (453.3435)	$C_{24}H_{45}N_4O_4$	2.608
^{12}C + methyl-$^2H_3$-met	583.4885 (583.4892)	$C_{32}{}^2H_9H_{47}N_5O_4$	1.101	462.3[a]	$C_{24}{}^2H_9H_{36}N_4O_4$	
^{12}C + -$^2H_{10}$-leu	583.5[a]	$C_{32}{}^2H_9H_{47}N_5O_4$		462.4[a]	$C_{24}{}^2H_9H_{36}N_4O_4$	
^{13}C	606.5389 (606.5400)	$^{13}C_{32}H_{56}N_5O_4$	1.806	477.3[a]	$^{13}C_{24}H_{45}N_4O_4$	
^{13}C + leu	600.5192 (600.5199)	$C_6{}^{13}C_{26}H_{56}N_5O_4$	1.126	471.4016 (471.4039)	$C_6{}^{13}C_{18}H_{45}N_4O_4$	4.898
^{13}C + val	591.4898 (591.4897)	$C_{15}{}^{13}C_{17}H_{56}N_5O_4$	0.164	462.3713 (462.3737)	$C_{15}{}^{13}C_9H_{45}N_4O_4$	5.159
^{13}C + phe	598.5129 (598.5132)	$C_8{}^{13}C_{24}H_{56}N_5O_4$	0.529	477.3[a]	$^{13}C_{24}H_{45}N_4O_4$	
	MeLeu – MeVal – Val			**MeLeu – MeVal**		
^{12}C	340.2592 (340.2595)	$C_{18}H_{34}N_3O_3$	0.906	241.2[a]	$C_{13}H_{25}N_2O_2$	
^{12}C + methyl-$^2H_3$-met	346.2[a]	$C_{18}{}^2H_6H_{28}N_3O_3$		247.2[a]	$C_{13}{}^2H_6H_{19}N_2O_2$	
^{12}C + -$^2H_{10}$-leu	349.3[a]	$C_{18}{}^2H_9H_{25}N_3O_3$		250.1[a]	$C_{13}{}^2H_9H_{16}N_2O_2$	
^{13}C	358.3[a]	$^{13}C_{18}H_{34}N_3O_3$		254.2[a]	$^{13}C_{13}H_{25}N_2O_2$	
^{13}C + leu	352.2982 (352.2997)	$C_6{}^{13}C_{12}H_{34}N_3O_3$	4.332	248.2[a]	$C_6{}^{13}C_7H_{25}N_2O_2$	
^{13}C + val	348.2848 (348.2863)	$C_{10}{}^{13}C_8H_{34}N_3O_3$	4.355	249.2293 (249.2179)	$C_5{}^{13}C_8H_{25}N_2O_2$	45.689
^{13}C + phe	358.3[a]	$^{13}C_{18}H_{34}N_3O_3$		n.d.	$^{13}C_{13}H_{25}N_2O_2$	
	MeLeu					
^{12}C	128.2[a]	$C_7H_{14}NO$				
^{12}C + methyl-$^2H_3$-met	131.2[a]	$C_7{}^2H_3H_{11}NO$				
^{12}C + -$^2H_{10}$-leu	137.2[a]	$C_7{}^2H_9H_5NO$				
^{13}C	135.2[a]	$^{13}C_7H_{14}NO$				
^{13}C + leu	129.1[a]	$C_6{}^{13}C_1H_{14}NO$				
^{13}C + val	n.d.	$^{13}C_7H_{14}NO$				
^{13}C + phe	n.d.	$^{13}C_7H_{14}NO$				

Rhabdopeptide 2 (2)	MeVal – MeLeu – MeVal – MeVal – PEA			MeVal – MeLeu – MeVal – MeVal		
labeling experiment	m/z det. (calc.) $[M+H]^+$	Sum formula $[H]^+$	Δppm	m/z det. (calc.) $[M+H]^+$	Sum formula $[H]^+$	Δppm
^{12}C	588.4469 (588.4483)	$C_{33}H_{58}N_5O_4$	2.433	467.3587 (467.3592)	$C_{25}H_{47}N_4O_4$	0.968
^{12}C + methyl-$^2H_3$-met	600.5228 (600.5237)	$C_{33}{}^2H_{12}H_{46}N_5O_4$	1.370	479.5[a]	$C_{25}{}^2H_{12}H_{35}N_4O_4$	
^{12}C + -$^2H_{10}$-leu	597.5[a]	$C_{33}{}^2H_9H_{49}N_5O_4$		476.5[a]	$C_{25}{}^2H_9H_{38}N_4O_4$	
^{13}C	621.5598 (621.5590)	$^{13}C_{33}H_{58}N_5O_4$	0.129	492.4294 (492.4431)	$^{13}C_{25}H_{47}N_4O_4$	27.765
^{13}C + leu	615.5385 (615.5389)	$C_6{}^{13}C_{27}H_{58}N_5O_4$	0.749	486.4213 (486.4229)	$C_6{}^{13}C_{19}H_{47}N_4O_4$	3.276
^{13}C + val	606.5077 (606.5087)	$C_{15}{}^{13}C_{18}H_{58}N_5O_4$	1.695	477.3925 (477.3927)	$C_{15}{}^{13}C_{10}H_{47}N_4O_4$	0.483
^{13}C + phe	613.5314 (613.5322)	$C_8{}^{13}C_{25}H_{58}N_5O_4$	1.258	492.3[a]	$^{13}C_{25}H_{47}N_4O_4$	
	MeVal – MeLeu – MeVal			**MeVal – MeLeu**		
^{12}C	354.2744 (354.2751)	$C_{19}H_{36}N_3O_3$	2.169	241.1907 (241.1911)	$C_{13}H_{25}N_2O_2$	0.305
^{12}C + methyl-$^2H_3$-met	363.4[a]	$C_{19}{}^2H_9H_{27}N_3O_3$		247.2[a]	$C_{13}{}^2H_6H_{19}N_2O_2$	
^{12}C + -$^2H_{10}$-leu	363.4[a]	$C_{19}{}^2H_9H_{27}N_3O_3$		250.3[a]	$C_{13}{}^2H_9H_{16}N_2O_2$	
^{13}C	373.3285 (373.3389)	$^{13}C_{19}H_{36}N_3O_3$	27.776	254.1[a]	$^{13}C_{13}H_{25}N_2O_2$	
^{13}C + leu	367.3177 (367.3187)	$C_6{}^{13}C_{13}H_{36}N_3O_3$	2.915	248.2136 (248.2145)	$C_6{}^{13}C_7H_{25}N_2O_2$	3.780
^{13}C + val	363.3054 (363.3053)	$C_{10}{}^{13}C_9H_{36}N_3O_3$	0.133	249.2180 (249.2179)	$C_5{}^{13}C_8H_{25}N_2O_2$	0.389
^{13}C + phe	373.2[a]	$^{13}C_{19}H_{36}N_3O_3$		254.1[a]	$^{13}C_{13}H_{25}N_2O_2$	
	MeVal					
^{12}C	114.0908 (114.0913)	$C_6H_{12}NO$	4.913			
^{12}C + methyl-$^2H_3$-met	117.1[a]	$C_6{}^2H_3H_9NO$				
^{12}C + -$^2H_{10}$-leu	114.1[a]	$C_6H_{12}NO$				
^{13}C	120.2[a]	$^{13}C_6H_{12}NO$				
^{13}C + leu	n.d.	$^{13}C_6H_{12}NO$				
^{13}C + val	n.d.	$C_5{}^{13}C_1H_{12}NO$				
^{13}C + phe	n.d.	$^{13}C_6H_{12}NO$				

Rhabdopeptide 3 (3)	MeLeu – MeVal – Val – MeVal – MeVal – PEA			MeLeu – MeVal – Val – MeVal – MeVal		
labeling experiment	m/z det. (calc.) $[M+H]^+$	Sum formula $[H]^+$	Δppm	m/z det. (calc.) $[M+H]^+$	Sum formula $[H]^+$	Δppm
^{12}C	687.5158 (687.5167)	$C_{38}H_{67}N_6O_5$	1.361	566.4265 (566.4276)	$C_{30}H_{56}N_5O_5$	1.918
^{12}C + methyl-$^2H_3$-met	699.5911 (699.5921)	$C_{38}{}^2H_{12}H_{55}N_6O_5$	1.439	578.5[a]	$C_{30}{}^2H_{12}H_{44}N_5O_5$	
^{12}C + -$^2H_{10}$-leu	696.6[a]	$C_{38}{}^2H_9H_{58}N_6O_5$		575.5[a]	$C_{30}{}^2H_9H_{47}N_5O_5$	
^{13}C	725.6445 (725.6442)	$^{13}C_{38}H_{67}N_6O_5$	0.416	596.5263 (592.5282)	$^{13}C_{30}H_{56}N_5O_5$	3.253
^{13}C + leu	719.6234 (719.6241)	$C_6{}^{13}C_{32}H_{67}N_6O_5$	0.958	590.5064 (590.5081)	$C_6{}^{13}C_{12}H_{56}N_5O_5$	2.932
^{13}C + val	705.5762 (705.5771)	$C_{20}{}^{13}C_{18}H_{67}N_6O_5$	1.378	576.4586 (576.4611)	$C_{20}{}^{13}C_{10}H_{56}N_5O_5$	4.275
^{13}C + phe	717.6168 (717.6174)	$C_8{}^{13}C_{30}H_{67}N_6O_5$	0.877	596.4[a]	$^{13}C_{30}H_{56}N_5O_5$	
	MeLeu – MeVal – Val – MeVal			**MeLeu – MeVal – Val**		
^{12}C	453.3428 (453.3435)	$C_{24}H_{45}N_4O_4$	1.682	340.2593 (340.2595)	$C_{18}H_{34}N_3O_3$	0.554
^{12}C + methyl-$^2H_3$-met	462.5[a]	$C_{24}{}^2H_9H_{36}N_4O_4$		346.4[a]	$C_{18}{}^2H_6H_{28}N_3O_3$	
^{12}C + -$^2H_{10}$-leu	462.3[a]	$C_{24}{}^2H_9H_{36}N_4O_4$		349.3[a]	$C_{18}{}^2H_9H_{25}N_3O_3$	
^{13}C	477.4229 (477.4240)	$^{13}C_{24}H_{45}N_4O_4$	2.342	358.3191 (358.3199)	$^{13}C_{18}H_{34}N_3O_3$	1.995
^{13}C + leu	471.4026 (471.4039)	$C_6{}^{13}C_{18}H_{45}N_4O_4$	2.776	352.2990 (352.2997)	$C_6{}^{13}C_{12}H_{34}N_3O_3$	1.976
^{13}C + val	462.3716 (462.3737)	$C_{15}{}^{13}C_9H_{45}N_4O_4$	4.446	348.2849 (348.2863)	$C_{10}{}^{13}C_8H_{34}N_3O_3$	3.838
^{13}C + phe	477.4[a]	$^{13}C_{24}H_{45}N_4O_4$		358.3[a]	$^{13}C_{18}H_{34}N_3O_3$	
	MeLeu – MeVal			**MeLeu**		
^{12}C	241.2[a]	$C_{13}H_{25}N_2O_2$		128.1[a]	$C_7H_{14}NO$	
^{12}C + methyl-$^2H_3$-met	247.1[a]	$C_{13}{}^2H_6H_{19}N_2O_2$		n.d.	$C_7{}^2H_3H_{11}NO$	
^{12}C + -$^2H_{10}$-leu	n.d.	$C_{13}{}^2H_9H_{16}N_2O_2$		n.d.	$C_6H_{12}NO$	
^{13}C	254.3[a]	$^{13}C_{13}H_{25}N_2O_2$		135.2[a]	$^{13}C_7H_{14}NO$	
^{13}C + leu	248.2[a]	$C_6{}^{13}C_7H_{25}N_2O_2$		n.d.	$C_6{}^{13}C_1H_{14}NO$	
^{13}C + val	n.d.	$C_5{}^{13}C_8H_{25}N_2O_2$		n.d.	$^{13}C_7H_{14}NO$	
^{13}C + phe	n.d.	$^{13}C_{13}H_{25}N_2O_2$		n.d.	$^{13}C_7H_{14}NO$	

Rhabdopeptide 4 (4)	**MeVal – MeLeu – MeVal – MeVal – MeVal – PEA**			**MeVal – MeLeu – MeVal – MeVal – MeVal**		
labeling experiment	**m/z det. (calc.) $[M+H]^+$**	**Sum formula $[H]^+$**	**Δppm**	**m/z det. (calc.) $[M+H]^+$**	**Sum formula $[H]^+$**	**Δppm**
^{12}C	701.5312 (701.5324)	$C_{39}H_{69}N_6O_5$	1.719	580.4426 (580.4432)	$C_{31}H_{58}N_5O_5$	1.165
^{12}C + methyl-$^2H_3$-met	716.5254 (716.6265)	$C_{39}{}^2H_{15}H_{54}N_6O_5$	1.559	595.6[a]	$C_{31}{}^2H_{15}H_{43}N_5O_5$	
^{12}C + -$^2H_{10}$-leu	710.5[a]	$C_{39}{}^2H_9H_{60}N_6O_5$		589.5[a]	$C_{31}{}^2H_9H_{49}N_5O_5$	
^{13}C	740.6625 (740.6632)	$^{13}C_{39}H_{69}N_6O_5$	1.016	611.4[a]	$^{13}C_{31}H_{58}N_5O_5$	
^{13}C + leu	734.6417 (734.6431)	$C_6{}^{13}C_{33}H_{69}N_6O_5$	1.884	605.5250 (605.5271)	$C_6{}^{13}C_{25}H_{58}N_5O_5$	3.528
^{13}C + val	720.5955 (720.5961)	$C_{20}{}^{13}C_{19}H_{69}N_6O_5$	0.953	591.4774 (591.4801)	$C_{20}{}^{13}C_{11}H_{58}N_5O_5$	4.597
^{13}C + phe	732.6361 (732.6361)	$C_8{}^{13}C_{31}H_{69}N_6O_5$	0.388	611.3[a]	$^{13}C_{31}H_{58}N_5O_5$	
	MeVal – MeLeu – MeVal – MeVal			**MeVal – MeLeu – MeVal**		
^{12}C	467.3586 (467.3592)	$C_{25}H_{47}N_4O_4$	1.310	354.2744 (354.2751)	$C_{19}H_{36}N_3O_3$	1.915
^{12}C + methyl-$^2H_3$-met	479.5[a]	$C_{25}{}^2H_{12}H_{35}N_4O_4$		363.4[a]	$C_{19}{}^2H_9H_{27}N_3O_3$	
^{12}C + -$^2H_{10}$-leu	476.5[a]	$C_{25}{}^2H_9H_{38}N_4O_4$		363.4[a]	$C_{19}{}^2H_9H_{27}N_3O_3$	
^{13}C	492.4501 (492.4431)	$^{13}C_{25}H_{47}N_4O_4$	14.372	373.2303 (373.3389)	$^{13}C_{19}H_{36}N_3O_3$	27.166
^{13}C + leu	486.4211 (486.4229)	$C_6{}^{13}C_{19}H_{47}N_4O_4$	3.667	367.3175 (367.3187)	$C_6{}^{13}C_{13}H_{36}N_3O_3$	3.324
^{13}C + val	477.3905 (477.3927)	$C_{15}{}^{13}C_{10}H_{47}N_4O_4$	4.693	363.3038 (363.3053)	$C_{10}{}^{13}C_9H_{36}N_3O_3$	4.216
^{13}C + phe	492.3[a]	$^{13}C_{25}H_{47}N_4O_4$		373.2[a]	$^{13}C_{19}H_{36}N_3O_3$	
	MeVal – MeLeu			**MeVal**		
^{12}C	241.1908 (241.1911)	$C_{13}H_{25}N_2O_2$	0.931	114.0908 (114.0913)	$C_6H_{12}NO$	5.089
^{12}C + methyl-$^2H_3$-met	247.0[a]	$C_{13}{}^2H_6H_{19}N_2O_2$		n.d.	$C_6{}^2H_3H_9NO$	
^{12}C + -$^2H_{10}$-leu	250.2[a]	$C_{13}{}^2H_9H_{16}N_2O_2$		n.d.	$C_6H_{12}NO$	
^{13}C	254.1[a]	$^{13}C_{13}H_{25}N_2O_2$		120.2[a]	$^{13}C_6H_{12}NO$	
^{13}C + leu	248.2137 (248.2145)	$C_6{}^{13}C_7H_{25}N_2O_2$	3.377	n.d.	$^{13}C_6H_{12}NO$	
^{13}C + val	249.2168 (249.2179)	$C_5{}^{13}C_8H_{25}N_2O_2$	4.426	n.d.	$C_5{}^{13}C_1H_{12}NO$	
^{13}C + phe	254.2[a]	$^{13}C_{13}H_{25}N_2O_2$		n.d.	$^{13}C_6H_{12}NO$	

Rhabdopeptide 5 (5)	**MeLeu – MeVal – Val – MeVal – MeVal – MeVal – PEA**			**MeLeu – MeVal – Val – MeVal – MeVal – MeVal**		
labeling experiment	**m/z det. (calc.) $[M+H]^+$**	**Sum formula $[H]^+$**	**Δppm**	**m/z det. (calc.) $[M+H]^+$**	**Sum formula $[H]^+$**	**Δppm**
^{12}C	800.6018 (800.6008)	$C_{44}H_{78}N_7O_6$	1.250	679.5119 (679.5117)	$C_{36}H_{67}N_6O_6$	0.353
^{12}C + methyl-$^{2}H_3$-met	815.6959 (815.6950)	$C_{44}{}^{2}H_{15}H_{63}N_7O_6$	0.747	694.6030 (694.6058)	$C_{36}{}^{2}H_{15}H_{52}N_6O_6$	4.004
^{12}C + -$^{2}H_{10}$-leu	844.7502 (844.7484)	$^{13}C_{44}H_{78}N_7O_6$	2.083	715.6325 (715.6324)	$^{13}C_{36}H_{67}N_6O_6$	0.108
^{13}C	838.7292 (838.7283)	$C_6{}^{13}C_{38}H_{78}N_7O_6$	1.071	709.6118 (709.6123)	$C_6{}^{13}C_{30}H_{67}N_6O_6$	0.654
^{13}C + leu	819.6652 (819.6646)	$C_{25}{}^{13}C_{19}H_{78}N_7O_6$	0.817	690.5425 (690.5486)	$C_{25}{}^{13}C_{11}H_{67}N_6O_6$	8.809
^{13}C + val	836.7209 (836.7216)	$C_8{}^{13}C_{36}H_{78}N_7O_6$	0.756	715.6322 (715.6323)	$C_8{}^{13}C_{28}H_{67}N_6O_6$	0.256
^{13}C + PEA	800.6018 (800.6008)	$C_{44}H_{78}N_7O_6$	1.250	679.5119 (679.5117)	$C_{36}H_{67}N_6O_6$	0.353
	MeLeu – MeVal – Val – MeVal – MeVal			**MeLeu – MeVal – Val – MeVal**		
^{12}C	566.4276(566.4276)	$C_{30}H_{56}N_5O_5$	0.082	453.3436 (453.3435)	$C_{24}H_{45}N_4O_4$	0.215
^{12}C + methyl-$^{2}H_3$-met	578.5043 (578.5029)	$C_{30}{}^{2}H_{12}H_{44}N_5O_5$	2.442	462.3998 (462.4000)	$C_{24}{}^{2}H_9H_{36}N_4O_4$	0.461
^{12}C + -$^{2}H_{10}$-leu	596.5283 (592.5282)	$^{13}C_{30}H_{56}N_5O_5$	0.150	477.4236 (477.4240)	$^{13}C_{24}H_{45}N_4O_4$	1.021
^{13}C	590.5083 (590.5081)	$C_6{}^{13}C_{12}H_{56}N_5O_5$	0.370	471.4038 (471.4039)	$C_6{}^{13}C_{18}H_{45}N_4O_4$	0.252
^{13}C + leu	576.4614(576.4611)	$C_{20}{}^{13}C_{10}H_{56}N_5O_5$	0.496	462.3735 (462.3737)	$C_{15}{}^{13}C_9H_{45}N_4O_4$	0.401
^{13}C + val	596.5283 (596.5282)	$^{13}C_{30}H_{56}N_5O_5$	0.134	477.4240 (477.4240)	$^{13}C_{24}H_{45}N_4O_4$	0.016
^{13}C + PEA	566.4276(566.4276)	$C_{30}H_{56}N_5O_5$	0.082	453.3436 (453.3435)	$C_{24}H_{45}N_4O_4$	0.215
	MeLeu – MeVal – Val			**MeLeu – MeVal**		
^{12}C	340.2595 (340.2595)	$C_{18}H_{34}N_3O_3$	0.152	n.d.	$C_{13}H_{25}N_2O_2$	
^{12}C + methyl-$^{2}H_3$-met	346.2994 (346.2971)	$C_{18}{}^{2}H_6H_{28}N_3O_3$	6.500	n.d.	$C_{13}{}^{2}H_6H_{19}N_2O_2$	
^{12}C + -$^{2}H_{10}$-leu	358.3198 (358.3199)	$^{13}C_{18}H_{34}N_3O_3$	0.181	n.d.	$^{13}C_{13}H_{25}N_2O_2$	
^{13}C	352.2998 (352.2997)	$C_6{}^{13}C_{12}H_{34}N_3O_3$	0.068	n.d.	$C_6{}^{13}C_7H_{25}N_2O_2$	
^{13}C + leu	348.2854 (348.2863)	$C_{10}{}^{13}C_8H_{34}N_3O_3$	2.604	n.d.	$C_5{}^{13}C_8H_{25}N_2O_2$	
^{13}C + val	358.3198 (358.3199)	$^{13}C_{18}H_{34}N_3O_3$	0.796	n.d.	$^{13}C_{13}H_{25}N_2O_2$	
^{13}C + PEA	340.2595 (340.2595)	$C_{18}H_{34}N_3O_3$	0.152	n.d.	$C_{13}H_{25}N_2O_2$	
	MeLeu					
^{12}C	n.d.	$C_7H_{14}NO$				
^{12}C + methyl-$^{2}H_3$-met	n.d.	$C_7{}^{2}H_3H_{11}NO$				
^{12}C + -$^{2}H_{10}$-leu	n.d.	$^{13}C_7H_{14}NO$				
^{13}C	n.d.	$C_6{}^{13}C_1H_{14}NO$				
^{13}C + leu	n.d.	$^{13}C_7H_{14}NO$				
^{13}C + val	n.d.	$^{13}C_7H_{14}NO$				
^{13}C + PEA	n.d.	$C_7H_{14}NO$				

Rhabdopeptide 6 (6)	**MeVal – MeLeu – MeVal – MeVal – MeVal – MeVal – PEA**			**MeVal – MeLeu – MeVal – MeVal – MeVal – MeVal**		
labeling experiment	**m/z det. (calc.) $[M+H]^+$**	**Sum formula $[H]^+$**	**Δppm**	**m/z det. (calc.) $[M+H]^+$**	**Sum formula $[H]^+$**	**Δppm**
^{12}C	814.6166 (814.6165)	$C_{45}H_{80}N_7O_6$	0.221	693.5271 (693.5273)	$C_{37}H_{69}N_6O_6$	0.303
^{12}C + methyl-$^{2}H_3$-met	832.7310 (832.7294)	$C_{45}{}^{2}H_{18}H_{62}N_7O_6$	1.896	711.6396 (711.6396)	$C_{37}{}^{2}H_{18}H_{51}N_6O_6$	0.930
^{12}C + -$^{2}H_{10}$-leu	859.7688 (859.7674)	$^{13}C_{45}H_{80}N_7O_6$	1.308	730.6506 (730.6514)	$^{13}C_{37}H_{69}N_6O_6$	1.147
^{13}C	853.7482 (853.7473)	$C_6{}^{13}C_{39}H_{80}N_7O_6$	1.023	724.6315 (724.6313)	$C_6{}^{13}C_{31}H_{69}N_6O_6$	0.222
^{13}C + leu	834.6841 (834.6836)	$C_{25}{}^{13}C_{30}H_{80}N_7O_6$	0.628	705.5690 (705.5676)	$C_{25}{}^{13}C_{12}H_{69}N_6O_6$	1.973
^{13}C + val	851.7419 (851.7406)	$C_8{}^{13}C_{37}H_{80}N_7O_6$	1.518	730.6515 (730.6514)	$^{13}C_{37}H_{69}N_6O_6$	0.030
^{13}C + PEA	814.6166 (814.6165)	$C_{45}H_{80}N_7O_6$	0.221	693.5271 (693.5273)	$C_{37}H_{69}N_6O_6$	0.303
	MeVal – MeLeu – MeVal – MeVal – MeVal			**MeVal – MeLeu – MeVal – MeVal**		
^{12}C	580.4431 (580.4432)	$C_{31}H_{58}N_5O_5$	0.338	467.3591 (467.3592)	$C_{25}H_{47}N_4O_4$	0.112
^{12}C + methyl-$^{2}H_3$-met	595.5373 (595.5374)	$C_{31}{}^{2}H_{15}H_{43}N_5O_5$	0.231	479.4344 (479.4345)	$C_{25}{}^{2}H_{12}H_{35}N_4O_4$	0.278
^{12}C + -$^{2}H_{10}$-leu	611.5471 (611.5472)	$^{13}C_{31}H_{58}N_5O_5$	0.188	492.4430 (492.4431)	$^{13}C_{25}H_{47}N_4O_4$	0.188
^{13}C	605.5274 (605.5271)	$C_6{}^{13}C_{25}H_{58}N_5O_5$	0.419	486.4223 (486.4229)	$C_6{}^{13}C_{19}H_{47}N_4O_4$	1.344
^{13}C + leu	591.4791 (591.4801)	$C_{20}{}^{13}C_{11}H_{58}N_5O_5$	1.283	477.3931 (477.3927)	$C_{15}{}^{13}C_{10}H_{47}N_4O_4$	0.774
^{13}C + val	611.5471 (611.5972)	$^{13}C_{31}H_{58}N_5O_5$	0.188	492.4429 (492.4431)	$^{13}C_{25}H_{47}N_4O_4$	0.309
^{13}C + PEA	580.4431 (580.4432)	$C_{31}H_{58}N_5O_5$	0.338	467.3591 (467.3592)	$C_{25}H_{47}N_4O_4$	0.112
	MeVal – MeLeu – MeVal			**MeVal – MeLeu**		
^{12}C	354.2753 (354.2751)	$C_{19}H_{36}N_3O_3$	0.428	n.d.	$C_{13}H_{25}N_2O_2$	
^{12}C + methyl-$^{2}H_3$-met	363.3312 (363.3316)	$C_{19}{}^{2}H_9H_{27}N_3O_3$	1.099	n.d.	$C_{13}{}^{2}H_6H_{19}N_2O_2$	
^{12}C + -$^{2}H_{10}$-leu	373.3389 (373.3389)	$^{13}C_{19}H_{36}N_3O_3$	0.135	n.d.	$^{13}C_{13}H_{25}N_2O_2$	
^{13}C	367.3178 (367.3187)	$C_6{}^{13}C_{13}H_{36}N_3O_3$	2.589	n.d.	$C_6{}^{13}C_7H_{25}N_2O_2$	
^{13}C + leu	363.3058 (363.3053)	$C_{10}{}^{13}C_9H_{36}N_3O_3$	1.427	n.d.	$C_5{}^{13}C_8H_{25}N_2O_2$	
^{13}C + val	373.3392(373.3389)	$^{13}C_{19}H_{36}N_3O_3$	0.858	n.d.	$^{13}C_{13}H_{25}N_2O_2$	
^{13}C + PEA	354.2753 (354.2751)	$C_{19}H_{36}N_3O_3$	0.428	n.d.	$C_{13}H_{25}N_2O_2$	
	MeVal					
^{12}C	n.d.	$C_6H_{12}NO$				
^{12}C + methyl-$^{2}H_3$-met	n.d.	$C_6{}^{2}H_3H_9NO$				
^{12}C + -$^{2}H_{10}$-leu	n.d.	$^{13}C_6H_{12}NO$				
^{13}C	n.d.	$^{13}C_6H_{12}NO$				
^{13}C + leu	n.d.	$C_5{}^{13}C_1H_{12}NO$				
^{13}C + val	n.d.	$^{13}C_6H_{12}NO$				
^{13}C + PEA	n.d.	$C_6H_{12}NO$				

Table S2. Proteins of the *rdp* cluster and open reading frames adjacent to the *rdp* cluster in *X. nematophila* ATCC 19061, their proposed function, protein size and closest homologues.

Protein	Size [aa]	Proposed function	Closest homologue		
			Origin	Identities/ Positives [%]	Accession number
XNC1_2227	462	pyridine nucleotide transhydrogenase	*Xenorhabdus bovienii* SS-2004	91/96	YP_003468253
RdpA (XNC1_2228)	1560	NRPS Plu0898	*Photorhabdus luminescens* subsp. *laumondii* TT01	73/84	NP_928234
RdpB (XNC1_2229)	1554	NRPS Plu0898	*Photorhabdus luminescens* subsp. *laumondii* TT01	75/85	NP_928234
RdpC (XNC1_2230)	1998	NRPS Plu0899	*Photorhabdus luminescens* subsp. *laumondii* TT01	72/86	NP_928235
XNC1_2231	65	hypothetical protein XNC1_2298	*Xenorhabdus nematophila* ATCC 19061	94/95	YP_003712532
XNC1_2232	72	hypothetical protein XNC1_0736	*Xenorhabdus nematophila* ATCC 19061	94/96	YP_003711031
XNC1_2233	1403	NRPS Plu0897	*Photorhabdus luminescens* subsp. *laumondii* TT01	64/78	NP_928233
XNC1_2234	338	integrase/ recombinase	*Xenorhabdus bovienii* SS-2004	90/98	YP_003468252

Table S3. Phenotypes[a] of the *rdpB::km* mutant compared to the wild type.

phenotype	Wild type	*rdpB*::*km*
pathogenesis in *M. sexta*	+	+
nematode colonization	+	+
antibiotic production towards		
Bacillus subtilis	+	+
Micrococcus luteus	+	+
pigment production	+	+
oral toxicity towards insects	+	+
siderophore production	+	+
haemolytic activity against		
mammalian RBCs	+	+
insect hemocytes	+	+
protease production	+	+
lipase production	+	+
hemagglutination of RBCs	+	+
motility	+	+
dye binding activity	+	+
growth rate	+	+

[a] + indicates wild type levels of activity. RBCs indicate red blood cells. Sheep, rabbit, and horse erythrocytes were used for hemolytic assays while hemagglutination assays used sheep erythrocytes. Growth rates were determined during growth in both LB medium and *M. sexta* hemolymph.

Table S4. Plasmids and strains used.

Plasmid or strain	Genotype	Reference
Plasmids		
pDS132	*ori*R6K oriT *sacB* Cm^r	Philippe *et al.* (2004)[8]
pDS132-XNC1_2228	*ori*R6K oriT *sacB* Cm^r, with 537 bp genomic DNA fragment of XNC1_2228	This work
pDS132-ΔXNC1_2233	*ori*R6K oriT *sacB* Cm^r, with 517 bp and 732 bp genomic DNA fragments flanking up- and downstream XNC1_2233	This work
pGY2	*ori*R6K, Mob_1 Ap^r r.with *Sph*I (*trpA-lacZY*) fragment replaced with *Sph*I (*aadA*) fragment, Str_r	Young *et al.*(1996)[3]
pKJN102	pGY2 ΔAp^r	This work
pBluescript SK+	Amp^r; general cloning vector	Stratagene, La Jolla, CA
pKR100	Cm^r; *ori*R6K suicide vector (a derivative of pGP704 [pJM703.1]	K. Visick Loyola University[23]
pBlueNRPS	12.9 kb *Eco*RI genomic fragment from HGB007 cloned into pBluescript; Amp^r	This work
pBlueNRPSkan	GeneJumper kanamycin insertion into pBlueNRPS at nt 3,151 of the total 4,665 nt of XNC1_2229	This work
pKR100NRPSkan	*Sph*I fragment from pBlueNRPSkan cloned into pKR100	This work
Strains		
E. coli S17-1λ*pir*	Tp^r Str^r *recA thi hsdR* RP4-2-TC::Mu-Km::Tn*7*,λ*pir* phage lysogen	Simon *et al.* (1983)[24]
X. nematophila HGB007	*X. nematophila* ATCC 19061, wild type (Amp^r)	American Type Culture Collection
X. nematophila HGB081	Wild type, phase I variant, ATCC19061::Rif^r	Orchard and Goodrich-Blair (2004)[9]
X. nematophila D11	HGB081 with unmapped Cm^r Tn*10* transposon insertion	Templeton and Goodrich-Blair, unpublished data
X. nematophila rdpA::*cat*	HGB081 XNC1_2228::pDS132	This work
X. nematophila ΔXNC1_*2233*	HGB081 ΔXNC1_2233	This work
X. nematophila HGB640	HGB007 *rdpB::km*	This work

Table S5. Oligonucleotides used for the construction of mutants and their verification (v). Restriction sites are marked in bold, complementary sequences used for overlap extension PCR are in lower case.

Experiment	Oligonucleotide	(5'-3') Sequence
Mutant	Xn2576fw	ATGCGAGCTCTTATCGAACGTACCGCGCCT
XNC1_2228	Xn2576rv	TATGCGCATGCCATTCGGTAGCGGTTTGCCT
	v2576f	CAGATAGTTTTTACGCTGGAGA
	v2576r	GACTATAAGCAATCACCGCC
Mutant	DelXn2564_up-F_SphI	ATGCAGCATGCTCTCCTTAACAATCGGCCAAAGA
XNC1_2233	DelXn2564_up-R	tggatgctctcttttcctgtccTAGCGTAATGCCATATTCCAAAGC
	DelXn2564_down-F	gctttggaatatggcattacgctaGGACAGGAAAAAGAGAGCATCCA
	DelXn2564_down-R_SacI	ATGCGAGCTCTCCGAGCATCTTTGCCACAA
	vDelXn2564_fw	TGGCTGCGGTGATTGATAACGTA
	vDelXn2564_rv	ACACCTACTCCGGCCACTTTTT
plasmid	pDS132fw	GATCGATCCTCTAGAGTCGACCT
	pDS132rv	ACATGTGGAATTGTGAGCGG
Confirm XNC1_2229 kanamycin	XpsKan2	CCGTCACATGTGCTGTCA
insertion	XpsKan3	CCAATATCGACAGACAGC
Sequence iip plasmid insertion	Arb102In	GGTTATTGTCTCATGAGCGG
site	Arb102Out	TGCACCCAACTGATCTTCAGC
	ArbCat2	CATATCACCAGCTCACCGTCT
	CatUp	CAACGGTGGTATATCCAGTG

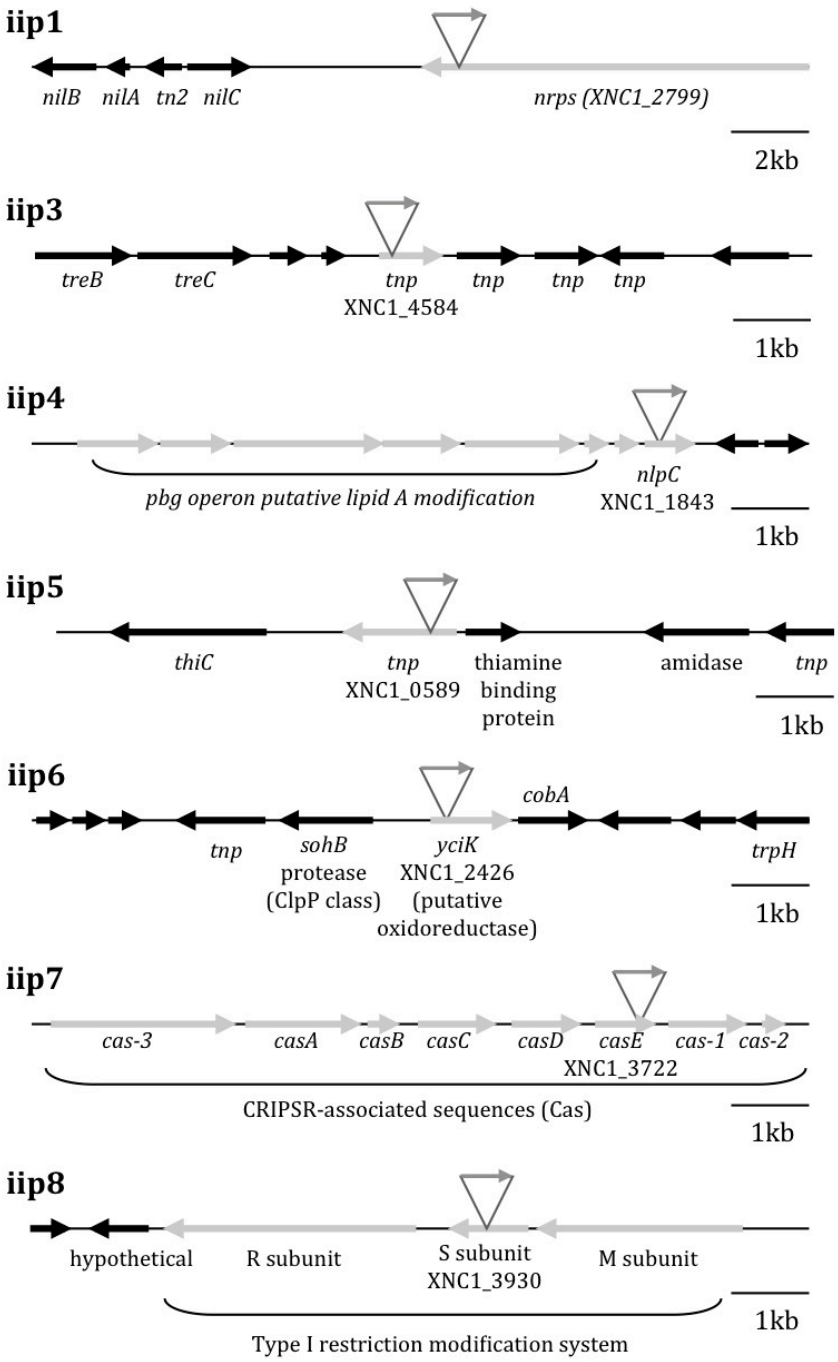

Figure S1. *X. nematophila* iip loci. Light gray arrows indicate the location (ORF or predicted operon) of IVET plasmid integration. Dark gray arrows designate orientation of *cat* gene. Black arrows denote flanking genes. Putative gene functions were assigned based on best hits from BLAST results.[25] iip1 = XNC1_2799, iip3 = XNC1_4584 iip4 = XNC1_1843, iip5 = XNC1_0589, iip6 = XNC1_2426, iip7 = XNC1_3722, iip8 = XNC1_3930.

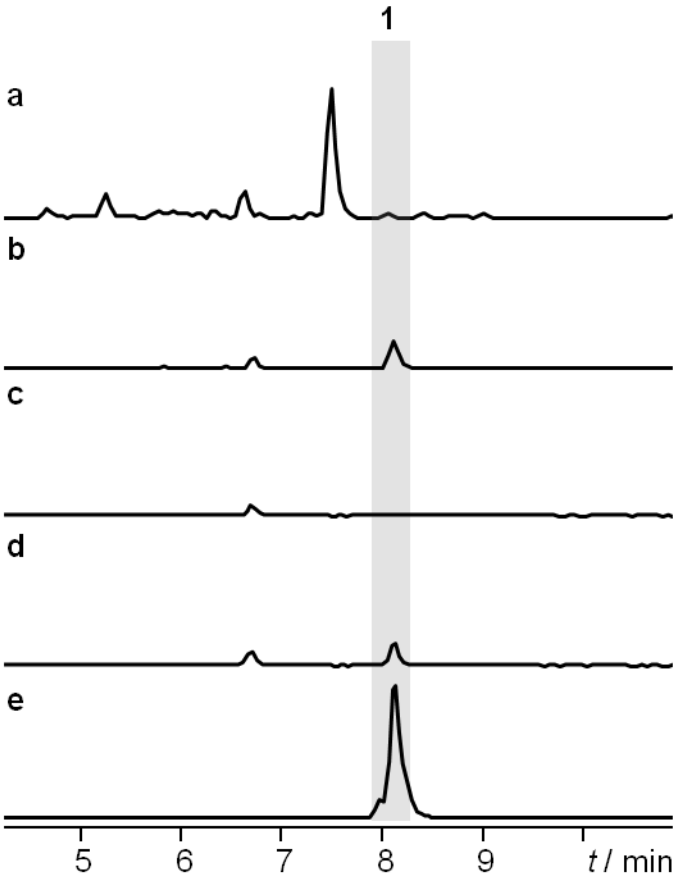

Figure S2. HPLC MS analysis of rhabdopeptides produced by *X. nematophila* mutant strains. Base peak chromatograms (BPC) and extracted ion chromatograms (EIC) traces specific for **1** (*m/z* 574 $[M+H]^+$) are shown. Depicted are (**a**) BPC of HGB081 wild type after 3 days of incubation (**b**) EIC of HGB081 wild type, (**c**) EIC of *rdpA*::*cat*, (**d**) EIC of ΔXNC1*_2233* and (**e**) EIC of HGB081wild type injected into *G. mellonella*. All chromatograms are scaled in the same intensity.

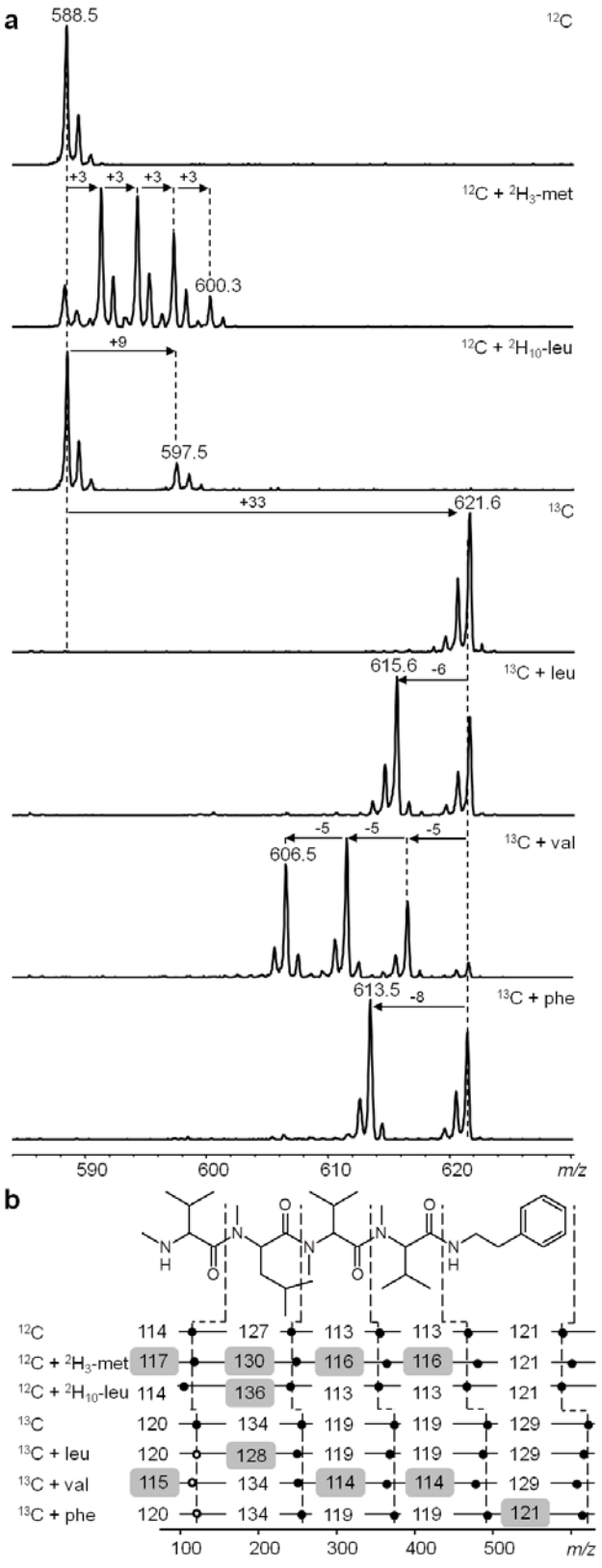

Figure S3. Structure elucidation of rhabdopeptide 2 (**2**) via fragmentation pattern and feeding experiments. *X. nematophila* was cultivated in ^{12}C LB medium supplemented with L-[methyl-D_3]methionine, L-[2,3,3,4,5,5,5,6,6,6-D_{10}]leucine and for an inverse feeding approach in [U-^{13}C] medium, supplemented with L-leucine, L-valine and L-phenylalanine (from top to bottom). (**a**) MS feeding experiments data of **2**. Identified mass shifts of incorporated precursors are indicated by arrows. (**b**) MS^2 fragmentation pattern of **2**. Positions of the possible b-ion MS^2 fragmentation sites are indicated with dashed lines. Precursor ion masses (filled circle on the right) and identified fragmentation ions *m/z* $[M+H]^+$ are indicated by a filled circle. Fragmentation b-ions which could not be detected in this experiment but could be concluded from other results are indicated with an open circle. Masses of fragments predicting the incorporated amino acid are highlighted in boxes.

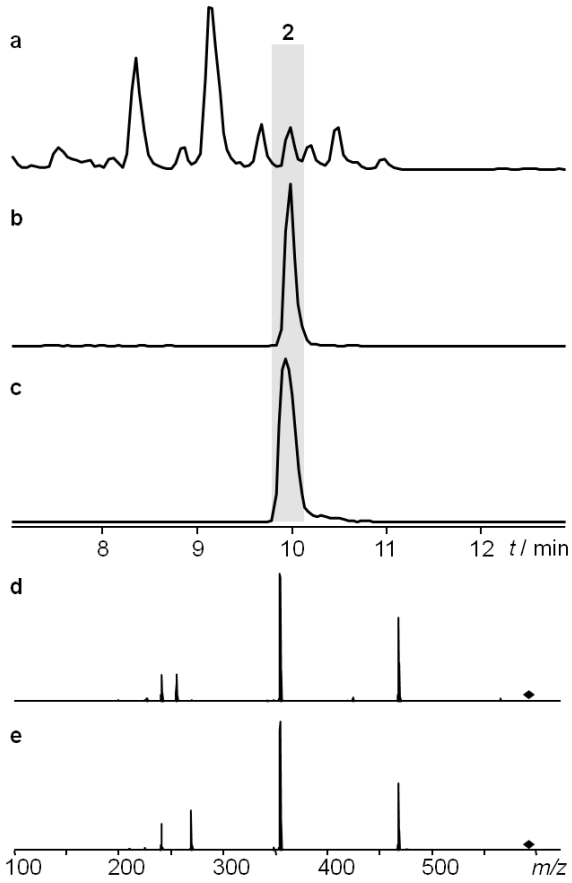

Figure S4. HPLC MS analysis of natural and synthetic rhabdopeptide 2 (**2**) produced by *X. nematophila.* Base peak chromatogram of HGB081 wild type (**a**), extracted ion chromatogram of natural **2** (**b**) and synthetic **2** (**c**) and the corresponding MS^2 fragmentation pattern of natural **2** (**d**) and synthetic **2** (**e**).

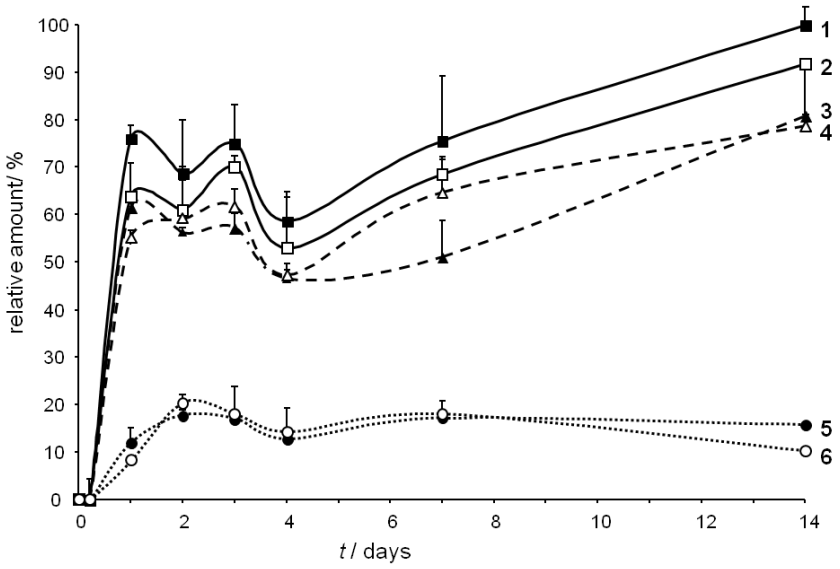

Figure S5. Rhabdopeptide (**1**-**6**) production of *X. nematophila*. Rhabdopeptide (**1**-**6**) production of *X. nematophila* cultivated in LB medium. 100% refers to the maximum production of **1**. **1** (filled squares), **2** (open squares), **3** (filled triangles), **4** (open triangles), **5** (filled circle) and **6** (open circle). Error bars represent standard deviation (n=2).

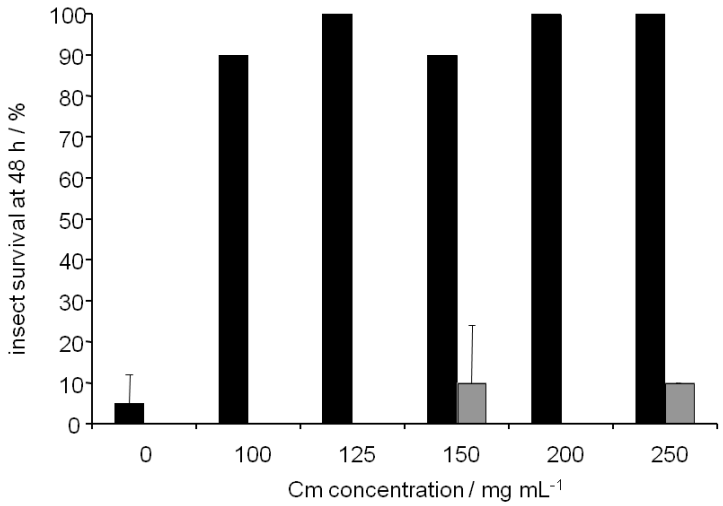

Figure S6. Effect of varying concentrations of chloramphenicol-succinate (Cm) on *X. nematophila* virulence towards insects. *X. nematophila* HGB007 (black bars) and a *X. nematophila* Tn*10* (Cm^R) mutant (gray bars) were injected into insects at approximately 20,000 cfu/insect. 10 µL of different concentrations of Cm were injected into insects 1 h post-bacterial injection. Insects were then monitored for survival for 48 h (n=2).

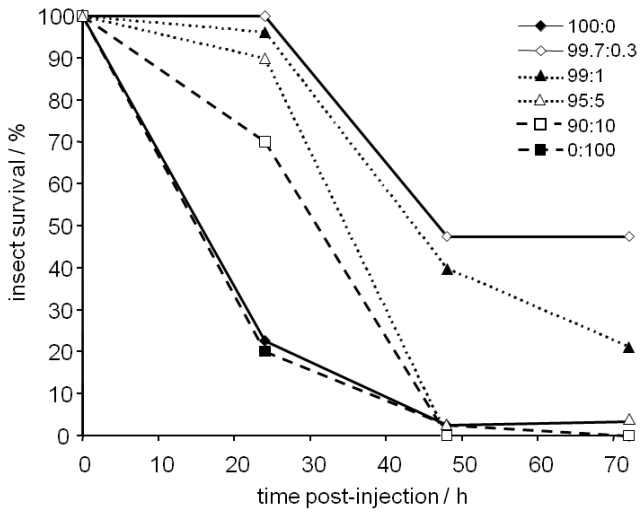

Figure S7. Optimization of IVET pool size. Wild type *X. nematophila* HGB007 (first number in legend) and a *X. nematophila* Tn*10* (Cm^R) mutant (second number) were mixed at different ratios (i.e. 99:1 corresponds to 99% wild type and 1% Tn*10* mutant) and injected into insects. The bacterial injection was followed by a 10 µL injection of 200 µg $µL^{-1}$ Cm after one hour (except in the case of the 100:0 injection where no Cm was injected). Insect survival was monitored for 72 h post-injection.

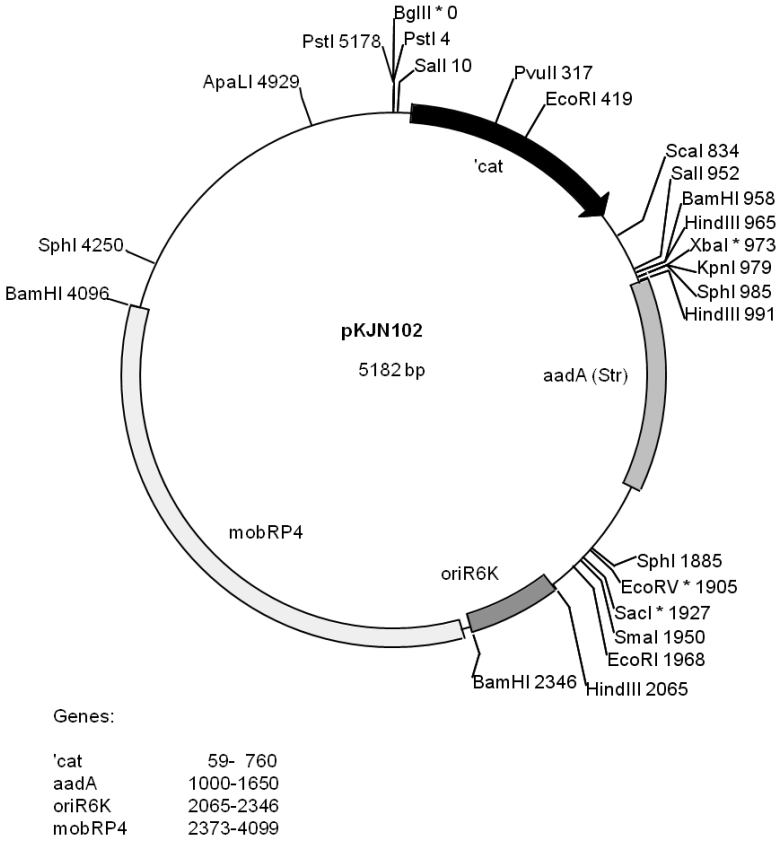

Figure S8. IVET plasmid pKJN102. Asterisks indicate unique restriction sites. Restriction site and plasmid element locations are rough estimates based on digest patterns and parent plasmid pGY2.

Reference List

[1] K. N. Cowles, H. Goodrich-Blair, *Cell Microbiol.* **2005,** *7*, 209-219.

[2] J. Sambrook, E. F. Fritsch, T. Maniatis, *Molecular cloning: A laboratory manual*, 2 ed. Cold Spring Harbor Laboratory Press, Cold Spring Harbor, NY **1989**.

[3] G. M. Young, D. Amid, V. L. Miller, *J.Bacteriol.* **1996,** *178*, 6487-6495.

[4] G. A. O'Toole, R. Kolter, *Mol.Microbiol.* **1998,** *28*, 449-461.

[5] G. Caetano-Anolles, *PCR Methods Appl.* **1993,** *3*, 85-94.

[6] J. M. Chaston, G. Suen, S. L. Tucker, A. W. Andersen, A. Bhasin, E. Bode, H. B. Bode, A. O. Brachmann, C. E. Cowles, K. N. Cowles, C. Darby, L. de Leon, K. Drace, Z. J. Du, A. Givaudan, E. E. H. Tran, K. A. Jewell, J. J. Knack, K. C. Krasomil-Osterfeld, R. Kukor, A. Lanois, P. Latreille, N. K. Leimgruber, C. M. Lipke, R. Y. Liu, X. J. Lu, E. C. Martens, P. R. Marri, C. Medigue, M. L. Menard, N. M. Miller, N. Morales-Soto, S. Norton, J. C. Ogier, S. S. Orchard, D. Park, Y. Park, B. A. Qurollo, D. R. Sugar, G. R. Richards, Z. Rouy, B. Slominski, K. Slominski, H. Snyder, B. C. Tjaden, R. van der Hoeven, R. D. Welch, C. Wheeler, B. S. Xiang, B. Barbazuk, S. Gaudriault, B. Goodner, S. C. Slater, S. Forst, B. S. Goldman, H. Goodrich-Blair, *PLoS ONE* **2011,** *6*, e27909.

[7] J. S. Gunn, S. S. Ryan, J. C. Van Velkinburgh, R. K. Ernst, S. I. Miller, *Infect.Immun.* **2000,** *68,* 6139-6146.

[8] N. Philippe, J. P. Alcaraz, E. Coursange, J. Geiselmann, D. Schneider, *Plasmid* **2004,** *51,* 246-255.

[9] S. S. Orchard, H. Goodrich-Blair, *Appl.Environ.Microbiol.* **2004,** *70,* 5621-5627.

[10] A. O. Brachmann, S. A. Joyce, H. Jenke-Kodama, G. Schwär, D. J. Clarke, H. B. Bode, *ChemBioChem* **2007,** *8,* 1721-1728.

[11] Hussa, E. and Goodrich-Blair, H. Rearing and Injection of Manduca sexta Larvae to Assess Bacterial Virulence. J.Vis.Exp. [70]. **2012**, in press.

[12] K. Heungens, C. E. Cowles, H. Goodrich-Blair, *Mol.Microbiol.* **2002,** *45,* 1337-1353.

[13] H. B. Bode, D. Reimer, S. W. Fuchs, F. Kirchner, C. Dauth, C. Kegler, W. Lorenzen, A. O. Brachmann, P. Grun, *Chemistry.* **2012,** *18,* 2342-2348.

[14] D. Reimer, E. Luxenburger, A. O. Brachmann, H. B. Bode, *ChemBioChem* **2009,** *10,* 1997-2001.

[15] I. Orhan, B. Sener, M. Kaiser, R. Brun, D. Tasdemir, *Mar.Drugs* **2010,** *8,* 47-58.

[16] D. Konz, M. A. Marahiel, *Chem.Biol.* **1999,** *6,* R39-R48.

[17] J. Ishikawa, K. Hotta, *FEMS Microbiol.Lett.* **1999,** *174,* 251-253.

[18] B. O. Bachmann, J. Ravel, *Methods in Enzymology* **2009,** *458,* 181-217.

[19] J. D. Thompson, D. G. Higgins, T. J. Gibson, *Nucleic Acids Res.* **1994,** *22,* 4673-4680.

[20] M. Z. Ansari, J. Sharma, R. S. Gokhale, D. Mohanty, *BMC.Bioinformatics.* **2008,** *9,* 454.

[21] C. J. Balibar, F. H. Vaillancourt, C. T. Walsh, *Chem.Biol.* **2005,** *12,* 1189-1200.

[22] M. Rottig, M. H. Medema, K. Blin, T. Weber, C. Rausch, O. Kohlbacher, *Nucleic Acids Res.* **2011,** *39,* W362-W367.

[23] V. L. Miller, J. J. Mekalanos, *J.Bacteriol.* **1988,** *170,* 2575-2583.

[24] R. Simon, U. Priefer, A. Pühler, *Bio.Technol.* **1983,** *1,* 784-791.

[25] S. F. Altschul, T. L. Madden, A. A. Schaffer, J. H. Zhang, Z. Zhang, W. Miller, D. J. Lipman, *Nucleic Acids Res.* **1997,** *25,* 3389-3402.

Concluding Remarks

A widespread natural prodrug activation mechanism in xenocoumacin biosynthesis

The most abundant secondary metabolites in *Xenorhabdus nematophila* are xenocoumacins, which belong to the class of dihydroisocoumarin-derived compounds. Dihydroisocoumarin derivatives represent a growing group of phenolic antibiotics with a wide range of significant activities. They are found in bacteria from different habitats such as *Bacillus*, *Streptomyces* and *Xenorhabdus* spp. but also in eukaryotes like in the marine fungus *Alternaria tenuis*.[44;65;76] In 1975, the first derivatives, baciphelacins, were isolated from the soil bacterium *Bacillus thiaminolyticus*.[72] All derivatives share a common structural element, a 3,4-dihydro-8-hydroxyisocoumarin chromophore consisting of a conserved leucine at the 3-position of the core structure (Figure 1). The broad spectrum of their biological activity originates from the variety of the hydroxylated amino acyl side chains. Side chain variations range from carboxylic amide and acids,[45] a hexahydropyrimidine ring,[61] unusual 7-membered rings,[44] rare 2-hydroxymorpholine substructures[3] to 8-phosphate esters.[36] They display a broad spectra of interesting characteristics like antibacterial activity[46;61;65;72] (e.g. PJS, baciphelacin, xenocoumacin), specific cytotoxic activity against several tumor cell lines[16;44;89] (e.g. PM94128, Sg17-1-4), antiulcer activity[46;65;89] (e.g. xenocoumacin, amicoumacin), herbicidal[3] and antiplasmodial activity[11] (e.g. bacilosarcin), as well as antiinflammatory activity[46] (e.g. amicoumacin). In addition to its antibiotic activity, xenocoumacin 1 also displays an antifungal activity.[65] Although they play an important role in the bacterial defense mechanism as discussed later in this section, the xenocoumacins are not widely distributed in *Xenorhabdus* spp. as one would expect. During the EC project GameXP (www.gamexp.eu) almost 250 *Xenorhabdus* and *Photorhabdus* strains were isolated from nematodes and/or collected, phylogenetically classified[99] as well as analyzed with respect to the produced compounds (Bode, H.B., unpublished). Though, xenocoumacins or the corresponding biosynthetic gene cluster were only be identified in 11 strains from seven *Xenorhabdus* subspecies (*X. nematophila* ATCC 19061[100], Xs85816 (B. Goldman, Monsanto), *X. indica* DSM 17382,[93] *X. miraniensis* DSM 17902,[98] PB62.2,[99] PB62.4,[99] PB63.3,[99] *X. stockiae* KJ12.1,[99] *X. kozodoii* DSM 17907,[98] *X. mauleonii* DSM 17908[98] and *X. doucetiae* DSM 17909[98]). Interestingly, several strains from the same phylogenetical clade showed different phenotypes of the secondary metabolome and only a few of them produced xenocoumacins (unpublished data). It can be speculated that different secondary metabolites deal with the same biological function dependent on their occurrence in their host.

Prior to this work, the structures of the two main xenocoumacin derivatives xenocoumacin 1 (XCN 1) and 2 (XCN 2) were known, but no corresponding biosynthetic pathway was assigned. The sequencing of the genome of *X. nematophila* ATCC 19061[19] and a detailed annotation of all biosynthetic gene clusters enabled us to identify the xenocoumacin gene cluster and to study the biosynthesis in detail.

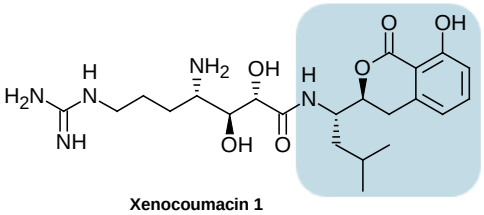

Xenocoumacin 1

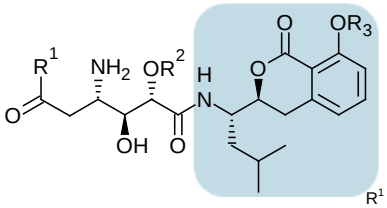

	R^1	R^2	R^3
Amicoumacin A or **AI-77-A**	NH_2	H	H
Amicoumacin B or **AI-77-B**	OH	H	H
Amicoumacin A-8'phospho derivative	NH_2	H_2PO_3	H
Amicoumacin B-8'phospho derivative	OH	H_2PO_3	H
6-[[1-(3,4-dihydro-8-methoxy-1-oxo-1H-2-benzopyran-3-yl)-3-methylbutyl]amino]-4,5-dihydroxy-6-oxo-3-ammoniohexanoate	OH	H	Me

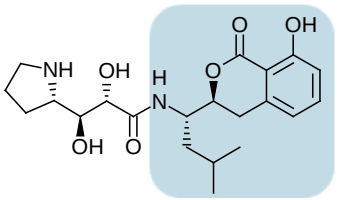

Xenocoumacin 2

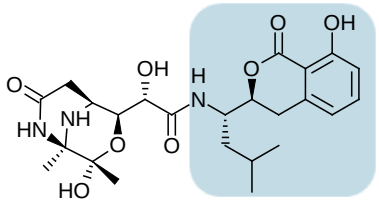

Bacilosarcin A

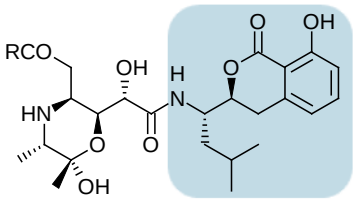

	R
Bacilosarcin B	NH_2
Bacilosarcin C	OH

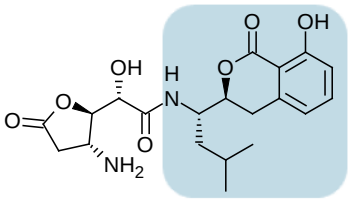

Amicoumacin C

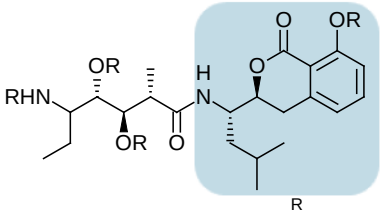

	R
Baciphelacin I	H
Baciphelacin II	$COCH_3$

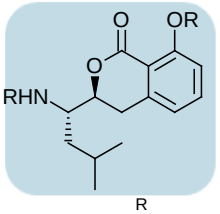

	R
Baciphelacin III	H
Baciphelacin IV	$COCH_3$

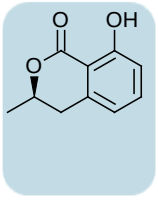

Baciphelacin V

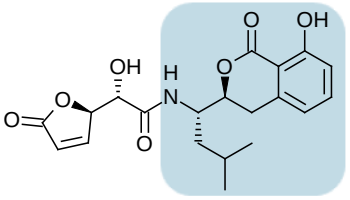

AI-77-F

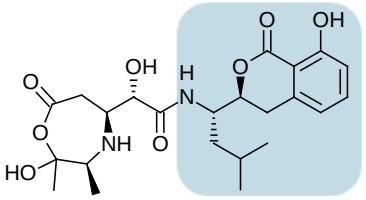

Sg17-1-4

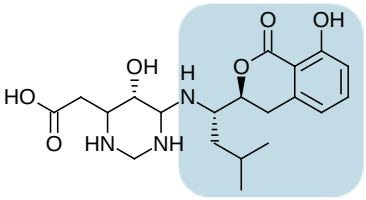

PJS

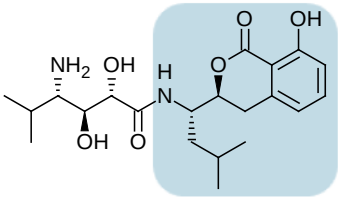

Y-05460M-A

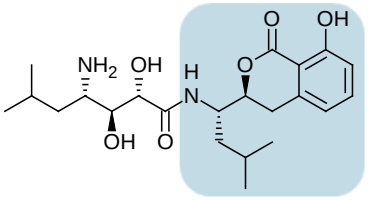

PM-94128

Figure 1. Dihydroisocoumarin derivatives from different bacterial taxa with the characteristic 3,4-dihydroisocoumarin chromophore extended with a leucine at the 3-position of the core (marked in blue). Xenocoumacins have been isolated from *Xenorhabdus* spp., amicoumacins[36;45;46] and AI-77[44;90] from soil and marine *Bacillus* spp. and from a *Norcardia* sp.[96], PM-94128[16] and bacilosarcins[3;11;60] from marine *Bacillus* spp., baciphelacin[72] and Y-05460M[89] from a soil *Bacillus* sp., Sg17-1-4[44] from the marine fungus *Alternaria tenuis* and PJS[61] from a plant associated *Bacillus* sp..

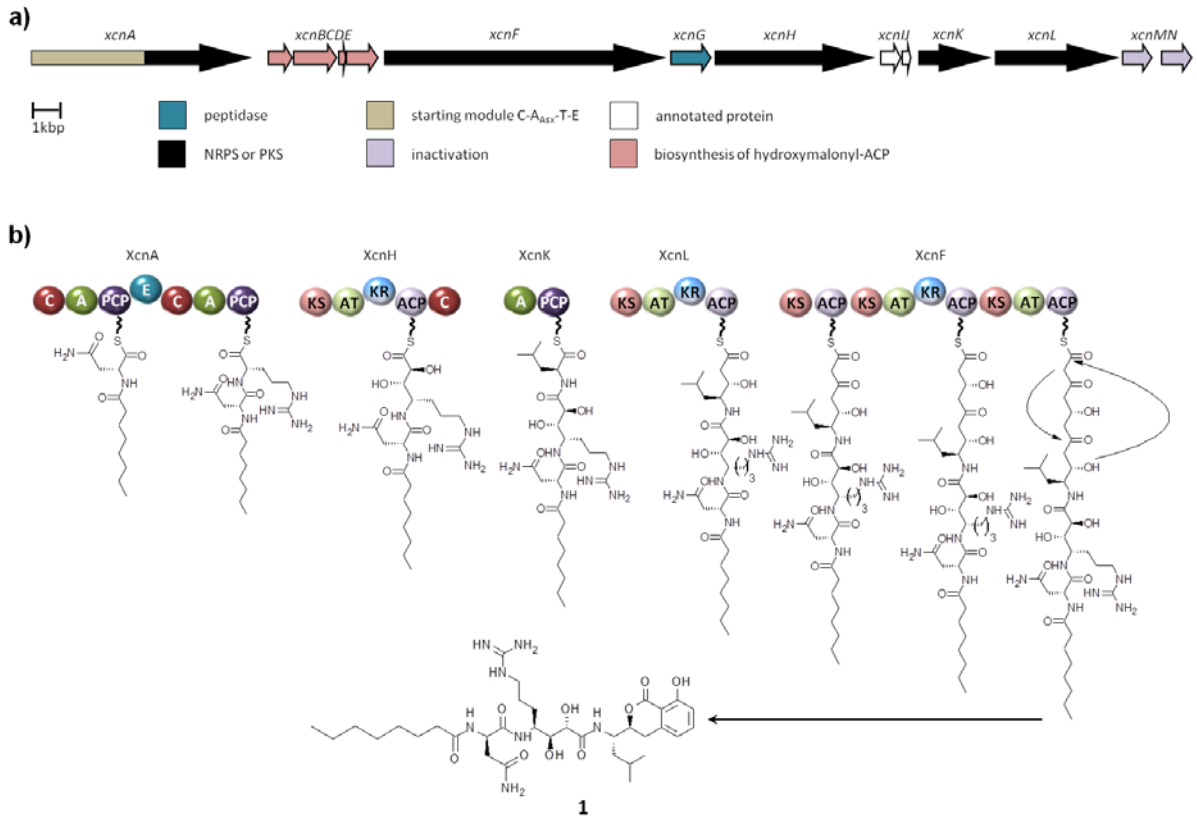

Figure 2. a) Organization of the xenocoumacin (*xcn*) biosynthesis gene cluster in *X. nematophila* ATCC 19061. b) Biosynthetic pathway for the formation of the polyketide-peptide backbone of prexenocoumacin B. A: adenylation domain, PCP: peptidyl carrier protein, C: condensation domain, E: epimerization domain, AT: acyltransferase domain, ACP: acyl carrier protein, KS: ketosynthase domain, KR: ketoreductase domain.

Xenocoumacins are synthesized via a non colinear hybrid polyketide synthase (PKS) and nonribosomal peptide synthetase (NRPS) multienzyme (Figure 2a), consisting of six transcriptional units identified by real time-PCR.[74;80] The biosynthesis can be divided into enzymes responsible for the biosynthesis of the core structure (Figure 2a, black), including the biosynthesis of the hydroxymalonyl-ACP (Figure 2a, pink), and in proteins involved in an interesting drug activation mechanism (Figure 2a, brown and teal) and a resistance conferring inactivation pathway (Figure 2a, purple).

A plasmid insertion into *xcnC* resulted in the total loss of xenocoumacin production[80] and allowed to identify *xcnB–E* as genes encoding enzymes required for the biosynthesis of hydroxymalonyl-ACP. This rare extender unit is derived from 1,3-bisphosphoglycerate, known and characterized in detail from the zwittermicin biosynthesis in *Bacillus cereus*.[17;18] On the basis of the known derivatives XCN 1 and XCN 2, the first attempt to elucidate the complete xenocoumacin biosynthetic machinery in the correct order of the acting proteins (XcnAHKLF, Figure 2b) was not successful. As the biosynthetic gene cluster harbors one more module as needed for the biosynthesis

of the main compounds, it was postulated as inactive.[80] Further investigations of all genes and deletion mutants thereof enabled to bridge the gap between the size of the structure and the biosynthetic pathway resulting in a new natural prodrug activation mechanism.[81]

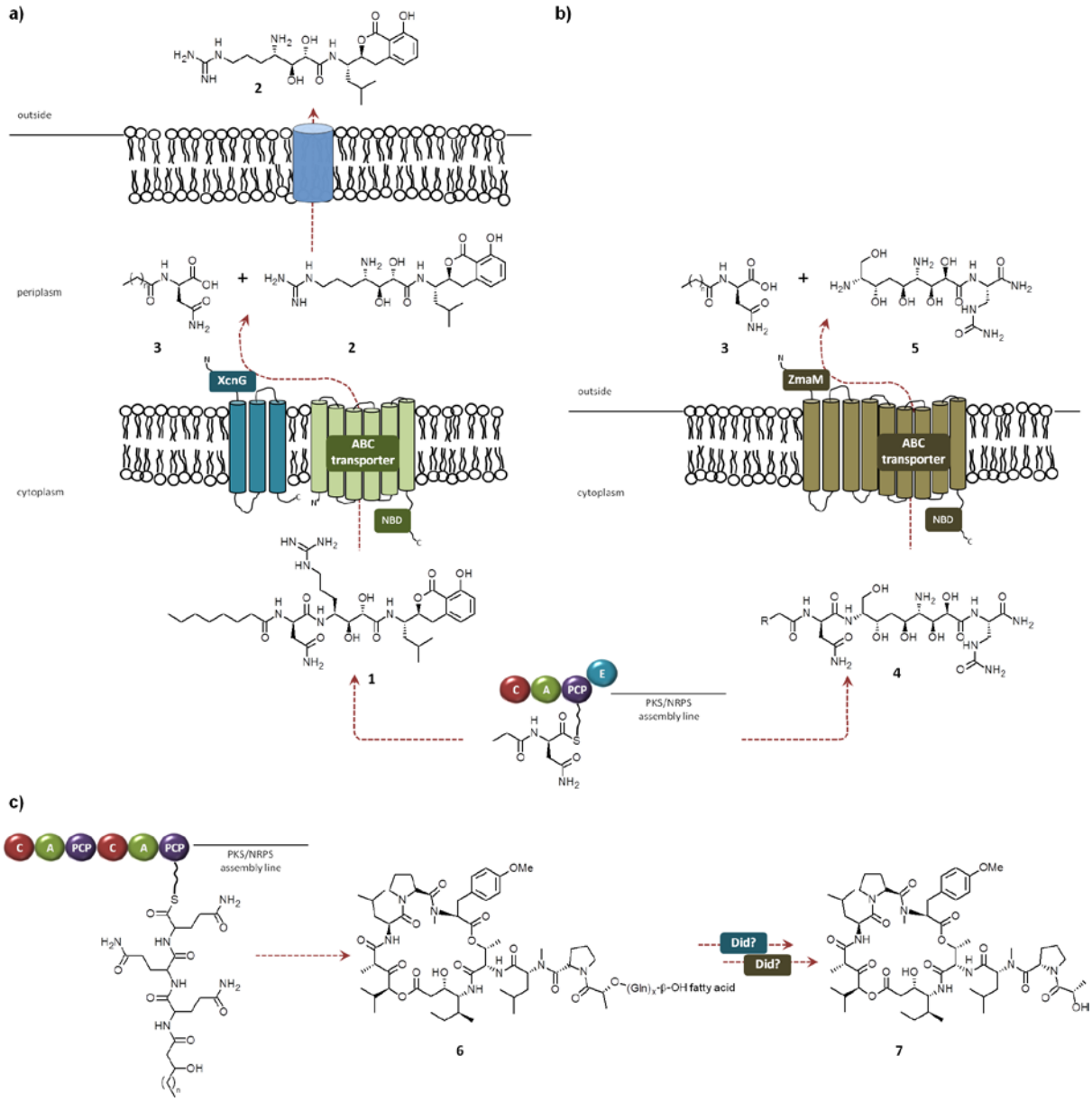

Figure 3. a) Natural prodrug activation mechanism in xenocoumacin biosynthesis in the Gram-negative *X. nematophila*. Prexenocoumacin B (**1**) and four additional derivatives are formed as inactive prodrugs and cleaved into XCN 1 (**2**) by releasing an acylated D-asparagine residue (**3**) via XcnG, a peptidase with type I architecture. b) Natural prodrug activation mechanism in zwittermicin biosynthesis in Gram-positive *Bacillus* spp.. Prezwittermicin (**4**) with an unknown fatty acid (R) is formed and cleaved by ZmaM (type II architecture peptidase) into **3** and the active zwittermicin A (**5**). c) Activation mechanism in didemnin biosynthesis from marine *Tistrella* spp. Didemnins X/Y (**6**) are produced as acylglutamine ester derivatives by the NRPS/PKS enzyme complex and are cleaved in the extracellular space by so far unknown proteins into the active didemnin B (**7**). A: adenylation domain, PCP: peptidyl carrier protein, C: condensation domain, E: epimerization domain.

Five inactive prexenocoumacins (**1**) are produced by the biosynthetic gene cluster inside the cytoplasm (Figure 2b, exemplarily for prexenocoumacin B and Figure 3a). XcnG, a bifunctional protein with a periplasmic peptidase domain and three additional transmembrane helices cleaves the acylated D-asparagine residue (**3**) from all prexenocoumacin derivatives synchronously. The bioactive XCN 1 (**2**) is secreted with an ABC transporter nucleotide binding domain (NBD) and presumably a TolC-like protein, which has not be identified yet (Figure 3a).[81] Astonishingly, homologues of the peptidase (XcnG) and the encoding NRPS C-A_{Asx}-T-E (for condensation, adenylation specific to Asx, thiolation and epimerization) starting module (XcnA) were identified in many different bacterial genera. Thus indicating a widespread and important mechanism for the activation of secondary metabolites.

Two homologues of XcnG and the corresponding NRPS for the starting module were identified in different *Bacillus* spp.[63;81] In the case of the structural related amicoumacin biosynthetic pathway, a peptidase (Bpum_0630) with the same domain architecture as XcnG, so called type I domain architecture is present.[81] Recently, four putatively amicoumacin prodrugs were identified in a marine *B. subtilis*.[60] These prodrugs are structural similar to amicoumacin C harboring a *N*-terminal asparagine or glutamine residue that is extended by a 9-methylundecanoic or 9-methyldodecanoic acid. However, these so called lipoamicoumacins exhibit no antibacterial activity.[60] Unfortunately, the authors missed to draw a link between their isolated structures and the prodrug strategy.

Several *Bacillus* species produce zwittermicin, another compound with a broad spectrum of activities, inhibiting Gram-positive and -negative microorganisms.[91] In the biosynthetic machinery of zwittermicin A (ZmA, **5**), a peptidase with type II architecture[81] (ZmaM) is available (Figure 3b). Although until now, no pre-structure has been detected, it is assumed that acyl-D-Asn-ZmA (prezwittermicin, **4**) contains a *N*-terminal fatty acid and a D-asparagine comparable to the prexenocoumacins.[51;63] In contrast to XcnG, ZmaM harbors the peptidase domain and an additional ABC-transporter domain with nine transmembrane helices. In xenocoumacin biosynthesis, transport and cleavage function is separated onto two proteins (XcnG and an unknown ABC-like transporter). Interestingly, in *Xenorhabdus bovienii* a cryptic biosynthetic gene cluster with a ZmaM-like peptidase (XbJ1_2693) was identified. The XcnG homologue XbJ1_2693 was able to cleave prexenocoumacin, indicating that the so far unknown substrate shows the same or at least a strong structural similarity to the *N*-terminus of prexenocoumacin. In contrast, ZmaM,[81] Bpum_0630[81] and the colibactin peptidase ClbP (unpublished data), were not able to cleave prexenocoumacin. These results indicate that not only the D-asparagine is responsible for the specificity but also the adjacent amino acid and therefore different classes of recognizing specific substrates might exist.

Colibactin is probably the most interesting compound produced by a NRPS/PKS hybrid harboring a peptidase homologue named ClbP.[28] The colibactin genome island is distributed across isolates of commensal and extraintestinal pathogenic *Escherichia coli* strains (ExPEC) but restricted

to the phylogenetic groups B1 and B2.[70] Highly conserved colibactin encoding regions were also found in the enterobacterial species *Klebsiella pneumoniae*, *Enterobacter aerogenes* and *Citrobacter koseri* and those are interestingly associated with yersiniabactin coding regions.[78] Colibactin causes DNA double strand breaks in mammalian cells and activates the DNA damage G_2 checkpoint in the cell cycle leading to a cell cycle arrest in G_2/M transition resulting in a nucleus enlargement called megalocytosis.[70] Recently, it was shown that colibactin might play a crucial role in chronic intestinal inflammation and has a carcinogenic impact in colorectal cancer.[2;24]

Detailed characterization of ClbP and XcnG revealed a strong structural homology to class C β-lactamases (AmpC). Peptidases of this class are periplasmic inner membrane proteins harboring a *N*-terminal signal sequence, a peptidase catalytic domain and a *C*-terminal three transmembrane helices consisting domain.[28;81] The *N*-terminal signal sequence is responsible for the translocation of the peptidase domain into the periplasm and the complete transmembrane domain is necessary for catalytic activity.[21;81] The peptidase domain of ClbP harbors two structural domains, an α/β-region with seven stranded antiparallel β-sheets packed on both sides with six α-helices and three β-strands and an all α-region with four helices. Its catalytic groove is located between the two structural domains and possesses the conserved motifs SxxK and YxS, typically for serine-type D-Ala-D-Ala carboxypeptidases of the MEROPS S12 enzyme family.[28] A striking feature in contrast to AmpC, is the unusual large catalytic groove and this could be interpreted as an adaption to a specific type of substrates. For ClbP, the catalytic triad comprises serine, lysine and tyrosine and six residues (E159, S188, H257, F316, G328, N331), which might be involved in substrate binding. These residues were identified on the basis of docking studies with imipenem, a substrate of the β-lactamase class.[28] Interestingly, the substrate binding residues of XcnG differ in five of six residues from that of ClbP, which might be due to a different substrate specificity as mentioned before. Nevertheless, involvement of these residues has to be proven *in vitro* with the natural compound colibactin. Although, the complete structure is still unknown, the *N*-terminal moiety of precolibactin could be characterized as a C_{12} or C_{14} *N*-acyl D-asparagine linked to L-alanine or L-valine.[12] Anyhow, a different behavior of the enzymes *in vitro* and *in vivo* should be taken into account. To get a clearer insight and understanding of XcnG functionality and the responsible specific recognition sites, the xenocoumacin peptidase should be investigated *in vitro* as it was done for ClbP.

In Gram-negative marine bacteria of the genus *Tistrella*, symbionts of tunicates, another related but not analogues mechanism was found in the NRPS/PKS hybrid biosynthesis of the didemnins. Didemnins X and Y are produced as acylglutamine ester derivatives and then are cleaved by so far unknown proteins into the active didemnin B (Figure 3c). In contrast to xenocoumacin biosynthesis, the cleavage might occur by an ester hydrolysis in the extracellular space as no peptidase like enzyme but two putative hydrolytic enzymes were identified in the gene cluster. However, the cellular export of the compound seems to be similar as membrane-associated transport proteins are existent.[103] Interestingly, the *N*-terminal moiety is more flexible as in the natural prodrug

activation mechanism in xenocoumacin biosynthesis as the acylglutamine ester exhibit three or up to four glutamine residues resulting from an iteratively usage of the starter module (Figure 3c).

Until now, further strategies of deacylation of natural compound precursors differing from the xenocoumacin mechanism were found in the pyoverdine, zeamine and saframycin biosynthesis. During the pyoverdine biosynthesis of *Pseudomonas aeruginosa*, a myristate moiety is removed by a periplasmic hydrolase (PvdQ) in the maturation pathway.[27] For the PKS/NRPS/FAS hybrid derived zeamine from *Serratia plymuthica* a post-assembly activation is postulated via an acyl-aminoacyl peptidase, cleaving short *N*-acylated peptides.[64] In saframycin and other tetrahydroisoquinoline (THIQ) antibiotics (e.g. ecteinascidin, quinocarcin) the acyl chain is used for a condensation (C) domain mediated Pictet-Spengler like reaction in forming the THIQ moiety followed by deacylation as the last important step to obtain bioactivity.[52;53]

Prior to this work, activation of compounds was only known as a common feature in the biosynthesis of ribosomal peptides,[1] where the bioactive peptide is often derived by proteolytic cleavage, but was not expected to play a role in nonribosomally synthesized peptides. The NRPS derived activation mechanism exhibits a remarkable similarity to the maturation process in ribosomal peptides. Microcin J25 for example is produced as a propeptide in *E. coli* and a cleavage of the *N*-terminal leader sequence by ATP-catalyzed proteases and successive maturation steps like cyclization results in the active peptide, exported by ABC transporters and an outer membrane TolC protein.[29;92]

Xenocoumacins are thought to be involved in clearing bacteria in the insect gut and thereby eliminating other food competitors like for example the Gram-negative *Bacillus subtilis*. It was shown that *B. subtilis* could be found in the gut of insects[42] and recently, Zhou *et al.* studied the global transcriptional response of *B. subtilis* to XCN 1.[105] They identified several processes, which are affected by xenocoumacin. For example, xenocoumacin induced downregulation of genes involved in amino acid (e.g. arginine, leucine), antibiotic and fatty acid biosynthesis, oligopeptide, amino acid and iron ion transport as well as aminoacyl-tRNA synthetases (AARSs). On the contrary, pyrimidine nucleotide biosynthesis and genes concerning the bacterial chemotaxis (e.g. flagellar synthesis) and the autolysis process were upregulated. As XCN 1 influences mainly processes, which are known to be affected by protein synthesis inhibitors, the authors presume the arginine tRNA ligase (ArgS) as possible target.[105] XCN 1 might have a similar mechanism like mupirocin, an isoleucyl-tRNA synthetase targeted antibiotic.[6;35] During treatment with XCN 1, *B. subtilis* possesses a low ArgS activity. An inhibition of ArgS resulted in an accumulation of uncharged $tRNA^{Arg}$. Finally, a raised ratio of uncharged to charged $tRNA^{Arg}$ will induce the transcription antitermination. Thereby, the expression of *argS* increases and the lower amount of charged $tRNA^{Arg}$ reduces the available amount of arginine for the translation elongation, resulting in an inhibition of the protein synthesis. As XCN 1 comprises an arginine in its structure, it can be speculated that the arginine

moiety acts as a competitive substrate for ArgS.[105] This hypothesis is congruent with the lower antibacterial activity of XCN 2,[65;81] which lacks the mentioned arginine in its structure. In this work, it was shown that production of XCN 1, accomplished by heterologous expression of the peptidase in *E. coli* and feeding of prexenocoumacin, could not be observed in high amounts as XCN 1 might stick to its target.[81] Moreover, a lysis of the cell culture suggested the induced upregulation of genes involved in autolysis as it was described for XCN 1 treated *Bacillus* cells.

Furthermore, xenocoumacins were tested for biological activity against the parasites *Trypanosoma brucei rhodesiense*, *Trypanosoma cruzi*, *Leishmania donovani* and *Plasmodium falciparum*, which are the causative agents of neglected tropical diseases like sleeping sickness, chagas disease, leishmaniasis and malaria, respectively. Good activities were observed against *T. b. rhodesiense* (IC_{50} 0.027 µg mL^{-1} (XCN 1), 0.03 µg mL^{-1} (XCN 2)) and *P. falciparum* (IC_{50} 0.011 µg mL^{-1} (XCN 1), 0.031 µg mL^{-1} (XCN 2)) (unpublished data). The commercial available treatments melarsoprol and chloroquine are active against *T. brucei rhodesiense* and *P. falciparum* with IC_{50} 0.004 µg mL^{-1} and 0.003 µg mL^{-1}, respectively. It might be possible and reasonable that XCN 1 is following a similar mode of action in *Plasmodium* as in *B. subtilis* and inhibits tRNA synthesis. In the meantime, it was shown that mupirocin inhibits the growth and division of the relic plastid, called apicoplast in *P. falciparum* by inhibiting the aminoacyl-tRNA synthetase in this compartment.[47] Moreover, an additional target of the 3,4-dihydroisocoumarin moiety might be possible. For instance, in a virtual screening of 50,000 functionally characterized natural and synthetic small molecules against nine binding sites from seven protein targets, a sulfotransferase (SULT1E1) for XCN 1 and a histone acetyltransferase (MYST3) were identified as potential targets for XCN 1 and XCN 2.[15] Nevertheless, all of these possible targets need further investigations to prove their evidence.

As *X. nematophila* is sensitive to XCN 1 itself, a detoxification process as self-resistance mechanism is present. Self-resistance is a common mechanism for antibiotic producing bacteria containing a target that is sensitive to the produced antibiotic.[43] Although, self-resistance and acquired resistance is mediated by same or related mechanisms, the next section will focus only on self-protection strategies. Bacteria exhibit different opportunities to cope with such cases. In the example of the erythromycin producer *Sachharopolyspora erythraea*, the sensitive target is modified to an insensitive form by a ribosomal RNA methyltransferase.[25] Another possibility is a rapid export of the compound by a transmembrane protein channel as it is described for tetracycline resistance in *Streptomyces*.[20] Furthermore, an inactivation due to a chemical modification of XCN itself as in the example of xenocoumacin could take place (Figure 4a).

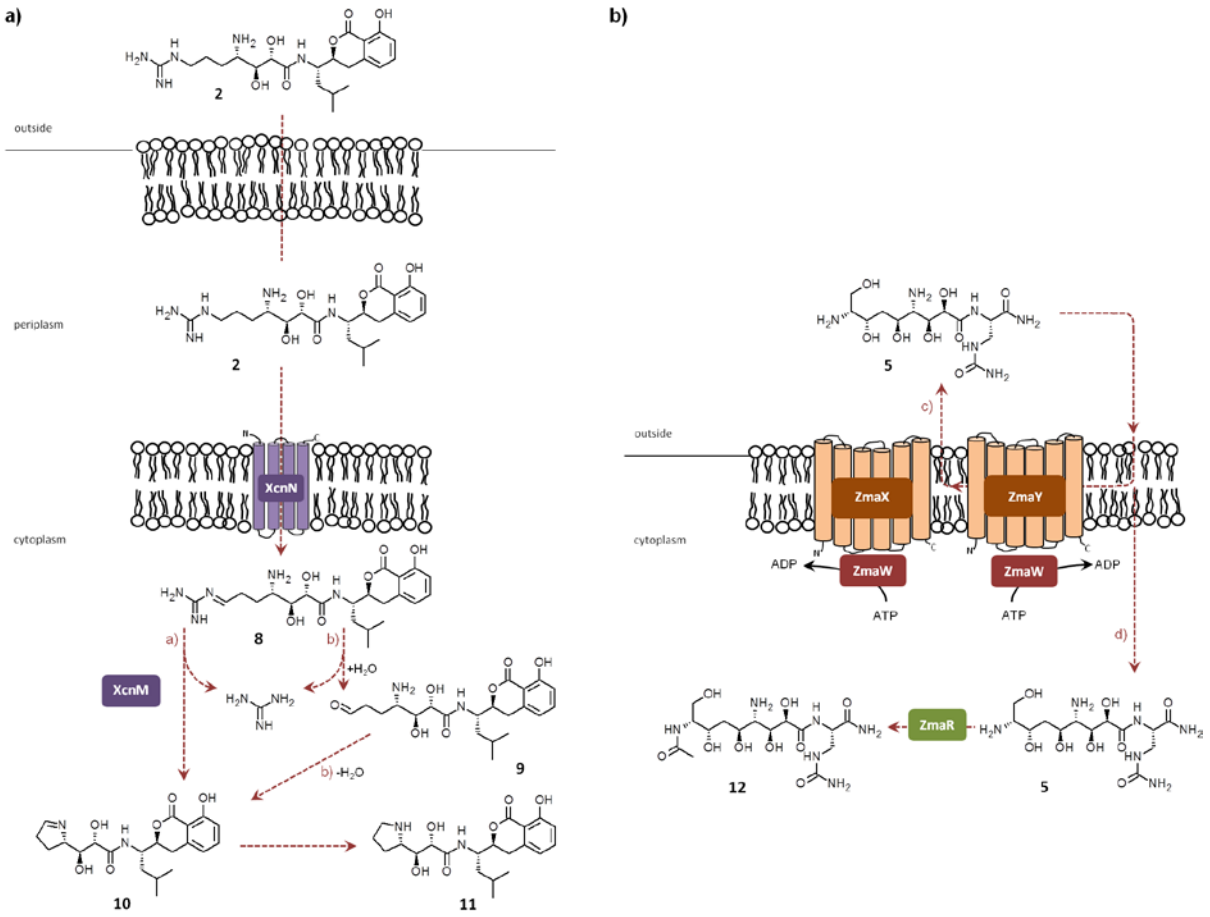

Figure 4. a) Self-resistance mechanism in xenocoumacin biosynthesis in the Gram-negative *X. nematophila*. XCN 1 (**2**) is oxidized by XcnN into the xenocoumacin intermediate XCN-464 (**8**), further conversion into XCN 3 (**10**) is catalyzed by XcnM via pathway (a) or (b) with XCN 4 (**9**) as intermediate and reduced in a further step into XCN 2 (**11**). b) Resistance mechanism in zwittermicin biosynthesis in Gram-positive *Bacillus* spp. via pathway (c) or/and (d). Zwittermicin A (ZmA, **5**) is transported by the membrane bound ZmaWXY out of the cell. Is the concentration higher than ZmaXWY's action, **5** is taken up into the cell and inactivated by acetylation via ZmaR into the inactivated zwittermicin (**12**).

Disruption of XcnMN eliminated conversion of XCN 1 to XCN 2 and resulted in an elevated XCN 1 production in a mutant strain with 20-fold reduced viability. This result strongly indicated a necessary balance between the required level of XCN 1 for suppression of competitors and a conversion to XCN 2 to maintain XCN 1 level below the threshold of self-toxicity.[74] Membrane bound *xcnN* encodes a protein similar to the family of fatty acid desaturases introducing regiospecifically double bounds into saturated fatty acids.[13] In XCN conversion, XCN 1 (**2**) is oxidized by XcnN to a probably unstable XCN-464 (**8**) intermediate with a double bond at the nitrogen position of the amino group in the arginine backbone (Figure 4a). XCN 2 formation is possible via two pathways, both presumably catalyzed by XcnM. XcnM shows similarity to saccharopine dehydrogenases, which are involved in the biosynthesis of lysine by catalyzing the formation of lysine and α-ketoglutarate from 2-aminoadipate-6 semialdehyde and glutamate with saccharopine as the key intermediate.[102] An

intramolecular nucleophilic attack of the former arginine amino group of **8** and cleavage of the guanidinium group catalyzed by XcnM results in the pyrrolidine formation of XCN 3 (**10**) (Figure 4a, pathway a). In an alternative pathway, XCN 4 (**9**) can be derived by hydrolysis or might be an intermediate of the conversion of **9** into **10** (Figure 4a, pathway b). In a further step, **10** is reduced into XCN 2 (**11**). Alternatively, XcnM might catalyze the formation of **11** from **8** or **10** directly in an NADPH-dependent reaction.[102] In this work, heterologous expression of XcnMN in *E. coli* has proven the involvement of these proteins in the conversion[80;81] but the exact role and the kind of reactions have to be investigated in more detail.

Xenocoumacin conversion as a detoxification mechanism supports the hypothesis of ArgS as a suitable target. Otherwise, a chemical modification of another XCN moiety would be expected.

Bacillus spp. use complementary to a self-resistance protein ZmaR an additionally membrane bound complex to cope in a sophisticated way with its sensitivity to zwittermicin A (ZmA, Figure 4b). During ZmA (**5**) interaction with the cytoplasmic membrane, the resistance transporter ZmaWXY senses the high concentration of ZmA and expel it from the membrane under consumption of ATP (Figure 4b, pathway c). Is the concentration of ZmA higher than ZmaXWY's action, **5** is taken up into the cell and inactivated by acetylation via ZmaR into the inactivated form (**12**) (Figure 4b, pathway d). ZmaR encodes an acetyltransferase and uses acetyl coenzyme A as donor group.[63;68;95]

A putative self-resistance mechanism can be proposed in amicoumacin biosynthesis just as well. On the one hand, the antimicrobial activity of amicoumacin B and C are weak compared to amicoumacin A[76] and it is not clear, if all derivatives are produced by the biosynthetic machinery at once or if only one derivative is synthesized and the others are derived by further enzymatic modifications. On the other hand, two C8' hydroxyl group phosphorylated derivatives of A and B with drastically lowered activity were identified.[36] Phosphorylation of antibiotics is commonly known as a mechanism of resistance (e.g. in the case of streptomycin).[38] In *B. pumilus* SAFR-32, a phosphotransferase enzyme (Bpum_0640), showing homology to the streptomycin 3"-phosphotransferase, can be found downstream of the NRPS/PKS encoding genes. An involvement can be assumed as this enzyme is localized in a transcriptional unit together with the PKS modules responsible for isocoumarin ring synthesis (unpublished data).

In summary, the data of this work and all the examples mentioned highlight the importance of different strategies for activation of NRPS and/or PKS derived natural products to avoid self-destruction of the producer strain during antibiotic production. Up to now, different strategies to cope with a bioactive produced antibiotic are well understand but this work discovered an astonished natural prodrug activation mechanisms in a similar way as it is known from ribosomal synthesized

protein research. This mechanism, which uses a D-asparagine specific carboxypeptidase is widespread among different bacterial taxa and thus adds a new layer of complexity to natural products. Moreover, such activation mechanisms seemed to have been evolved independently as multiple activation strategies have been found across different genera. Furthermore, the xenocoumacins are the first example for which inactive pre-structures and active structures were described and a detailed study of the biosynthesis has moreover uncovered a new type of resistance mechanism as a system of self-protection.

Rapid structure elucidation of linear and cyclic nonribosomally produced peptides by stable isotope labeling and mass spectrometry

Structure elucidation of natural products of interest is usually performed after their isolation by NMR spectroscopy and chemical derivatization to determine the absolute configuration. However, isolation of compounds might be a challenging task as microorganisms produce interesting compounds very often in minute amounts or with many different derivatives in complex mixtures leading to purification problems.[79;104] Thus, identification of known compounds via high-resolution (HR) mass spectrometry (MS) using databases like "The dictionary of natural products" (http://dnp.chemnetbase.com) or Scifinder (https://scifinder.cas.org) gains popularity. However, as natural products are not as "simple" as ribosomally derived peptides and very often harbor unusual building blocks resulting in different possible sum formula, compound identification by HR MS analysis is limited.

In the last years, development of bioinformatic and mass spectrometric methods enabled rapid methods to identify and annotate secondary metabolites and their corresponding biosynthetic gene clusters (e.g. antiSMASH,[66] PKS/NRPS Analysis Web-site,[4] NAPDoS[106]). These tools facilitate structure elucidation based on building block predictions. For ribosomally or nonribosomally derived peptides, a possible structure (chemotype) can be predicted using tandem mass spectrometry (MS^n)[69] linked with the genotypes using natural product peptidogenomics (NPP)[50] or with the proteome.[14] Based on the resulting fragmentation pathway[73] very often a possible structure can be determined. However, this method is not able to distinguish between isobar building blocks like leucine and isoleucine as well as the nonribosomally derived *N*-methylvaline. At this point, a combination of mass spectrometry and bioinformatic prediction is beneficial. For instance, prediction of adenylation domain specificity[77;86] could be suggestive of incorporated amino acids and can be used for labeling experiments. In general, stable isotope labeling experiments are used to determine the number of carbons and nitrogens of a compound. Moreover, if building blocks of natural abundance are fed to a culture of a bacterium grown in [U-^{13}C] medium, an incorporation can easily be concluded by a mass

shift to a lower mass. Naturally, this method can also be applied *vice versa*, using normal medium in addition to labeled building blocks.[7;80] In this work, nonribosomally produced peptides such as the cyclic GameXPeptides from *P. luminescens* and the linear rhabdopeptides from *X. nematophila* were identified and elucidated by exploiting genomic analysis and isotopic feeding experiments.[7;79] For rhabdopeptide structure elucidation, labeling experiments and tandem MS analysis were combined to distinguish between *N*-methylvaline and leucine. In short, *X. nematophila* was cultivated in LB medium supplemented with [D_{10}]leucine or [D_3]methionine (Figure 5a). The incorporation of a building block is marked by an increasing mass shift, which is highlighted in blue. For example, leucine as building block has a *m/z* of 113, supplemented with [D_{10}]leucine resulted in a mass increase of +9 Da (*m/z* 122). Nevertheless, bioinformatic predictions like the NRPSpredictor2[86] are based on standard consensus sequences resulted from limited organisms investigated and are not always correct in *Xenorhabdus* and *Photorhabdus*.

For isolated compounds, absolute amino acid configuration is determined by the advanced Marfey's method, where the stereochemistry is analyzed by comparison of the eluting profiles in HPLC MS analysis of 1-fluoro-2,4-dinitrophenyl-5-L-leucinamide (L-FDLA) and 1-fluoro-2,4-dinitrophenyl-5-DL-leucinamide (DL-FDLA) derivatized amino acids.[31;32;71] In addition to building block elucidation, isotope labeling can be used as a method to determine the absolute amino acid configuration of compounds directly in the producer strain.[7] In nonribosomal peptide synthetases, epimerization (E) domains catalyze the conversion of L- into D-amino acids and the D-amino acid derivative is further processed.[49;94] Labeling of amino acids with ^2H at the α-position used in transaminase deficient mutant strains (e.g. Δ*ilvE*Δ*tyrB*) enables to determine the absolute configuration as in a conversion to a D-amino acid one ^2H label is exchanged for one ^1H from the medium. In the case of the GameXPeptides, feeding of [$^2H_8$]L-phenylalanine ([D_8]L-Phe) resulted in in a labeling of $^2H_7$ using the Δ*ilvE*Δ*tyrB* mutant strain (Figure 5b, highlighted in blue). On the contrary, a L-amino acid, as shown for [$^2H_{10}$]L-leucine ([D_{10}]L-Leu) maintains the complete label (Figure 5b, highlighted in blue). Harbors the compound different configuration of the same amino acid, both labeling masses can be observed. In wild type strains such a comparison is not possible as the transaminases catalyze the conversion of amino acids into 2-keto carboxylic acids in amino acid biosynthesis and degradation (e.g. *ilvE* specific for branched-chain amino acids such as leucine and valine and *tyrB* specific for aromatic amino acids such as phenylalanine and tyrosin).[67]

However, structure elucidation without isolation and mapping of genotypes with chemotypes[50] could be misleading. PKS and NRPS derived secondary metabolites are not always produced via a colinear biosynthesis and there are some examples described where an iterative usage of discrete modules or a skipping of modules lead to unexpected compounds.[26;56;101]

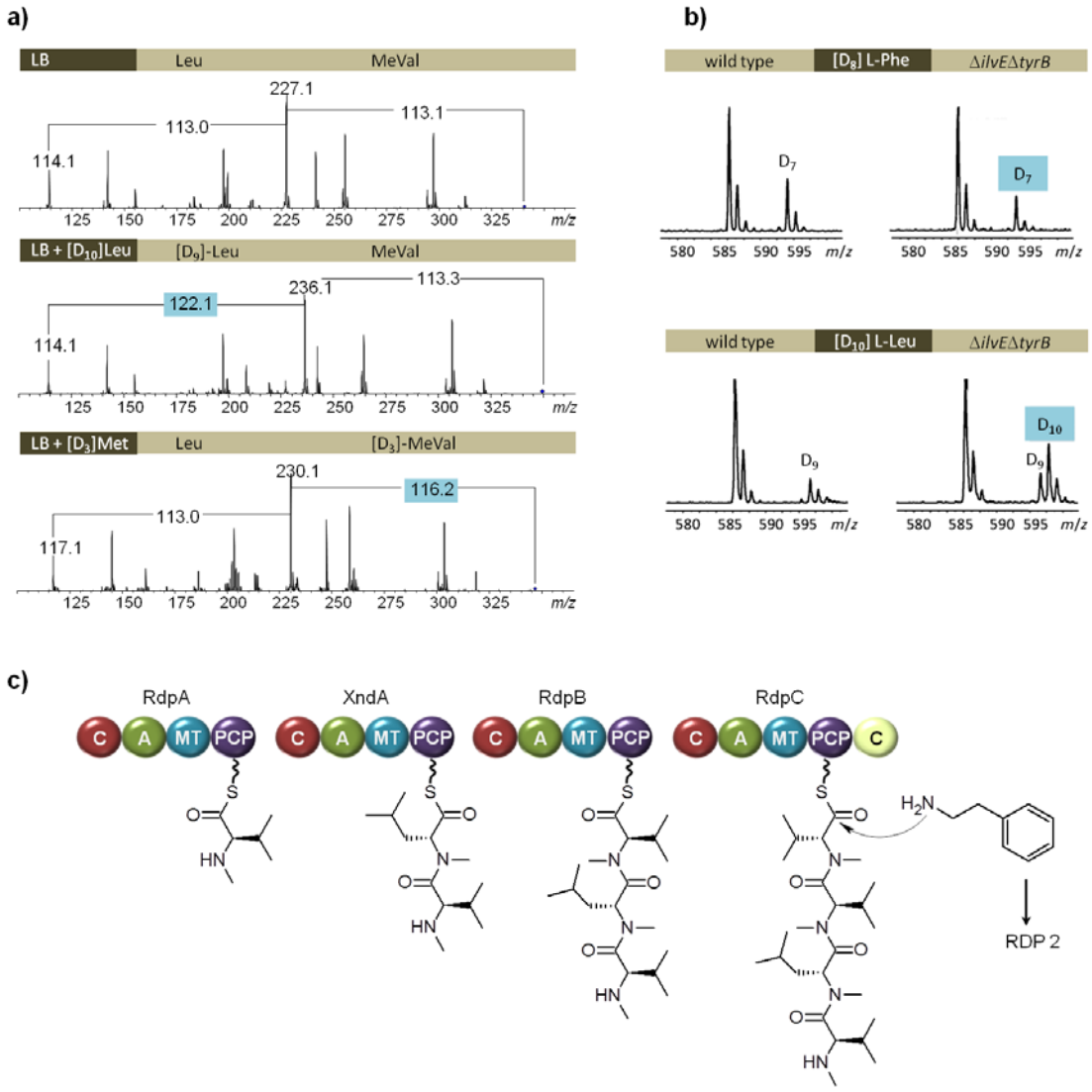

Figure 5. Structure elucidation by stable isotope labeling and mass spectrometry. a) Isotope labeling experiments to distinguish between isobar building blocks such as leucine (Leu) and *N*-methylvaline (MeVal) using the example of the rhabdopeptides. *X. nematophila* is cultivated in LB medium supplemented with [$^2H_{10}$]leucine ([D_{10}]Leu) or [$^2H_3$]methionine ([D_3]Met). Incorporation of a building block is marked by a increasing mass shift (highlighted in blue). b) Determination of the absolute configuration of amino acids by labeling with ^2H at the α-position used in transaminase deficient mutant strain (Δ*ilvE*Δ*tyrB*). Feeding of [$^2H_8$]L-phenylalanine ([D_8]L-Phe) resulted in the case of a D-amino acid in the transaminase mutant strain with a labeling of $^2H_7$ (highlighted in blue) as one ^2H label is exchanged for one ^1H from the medium. In the case of a L-amino acid, as shown for [$^2H_{10}$L]-leucine ([D_{10}]L-Leu), it resulted in a complete labeling (highlighted in blue). Harbors the compound different configuration of the same amino acid, both labeling masses can be observed. c) Proposed biosynthesis of rhabdopeptide 2 (RDP 2) via a crosstalk between rhabdopeptide (Rdp) and xenortide (Xnd) modules. A: adenylation domain, PCP: peptidyl carrier protein, C: condensation domain, MT: *N*-methyltransferase domain.

In the rhabdopeptide biosynthesis an iterative usage of one or more modules and a crosstalk between the biosynthesis gene clusters for the rhabdopeptides and xenortides is proposed (Figure 5c, unpublished data). The first amino acid of rhabdopeptide 2 (RDP 2) is synthesized by module RdpA and the intermediate is translocated to XndA of the biosynthetic gene cluster of the xenortides located

only 60 kb downstream of the RDP gene cluster. Subsequently a back translocation to the Rdp modules occurred and the remaining modules act colinear. Due the presence of only three modules in the RDP biosynthetic gene cluster and larger derivatives available, for RDP 1 and RDP 3-6 an iterative usage of module RdpB must be assumed as has been proposed previously for coelichelin,[56] fuscachelin[26] and thalassospiramide[85] (unpublished data). Only a few examples for a crosstalk between different NRPS or PKS biosynthetic gene clusters are described in literature. In the biosynthesis of the siderophores erythrochelin and rhodochelin, a δ-*N*-acetyltransferase is encoded within a remote NRPS gene cluster[57] and the required genes are located on three distinct gene clusters,[10] respectively. However, the complete rhabdopeptide biosynthesis in detail is currently investigated.

Distribution of insect-associated highly *N*-methylated rhabdopeptide derivatives in *Xenorhabdus* and *Photorhabdus* spp.

The group of the rhabdopeptides, xenortides and mevalagmapeptides are the first example of highly *N*-methylated nonpolar linear NRPS-derived peptides from *Xenorhabdus* and *Photorhabdus* spp.. Other structural related peptides are reported in diversity in marine-derived bacteria and fungi and are shown in Figure 6. These peptides are composed by a variety of nonpolar amino acids and harbor partially unusual *N*- and *C*-terminal modifications (e.g. free amides,[88] cinnamoyl groups,[55] (2*R*)-methyloct-7-ynoic acids[88] or methylamides[55]). The almiramides and dragonamides produced by the cyanobacterium *Lyngbya majuscula* represent a new class of Leishmaniasis lead compounds with a mentionable activity against the protozoan parasite *Leishmania donovani* (IC_{50} 1.9 µM for almiramide C, IC_{50} 6.5 µM for dragonamide A) and no significant cytotoxicity against mammalian Vero cells. Comparisons of different derivatives have shown a strong influence of specific moieties on the activity. Unsaturated *N*-termini and an aromatic ring-containing residue at the *C*-terminus are necessary for activity compared to the insufficient alkyne and primary amide termini.[5;88] Pterulamides[55] isolated from fruiting bodies of a Malaysian fungus *Pterula* sp. with an unusual *C*-terminal methylamide possess cytotoxicity against murine leukemia cells and RHMs,[8;9] from a marine sponge-derived *Acremonium* fungus, show antibiotic activity. For none of the mentioned natural products the biological function in the host is known. Although, rhabdopeptides share some structural similarities, they clearly differ from the mentioned peptides by the presence of a larger *C*-terminal amine.[79]

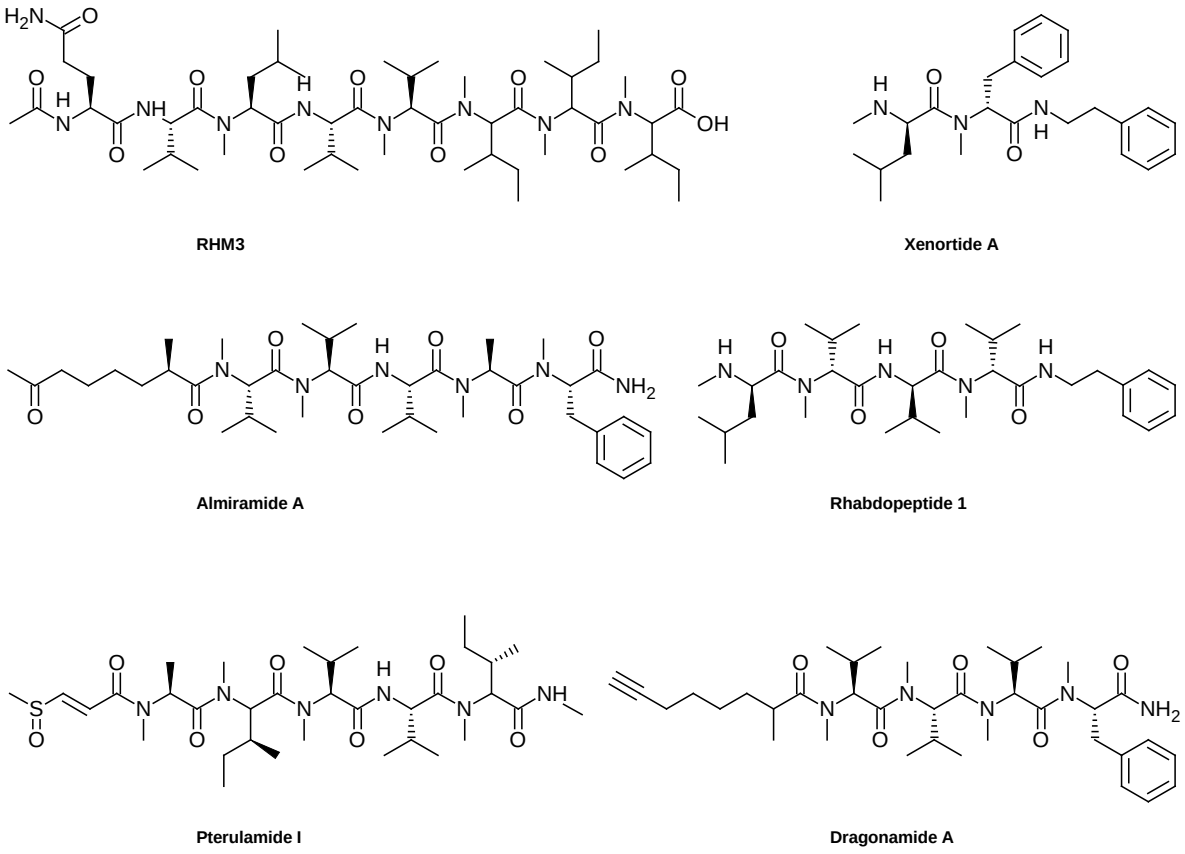

Figure 6. Highly *N*-methylated linear peptides from bacteria and fungi. Xenortide A[54] and rhabdopeptide 1[79] from *X. nematophila*, RHM3[8] from an *Acremonium* fungus and pterulamide I[55] from a *Pterula* fungus, as well as dragonamide A[5] and almiramide A[88] from the cyanobacterium *Lyngbya majuscula.*

In addition to the structures discussed in chapter 5, rhabdopeptide-like structures could be found in diversity in different *Xenorhabdus* and *Photorhabdus* species. The class of rhabdopeptides differs in length from two to eight amino acids, in their methylation pattern and in combination with different amines like phenylethylamine, tryptamine and agmatine. *P. luminescens* TT01,[30] *P. temperata thracensis* DSM 15199,[37;97] *X. budapestensis* DSM 16342[58] and an unknown *Xenorhabdus* strain KK7.4[99] demonstrate a high grade of similarity of the rhabdopeptide-like gene cluster consisting of three modules. In each case, in the first module the *N*-methyltransferase (MT) domain is missing and the structures are composed of one or two valine and three or four *N*-methylvalines bound to an agmatine (named mevalagmapeptide[7]). Interestingly, in DSM 16342 none of these compounds could be identified. Instead, a variety of eight derivatives possessing five or six building blocks with phenylethylamine or tryptamine incorporated are produced. The incorporation of different amines is not only a question of the specificity of the responsible terminal condensation (C) domain but rather of the availability of a decarboxylase catalyzing the decarboxylation of specific amino acids. For the xenortides, a mutasynthesis strategy, where different amines where fed to an *E. coli* strain harboring the corresponding xenortide biosynthetic gene cluster, has shown a possible incorporation of different amines by the terminal C-domain (unpublished data). Worth

mentioning is *X. innexi* DSM 16336[58] as with eight amino acids it is not only producing the biggest rhabdopeptides identified so far, but furthermore incorporates similar to the xenortides *N*-methylphenylalanine besides valine as building blocks. *X. miraniensis* DSM 17902[98] and PB62.4[99] harbor *N*-terminal a disrupted condensation domain, which might be inactive and can not be used iteratively as the strains produce only four small derivatives with two (*N*-methyl)valines and the amine. Furthermore, as this compound class is so widely distributed and similar biosynthetic gene clusters could also be found in *X. stockiae* DSM 17904[98] and KJ12.1,[99] *X. indica* DSM 17382[93] and *X. szentirmaii* DSM 16338[58] an important biological role of the rhabdopeptides can be proposed (unpublished data).

Rhabdopeptides were identified by a promoter trap strategy using an *in vivo* expression technology (IVET) for the detection of insect inducible promoters. Although, the promoter is upregulated 1 h post-infection and the production is dramatically upregulated during *X. nematophila infection* of *Manduca sexta* or *Galleria mellonella* insect hosts, only a slight increase of virulence was detected. Furthermore, no differences in nematode colonization or other phenotypes can be observed. As a rhabdopeptide negative mutant displays no severe virulence defect and the production reaches its maximum 10 days post-infection, rhabdopeptides might play a role in protecting the insect cadaver against food competitors or nematode reproduction phases of the *Xenorhabdus* life cycle.[79]

Rhabdopeptide-like compounds, especially the tryptamine derivatives, display an anti-protozoan activity against the protists *Trypanosoma brucei rhodesiense* (sleeping sickness) and *Plasmodium falciparum* (malaria) with IC_{50} values of 0.202 µg mL^{-1} (rhabdopeptide *m/z* 698.4 $[M+H]^+$, DSM 17382), 0.731 µg mL^{-1} (xenortide B, ATCC 19061) and 0.367 µg mL^{-1} (rhabdopeptide m/z 698.4 $[M+H]^+$, DSM 17382), 0.343 µg mL^{-1} (xenortide B, ATCC 19061), respectively (unpublished data). Activity against pathogenic protists might be explained by the relationship between protozoa causing tropical diseases and amoebae. Amoebae belong to the protozoa and are common soil inhabitants,[84] which might act as a food competitor to *Xenorhabdus* during the nematode-bacteria life cycle as free-living amoebae feed mainly on bacteria. Some microorganisms are described, which have evolved to become resistant to amoeba as a system of self-protection or use them as a kind of Trojan horse (e.g. *Legionella pneumophila, Pseudomonas aeruginosa*).[34]

Recently, membrane associated proteins of glycosomes of the parasite *Trypanosoma brucei* were identified as potential targets of the *N*-methylated almiramides. Glycosomes are the globular organelles and compartmentalize steps of the glycolysis and are consequently essential for parasite survival in the bloodstream. Almiramide might disrupt the membrane and therefore perturb the functionality of the glycosomes.[87] Targeting the cell membrane by *N*-methylated peptides is also described for the cyclic hexadepsipeptides enniatins from different *Fusarium* species. Enniatins

incorporate into the cell membrane, form vertically complexes and act as ionophores disrupting the membrane potential.[48]

In future, the biological role and the behavior of the rhabdopeptides need to be investigated but a similar or related mode of action as described for the almiramides should be considered.

Regulation of secondary metabolite biosynthesis in *Xenorhabdus nematophila*

Xenorhabdus features the capability to respond to environmental changes for microbial adaptation to hosts and regulation between mutualism and pathogenesis involving the regulation of secondary metabolite production.[41] The global regulator Lrp (leucine responsive regulatory protein) is one of the key player in this highly regulated system.[22;39-41;83] HPLC MS analysis of *lrp* mutant strains (kindly provided by Heidi Goodrich-Blair, University of Wisconsin-Madison, USA) demonstrated an dramatic influence of the regulator to the secondary metabolite production (Figure 7a). A *lrp* deficient mutant offers a HLPC MS chromatogram, which is comparable with a chromatogram of *X. nematophila* secondary form variants (Figure 7a, iv and data not shown). Expression of *lrp* at a low-level (Figure 7a, ii) and high-level (Figure 7a, iii) compared to the wild type (Figure 7a, i) resulted in higher amounts of produced secondary metabolites. Xenortide production is 4- to 5-fold increased in low- or high-level *lrp* expression, respectively (Figure 7b). Rhabdopeptides show a more drastically upregulation about 10-fold increase (Figure 7c) (unpublished data).

In 2011, Crawford *et al.* have shown that L-proline's present in the insect hemolymph results in a significant upregulation of virulence factors and secondary metabolites. Addition of L-proline to *X. nematophila* cultivated under lab conditions mimics the insect host. Compounds like nematophin or the related tryptamide derivatives possessing little to no antibiotic activity are upregulated implying an important biological function.[23;59] Proline transport is regulated by the transcriptional regulator LrhA, one of the key controlling virulence factors in *X. nematophila*[41;83] Therefore, an inhibition of the proline transport by LrhA suggests LrhA as important virulence inductor.[62]

Xenocoumacin production is positively influenced by Lrp and independent of LrhA[62] and an increase up to 5-fold could be observed in the production using the high-level expression strain of *lrp* (Figure 7d) (unpublished data). Furthermore, the biosynthesis is regulated by the response regulator OmpR.[74] The OmpR/EnvZ two-component system was shown to repress flagella synthesis and exoenzyme production in *X. nematophila* by negatively regulating the *flhDC* operon. FlhDC activates the class II flagella genes required for flagellin and exoenzyme gene expression.[75] OmpR was identified as a negative regulator of *xcnA–L* required for the biosynthesis of xenocoumacin 1. XcnMN, responsible for the self-resistance mechanism and the conversion of active XCN 1 into

inactive XCN 2 is positively regulated by OmpR.[74] A different regulation of separate transcriptional units in one biosynthetic gene cluster could be explained by two possible scenarios: OmpR might act as an repressor by binding near to the transcription start of *xcnA-L* and as an activator by binding further upstream of xcnMN[33;82] or OmpR controls indirectly a repressor controlling *xcnA-L* and an activator regulating the expression of *xcnMN*.[74] As mentioned earlier in this chapter, the differential expression may therefore be part of a response to balance the necessary level between XCN 1 and XCN 2 and as a result optimize the fitness of the strain. This is underlined by the fact that inactivation of OmpR compensate the reduced viability in a *xcnM* mutant strain by reducing outer membrane permeability due the missing positive regulation of outer membrane porins by OmpR.[74]

Nevertheless, how global regulators control the mechanisms of xenocoumacin and further secondary metabolite biosynthesis remain to be determined.

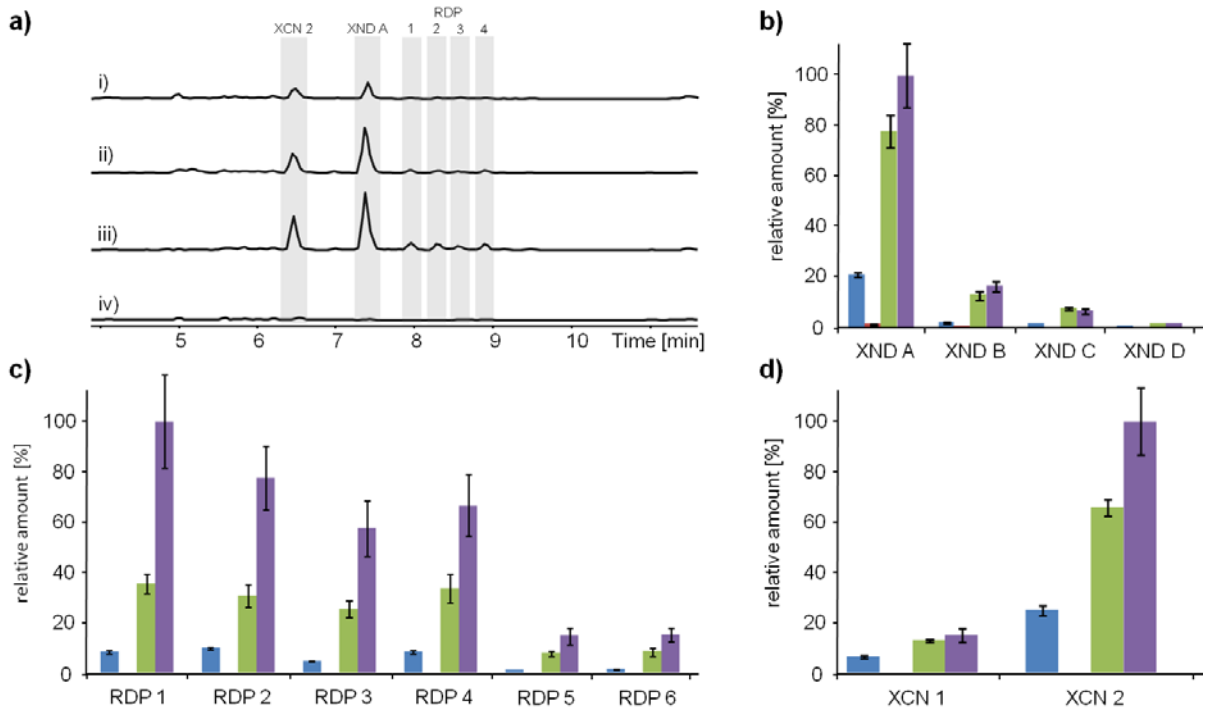

Figure 7. HPLC MS analysis of xenortide (XND) , rhabdopeptide (RDP) and xenocoumacin (XCN) production in *X. nematophila* strains. a) Base peak chromatograms of i) *X. nematophila* wild type, ii) low-level expression of *lrp*, iii) high-level expression of *lrp* and iv) inactivation mutant of *lrp* in *X. nematophila*. All chromatograms are scaled in the same intensity. b) Relative amount of xenortide derivatives, c) relative amount of rhabdopeptide derivatives and d) relative amount of xenocoumacin derivatives produced in wild type strain (blue), *lrp* inactivation mutant (red), low-level expression *lrp* mutant (green) and high-level expression *lrp* mutant (violet). 100% refers to the maximum production of XND A, RDP 1 and XCN 2, respectively, in the *lrp* high-level expression mutant (unpublished data).

Reference list

1. **Arnison, P. G., M. J. Bibb, G. Bierbaum, A. A. Bowers, T. S. Bugni, G. Bulaj, J. A. Camarero, D. J. Campopiano, G. L. Challis, J. Clardy, P. D. Cotter, D. J. Craik, M. Dawson, E. Dittmann, S. Donadio, P. C. Dorrestein, K. D. Entian, M. A. Fischbach, J. S. Garavelli, U. Goransson, C. W. Gruber, D. H. Haft, T. K. Hemscheidt, C. Hertweck, C. Hill, A. R. Horswill, M. Jaspars, W. L. Kelly, J. P. Klinman, O. P. Kuipers, A. J. Link, W. Liu, M. A. Marahiel, D. A. Mitchell, G. N. Moll, B. S. Moore, R. Müller, S. K. Nair, I. F. Nes, G. E. Norris, B. M. Olivera, H. Onaka, M. L. Patchett, J. Piel, M. J. Reaney, S. Rebuffat, R. P. Ross, H. G. Sahl, E. W. Schmidt, M. E. Selsted, K. Severinov, B. Shen, K. Sivonen, L. Smith, T. Stein, R. D. Sussmuth, J. R. Tagg, G. L. Tang, A. W. Truman, J. C. Vederas, C. T. Walsh, J. D. Walton, S. C. Wenzel, J. M. Willey, and W. A. van der Donk**. 2013. Ribosomally synthesized and post-translationally modified peptide natural products: overview and recommendations for a universal nomenclature. Nat. Prod. Rep. 30:108-160.

2. **Arthur, J. C., E. Perez-Chanona, M. Muhlbauer, S. Tomkovich, J. M. Uronis, T. J. Fan, B. J. Campbell, T. Abujamel, B. Dogan, A. B. Rogers, J. M. Rhodes, A. Stintzi, K. W. Simpson, J. J. Hansen, T. O. Keku, A. A. Fodor, and C. Jobin**. 2012. Intestinal inflammation targets cancer-inducing activity of the microbiota. Science 338:120-123.

3. **Azumi, M., K. Ogawa, T. Fujita, M. Takeshita, R. Yoshida, T. Furumai, and Y. Igarashi**. 2008. Bioactive microbial metabolites Part 33. Bacilosarcins A and B, novel bioactive isocoumarins with unusual heterocyclic cores from the marine-derived bacterium *Bacillus subtilis*. Tetrahedron 64:6420-6425.

4. **Bachmann, B. O. and J. Ravel**. 2009. Methods for in silico prediction of microbial polyketide and nonribosomal peptide biosynthetic pathways from DNA sequence data. Methods Enzymol. 458:181-217.

5. **Balunas, M. J., R. G. Linington, K. Tidgewell, A. M. Fenner, L. D. Urena, G. D. Togna, D. E. Kyle, and W. H. Gerwick**. 2010. Dragonamide E, a modified linear lipopeptide from *Lyngbya majuscula* with antileishmanial activity. J. Nat. Prod. 73:60-66.

6. **Bandow, J. E., H. Brotz, L. I. Leichert, H. Labischinski, and M. Hecker**. 2003. Proteomic approach to understanding antibiotic action. Antimicrob. Agents Chemother. 47:948-955.

7. **Bode, H. B., D. Reimer, S. W. Fuchs, F. Kirchner, C. Dauth, C. Kegler, W. Lorenzen, A. O. Brachmann, and P. Grün**. 2012. Determination of the absolute configuration of peptide natural products by using stable isotope labeling and mass spectrometry. Chem. Eur. J. 18:2342-2348.

8. **Boot, C. M., T. Amagata, K. Tenney, J. E. Compton, H. Pietraszkiewicz, F. A. Valeriote, and P. Crews**. 2007. Four classes of structurally unusual peptides from two marine-derived fungi: structures and bioactivities. Tetrahedron 63:9903-9914.

9. **Boot, C. M., K. Tenney, F. A. Valeriote, and P. Crews**. 2006. Highly N-methylated linear peptides produced by an atypical sponge-derived *Acremonium* sp. J. Nat. Prod. 69:83-92.

10. **Bosello, M., L. Robbel, U. Linne, X. Xie, and M. A. Marahiel**. 2011. Biosynthesis of the siderophore rhodochelin requires the coordinated expression of three independent gene clusters in *Rhodococcus jostii* RHA1. J. Am. Chem. Soc. 133:4587-4595.

11. **Boya, C. A., L. Herrera, H. M. Guzman, and M. Gutierrez**. 2012. Antiplasmodial activity of bacilosarcin A isolated from the octocoral-associated bacterium *Bacillus* sp. collected in Panama. J. Pharm. Bioallied. Sci. 4:66-69.

12. **Brotherton, C. A. and E. P. Balskus**. 2013. A prodrug resistance mechanism is involved in colibactin biosynthesis and cytotoxicity. J. Am. Chem. Soc. 135:3359-3362.

13. **Buist, P. H.** 2004. Fatty acid desaturases: selecting the dehydrogenation channel. Nat. Prod. Rep. 21:249-262.

14. **Bumpus, S. B., B. S. Evans, P. M. Thomas, I. Ntai, and N. L. Kelleher**. 2009. A proteomics approach to discovering natural products and their biosynthetic pathways. Nat. Biotechnol. 27:951-956.

15. **Campagna-Slater, V. and M. Schapira**. 2009. Evaluation of virtual screening as a tool for chemical genetic applications. J. Chem. Inf. Model. 49:2082-2091.

16. **Canedo, L. M., J. L. Fernandez Puentes, B. J. Perez, C. Acebal, F. de la Calle, G. D. Garcia, and T. Garcia de Quesada**. 1997. PM-94128, a new isocoumarin antitumor agent produced by a marine bacterium. J. Antibiot. 50:175-176.

17. **Chan, Y. A., M. T. Boyne, A. M. Podevels, A. K. Klimowicz, J. Handelsman, N. L. Kelleher, and M. G. Thomas**. 2006. Hydroxymalonyl-acyl carrier protein (ACP) and aminomalonyl-ACP are two additional type I polyketide synthase extender units. P. Natl. Acad. Sci. 103:14349-14354.

18. **Chan, Y. A. and M. G. Thomas**. 2009. Formation and characterization of acyl carrier protein-linked polyketide synthase extender units. Methods Enzymol. 459:143-163.

19. **Chaston, J. M., G. Suen, S. L. Tucker, A. W. Andersen, A. Bhasin, E. Bode, H. B. Bode, A. O. Brachmann, C. E. Cowles, K. N. Cowles, C. Darby, L. de Leon, K. Drace, Z. J. Du, A. Givaudan, E. E. H. Tran, K. A. Jewell, J. J. Knack, K. C. Krasomil-Osterfeld, R. Kukor, A. Lanois, P. Latreille, N. K. Leimgruber, C. M. Lipke, R. Y. Liu, X. J. Lu, E. C. Martens, P. R. Marri, C. Medigue, M. L. Menard, N. M. Miller, N. Morales-Soto, S. Norton, J. C. Ogier, S. S. Orchard, D. Park, Y. Park, B. A. Qurollo, D. R. Sugar, G. R. Richards, Z. Rouy, B. Slominski, K. Slominski, H. Snyder, B. C. Tjaden, R. van der Hoeven, R. D. Welch, C. Wheeler, B. S. Xiang, B. Barbazuk, S. Gaudriault, B. Goodner, S. C. Slater, S. Forst, B. S. Goldman, and H. Goodrich-Blair**. 2011. The entomopathogenic bacterial endosymbionts *Xenorhabdus* and *Photorhabdus*: Convergent lifestyles from divergent genomes. PLoS ONE 6:e27909.

20. **Coleman, D. C., I. Chopra, S. W. Shales, T. G. Howe, and T. J. Foster**. 1983. Analysis of tetracycline resistance encoded by transposon Tn10: deletion mapping of tetracycline-sensitive point mutations and identification of two structural genes. J. Bacteriol. 153:921-929.

21. **Cougnoux, A., L. Gibold, F. Robin, D. Dubois, N. Pradel, A. Darfeuille-Michaud, G. Dalmasso, J. Delmas, and R. Bonnet**. 2012. Analysis of structure-function relationships in the colibactin-maturating enzyme ClbP. J. Mol. Biol. 424:203-214.

22. **Cowles, K. N., C. E. Cowles, G. R. Richards, E. C. Martens, and H. Goodrich-Blair**. 2007. The global regulator Lrp contributes to mutualism, pathogenesis and phenotypic variation in the bacterium *Xenorhabdus nematophila*. Cell. Microbiol. 9:1311-1323.

23. **Crawford, J. M., R. Kontnik, and J. Clardy**. 2010. Regulating alternative lifestyles in entomopathogenic bacteria. Curr. Biol 20:69-74.

24. **Cuevas-Ramos, G., C. R. Petit, I. Marcq, M. Boury, E. Oswald, and J. P. Nougayrede**. 2010. *Escherichia coli* induces DNA damage in vivo and triggers genomic instability in mammalian cells. Proc. Natl. Acad. Sci. 107:11537-11542.

25. **Dhillon, M. and P. F. Leadlay**. 1990. A repeated decapeptide motif in the C-terminal domain of the ribosomal RNA methyltransferase from the erythromycin producer *Saccharopolyspora erythraea*. FEBS 262:189-193.

26. **Dimise, E. J., P. F. Widboom, and S. D. Bruner**. 2008. Structure elucidation and biosynthesis of fuscachelins, peptide siderophores from the moderate thermophile *Thermobifida fusca*. Proc. Natl. Acad. Sci. 105:15311-15316.

27. **Drake, E. J. and A. M. Gulick**. 2011. Structural characterization and high-throughput screening of inhibitors of PvdQ, an NTN hydrolase involved in pyoverdine synthesis. ACS Chem. Biol. 6:1277-1286.

28. **Dubois, D., O. Baron, A. Cougnoux, J. Delmas, N. Pradel, M. Boury, B. Bouchon, M. A. Bringer, J. P. Nougayrede, E. Oswald, and R. Bonnet**. 2011. ClbP is a prototype of a peptidase subgroup involved in biosynthesis of nonribosomal peptides. J. Biol. Chem. 286:35562-35570.

29. **Duquesne, S., D. Destoumieux-Garzon, S. Zirah, C. Goulard, J. Peduzzi, and S. Rebuffat**. 2007. Two enzymes catalyze the maturation of a lasso peptide in *Escherichia coli*. Chem. Biol. 14:793-803.

30. **Fischer-Le Saux, M., V. Viallard, B. Brunel, P. Normand, and N. E. Boemare**. 1999. Polyphasic classification of the genus *Photorhabdus* and proposal of new taxa: *P. luminescens* subsp. *luminescens* subsp. nov., *P. luminescens* subsp. *akhurstii* subsp. nov., *P. luminescens* subsp. *laumondii* subsp. nov., *P. temperata* sp. nov., *P. temperata* subsp. *temperata* subsp. nov. and *P. asymbiotica* sp. nov. Int. J. Syst. Bacteriol. 49 Pt 4:1645-1656.

31. **Fujii, K., Y. Ikai, T. Mayumi, H. Oka, M. Suzuki, and K. Harada**. 1997. A nonempirical method using LC/MS for determination of the absolute configuration of constituent amino acids in a peptide: Elucidation of limitations of Marfey's method and of its separation mechanism. Anal. Chem. 69:3346-3352.

32. **Fujii, K., T. Shimoya, Y. Ikai, H. Oka, and K. Harada**. 1998. Further application of advanced Marfey's method for determination of absolute configuration of primary amino compound. Tetrahedron Lett. 39:2579-2582.

33. **Goh, E. B., D. F. Siino, and M. M. Igo**. 2004. The *Escherichia coli* tppB (ydgR) gene represents a new class of OmpR-regulated genes. J. Bacteriol. 186:4019-4024.

34. **Greub, G. and D. Raoult**. 2004. Microorganisms resistant to free-living amoebae. Clin. Microbiol. Rev. 17:413-433.

35. **Grundy, F. J., M. T. Haldeman, G. M. Hornblow, J. M. Ward, A. F. Chalker, and T. M. Henkin**. 1997. The *Staphylococcus aureus ileS* gene, encoding isoleucyl-tRNA synthetase, is a member of the T-box family. J. Bacteriol. 179:3767-3772.

36. **Hashimoto, M., T. Taguchi, S. Nishida, K. Ueno, K. Koizumi, M. Aburada, and K. Ichinose**. 2007. Isolation of 8'-phosphate ester derivatives of amicoumacins: structure-activity relationship of hydroxy amino acid moiety. J. Antibiot. 60:752-756.

37. **Hazir, S., E. Stackebrandtz, E. Lang, P. Schumann, R. U. Ehlers, and N. Keskin**. 2004. Two new subspecies of *Photorhabdus luminescens*, Isolated from *Heterorhabditis bacteriophora* (Nematoda : Heterorhabditidae): *Photorhabdus luminescens* subsp *kayaii* subsp nov and *Photorhabdus luminescens* subsp *thracensis* subsp nov. Syst. Appl. Microbiol. 27:36-42.

38. **Heinzel, P., O. Werbitzky, J. Distler, and W. Piepersberg**. 1988. A second streptomycin resistance gene from *Streptomyces griseus* codes for streptomycin-3"-phosphotransferase. Relationships between antibiotic and protein kinases. Arch. Microbiol. 150:184-192.

39. **Herbert Tran, E. E., A. W. Andersen, and H. Goodrich-Blair**. 2009. CpxRA influences *Xenorhabdus nematophila* colonization initiation and outgrowth in *Steinernema carpocapsae* nematodes through regulation of the nil locus. Appl. Environ. Microbiol. 75:4007-4014.

40. **Herbert, E. E., K. N. Cowles, and H. Goodrich-Blair**. 2007. CpxRA regulates mutualism and pathogenesis in *Xenorhabdus nematophila*. Appl. Environ. Microbiol. 73:7826-7836.

41. **Herbert, E. E. and H. Goodrich-Blair**. 2007. Friend and foe: the two faces of *Xenorhabdus nematophila*. Nat. Rev. Microbiol. 5:634-646.

42. **Hong, H. A., l. H. Duc, and S. M. Cutting**. 2005. The use of bacterial spore formers as probiotics. FEMS Microbiol. Rev. 29:813-835.

43. **Hopwood, D. A.** 2007. How do antibiotic-producing bacteria ensure their self-resistance before antibiotic biosynthesis incapacitates them? Mol. Microbiol. 63:937-940.

44. **Huang, Y. F., L. H. Li, L. Tian, L. Qiao, H. M. Hua, and Y. H. Pei**. 2006. Sg17-1-4, a novel isocoumarin from a marine fungus *Alternaria tenuis* Sg17-1. J. Antibiot. 59:355-357.

45. **Itoh, J., S. Omoto, N. Nishizawa, Y. Kodama, and S. Inouye**. 1982. Chemical structures of amicoumacins produced by *Bacillus pumilus*. Agric. Biol. Chem. 46:2659-2665.

46. **Itoh, J., S. Omoto, T. Shomura, N. Nishizawa, S. Miyado, Y. Yuda, U. Shibata, and S. Inouye**. 1981. Amicoumacin-A, a new antibiotic with strong antiinflammatory and antiulcer activity. J. Antibiot. 34:611-613.

47. **Jackson, K. E., J. S. Pham, M. Kwek, N. S. De Silva, S. M. Allen, C. D. Goodman, G. I. McFadden, L. R. de Pouplana, and S. A. Ralph**. 2012. Dual targeting of aminoacyl-tRNA synthetases to the apicoplast and cytosol in *Plasmodium falciparum*. Int. J. Parasitol. 42:177-186.

48. **Kamyar, M., P. Rawnduzi, C. R. Studenik, K. Kouri, and R. Lemmens-Gruber**. 2004. Investigation of the electrophysiological properties of enniatins. Arch. Biochem. Biophys. 429:215-223.

49. **Keating, T. A., C. G. Marshall, C. T. Walsh, and A. E. Keating**. 2002. The structure of VibH represents nonribosomal peptide synthetase condensation, cyclization and epimerization domains. Nat. Struct. Biol. 9:522-526.

50. **Kersten, R. D., Y. L. Yang, Y. Q. Xu, P. Cimermancic, S. J. Nam, W. Fenical, M. A. Fischbach, B. S. Moore, and P. C. Dorrestein**. 2011. A mass spectrometry-guided genome mining approach for natural product peptidogenomics. Nat. Chem. Biol 7:794-802.

51. **Kevany, B. M., D. A. Rasko, and M. G. Thomas**. 2009. Characterization of the complete zwittermicin A biosynthesis gene cluster from *Bacillus cereus*. Appl. Environ. Microbiol. 75:1144-1155.

52. **Koketsu, K., A. Minami, K. Watanabe, H. Oguri, and H. Oikawa**. 2012. Pictet-Spenglerase involved in tetrahydroisoquinoline antibiotic biosynthesis. Curr. Opin. Chem. Biol. 16:142-149.

53. **Koketsu, K., A. Minami, K. Watanabe, H. Oguri, and H. Oikawa**. 2012. The Pictet-Spengler mechanism involved in the biosynthesis of tetrahydroisoquinoline antitumor

antibiotics: a novel function for a nonribosomal peptide synthetase. Methods Enzymol. 516:79-98.

54. **Lang, G., T. Kalvelage, A. Peters, J. Wiese, and J. F. Imhoff**. 2008. Linear and cyclic peptides from the entomopathogenic Bacterium *Xenorhabdus nematophilus*. J. Nat. Prod. 71:1074-1077.

55. **Lang, G., M. I. Mitova, A. L. Cole, L. B. Din, S. Vikineswary, N. Abdullah, J. W. Blunt, and M. H. Munro**. 2006. Pterulamides I-VI, linear peptides from a Malaysian *Pterula* sp. J. Nat. Prod. 69:1389-1393.

56. **Lautru, S., R. J. Deeth, L. M. Bailey, and G. L. Challis**. 2005. Discovery of a new peptide natural product by *Streptomyces coelicolor* genome mining. .Nat. Chem. Biol. 1:265-269.

57. **Lazos, O., M. Tosin, A. L. Slusarczyk, S. Boakes, J. Cortes, P. J. Sidebottom, and P. F. Leadlay**. 2010. Biosynthesis of the putative siderophore erythrochelin requires unprecedented crosstalk between separate nonribosomal peptide gene clusters. Chem. Biol. 17:160-173.

58. **Lengyel, K., E. Lang, A. Fodor, E. Szallas, P. Schumann, and E. Stackebrandt**. 2005. Description of four novel species of *Xenorhabdus*, family Enterobacteriaceae: *Xenorhabdus budapestensis* sp. nov., *Xenorhabdus ehlersii* sp. nov., *Xenorhabdus innexi* sp. nov., and *Xenorhabdus szentirmaii* sp. nov. Syst. Appl. Microbiol. 28:115-122.

59. **Li, J. X., G. H. Chen, and J. M. Webster**. 1997. Synthesis and antistaphylococcal activity of nematophin and its analogs. Bioorg. Med. Chem. Lett. 7:1349-1352.

60. **Li, Y., Y. Xu, L. Liu, Z. Han, P. Y. Lai, X. Guo, X. Zhang, W. Lin, and P. Y. Qian**. 2012. Five new amicoumacins isolated from a marine-derived bacterium *Bacillus subtilis*. Mar. Drugs 10:319-328.

61. **Liu, S. W., J. Jin, C. Chen, J. M. Liu, J. Y. Li, F. F. Wang, Z. K. Jiang, J. H. Hu, Z. X. Gao, F. Yao, X. F. You, S. Y. Si, and C. H. Sun**. 2013. PJS, a novel isocoumarin with hexahydropyrimidine ring from *Bacillus subtilis* PJS. J. Antibiot. in press, http://dx.doi.org/10.1038/ja.2012.118

62. **Lu, X.** Examining pathogenic and mutualistic regulatory networks in the bacterium *Xenorhabdus nematophila* . 2012, Thesis, 1-184. University of Wisconsin-Madison, USA.

63. **Luo, Y., L. F. Ruan, C. M. Zhao, C. X. Wang, D. H. Peng, and M. Sun**. 2011. Validation of the intact zwittermicin A biosynthetic gene cluster and discovery of a complementary resistance mechanism in *Bacillus thuringiensis*. Antimicrob. Agents Chemother. 55:4161-4169.

64. **Masschelein, J., W. Mattheus, L. J. Gao, P. Moons, H. R. Van, B. Uytterhoeven, C. Lamberigts, E. Lescrinier, J. Rozenski, P. Herdewijn, A. Aertsen, C. Michiels, and R. Lavigne**. 2013. A PKS/NRPS/FAS hybrid gene cluster from *Serratia plymuthica* RVH1 encoding the biosynthesis of three broad spectrum, zeamine-related antibiotics. PLoS. ONE. 8:e54143.

65. **McInerney, B. V., W. C. Taylor, M. J. Lacey, R. J. Akhurst, and R. P. Gregson**. 1991. Biologically active metabolites from *Xenorhabdus* spp., Part 2. Benzopyran-1-one derivatives with gastroprotective activity. J. Nat. Prod. 54:785-795.

66. **Medema, M. H., K. Blin, P. Cimermancic, V. de Jager, P. Zakrzewski, M. A. Fischbach, T. Weber, E. Takano, and R. Breitling**. 2011. antiSMASH: rapid identification, annotation and analysis of secondary metabolite biosynthesis gene clusters in bacterial and fungal genome sequences. Nucleic Acids Res. 39:W339-W346.

67. **Michal, G.** 1999. Biochemical Pathways. Spektrum Akad. Verlag, Heidelberg.

68. **Milner, J. L., E. A. Stohl, and J. Handelsman**. 1996. Zwittermycin A resistance gene from *Bacillus cereus*. J. Bacteriol. 178:4266-4272.

69. **Mohimani, H., W. T. Liu, Y. L. Yang, S. P. Gaudencio, W. Fenical, P. C. Dorrestein, and P. A. Pevzner**. 2011. Multiplex de novo sequencing of peptide antibiotics. J. Comput. Biol. 18:1371-1381.

70. **Nougayrede, J. P., S. Homburg, F. Taieb, M. Boury, E. Brzuszkiewicz, G. Gottschalk, C. Buchrieser, J. Hacker, U. Dobrindt, and E. Oswald**. 2006. *Escherichia coli* induces DNA double-strand breaks in eukaryotic cells. Science 313:848-851.

71. **Nozawa, Y., N. Sakai, K. Arai, Y. Kawasaki, and K. Harada**. 2007. Reliable and sensitive analysis of amino acids in the peptidoglycan of actinomycetes using the advanced Marfey's method. J. Microbiol. Methods 70:306-311.

72. **Okazaki, H., T. Kishi, T. Beppu, and K. Arima**. 1975. Letter: A new antibiotic, baciphelacin. J. Antibiot. 28:717-719.

73. **Paizs, B. and S. Suhai**. 2005. Fragmentation pathways of protonated peptides. Mass Spectrom. Rev. 24:508-548.

74. **Park, D., K. Ciezki, R. van der Hoeven, S. Singh, D. Reimer, H. B. Bode, and S. Forst**. 2009. Genetic analysis of xenocoumacin antibiotic production in the mutualistic bacterium *Xenorhabdus nematophila*. Mol. Microbiol. 73:938-949.

75. **Park, D. and S. Forst**. 2006. Co-regulation of motility, exoenzyme and antibiotic production by the EnvZ-OmpR-FlhDC-FliA pathway in *Xenorhabdus nematophila*. Mol. Microbiol. 61:1397-1412.

76. **Pinchuk, I. V., P. Bressollier, I. B. Sorokulova, B. Verneuil, and M. C. Urdaci**. 2002. Amicoumacin antibiotic production and genetic diversity of *Bacillus subtilis* strains isolated from different habitats. Res. Microbiol. 153:269-276.

77. **Prieto, C., C. Garcia-Estrada, D. Lorenzana, and J. F. Martin**. 2012. NRPSsp: non-ribosomal peptide synthase substrate predictor. Bioinformatics 28:426-427.

78. **Putze, J., C. Hennequin, J. P. Nougayrede, W. Zhang, S. Homburg, H. Karch, M. A. Bringer, C. Fayolle, E. Carniel, W. Rabsch, T. A. Oelschlaeger, E. Oswald, C. Forestier, J. Hacker, and U. Dobrindt**. 2009. Genetic structure and distribution of the colibactin genomic island among members of the family Enterobacteriaceae. Infect. Immun. 77:4696-4703.

79. **Reimer, D., K. N. Cowles, F. I. Nollmann, H. Goodrich-Blair, and H. B. Bode**. 2013. Rhabdopeptides from entomopathogenic bacteria as examples for insect-associated secondary metabolites. ChemBioChem, submitted.

80. **Reimer, D., E. Luxenburger, A. O. Brachmann, and H. B. Bode**. 2009. A new type of pyrrolidine biosynthesis is involved in the late steps of xenocoumacin production in *Xenorhabdus nematophila*. ChemBioChem 10:1997-2001.

81. **Reimer, D., K. M. Pos, M. Thines, P. Grün, and H. B. Bode**. 2011. A natural prodrug activation mechanism in nonribosomal peptide synthesis. Nat. Chem. Biol. 7:888-890.

82. **Rhee, J. E., W. Sheng, L. K. Morgan, R. Nolet, X. Liao, and L. J. Kenney**. 2008. Amino acids important for DNA recognition by the response regulator OmpR. J. Biol. Chem. 283:8664-8677.

83. **Richards, G. R., E. E. Herbert, Y. Park, and H. Goodrich-Blair**. 2008. *Xenorhabdus nematophila lrhA* is necessary for motility, lipase activity, toxin expression, and virulence in *Manduca sexta* insects. J. Bacteriol. 190:4870-4879.

84. **Rodriguez-Zaragoza, S.** 1994. Ecology of free-living amoebae. Crit. Rev. Microbiol. 20:225-241.

85. **Ross, A. C., Y. Xu, L. Lu, R. D. Kersten, Z. Shao, A. M. Al-Suwailem, P. C. Dorrestein, P. Y. Qian, and B. S. Moore**. 2013. Biosynthetic multitasking facilitates thalassospiramide structural diversity in marine bacteria. J. Am. Chem. Soc. 135:1155-1162.

86. **Röttig, M., M. H. Medema, K. Blin, T. Weber, C. Rausch, and O. Kohlbacher**. 2011. NRPSpredictor2--a web server for predicting NRPS adenylation domain specificity. Nucleic Acids Res. 39:W362-W367.

87. **Sanchez, L. M., G. M. Knudsen, C. Helbig, M. G. De, S. M. Mascuch, Z. B. Mackey, L. Gerwick, C. Clayton, J. H. McKerrow, and R. G. Linington**. 2013. Examination of the mode of action of the almiramide family of natural products against the kinetoplastid parasite *Trypanosoma brucei*. J. Nat. Prod. in press, http://dx.doi.org/10.1021/np300834q

88. **Sanchez, L. M., D. Lopez, B. A. Vesely, T. G. Della, W. H. Gerwick, D. E. Kyle, and R. G. Linington**. 2010. Almiramides A-C: discovery and development of a new class of leishmaniasis lead compounds. J. Med. Chem. 53:4187-4197.

89. **Sato, T., K. Nagai, K. Suzuki, M. Morioka, T. Saito, C. Nohara, K. Susaki, and Y. Takebayashi**. 1992. A new isocoumarin antibiotic, Y-05460M-A. J. Antibiot. 45:1949-1952.

90. **Shimojima, Y., H. Hayashi, T. Ooka, M. Shibukawa, and Y. Iitaka**. 1984. Studies an AI-77s, microbial products with gastroprotective activity. Structures and the chemical nature of AI-77s. Tetrahedron 40:2519-2527.

91. **Silo-Suh, L. A., B. J. Lethbridge, S. J. Raffel, H. He, J. Clardy, and J. Handelsman**. 1994. Biological activities of two fungistatic antibiotics produced by *Bacillus cereus* UW85. Appl. Environ. Microbiol. 60:2023-2030.

92. **Solbiati, J. O., M. Ciaccio, R. N. Farias, J. E. Gonzalez-Pastor, F. Moreno, and R. A. Salomon**. 1999. Sequence analysis of the four plasmid genes required to produce the circular peptide antibiotic microcin J25. J. Bacteriol. 181:2659-2662.

93. **Somvanshi, V. S., E. Lang, S. Ganguly, J. Swiderski, A. K. Saxena, and E. Stackebrandt**. 2006. A novel species of *Xenorhabdus*, family Enterobacteriaceae: *Xenorhabdus indica* sp. nov., symbiotically associated with entomopathogenic nematode *Steinernema thermophilum* Ganguly and Singh, 2000. Syst. Appl. Microbiol. 29:519-525.

94. **Stachelhaus, T. and C. T. Walsh**. 2000. Mutational analysis of the epimerization domain in the initiation module PheATE of gramicidin S synthetase. Biochemistry 39:5775-5787.

95. **Stohl, E. A., S. F. Brady, J. Clardy, and J. Handelsman**. 1999. ZmaR, a novel and widespread antibiotic resistance determinant that acetylates zwittermicin A. J. Bacteriol. 181:5455-5460.

96. **Sun, W., Y. Q. Zhang, Y. Huang, Y. Q. Zhang, Z. Y. Yang, and Z. H. Liu**. 2009. *Nocardia jinanensis* sp. nov., an amicoumacin B-producing actinomycete. Int. J. Syst. Evol. Microbiol. 59:417-420.

97. **Tailliez, P., C. Laroui, N. Ginibre, A. Paule, S. Pages, and N. Boemare**. 2010. Phylogeny of *Photorhabdus* and *Xenorhabdus* based on universally conserved protein-coding sequences and implications for the taxonomy of these two genera. Proposal of new taxa: *X. vietnamensis* sp. nov., *P. luminescens* subsp. *caribbeanensis* subsp. nov., *P. luminescens* subsp. *hainanensis* subsp. nov., *P. temperata* subsp. *khanii* subsp. nov., *P. temperata* subsp. *tasmaniensis* subsp. nov., and the reclassification of *P. luminescens* subsp. *thracensis* as *P. temperata* subsp. *thracensis* comb. nov. Int. J. Syst. Evol. Microbiol. 60:1921-1937.

98. **Tailliez, P., S. Pages, N. Ginibre, and N. Boemare**. 2006. New insight into diversity in the genus *Xenorhabdus*, including the description of ten novel species. Int. J. Syst. Evol. Microbiol. 56:2805-2818.

99. **Thanwisai, A., S. Tandhavanant, N. Saiprom, N. R. Waterfield, L. P. Ke, H. B. Bode, S. J. Peacock, and N. Chantratita**. 2012. Diversity of *Xenorhabdus* and *Photorhabdus* spp. and their symbiotic entomopathogenic nematodes from Thailand. PLoS. ONE. 7:e43835.

100. **Thomas, G. M. and G. O. Jr. Poinar**. 1965. A new bacterium, *Achromobacter nematophilus* sp. nov. (Achromobacteriaceae: Eubacteriales) associated with a nematode. Int. Bull. Bacteriol. Nomencl. .Taxon. 15:249-254.

101. **Wenzel, S. C. and R. Müller**. 2007. Myxobacterial natural product assembly lines: fascinating examples of curious biochemistry. Nat. Prod. Rep. 24:1211-1224.

102. **Xu, H., S. S. Alguindigue, A. H. West, and P. F. Cook**. 2007. A proposed proton shuttle mechanism for saccharopine dehydrogenase from *Saccharomyces cerevisiae*. Biochemistry 46:871-882.

103. **Xu, Y., R. D. Kersten, S. J. Nam, L. Lu, A. M. Al-Suwailem, H. Zheng, W. Fenical, P. C. Dorrestein, B. S. Moore, and P. Y. Qian**. 2012. Bacterial biosynthesis and maturation of the didemnin anti-cancer agents. J. Am. Chem. Soc. 134:8625-8632.

104. **Zhou, Q., A. Dowling, H. Heide, J. Wöhnert, U. Brandt, J. Baum, R. ffrench-Constant, and H. B. Bode**. 2012. Xentrivalpeptides A-Q: depsipeptide diversification in *Xenorhabdus*. J. Nat. Prod. 75:1717-1722.

105. **Zhou, T., H. Zeng, D. Qiu, X. Yang, B. Wang, M. Chen, L. Guo, and S. Wang**. 2011. Global transcriptional responses of *Bacillus subtilis* to xenocoumacin 1. J. Appl. Microbiol. 111:652-662.

106. **Ziemert, N., S. Podell, K. Penn, J. H. Badger, E. Allen, and P. R. Jensen**. 2012. The natural product domain seeker NaPDoS: a phylogeny based bioinformatic tool to classify secondary metabolite gene diversity. PLoS. ONE. 7:e34064.

Acknowledgment

Mein besonderer Dank gilt Prof. Dr. Helge B. Bode für die Möglichkeit in seiner Arbeitsgruppe an einem spannenden Thema zu promovieren. Sein Interesse am Fortgang des Projektes, die große Unterstützung und das Vertrauen in allen Dingen und seine Begeisterung haben mich stets motiviert. Ich danke ihm auch für die Möglichkeit, an vielen Tagungen teilnehmen zu können um meine Forschung zu präsentieren.

Besonders danken möchte ich auch Prof. Dr. Eckhard Boles für die Übernahme des Zweitgutachtens.

Ganz herzlich bedanke ich mich bei Dr. Alexander Brachmann für die vielen hilfreichen Gespräche, Hilfestellungen im Labor und die vielen lustigen Zeiten und Kabbeleien. Danke, dass du einfach da warst.

Meinem Büro und meinem Labor in den verschiedenen Konstellationen danke ich für die lustigen gemeinsamen Arbeitsstunden. Schön, dass ihr bei meinem Ordnungssinn nicht geflüchtet seid und meine Launen und Späße ertragen habt.

Den Amazon-Mädels Qiuqin Zhou, Yvonne Engel und Olivia Schwimming danke ich für die vielen Stunden, die wir zusammen im MS Raum verbracht haben und dass wir trotz den Eigenschaften unseres "Lieblingsspielzeugs" nie die gute Laune verloren haben. Der Dank geht hierbei besonders an Qiuqin, die mit mir zusammen viele Probleme gelöst hat.

Besonders danken möchte ich auch Peter Grün, für alles, was er für die Gruppe tut und für die Unterstützung bei preparativen Fragestellungen.

Wolfram Lorenzen danke ich für die GC-Messungen und die kräftige Unterstützung im "Kalbach-Bonames Revier Derby".

Danke, Sebastian Fuchs für die Maldi-MS Messungen.

Ein großer Dank geht auch an Dr. Carsten Kegler für die vielen Tipps, wenn einen die Molekularbiologie mal wieder in den Wahnsinn treibt.

Friederike Nollmann, Christina Dauth und Max Kronenwerth danke ich, dass ihr mir die Chemie ein bisschen näher gebracht habt und an meinem Unverständnis nicht verzweifelt seid ;-) Danke auch für die vielen Biologen-Chemiker-Gespräche, die für beide Seiten sehr fruchtvoll waren.

Meinen Studenten Marek Kijonka, Tanja Schipper, Charlotte Hannig, Christian Sachs, Anna Venneri, Sandra Dramac, Eduardo Augusto Alonso, Kerstin Tusch, Patrice Lubuta und Carina Windhorst möchte ich auch danken. Es hat mir viel Spaß gemacht, euch Dinge beizubringen und es war toll, dass ihr euch für meine Projekte interessiert habt. Ein besonderer Dank geht hier aber vor allem an Anna, die zu einer gute Freundin geworden ist. Unsere vielen "Gele-Interpretations-Stunden" werden mir in guter Erinnerung bleiben und der kleine *E. coli* wird mich sicherlich noch weiterhin begleiten.

Danke auch an die ganze Arbeitsgruppe für die tolle Arbeitsatmosphäre und den Spaß, den wir zusammen hatten.

Alexander, Carsten, Friederike und Yvonne danke ich für die kritischen Kommentare zu meiner Arbeit.

Ich möchte auch meinen ehemaligen Kollegen aus dem Saarbrücker Labor danken, hier vor allem Eva Luxenburger für die analytischen Messungen, Gertrud Schwär für die labortechnischen Tipps, Katharina Schultz für eine lustige Laborbank-Nachbarschaft und Dr. Kathrin Buntin für die Hilfe bei meinen ersten Annotationsversuchen. Danke auch an Prof. Dr. Rolf Müller für das Beherbergen unserer kleinen Gruppe und die Aufnahme in seine Arbeitsgruppe.

Darüber hinaus möchte ich weiterhin, unseren Kollaborationspartnern Prof. Heidi Goodrich-Blair (University of Wisconsin-Madison, USA) und Prof. Steven Forst (University of Wisconsin-Milwaukee, USA) für das Austauschen unveröffentlichter Daten und die Zusammenarbeit an den Xenocoumacinen und Rhabdopeptiden danken.

Zuletzt geht ein riesengroßes Dankeschön an meine Eltern, Sylvia und Frank Reimer, die immer hinter mir standen, an mich geglaubt haben und mir vieles ermöglicht haben.

Ein großer Dank auch an Malte Burkhardt für die schönen biologiefreien Stunden.

Eidesstattliche Erklärung

Ich erkläre hiermit an Eides Statt, dass ich die vorgelegte Dissertation über "Identification and characterization of selected secondary metabolite biosynthetic pathways from *Xenorhabdus nematophila*" selbständig angefertigt und mich anderer Hilfsmittel als der in ihr angegebenen nicht bedient habe, insbesondere, dass alle Entlehnungen aus anderen Schriften mit Angabe der betreffenden Schrift gekennzeichnet sind.

Ich versichere, nicht die Hilfe einer kommerziellen Promotionsvermittlung in Anspruch genommen zu haben.

Ich erkläre hiermit weiterhin, dass ich mich bisher keiner Doktorprüfung unterzogen habe.

Frankfurt, 22.04.2013